Universitá degli Studi di Roma Tre
e
Consorzio Nazionale Interuniversitario per le Scienze Fisiche della Materia

Dottorato di Ricerca in Scienze Fisiche della Materia
XXIII ciclo

Generation and manipulation of multiphoton quantum fields
Tesi di dottorato della dott. Chiara Vitelli

Relatori:
Prof. Francesco De Martini
Dr. Fabio Sciarrino

Coordinatore Dottorato:
Prof. Settimio Mobilio

AA 2009/2010

Contents

Introduction

In the context of modern science, Quantum Information opens a new chapter, whose origins can be traced down to a proposal by Richard Feynman in the early eighties of the last century [Fey82]. According to Feynman a *quantum computer*, i.e. a device working on the basis of the algorithms of information theory re-formulated within the Hilbert space scenario, would be a necessary tool to simulate and investigate properly any natural quantum process. Owing to its insightful predictive character and to its intrinsic multidisciplinary nature, Quantum Information has attracted scientists from diverse areas of theoretical and experimental physics, e.g. atomic physics, quantum optics and laser physics, condensed matter, etc., and from other disciplines such as computer science, mathematical complexity, material sciences and engineering. In the last two decades it has undergone a huge and rapid growing, both on the theoretical and experimental sides and, in a world moving fast towards an increasing miniaturization approaching the quantum limits, it is expected to revolutionize many areas of Science and Technology. Today one of the main goals of QI is to understand the subtle aspects of quantum mechanics in order to learn how to formulate, manipulate, process and communicate the information in the most efficient way using realizable physical systems that operate on quantum principles. This is quite a hard task which necessarily implies a nearly decoherence-free intersection between the *microscopic* world of single quantum particles (photons, atoms etc.) and the *macroscopic* preparing or measuring devices that transfer the information to the human world.
QI usually deals with quantum bits, or *qubits*, i.e. 2-dimensional quantum systems that generally do not possess the definite values of 0 or 1 of classical bits, but rather are in a so-called *coherent superposition*, $|\psi\rangle = \alpha|0\rangle + \beta|1\rangle$ of the two orthogonal basis states $\{|0\rangle, |1\rangle\}$. Such state reveals unusual properties, especially when dealing with composite systems. Indeed the most distinctive feature of quantum physics is given by the possibility of entangling different qubits. First recognized by Erwin Schroedinger as "the characteristic trait of quantum mechanics", quantum entanglement represents the key resource for modern QI processing. It derives from subtle non-local correlations between the parts of a quantum system and combines three basic structural elements of quantum theory, i.e. the superposition principle, the quantum non-separability property and the exponential scaling of the state space with the number of partitions. Quantum entanglement has no classical analogue. This resource, associated with non-classical correlations among separated quantum systems, can be used to perform computational and cryptographic tasks

that are impossible with classical systems. An entangled state shared by two or more separated parties is a valuable resource for fundamental quantum communication protocols, such as quantum cryptography and quantum teleportation. While quantum communication tasks can be suitably realized with "flying" photonic qubits, there are at present a number of technologies under investigation for their suitability to implement a quantum computer. No single technology meets currently all of these requirements in a completely satisfactory way. Indeed, besides photons, qubits can be in principle realized by using different resources, for instance trapped ions, neutral atoms in interaction with optical cavities, superconducting circuits, semiconductor quantum dots, impurity in solids and also by the nuclear magnetic resonance.

Quantum optics represents an excellent experimental test bench for various novel concepts introduced within the framework of QI theory. Indeed, quantum states of photons can be easily and accurately manipulated using linear and non-linear (NL) optical devices and can be efficiently measured by efficient single-photon detectors. Pairs of entangled photonic qubits are usually generated by the *spontaneous parametric down conversion* (SPDC) process in a NL crystal where, under suitable conditions a pump photon of frequency ω_p is annihilated and two photons of frequencies ω_1 and ω_2 are created, such that $\omega_1 + \omega_2 = \omega_p$.

Nevertheless, as said the main problem of quantum resources resides on the extremely fragile nature of quantum systems and on the decoherence process that affects the quantum world. A possible approach in order to overcome this limitation is to exploit an amplification process performed over the photonic qubit establishing a tight connection between the microscopic and the macroscopic fields. Such an approach is at the heart of this work, whose starting point is the possibility of generating multiphoton quantum states through non linear optical methods. The generated fields have been obtained through the interaction of a non linear crystal with a high power pump beam, by amplification of single photon states or by spontaneous emission in a high gain regime. The interest for the study of multiphoton fields generated by the optical parametric amplifier is double: on one hand there is the investigation about the nature of quantum mechanics and about the transition from the microscopic to the macroscopic world, i.e. from the quantum to the classical world. The study and the realization of the entanglement between macroscopic quantum fields, generated by high gain spontaneous parametric amplifiers, fits in with this context. On the other hand there is the practical interest of the quantum information field for the possibility of generating macro-qubits, resilient to decoherence and to losses, able to be used in different quantum information and quantum communication protocols.

A further application of these states is related to the possibility of performing measurements able to influence the following overall state system evolution. Concerning this property, we have developed the idea of exploiting the high resilience to losses of the macro-qubit states in order to beat the decoherence in quantum metrology applications. Furthermore, in the quantum metrology context, the employ of this multiphoton states into interferometric schemes has been studied. More specifically the amplification of

NOON states has been investigated, theoretically and experimentally, [VSSD09]; these states enable to increase the optical resolution in interferometric experiments, beating the Heisenberg limit, and resulting as a resource in the context of quantum lithography.
Finally the interaction between multiphoton fields with atomic systems such as a Bose Einstein condensate (BEC) [DSVC10], by realizing the merging between different technologies, could open a new scenario in the context of quantum information. For example the creation of the light-matter entanglement would represent a long term perspective for this application. The simultaneous adoption of different methods and concepts, i.e. the optical phenomena and the BEC, would led to the development of an *hybrid technology* for the quantum information. The hybrid system would consist in the use of the two subsystems , the optical and the atomic ones, that can be prepared, manipulated and measured through different and independent experimental technologies.
The present work is divided into four parts: in the first part the necessary elements of quantum information and quantum optics are presented: in chapter 1 the quantum state representation and the more important features of quantum states are addressed, while in chapter 2 the optical implementation of quantum states is investigated. Particular attention is devoted to the concept of quantum cloning which is at the heart of the realization of multiphoton states of light. In part two two fundamental schemes for the macro states generation are then introduced: the quantum injected optical parametric amplifier (chapter 3), and the high gain optical parametric amplifier working in a spontaneous regime (chapter4). In both cases the quantum properties and the measurement strategy suitable for the observation of quantum nature are investigated. In this context the problem of finding a measurement able to catch the quantum structure of macro states arises. Hence in part three, by making use of optical devices such as an experimentally developed ultrafast optical shutter (chapter 5), we exploit different manipulation strategy in order to obtain the maximum amount of information about the multiphoton fields (chapter 6). Finally different applications of macro-states are investigated in part four: the high flux regime combined with the sub Rayleigh resolution available with an optical parametric amplifier working in a spontaneous emission regime turns out to be a promising ingredient to perform efficient lithography experiments (chapter 7). In the quantum metrology context the robustness of macro states obtained by the amplification of single qubits has then been exploited for improving the sensitivity in interferometrical experiments performed in high losses conditions (chapter 8. The same robustness allows in principle the non resonant interaction between the multiphoton state and a BEC system, theoretically investigated in chapter 9.

Part I

Preliminary notions

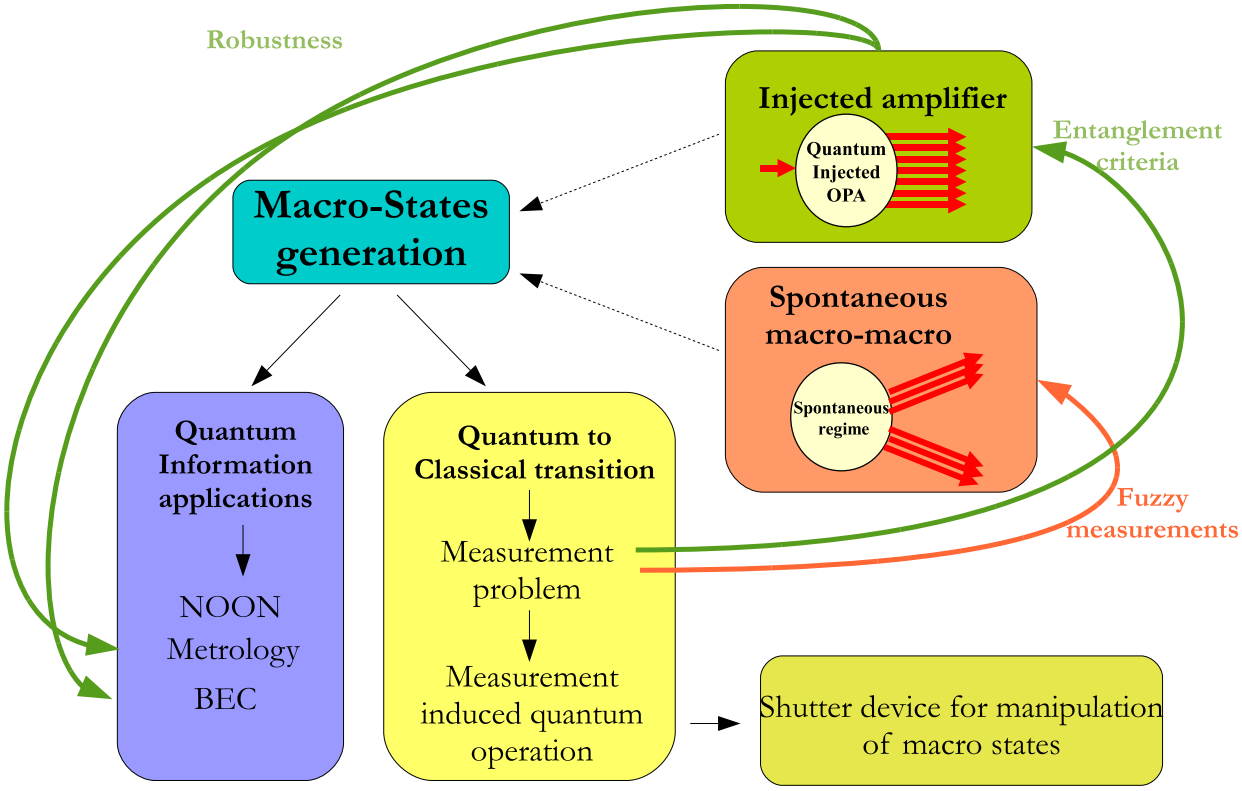

Figure 1: Conceptual scheme of the present work: the possibility of generating macroscopic states of light is at the basis of the thesis. The multiphoton states can be generated through different amplification schemes. In both cases the measurement problem is a key ingredient for the observation of quantum properties. The macro-states can then be studied as a paradigmatic example for the quantum to classical transition investigation. On the other hand the interest in investigating macroscopic states of light concerns the implementation of quantum information protocols related to quantum metrology and light atom efficient interactions.

The framework of the present thesis is reported in figure 2.8. The starting point of this research work is the generation of multiphoton quantum states, through different optical systems based on the laws of quantum mechanics and realized with the tools of non linear optics.
In this part the preliminary notions about the basic concepts of quantum information and quantum optics are then given. The problem of representation of quantum states and their measurement, which is strictly connected with the possibility of observing quantum phenomena in an increasing size quantum system, is firstly approached. The concept of quantum cloning and its implementation through the optical parametric amplifier, which is at the basis of the experiments addressed in the next chapters, is investigated in connection with the quantum correlation measurements problem.

Chapter 1

Elements of Quantum Information

Quantum information is a generalization of classical information, a deep difference among the two is shown by Bell's work (1964) [Bel64], in which is demonstrated that quantum reality cannot be reproduced by a local hidden variables model.
Quantum Information is then a non trivial extension of classical information which presents some limitation due to the laws of quantum mechanics: for instance two non commutative observables cannot be measured simultaneously, the acquisition of information about the system perturbs the system itself. This problem is strictly related with another difference between quantum and classical information: quantum information cannot be cloned (no-cloning theorem, demonstrated by Wooters and Zurek in 1982 [WZ82]).
The different resources and the "unusual" properties of quantum mechanics, for instance the concept of entanglement and the parallelism with which different logical functions can evolve, make quantum computation a precious instrument when the requirement is to solve *complex* problems. *Complex* or *not complex* in the information language refer to the time needed to solve a given problem: there is a distinction between algorithms which can be solved in a *polynomial time* or in a *exponential time*. To an algorithm A it can be associated a *complexity function* $T_A(N)$, where N is the input length calculated in bits. $T_A(N)$ is then the maximum time required to solve the algorithm A. If, for instance, algorithm A is the factorization algorithm, the required time for a *quantum* implementation (Shor algorithm) is polynomial. This problem is instead unsolvable by a *classical* implementation, and the problem is said to have a "NP complexity".
In this chapter the resources of quantum information will be addressed: starting from the *quantum bit* to the concept of entanglement, we will address the problem of representation and measurement of quantum states. Finally the problem of *quantum cloning* will be introduced.

1.1 Quantum states and their representation

The Quantum information carrier, the *qubit*, is defined into a bidimensional Hilbert space $\{|0\rangle, |1\rangle\}$, and then, differently respect to the classical *bit*, which can assume only 0 or 1

values, a general quantum state can be defined as:

$$|\psi\rangle = \alpha|0\rangle + \beta|1\rangle \tag{1.1}$$

with α and β complex numbers, such that $|\alpha|^2 + |\beta|^2 = 1$. Thanks to the superposition principle, a qubit can then be codified in an infinite number of states, while the classical bit lives in a bidimensional space.
A projective measurement of the state $|\psi\rangle$ upon the basis $\{|0\rangle, |1\rangle\}$ will give as a result $|0\rangle$ with probability $|\alpha|^2$ and $|1\rangle$ with probability $|\beta|^2$. Classically a probabilistic bit measurement can give 0 or 1 values with a probability p_0 and p_1 respectively, such that $p_0 + p_1 = 1$. The two measurement processes are not equivalent: the first difference resides into the perturbative character of a measurement in quantum mechanics, whose action modifies the state. The second difference is given by the continuous parameters α and β, which not only define the probability of a given result but define also a vector into the tridimensional space of spins. We can indeed consider the qubit as a $\frac{1}{2}$ spin state, the parameters α and β determine then the polar and the azimuthal angles θ and ϕ.
The evolution of a quantum state is reversible and is given by the Schrödinger equation:

$$H|\psi\rangle = i\hbar\frac{\partial|\psi\rangle}{\partial t} \tag{1.2}$$

where $|\psi\rangle$ can be a single qubit or a complex system composed by several interacting degrees of freedom, and H is the system hamiltonian. At a fixed time t the state vector of the system can be written as:

$$|\psi(t)\rangle = U|\psi(0)\rangle \tag{1.3}$$

where $U = \exp\left[-\frac{i}{\hbar}\int_0^t dt' H\right]$ is an unitary operator.
The qubit evolution can then be found by applying unitary operators to the state vector $|\psi\rangle$, corresponding to different continuous symmetries acting on the physical system. For each continuous symmetry R acting on the system there is a corresponding unitary operator $\mathbf{U}(R)$ commuting with the system hamiltonian $\mathbf{H}$. Generally:

$$\mathbf{U}(R) = e^{i\theta\mathbf{Q}} \tag{1.4}$$

where $\mathbf{Q}$ is the symmetry generator.
A particular symmetry class is the one of rotations: given the angular momentum $\mathbf{J} = (J_1, J_2, J_3)$, a rotation around the axis $\mathbf{n}$ of an angle θ, is represented by the following operator [Sak94]:

$$\mathbf{R}(\mathbf{n}, \theta) = e^{i\theta\mathbf{n}\cdot\mathbf{J}} \tag{1.5}$$

The rotation generator is then the angular momentum operator. The rotations group has an irreducible bidimensional representation:

$$\mathbf{J_k} = \frac{1}{2}\sigma_\mathbf{k} \tag{1.6}$$

where:

$$\sigma_1 = \begin{pmatrix} 0 & 1 \\ 1 & 0 \end{pmatrix}, \quad \sigma_2 = \begin{pmatrix} 0 & -i \\ i & 0 \end{pmatrix}, \quad \sigma_3 = \begin{pmatrix} 1 & 1 \\ 0 & -1 \end{pmatrix}$$

are the Pauli matrices, which with the unitary matrix form a complete basis for the 2×2 matrices. A generic 2×2 matrix can then be written as:

$$\mathbf{U}(\mathbf{n}, \theta) = e^{i\frac{\theta}{2}\mathbf{n}\cdot\sigma} = \mathbf{1}\cos\frac{\theta}{2} - i\mathbf{n}\cdot\sigma\sin\frac{\theta}{2} \tag{1.7}$$

In conclusion the qubit is a $1/2$ spin state and a unitary rotation acting upon it is equivalent to a rotation of the spin itself.
A measurement on the qubit results in an *irreversible* change of the system's state and it will always give a result equal to **0** or **1**, corresponding to the projection of the qubit into the state $|0\rangle$ or $|1\rangle$. It is impossible to know the state of a qubit through a single measurement, nor if, before the projection, it was in a pure state or in a superposition of states. It turns out that the infinite amount of information contained into a qubit is reduced, at the measurement stage, to the one carried by a classical bit.

1.1.1 Density matrix

Let us consider a large number of non interacting quantum states, in which each element of the ensemble can be described by the state $|\psi\rangle$. The overall ensemble is then described by the *density operator*:

$$\rho = |\psi\rangle\langle\psi| \tag{1.8}$$

which in the notation of states vector (1.1), can be written as:

$$\rho = \begin{pmatrix} \alpha \\ \beta \end{pmatrix} \begin{pmatrix} \alpha^* & \beta^* \end{pmatrix} = \begin{pmatrix} |\alpha|^2 & \alpha\beta^* \\ \beta\alpha^* & |\beta|^2 \end{pmatrix} \tag{1.9}$$

The density matrix is connected with the information content, and then with the system entropy S by the relation:

$$S = -kTr(\rho\ln\rho) \tag{1.10}$$

where k is the Boltzmann constant. A pure ensemble, in which each member of the ensemble is in the same state, the entropy is zero, this means that there is no lack of knowledge about the state of the system.
The density operator evolves with the Schödinger equation according to:

$$\frac{\partial \rho}{\partial t} = \frac{-i}{\hbar}[H, \rho] \tag{1.11}$$

from which $\rho(t) = U\rho(0)U^{\dagger}$. The unitary evolution of the density operator preserves the system's entropy $\frac{\partial S}{\partial t} = 0$.
The density matrix allows to describe the properties of a complex system, which is not representable by a single qubit. If we have a two-qubit system, being A and B the two subsystems; for instance in the state:

$$|\psi\rangle_{AB} = \alpha\,|0\rangle_A\,|0\rangle_B + \beta\,|1\rangle_A\,|1\rangle_B \tag{1.12}$$

a measurement on the state A corresponds to the application of the operator $(\mathbf{M_A} \otimes \mathbf{1_B})$ to $|\psi\rangle_{AB}$. The expectation value of such an observable is:

$${}_{AB}\langle\psi|\,(\mathbf{M_A} \otimes \mathbf{1_B})\,|\psi\rangle_{AB} = |\alpha|^2\,{}_A\langle 0|\,\mathbf{M_A}\,|0\rangle_A + |\beta|^2_A\,\langle 1|\,\mathbf{M_A}\,|1\rangle_A \tag{1.13}$$

which can be written as:

$$\langle \mathbf{M_A} \rangle = tr(\rho_{\mathbf{A}}\mathbf{M_A}) \tag{1.14}$$

where $\rho_{\mathbf{A}} = |\alpha|^2\,|0\rangle_A\,\langle 0| + |\beta|^2\,|1\rangle_A\,\langle 1|$ *reduced density matrix* of the qubit A.
Since the expectation value of every observable $\mathbf{M}$ acting upon the subsystem can be written as: $\langle M\rangle = tr(\mathbf{M}\rho) = \sum_a p_a\,\langle\psi_a|\mathbf{M}\,|\psi_a\rangle$, the density operator ρ_A represents the *ensemble* of the all possible quantum states in which the subsystem can be with probability p_a.
Generally for a bipartite system $\mathscr{H}_A \otimes \mathscr{H}_B$, if $\{|i\rangle_A\}$ is an orthonormal basis for the system A and $\{|\mu\rangle_B\}$ is an orthonormal basis for the system B, an arbitrary pure state $\mathscr{H}_A \otimes \mathscr{H}_B$ is written as:

$$|\psi\rangle_{AB} = \sum_{i,\mu} a_{i,\mu}\,|i\rangle_A \otimes |\mu\rangle_B \tag{1.15}$$

where $\sum_{i,\mu} a_{i,\mu} = 1$. The reduced density matrix of the system A, is then obtained by tracing over B the total density matrix AB, and is:

$$\begin{aligned} \rho_{\mathbf{A}} &= tr_B(|\psi\rangle_{AB}\,\langle\psi|) \\ &= \sum_{i,j,\mu} a_{i,j}a^*_{j,\mu}\,|i\rangle_A\,\langle j| \end{aligned} \tag{1.16}$$

which has the following properties:

- $\rho_{\mathbf{A}}$ is selfadjoint: $\rho_{\mathbf{A}} = \rho_{\mathbf{A}}\dagger$
- $\rho_{\mathbf{A}}$ is positive: for each $|\psi\rangle_A$ ${}_A\langle\psi|\,\rho\,|\psi\rangle_A = \sum_\mu \left|\sum_i a_{i,\mu}\,{}_A\langle\psi|\,i\rangle_A\right|^2 \geq 0$

- $tr(\rho_{\mathbf{A}}) = 1$

Generally the density matrix state can be *pure* or *mixed*, in the first case $\rho_{\mathbf{A}} = |\psi\rangle_A \langle\psi|$ is a projector which acts on the unidimesional space of the vector $|\psi\rangle_A$ for which holds $\rho^{\mathbf{2}} = \rho$; in the second case the density matrix is given by the sum: $\rho_{\mathbf{A}} = \sum_a p_a |\psi\rangle_A \langle\psi|$ where $0 < p_a < 1$ and $\sum_a p_a = 1$. In the last case ρ is given by the incoherent superposition of states and the relative phases between the various $|\psi\rangle_A$ are experimentally inaccessible.

1.1.2 Bloch sphere

Let us consider the case in which the system A is a single qubit, a graphical representation of the density matrix can then be given by the Bloch sphere. In a 2×2 Hilbert space a generic self-adjoint operator has 4 parameters and can be expressed in the basis $\{\mathbf{1}, \sigma_{\mathbf{1}}, \sigma_{\mathbf{2}}, \sigma_{\mathbf{3}}\}$. The density matrix ρ can be written as:

$$\rho(P) = \frac{1}{2}\left(1 + \overrightarrow{P} \cdot \overrightarrow{\sigma}\right) \tag{1.17}$$

where $det(\rho) = \frac{1}{4}(1 - \overrightarrow{P}^2)$. In order to have $det(\rho) \geq 0$ it is necessary that $\overrightarrow{P}^2 \leq 1$; there is then a correspondence $1-1$ between all the possible matrices of the single qubit and the points of the tridimensional space $0 \leq |\overrightarrow{P}| \leq 1$. This sphere is usually called *Bloch sphere*.

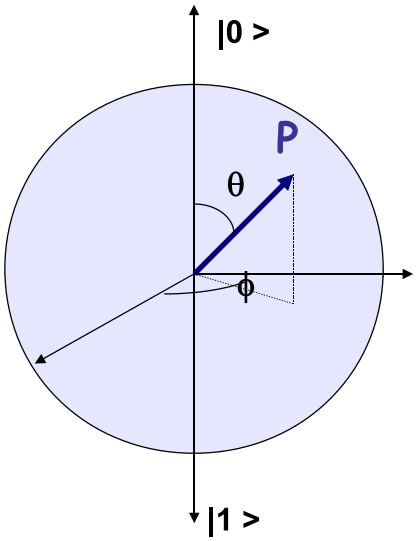

Figure 1.1: Bloch sphere: there is a $1-1$ correspondence between the points of the sphere and the single qubit's density matrix. The length of vector P defines the purity of the state, the states on the surface are pure while the mixed ones are internal vectors.

The states with $|\overrightarrow{P}| = 1$ on the surface correspond to the states whose density matrix has determinant equal to zero, and, since $tr(\rho) = 1$, the density matrix must have eigenvalues 0 and 1. This means that the operators corresponding to the points on the surface are unidimensional projectors over pure states.

The state of the single qubit $|\psi(\theta,\phi)\rangle$ can be seen as a $\frac{1}{2}$ spin vector on the direction identified by the angles $\overrightarrow{r}$ and (θ,ϕ):

$$|\psi(\theta,\phi)\rangle = \begin{pmatrix} e^{-i\phi/2}\cos(\frac{\theta}{2}) \\ e^{i\phi/2}\sin(\frac{\theta}{2}) \end{pmatrix} \tag{1.18}$$

the density matix can then be written as:

$$\rho(\mathbf{r}) = \frac{1}{2}(1+\overrightarrow{r}\cdot\overrightarrow{\sigma}) \tag{1.19}$$

where the length of r determines the purity of the state.
The qubit state can be implemented via a two level system, such as the photon's polarization [DS05], the state 1.1 can then be written as:

$$|\psi\rangle = \alpha|H\rangle + \beta|V\rangle \tag{1.20}$$

where $|H\rangle$ and $|V\rangle$ are the horizontal and vertical polarizations and can be represented by the column vectors $\begin{pmatrix} 1 \\ 0 \end{pmatrix}$ e $\begin{pmatrix} 0 \\ 1 \end{pmatrix}$.
In this case the three axis of the Bloch sphere represent the linear polarizations $(\overrightarrow{\pi_H},\overrightarrow{\pi_V})$, linear at 45° degrees 45° $(\overrightarrow{\pi_+},\overrightarrow{\pi_-})$, and circular polarization $(\overrightarrow{\pi_R},\overrightarrow{\pi_L})$.

1.2 Measurement and evolution of quantum states

Let us imagine, we have with equal probability some $\frac{1}{2}$ spin particles in one of the two non-orthogonal states $|\psi_1\rangle$ and $|\psi_2\rangle$, such that:

$$|\langle\psi_1|\psi_2\rangle| \equiv \cos\alpha \neq 0 \tag{1.21}$$

These non orthogonal states cannot be identified with certainty, by performing a standard or von Neumann measurement,the best we can do is indeed to project the particle state in one of the two orthogonal states $|\phi_1\rangle$ or $|\phi_2\rangle$, chosen as near as possible to the original states (see figure 1.2).

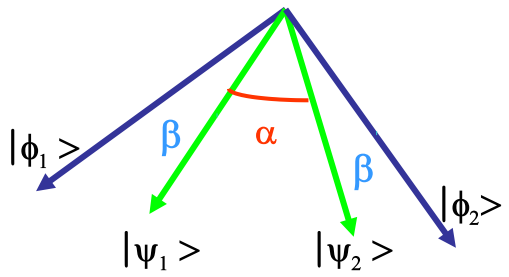

Figure 1.2: The identification of the two non orthogonal states $|\psi_1\rangle$ and $|\psi_2\rangle$ through a standard quantum measurement.

The measurement result will give $|\phi_1\rangle$ or $|\phi_2\rangle$, which will identify $|\psi_1\rangle$ or $|\psi_2\rangle$ respectively [HMG$^+$96]. This process has an error probability:

$$q \equiv Prob(err) = |\langle\psi_1|\phi_2\rangle|^2 = |\langle\psi_2|\phi_1\rangle|^2 = \frac{1}{2}(1-\sin\alpha) \tag{1.22}$$

In some cases this strategy can be the non optimal one: instead of having a binary answer $|\psi_1\rangle$ or $|\psi_2\rangle$ with a given error probability, we can add a third option: the inconclusive result. After the test the state of the particle will determined as $|\psi_1\rangle$ or $|\psi_2\rangle$, or unknown . A way to implement this test is to choose in a casual way, adding an auxiliary system, to project the particle's state over the orthogonal space to $|\psi_1\rangle$ or to $|\psi_2\rangle$. If the state is projected on the space orthogonal to $|\psi_1\rangle$ and the measurement's result is positive, we know with certainty that the initial state couldn't be $|\psi_1\rangle$ and it was $|\psi_2\rangle$. On the other hand if we obtain a negative result no deterministic conclusion can be reached: the particle could be in both the states. In this case the measurement is inconclusive and the result must be discarded. This kind of test is an example of generalized measurement, or POVM (Positive-Operator-Valued Measurement).

1.2.1 Orthogonal measurements

Each measurable physical quantity $\mathscr{A}$ is represented by an hermitian operator A into the Hilbert space $\mathscr{H}$, and is known as an observable.
The principal property of an observable is that it has a continuous and complete set of eigenvalues, furthermore two eigenvectors corresponding to different eigenvalues result to be orthogonal. In a n-dimensional Hilbert space it is possible to write the completeness condition as:

$$\sum_{i=1}^{n} P_i = 1 \tag{1.23}$$

where P_i is the projection operator on the eigenvector $|\phi_i\rangle$.
A measurement of the physical quantity $\mathscr{A}$ can only give as a result one of the eigenvalues of A, and the state $|\psi\rangle$ is projected on the corresponding eigenvector. This measurement is known as a *standard* or *orthogonal* measurement. The probability of obtaining the result i is given by the superposition of the corresponding eigenvector:

$$p(i) = |\langle\phi_i|\psi\rangle|^2 \tag{1.24}$$

More in general, if the initial state is described by the density matrix ρ, the probability of obtaining the result i becomes:

$$p(i) = Tr(\rho P_i). \tag{1.25}$$

1.2.2 Generalized measurements

A generalized measurement corresponds to couple the system under investigation to an auxiliary one, the ancilla, and then perform a standard measurement on the overall system. A generalized measurement can be mathematically described through a set of positive non-commutative operators Q_i, which satisfy the condition:

$$\sum_{i}^{m} Q_i = 1 \tag{1.26}$$

where m can be greater than the Hilbet space dimensionality of the system under examination. Since the operators Q_i are non orthogonal projection operators, this measurement is known as non-orthogonal measurement. In the case of the discrimination between the states $|\psi_1\rangle$ and $|\psi_2\rangle$, even in a bidimensional space, we need a measurement which gives three results: the $|\psi_1\rangle$, the state $|\psi_2\rangle$, or the inconclusive one. The probability of obtaining a result i is :

$$p(i) = Tr(\rho Q_i). \tag{1.27}$$

with ρ density matrix of the initial state.

1.2.3 Geometric representation

The bidimensional space identified by the vectors $|\psi_1\rangle$ and $|\psi_2\rangle$ can placed into a tridimensional space, whose third dimension is given by the state $|\phi_0\rangle$, orthogonal to the initial states (figure 1.3).

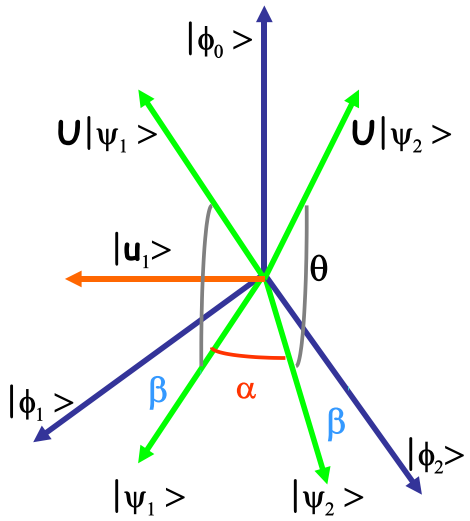

Figure 1.3: Identification of twonon-orthogonal states $|\psi_1\rangle$ and $|\psi_2\rangle$ through a generalized quantum measurement.

We can imagine the unitary evolution U of the system in a three dimensional space as a three-dimensional rotation around the vector $u_1 = \frac{1}{\sqrt{2}}(|\phi_1\rangle - |\phi_2\rangle)$ of an angle θ. The initial state $|\psi_1\rangle$ is then transformed into:

$$U|\psi_1\rangle = \frac{1}{\sqrt{2}}\left(\sin\frac{\alpha}{2}+\cos\frac{\alpha}{2}\cos\theta\right)|\phi_1\rangle+\frac{1}{\sqrt{2}}\left(-\sin\frac{\alpha}{2}+\cos\frac{\alpha}{2}\cos\theta\right)|\phi_2\rangle+\cos\frac{\alpha}{2}\sin\theta|\phi_0\rangle \tag{1.28}$$

while the state $|\psi_2\rangle$ transforms into:

$$U|\psi_2\rangle = \frac{1}{\sqrt{2}}\left(-\sin\frac{\alpha}{2}+\cos\frac{\alpha}{2}\cos\theta\right)|\phi_1\rangle+\frac{1}{\sqrt{2}}\left(\sin\frac{\alpha}{2}+\cos\frac{\alpha}{2}\cos\theta\right)|\phi_2\rangle+\cos\frac{\alpha}{2}\sin\theta|\phi_0\rangle \tag{1.29}$$

Defining the roation angle θ such that $\cos\theta = \tan\frac{\alpha}{2}$, we obtain:

$$U|\psi_1\rangle = \sqrt{2}\sin\frac{\alpha}{2}|\phi_1\rangle+\sqrt{\cos\alpha}|\phi_0\rangle \tag{1.30}$$

$$U|\psi_2\rangle = \sqrt{2}\sin\frac{\alpha}{2}|\phi_2\rangle+\sqrt{\cos\alpha}|\phi_0\rangle \tag{1.31}$$

Since now $|\phi_0\rangle$, $|\phi_1\rangle$ and $|\phi_2\rangle$ are orthogonal, it is possible to separate them with an orthogonal measurement. The probability of obtaining an inconclusive result is then:

$$p(\textit{inconclusive result}) = \cos\alpha. \tag{1.32}$$

In such a way the state can be identified with certainty at the cost of discard part of the data corresponding to the inconclusive results.

1.3 Entanglement

Quantum entanglement consists in a strong correlation between subsystems of the same physical system. It is a quantum non-local connection that characterizes the quantum mechanical state of a system containing two or more objects: the objects that make up the system are linked in a way such that one cannot adequately describe the quantum state of a constituent of the system without full mention of its counterparts, even if the individual objects are spatially separated. This interconnection leads to non-classical correlations between observable physical properties of remote systems, often referred to as nonlocal correlations. This feature cannot be produced by acting locally upon a single subsystem of the overall system [HKPS99].
Let us consider a bipartite system $\mathscr{H}_A \otimes \mathscr{H}_B$, in which $\{|i_A\rangle\}$ and $\{|j\rangle_B\}$ are orthonormal basis for systems A and B respectively; a generic state of $\mathscr{H}_{AB}$ can be written as:

$$|\psi\rangle_{AB} = \sum_{i,j} c_{ij}\,|i\rangle_A\,|j\rangle_B \tag{1.33}$$

where $\sum_{i,j}|c_{i,j}|^2 = 1$. If the state $|\psi\rangle_{AB}$ is a product state, it can be written in a convenient basis as:

$$|\psi\rangle_{AB} = |\phi\rangle_A|\xi\rangle_B = \left(\sum_i c_i^A |i\rangle_A\right)\left(\sum_j c_j^B |j\rangle_B\right) \tag{1.34}$$

in this case the state is separable. If $|\psi\rangle_{AB}$ is not separable, then it is entangled.
An entanglement criterion for pure states is the following. For a bipartite state $|\psi\rangle_{AB} \in \mathscr{H}_{AB}$ the Schmidt decomposition can be defined as:

$$|\psi\rangle_{AB} = \sum_i \sqrt{p_i}|i\rangle_A|i'\rangle_B \tag{1.35}$$

A bipartite state is entangled if the number of terms in the Schmidt decomposition, the Schmidt number n, is greater than 1, otherwise it is separable.
Given a bipartite mixed state $\mathscr{H} = \mathscr{H}_A \otimes \mathscr{H}_B$, the density matrix ρ represents a separable state if it can be written as:

$$\rho = \sum_i p_i \rho_i^A \otimes \rho_i^B \tag{1.36}$$

A necessary criterion for the separability is the Peres' one: if ρ is separable, the partial transpose must be positive: $\rho_A^T \geq 0$ [Per96]. This criterion becomes also sufficient in a $2 \otimes 2$ or $2 \otimes 3$ Hilbert space.
A particular example of entangled state is the one given by Werner states, whose density matrix can be written as:

$$\rho = \frac{1}{2}\mathbf{I} + \frac{1}{2}|\psi^-\rangle\langle\psi^-| \tag{1.37}$$

where $|\psi^-\rangle = \frac{|1\rangle|0\rangle - |0\rangle|1\rangle}{\sqrt{2}}$. The density matrix and its partial transpose are then:

$$\begin{pmatrix} \frac{1-p}{4} & 0 & 0 & 0 \\ 0 & \frac{1+p}{4} & -\frac{p}{2} & 0 \\ 0 & -\frac{p}{2} & \frac{1+p}{4} & 0 \\ 0 & 0 & 0 & \frac{1-p}{4} \end{pmatrix} \Rightarrow \begin{pmatrix} \frac{1-p}{4} & 0 & 0 & -\frac{p}{2} \\ 0 & \frac{1+p}{4} & 0 & 0 \\ 0 & 0 & \frac{1+p}{4} & 0 \\ -\frac{p}{2} & 0 & 0 & \frac{1-p}{4} \end{pmatrix} \tag{1.38}$$

The eigenvalues of the partial transpose are then: $\lambda = \{\frac{1+p}{4}, \frac{1+p}{4}, \frac{1+p}{4}, \frac{1+3p}{4}\}$, and the state is separable if $p \leq \frac{1}{3}$ or entangled if $p > \frac{1}{3}$.
Another example of entangled state is the singlet one:

$$|\psi^-\rangle_{AB} = \frac{1}{\sqrt{2}}(|0\rangle_A|1\rangle_B - |1\rangle_A|0\rangle_B) \tag{1.39}$$

the density matrix of the overall system is:

$$\rho_{\mathbf{AB}} = \begin{pmatrix} 0 & 0 & 0 & 0 \\ 0 & \frac{1}{2} & -\frac{1}{2} & 0 \\ 0 & -\frac{1}{2} & \frac{1}{2} & 0 \\ 0 & 0 & 0 & 0 \end{pmatrix} \tag{1.40}$$

where the correlation between A and B is expressed by the out of diagonal terms. If one looks only at one subsystem, it is found to be in a completely mixed, it turns out that the reduced density matrices for the subsystems A and B are:

$$\rho_{\mathbf{A}} = \rho_{\mathbf{B}} = \frac{\mathbf{I}}{2} \tag{1.41}$$

which represent the complete mixed states of the two subsystems. As said, it is then impossible to deduce the nature of the overall entangled state by looking at the state of the single subsystems alone.

1.4 Bell's inequalities

Bells theorem shows that there are limits which apply to local hidden-variable models of quantum systems, and quantum mechanics predicts that they will be exceeded by measurements performed on entangled pairs of particles. The predictions of quantum mechanics are consistent with the results of experiments, and turns out to be inconsistent with local hidden variable models of quantum mechanics. This can be shown by taking into account an entangled pair, as the one in equation (1.39), and tracing back the arguments of Clauser, Horne, Shimony and Holt against the Einstein Podolsky and Rosen paradox.
The structure of the state (1.39) implies that a measurement on the subsystem A determines univocally the state of subsystem B, even if they are non-interacting and spatially separated. Einstein Podolsky e Rosen (EPR) [EPR35] proposed to restore the reality principle by assuming the existance of local hidden variables (LHV) able to determine the result of the measurement before the measurement itself. Precisely, assuming the principles of di *reality*(if, without disturbing the system, we can predict with certainty the value of a given physical quantity, then there is an element of physical reality corresponding to it), *completeness* (each element of physical reality must have a counter-party into the physics theory) and *locality* (each action upon the system A cannot change the physical reality of a system B spatially separeted from A), EPR concluded that quantum mechanics was not complete. In order to confute the EPR argumentation, Bell demonstrated that an LHV-based theory couldn't reproduce the locality features of classical mechanics, by introducing a mathematical inequality satisfied by the correlations of the two subsystems. The Bell's inequality has been demonstrated in different schemes. The one proposed by Clauser, Horne, Shimony and Holt (CHSH) in 1969 is the following [CHSH69]. Let us consider the singlet state (1.39), and imagine it is composed by two $\frac{1}{2}$ spin particles moving along opposite directions towards different points, **A** and **B** respectively, in which a measurement of the spin along two different direction, $\overrightarrow{a}, \overrightarrow{a'}$ in **A**, and $\overrightarrow{b}, \overrightarrow{b'}$ in **B**, is performed. The possible results of the measurement in $A(\overrightarrow{a})$ and $B(\overrightarrow{b})$ can assume values $+1$ or -1. The hypothesis of locality implies that the result of the measurement **A** depends only on $\overrightarrow{a}$ and not on $\overrightarrow{b}$, conversely for **B**. Both the measurements, in the LHV

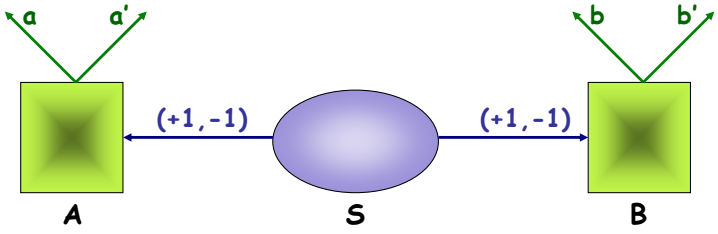

Figure 1.4: Apparatus for the measurement of Bell's inequality: **S** is the singlet state's source, the two particles are sent through the different apparata **A** and **B** which perform a dichotomic measurement, along two different directions.

model, depend from an ensemble of hidden variables λ such that $\int_\Gamma \rho(\lambda)d\lambda = 1$, with $\rho(\lambda)$ density probability and Γ hidden variable's space.

Let us introduce the correlation function $E(\vec{a},\vec{b})$ between the observables $A(\vec{a},\lambda)$ e $B(\vec{b},\lambda)$:

$$E(\vec{a},\vec{b}) = \left\langle A(\vec{a},\lambda)B(\vec{b},\lambda)\right\rangle = \int_\Gamma A(\vec{a},\lambda)B(\vec{b},\lambda)\rho(\lambda)d\lambda \tag{1.42}$$

Poichè $|A(\vec{a},\lambda)| = |B(\vec{b},\lambda)| = 1$ The following inequalities are satisfied:

$$\begin{aligned} |E(\vec{a},\vec{b}) - E(\vec{a},\vec{b'})| &\leq \int_\Gamma |B(\vec{b},\lambda) - B(\vec{b'},\lambda)|\rho(\lambda)d\lambda \\ |E(\vec{a'},\vec{b}) + E(\vec{a'},\vec{b'})| &\leq \int_\Gamma |B(\vec{b},\lambda) + B(\vec{b'},\lambda)|\rho(\lambda)d\lambda \end{aligned} \tag{1.43}$$

by summing the two terms and remembering that the observable B can assume only $+1$ or -1 values, the following relation is satisfied:

$$|E(\vec{a},\vec{b}) - E(\vec{a},\vec{b'})| + |E(\vec{a'},\vec{b}) + E(\vec{a'},\vec{b'})| \leq 2 \tag{1.44}$$

This relation provides a different prediction respect to the quantum mechanics' one: the singlet state violate the inequality 1.44.
The quantum correlation function is defined as:

$$E(\vec{a},\vec{b}) = \left\langle (\widehat{\sigma_1}\cdot\vec{a})\otimes(\widehat{\sigma_2}\cdot\vec{b})\right\rangle_{|\psi^-\rangle} \tag{1.45}$$

where $|\psi^-\rangle$ is the singlet state, $\widehat{\sigma_1} = (\sigma_{1x}, \sigma_{1y}, \sigma_{1z})$ and $\widehat{\sigma_2} = (\sigma_{2x}, \sigma_{2y}, \sigma_{2z})$ Pauli operators. Taking $\vec{a}$ coincident with the $\hat{z}$ axis and choosing $\vec{x}$ such that $\vec{b}$ is into the $\hat{xz}$ plane and makes an angle θ_{ab} with the direction of $\vec{a}$, the correlation function becomes:

$$E(\vec{a}, \vec{b}) = \left\langle \widehat{\sigma_{1z}} \otimes (\widehat{\sigma_{2z}} \cos\theta_{ab} + \widehat{\sigma_{2x}} \sin\theta_{ab}) \right\rangle \tag{1.46}$$

the calcolus of the correlation function upon the singlet state gives:

$$E(\vec{a}, \vec{b}) = -\cos(\theta_{ab}) \tag{1.47}$$

which can be rewritten into the Bell's inequality expression:

$$|E(\vec{a}, \vec{b}) - E(\vec{a}, \vec{b}') + E(\vec{a}', \vec{b}) + E(\vec{a}', \vec{b}')| \leq 2 \tag{1.48}$$

with $\vec{a}, \vec{a}', \vec{b}, \vec{b}'$ in the same plane $\vec{a} \equiv \hat{k}$, versor of $\hat{z}$, $\vec{a}' \equiv \hat{i}$, versor of $\hat{x}$, $\vec{b} \equiv \frac{\vec{k}+\vec{i}}{\sqrt{2}}$, $\vec{b}' \equiv \frac{\vec{k}-\vec{i}}{\sqrt{2}}$, we find:

$$|E(\vec{a}, \vec{b}) - E(\vec{a}, \vec{b}') + E(\vec{a}', \vec{b}) + E(\vec{a}', \vec{b}')| = 2\sqrt{2} \tag{1.49}$$

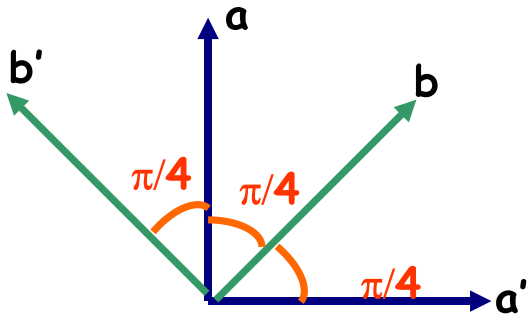

Figure 1.5: Choice of the directions along which measure the spin of the singlet state in order to observe a violation of Bell's inequality in the CHSH formulation.

In summary Bell's theorem establishes that no deterministic and local theory can reproduce the results of quantum mechanics.

1.5 Quantum Cloning

The impossibility of cloning perfectly every quantum state can be traced back to the work of Wooters and Zurek in 1982 [WZ82]. An immediate demonstration of the *no-cloning theorem* can be obtained in the following way: let us imagine to possess a perfect quantum cloning machine able to reproduce the two quantum states, encoded in the linear single photon polarization, $|H\rangle$ and $|V\rangle$:

$$|H\rangle|C\rangle \rightarrow |HH\rangle|C_H\rangle, \qquad |V\rangle|C\rangle \rightarrow |VV\rangle|C_V\rangle \tag{1.50}$$

$|C\rangle$ and $|C_i\rangle$ $(i = H,V)$ are the cloning machine's states before and after cloning process respectively.The circular polarization states $|L\rangle = \frac{|H\rangle - i|V\rangle}{\sqrt{2}}$ and $|R\rangle = \frac{|H\rangle + i|V\rangle}{\sqrt{2}}$ will then be transformed into:

$$\begin{aligned} |L\rangle|C\rangle &\rightarrow \frac{1}{\sqrt{2}}(|HH\rangle|C_H\rangle - i|VV\rangle|C_V\rangle) \neq |LL\rangle|C_L\rangle \\ |R\rangle|C\rangle &\rightarrow \frac{1}{\sqrt{2}}(|HH\rangle|C_H\rangle + i|VV\rangle|C_V\rangle) \neq |RR\rangle|C_R\rangle \end{aligned} \tag{1.51}$$

The previous relations (1.51) show the impossibility of building an universal quantum cloning machine, due to the linearity of quantum mechanics. Nevertheless, in order to reproduce a copy characterized by the maximum overlap with a given quantum state, an *optimal* cloning can be performed [BcvH96].

1.5.1 Optimal Universal Cloning

Let us consider the qubit $|\psi\rangle = \alpha|0\rangle + \beta|1\rangle$, and imagine we are able to operate upon an auxiliary system (the cloning machine) in order to produce two clones of the same state with the same fidelity; if this process is independent from the initial state, it is called *universal cloning*.
If the cloning machine was initially in the state $|C\rangle$, then:

$$|0\rangle|C\rangle \rightarrow |\Sigma_0\rangle, \qquad |1\rangle|C\rangle \rightarrow |\Sigma_1\rangle \tag{1.52}$$

with $|\Sigma_0\rangle$ and $|\Sigma_1\rangle$ final states of the system, defined in the Hilbert space $\mathscr{H}_A \otimes \mathscr{H}_B \otimes \mathscr{H}_C$, where $\mathscr{H}_A$ and $\mathscr{H}_B$ refer to the space of the two clones A and B.

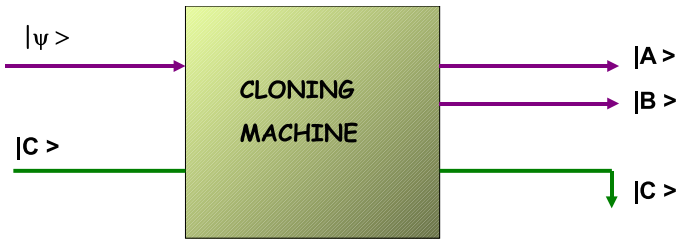

Figure 1.6: Universal cloning machine: the state $|\psi\rangle$ is reproduced into the states $|A\rangle$ and $|B\rangle$, the ancilla is represented by the cloning machine in the state $|C\rangle$

Due to linearity:

$$|\psi\rangle|C\rangle \rightarrow \alpha|\Sigma_0\rangle + \beta|\Sigma_1\rangle \equiv |\Sigma\rangle. \tag{1.53}$$

The fidelity of clones, which measures the superposition between the input state and the clone, is given by:

$$\mathscr{F}_A(\psi) = \langle\psi|Tr_{BC}(\Sigma)|\psi\rangle, \qquad \mathscr{F}_B(\psi) = \langle\psi|Tr_{AC}(\Sigma)|\psi\rangle \tag{1.54}$$

It can be demonstrated that if $\mathscr{F}_A(\psi) = \mathscr{F}_B(\psi)$ are independent of ψ [BcvH96], then the quantum mechanics allows the existence of a cloning transformation able to obtain a fidelity equal to:

$$\mathscr{F}^{univ} = \frac{5}{6} \simeq 0.833 \tag{1.55}$$

for which the following relations hold:

$$\begin{aligned} |0\rangle|C\rangle &\rightarrow |\Sigma_0\rangle \equiv \sqrt{\frac{2}{3}}|00\rangle_{AB}|0\rangle_C + \sqrt{\frac{1}{3}}|\psi^+\rangle_{AB}|1\rangle_C, \\ |1\rangle|C\rangle &\rightarrow |\Sigma_1\rangle \equiv \sqrt{\frac{2}{3}}|11\rangle_{AB}|1\rangle_C + \sqrt{\frac{1}{3}}|\psi^+\rangle_{AB}|0\rangle_C \end{aligned} \tag{1.56}$$

where $|\psi^+\rangle = \frac{|01\rangle+|10\rangle}{\sqrt{2}}$. By tracing out the degrees of freedom of C, we found that the states A,B remain in the joint state:

$$\rho_{AB} = Tr_C(\Sigma) = \frac{2}{3}|00\rangle\langle 00| + \frac{1}{3}|\psi^+\rangle\langle\psi^+| \tag{1.57}$$

Tracing out one of the two clones state:

$$\rho_A = Tr_{BC}(\Sigma) = \frac{2}{3}|\psi\rangle\langle\psi| + \frac{1}{6}I, \qquad \rho_B = Tr_{AC}(\Sigma) = \frac{2}{3}|\psi\rangle\langle\psi| + \frac{1}{6}I \tag{1.58}$$

where I is the identity operator. From the relations (1.58), we note that the two clones are in the same state , and with probability $\frac{2}{3}$ are in the state $|\psi\rangle$, while with probability

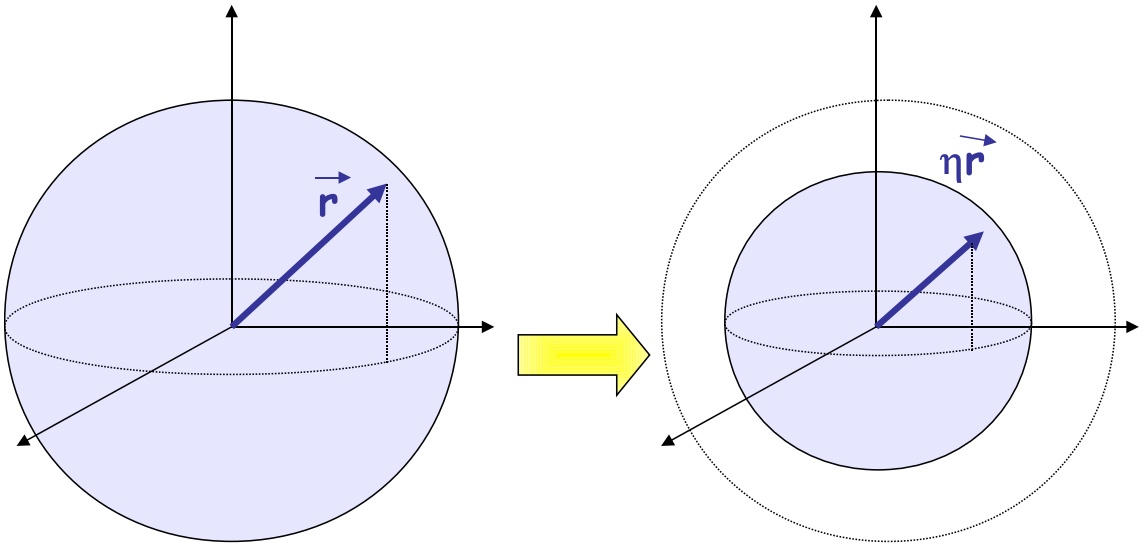

Figure 1.7: Cloning transformation reduces the state's purity: the ray of the Bloch sphere is reduced by the shrinking factor η.

$\frac{1}{3}$ are in a complete mixed state $I/2$. This transformation can be represented graphically through the Bloch sphere: the density matrix for a qubit can be written as in equation (1.19): with $|\overrightarrow{r}| = 1$ for pure states. The depolarizing effect of the cloning process can be thought as a reduction of vector $\overrightarrow{r}$ for a factor η, said shrinking factor, and the density matrix of the output state reads:

$$\rho'(\mathbf{r}) = \frac{1}{2}(1 + \eta\,\overrightarrow{r}\cdot\overrightarrow{\sigma}) \tag{1.59}$$

η and the Fidelity of the cloning process are linked by the relation:

$$\mathscr{F} = \frac{1+\eta}{2}. \tag{1.60}$$

1.5.2 Universal cloning N → M

Gisin and Massar [GM97] in 1997 introduced the concept of $N \to M$ cloning machine, able to transform N identical copy of an arbitrary state $|\psi\rangle^{\otimes N}$ into $M > N$ identical clones. This process can be realized with a fidelity equal to:

$$\mathscr{F}^{univ}_{N\to M} = \frac{M(N+1)+N}{M(N+2)} = \frac{(N+1)+N/M}{N+2} \tag{1.61}$$

When fixed N the number of clones increases, since the information has to be shared between a greater number of partners, the Fidelity decreases. In the limit $M \to \infty$ the cloning transformation approaches the fidelity of the perfect measurement over N identical qubits in the state $|\psi\rangle^{\otimes N}$ [MP95]:

$$\mathscr{F}^{univ}_{N\to\infty} = \frac{N+1}{N+2} \tag{1.62}$$

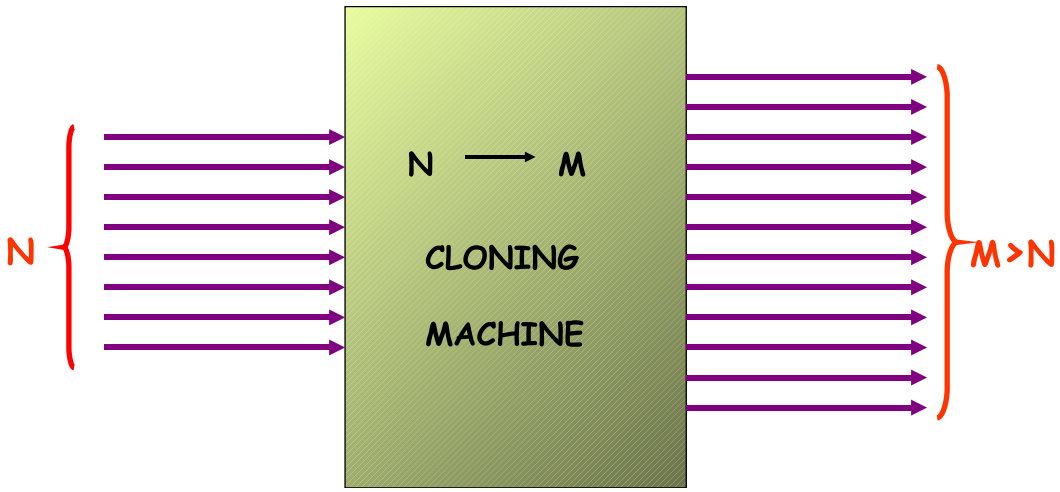

Figure 1.8: Universal quantum cloning machine $N \to M$

1.5.3 Phase-covariant cloning

If we restrict our attention to a particular class of states, for instance the one that lay on the equatorial plane of the Bloch states:

$$|\phi\rangle = \frac{|0\rangle + e^{i\phi}|1\rangle}{\sqrt{2}} \tag{1.63}$$

we obtain a value of the Fidelity greater respect to the universal cloning case.This is indeed the case of the *phase covariant cloning* process. The Fidelity results to be independent of the phase ϕ of the input qubit, and it has been demonstrated that its optimal value in the $N \to M$ case is [Fen02]:

$$\mathscr{F}^{pc}_{N\to M} = \frac{1}{2} + \frac{1}{M2^N}\sum_{j=0}^{N-1}\sqrt{\binom{N}{j}\binom{N}{j+1}}\sqrt{(N+L-j)(L+j+1)} \tag{1.64}$$

in the limit $1 \to \infty$ the cloning precess is equivalent to the state estimation, whose Fidelity is: $\mathscr{F}^{pc}_{N=1\to\infty} = \mathscr{F}^{est}_{N=1} = \frac{3}{4}$.

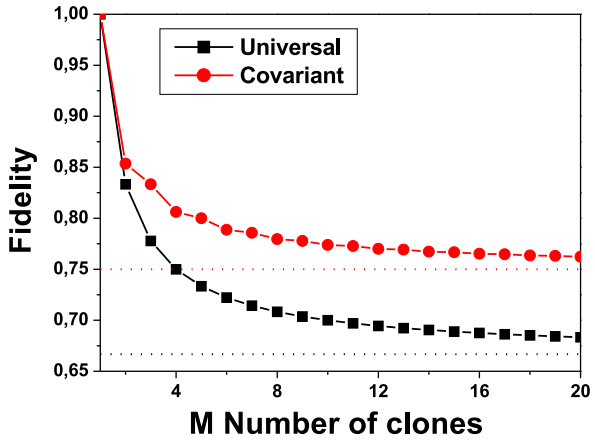

Figure 1.9: Trend of Fidelity as a function of the number M of clones in the universal and the phase covariant schemes.

In figure 1.9 a comparison between the trends of fidelity as a function of the number of clones, in the phase covariant and universal schemes, is reported. We see that the fidelity value in the phase covariant case results to be higher than the universal one for each number of reproduced clones. This is due to the deeper knowledge about the state to be cloned, which spans only the equatorial plane of the Block sphere and not the overall sphere itself, which characterize the phase covariant cloning process respect to the complete uncertainty about the state in a universal scheme.

Chapter 2

Theory of the Optical Parametric Amplifier

The optical implementation of a qubit exploits the resources of both linear and non-linear optics. In this chapter we will show that quantum cloning can be implemented by the optical process of parametric down conversion.
We will address the concept of spontaneous-parametric-down-conversion (SPDC) in the context of non-linear optics, and the optical parametric amplifier, in both the collinear and non collinear configuration, will be characterized. The case of single photon amplification through a phase covariant amplifier will be then investigated in a more detail.

2.1 Elements of non-linear optics

The presence of radiation into an optical system can produce different changes inside the material, for instance in the index of refraction due to the electro-optic effect, or produce a variation in the radiation itself, as it happens in the *sum* and *difference-frequency generation* phenomena [Boy]. The interaction between the radiation and the system produce "non linear" phenomena, since the response of the material depends quadratically on the electromagnetic field.
In the linear case, the medium polarization $P(t)$ is a function of the applied electric field $E(t)$:

$$P(t) = \chi^{(1)} E(t) \tag{2.1}$$

where $\chi^{(1)}$ is the linear suscettivity.
In non-linear optics the response of the medium is expressed through a generalization of equation (2.1):

$$P(t) = \chi^{(1)} E(t) + \chi^{(2)} E^2(t) + \chi^{(3)} E^3(t) \tag{2.2}$$

where $\chi^{(2)}$ and $\chi^{(3)}$ are the optical suscettivity at the send and third order respectively.
The response of the medium can be considered instantaneous if the medium is not disper-

sive and without losses, in this case the suscettivity is independent of the applied electric field's frequency.
Sum and Difference-Frequency Generation (SFG) and (DFG) are examples of non linear second order processes, which happen in a non-centrosymmetric and non linear material, when a two-frequency (ω_1 and ω_2) incident field impinges on it:

$$E(t) = E_1 \exp(-i\omega_1 t) + E_2 \exp(-i\omega_2 t) + c.c. \tag{2.3}$$

by considering only the second order term in equation (2.2), we obtain the expression of the second order polarization:

$$P^{(2)}(t) = \sum_n P(\omega_n) \exp(-i\omega_n t) \tag{2.4}$$

where the sum over n is extended to negative and positive frequencies, and the amplitudes of different frequency components describe different physical phenomena: Sum-Frequency-Generation(SFG), Difference-Frequency-Generation (DFG), Second-Harmonic-Generation (SHG) (which is obtained when a radiation with frequency ω_i is converted into the second harmonic frequency $2\omega_i$ (with $i = 1,2$) radiation) , and Optical-Rectification (OR):

$$\begin{aligned} P(2\omega_1) &= \chi^{(2)} E_1^2(t)\ (SHG) \\ P(2\omega_2) &= \chi^{(2)} E_2^2(t)\ (SHG) \\ P(\omega_1+\omega_2) &= 2\chi^{(2)} E_1(t)E_2(t)\ (SFG) \\ P(\omega_1-\omega_2) &= 2\chi^{(2)} E_1(t)E_2^*(t)\ (DFG) \\ P(0) &= 2\chi^{(2)}(E_1E_1^* + E_2E_2^*)\ (OR) \end{aligned} \tag{2.5}$$

Generally no more than one frequency component is present in the radiation after the interaction with the material, since each of the process described in equation (2.5) requires a different phase matching condition.
The difference between the processes of SFG e DFG is highlighted in figure 2.1:
in the SFG process two input photons at frequency ω_1 and ω_2 are annihilated and a photon at a greater frequency ω_3 is generated.
In DFG case for the energy conservation to generate a photon at frequency ω_3, a photon at greater frequency ω_1 must be destroyed and a photon at lower frequency ω_2 has to be created.The DFG process amplifies the input field at the lowest frequency, for this reason it is also known as parametric amplifier.
According to the energy levels scheme, the DFG process can be described as follows: first an atom absorbs a photon at frequency ω_1 and jumps up to a virtual energy level which decays emitting two photons; this process is stimulated by the presence of the input field at frequency ω_2. Nevertheless the two-photon emission can happen even in absence of

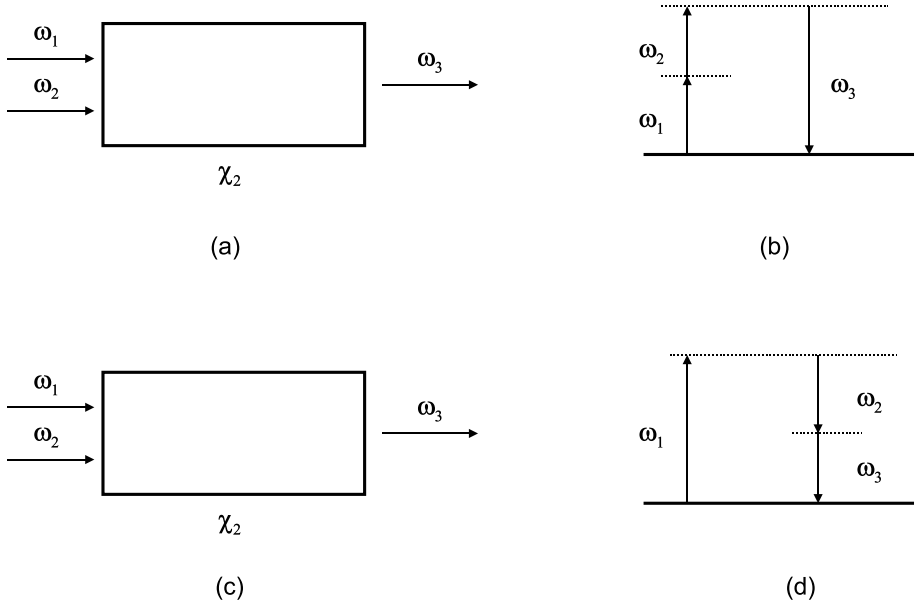

Figure 2.1: (a) Geometry of the SFG interaction. (b) Description of energy levels for SFG. (c) Geometry o9f the DFG interaction. (d) Description of energy levels for DFG.

the ω_2 field: in this case we have *parametric fluorescence*, and the process cannot be explained classically but through the use of quantum optics.

2.2 Parametric Fluorescence

The parametric fluorescence phenomenon cannot be explained by classical theory but it is well described by quantum theory. As said, spontaneous parametric down conversion (SPDC) or parametric fluorescence is the nonlinear process whereby two photons (called idler and signal) are created from a parent photon (called the pump photon).
The interaction Hamiltonian between the radiation and the crystal reads:

$$H = \frac{1}{2}\int_V d^3r \overrightarrow{P}\cdot\overrightarrow{E} = \int_V d^3r(\chi^{(1)}_{ij}E_jE_i + \chi^{(2)}_{ijk}E_jE_kE_i) \tag{2.6}$$

If the pump field is intense, such as the one of the laser, it can be treated classically, while the field at frequency ω_1 and ω_2, called *signal* e *idler*, are quantized:

$$E_p = \varepsilon_p \int dk_p \exp(-4\log 2\frac{[\omega_p(k_p)-\Omega_p]^2}{\sigma_p^2})\exp[k_pz-\omega_p(k_p)t] \tag{2.7}$$

$$\widehat{E}^{(-)}_j = i\int dk_j \sqrt{\frac{\hbar_j\omega_j}{2\varepsilon_0 n^2(k_j)V}}\widehat{a}^{\dagger}_{\overrightarrow{k_j}}\exp(-i[k_{jz}z+\overrightarrow{k_{j\perp}}\cdot\overrightarrow{r_\perp}-\omega_j(k_j)t]) \tag{2.8}$$

where $j = s,i$, and $\widehat{a}^{\dagger}_j$ is the creation operator on spatial mode k_j. The interaction Hamiltonian can then be written as:

$$\widehat{H} = C\int dk_p\int dk_s\int dk_i \exp^{(-4\log 2\frac{[\omega_p(k_p)-\Omega_p]^2}{\sigma_p^2})}\exp^{i(\omega_s+\omega_i-\omega_p)}\int_0^L dz\times$$
$$\times\exp^{i[k_p-k_{sz}-k_{iz}]z}\int_A d^2r_\perp \exp^{-i[\overrightarrow{k_{\perp i}}+\overrightarrow{k_{\perp s}}]\cdot\overrightarrow{r_\perp}}\widehat{a}^{\dagger}_{\overrightarrow{k_s}}\widehat{a}^{\dagger}_{\overrightarrow{k_i}} + h.c. \tag{2.9}$$

where C is a constant and L is the length of the crystal. The area A of the crossed transverse section can be considered infinite, since the transverse dimensions of the pump field are order of magnitude greater than the radiation wavelength. The integral in dr becomes then a $\delta(\overrightarrow{k_p}-\overrightarrow{k_s}-\overrightarrow{k_i})$ function, responsible for one of the two phase-matching conditions of the fluorescence process.
Since the second order interaction are considered to be weak, the exponential operator of the temporal evolution can be approximated with it's first order expression:

$$\widehat{U}(t) = \exp\left(-\frac{i}{\hbar}\int_{-\infty}^{+\infty}dt\widehat{H}(t)\right) \simeq \mathbf{I} - \frac{i}{\hbar}\int_{-\infty}^{+\infty}dt\widehat{H}(t) \tag{2.10}$$

The dt integral in equation (2.9) gives then the second energy conservation condition: $\delta(\omega_p-\omega_i-\omega_s)$. The two phase matching conditions express the necessity of conserving both the energy and the momentum between the three fields:

$$\begin{aligned}\omega_p &= \omega_s+\omega_i\\ \overrightarrow{k_p} &= \overrightarrow{k_i}+\overrightarrow{k_s}\end{aligned}$$

If $\omega_i = \omega_s = \frac{1}{2}\omega_p$ we talk about *degenerate emission* in frequency.
If the beams involved in the interaction are collinear, the condition of momentum conservation can be written as:

$$\frac{n_p\omega_p}{c} = \frac{n_s\omega_s}{c} + \frac{n_i\omega_i}{c} \tag{2.11}$$

this condition cannot be realized in linear crystals due to the normal dispersion phenomenon, for which the index of refraction increases monotonically with the radiation frequency. The use of anomalous dispersion regions makes the phase matching condition difficult to realize, due to the extreme variability of the index of refraction.
A better solution consists in using birefringent crystals, in which the index of refraction depends on the polarization of the impinging beam: an incident beam which makes an angle θ with the optical axis of the crystal experiences an index of refraction equal to:

$$\frac{1}{n_e(\theta)^2} = \frac{\sin^2\theta}{n_o^2} + \frac{\cos^2\theta}{n_e^2}$$

where n_e and n_o are the index of refraction extraordinary and ordinary seen by the radiation propagating towards the directions of the two optical axes.
For uniaxial crystals $n_e < n_o$, it's then more convenient to choose a pump beam at greater frequency with extraordinary polarization, in this case signal and idler can have both the same polarization o (type I phase matching) or orthogonal polarizations (type II phase matching). In the first case the fluorescence is emitted over an ensemble of concentric circumferences, each of which is given by photons with the same wavelength, the correlated photons (signal and idler) are in the diametrically opposite directions and on different circumferences if $\lambda_i \neq \lambda_s$.
In type II phase matching case the photons are emitted over two non-coaxial cones, whose vertex is in the generation point of the parametric fluorescence inside the crystal and the aperture depends on the frequency (as shown in figure 2.2). One of the two cones contains photons with extraordinary polarization, the other the ones with ordinary polarization. If the emission is degenerate the two cones have the same aperture. The intersection between them depends on the inclination of the pump beam respect to the optical axis of the crystal, and is responsible for the generation of entangled photons.

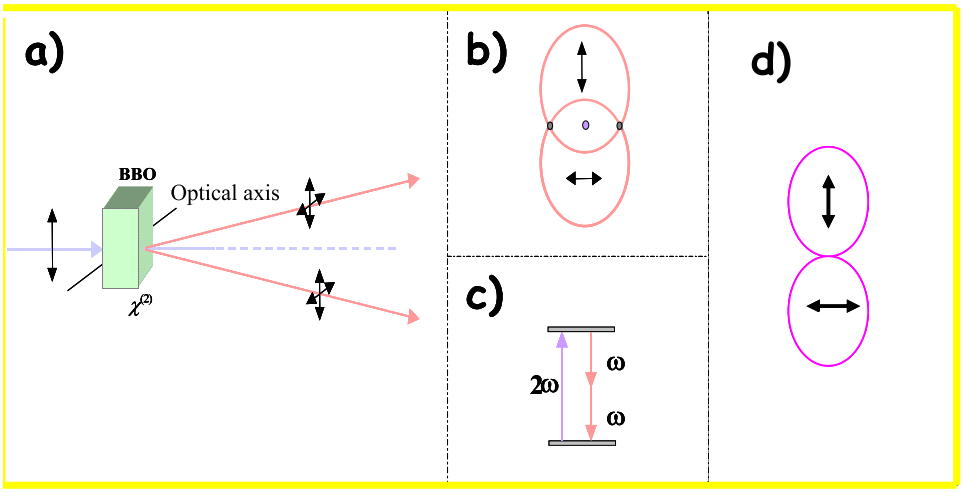

Figure 2.2: (a) Intersection between the ordinary and extraordinary cones. (b) Orthogonal polarizations of the generated beams. (c) Energy levels scheme in the degenerate fluorescence case, (d) Collinear case: entangled photons are generated over the same spatial mode.

2.3 The Optical Parametric Amplifier

The interaction between a radiation field at frequency ω_p and a crystal with second order non-linear suscettivity in order to generate field at frequencies ω_1 and ω_2 such that $\omega_1 + \omega_2 = \omega_p$ can be exploited by the optical parametric amplifier (OPA).
If the radiation fields have the same frequencies $2\omega = \omega_p$ and are generated over the same spatial mode the optical parametric amplifier is degenerate, if on the contrary the generated fields are different in frequency or in spatial mode, the amplifier is non degenerate [WM94].

2.3.1 Degenerate amplifier

In a degenerate parametric amplifier the signal at frequency ω is amplified through the excitation of a crystal characterized by $\chi^{(2)} \neq 0$ with a beam at frequency 2ω. We consider the intense beam at frequency 2ω classically, while the one at frequency ω within the quantum theory, through the creation and destruction operator $\hat{a}^\dagger$ and $\hat{a}$.
The interaction Hamiltonian reads:

$$\hat{H} = \hbar\omega\hat{a}^\dagger\hat{a} - i\hbar\frac{\chi}{2}(\hat{a}^2 e^{2i\omega t} - \hat{a}^{\dagger\,2} e^{-2i\omega t}) \tag{2.12}$$

where χ is proportional to the non linear suscettivity and to the pump beam's amplitude.
In the interaction picture we can write:

$$\hat{H}_I = -i\hbar\frac{\chi}{2}(\hat{a}^2 - \hat{a}^{\dagger\,2}) \tag{2.13}$$

and the Heisenberg motion equations are:

$$\begin{aligned} \frac{d\widehat{a}}{dt} &= \frac{1}{i\hbar}\left[\widehat{a},\widehat{H}_I\right] = \chi\widehat{a}^\dagger \\ \frac{d\widehat{a}^\dagger}{dt} &= \frac{1}{i\hbar}\left[\widehat{a}^\dagger,\widehat{H}_I\right] = \chi\widehat{a} \end{aligned} \tag{2.14}$$

These equations have the following solution:

$$\widehat{a}(t) = \widehat{a}(0)\cosh(\chi t) + \widehat{a}^\dagger(0)\sinh(\chi t) \tag{2.15}$$

The expression of the destruction operator's solution reminds to the one of squeezing generator, the light produced by the parametric amplifier will then be squeezed. This can be verified by introducing the quadratures operator, and looking at their time evolution:

$$\begin{aligned} \widehat{X}_1 &= \widehat{a}+\widehat{a}^\dagger \\ \widehat{X}_2 &= \frac{\widehat{a}-\widehat{a}^\dagger}{i} \end{aligned} \tag{2.16}$$

The equation which describe the quadratures' motion are:

$$\begin{aligned} \frac{d\widehat{X}_1}{dt} &= \chi\widehat{X}_1 \\ \frac{d\widehat{X}_2}{dt} &= -\chi\widehat{X}_2 \end{aligned} \tag{2.17}$$

These equations demonstrate that the parametric amplifier is phase sensitive, since a quadrature is amplified while the other is attenuated:

$$\begin{aligned} \widehat{X}_1(t) &= e^{\chi t}\widehat{X}_1(0) \\ \widehat{X}_2(t) &= e^{-\chi t}\widehat{X}_2(0) \end{aligned} \tag{2.18}$$

the temporal evolution operator $\widehat{U} = e^{-i\widehat{H}_I t/\hbar}$ coincides with the squeezing operator, furthermore the mean number of generated photons, obtained with the injection of vacuum state is:

$$\langle\widehat{n}\rangle = \langle\widehat{a}^\dagger(t)\widehat{a}(t)\rangle = \sinh(g)^2 \tag{2.19}$$

with $g = \chi t$ gain of the amplifier. The expression (2.19) correspond to the mean number of photons in the squeezed vacuum.

2.3.2 Non degenerate amplifier

In the non degenerate amplifier case, the classical field at frequency 2ω interacts with a non linear medium and generates two fields at frequency ω_1 and ω_2, such that $\omega_1 + \omega_2 = 2\omega$ over two spatial modes $\overrightarrow{k_1}$ and $\overrightarrow{k_2}$ called signal and idler.
The Hamiltonian of the system reads:

$$\widehat{H} = \hbar\omega_1 \widehat{a}_1^\dagger \widehat{a}_1 + \hbar\omega_2 \widehat{a}_2^\dagger \widehat{a}_2 + i\chi\hbar(\widehat{a}_1^\dagger \widehat{a}_2^\dagger e^{-2i\omega t} - \widehat{a}_1 \widehat{a}_2 e^{2i\omega t}) \tag{2.20}$$

where $\widehat{a}_1$ and $\widehat{a}_2$ are the annihilation operator for signal and idler. The motion equations in the interacting picture are:

$$\begin{aligned} \frac{d\widehat{a}_1}{dt} &= \chi \widehat{a}_2^\dagger \\ \frac{d\widehat{a}_2^\dagger}{dt} &= \chi \widehat{a}_1 \end{aligned} \tag{2.21}$$

and the solutions are:

$$\begin{aligned} \widehat{a}_1(t) &= \widehat{a}_1 \cosh(\chi t) + \widehat{a}_2^\dagger \sinh(\chi t) \\ \widehat{a}_2(t) &= \widehat{a}_2 \cosh(\chi t) + \widehat{a}_1^\dagger \sinh(\chi t) \end{aligned} \tag{2.22}$$

the number of generated photons is given by: $\langle \widehat{n_1} \rangle = \langle \widehat{n_2} \rangle = \sinh(g)^2$.

2.4 Correlation functions

The classical optics interferometric experiments correspond to a measurement of the first order correlation function of the radiation field [Lou00]. Given two fields temporally separated for a time interval τ, a first order correlation function $g^{(1)}(\tau)$ can be defined as:

$$g^{(1)}(\tau) = \frac{\langle E^*(t)E(t+\tau)\rangle}{\langle E^*(t)E(t)\rangle} \tag{2.23}$$

this coherence value gives an extimation of the fringe pattern visibility $\mathscr{V}$:

$$\mathscr{V} = |g^{(1)}(\tau)| \quad 0 \leq |g^1(\tau)| \leq 1 \tag{2.24}$$

then completely coherent light, such as the laser one, has $g^{(1)}(\tau) = 1$, while for chaotic light $g^{(1)}(\tau) \to 0$ as τ increases.
In terms of quantized fields $g^{(1)}$ refers to the estimation of the average number of photons contained in the radiation:

$$g^{(1)}(\tau) \quad \Leftrightarrow \quad <\widehat{n}> = <\widehat{a}^\dagger \widehat{a}> \tag{2.25}$$

a first order coherence measurement of the radiation field coincides then with the extimation of the mean number of photons.
The study of second order correlation functions allows to distinguish between quantum and classical fields, which cannot be discriminated between a measurement of first order correlation one.
The second order correlation function is defined as:

$$g^{(2)}(\tau) = \frac{\langle E^*(t)E^*(t+\tau)E(t+\tau)E(t)\rangle}{\langle E^*(t)E(t)\rangle \langle E^*(t+\tau)E(t+\tau)\rangle} \tag{2.26}$$

in terms of quantized fields it reads:

$$g^{(2)}(\tau) = \frac{\langle \widehat{a}^\dagger \widehat{a}^\dagger \widehat{a}\widehat{a}\rangle}{\langle \widehat{a}^\dagger \widehat{a}\rangle^2} = \frac{\langle \widehat{n}(\widehat{n}-1)\rangle}{\langle \widehat{n}\rangle^2} \tag{2.27}$$

for number state:

$$g^{(2)}(\tau) = \begin{cases} (n-1)/n & se\ \ n \geq 2 \\ 0 & se\ \ n = 0 \end{cases} \tag{2.28}$$

it is worth noting that, while for classical light $1 \leq g^{(2)}(\tau) \leq \infty$, for quantum light $0 \leq g^{(2)}(\tau) \leq \infty$.

Another interesting physical quantity is the two modes correlation function, which can be addressed by analyzing the two different modes 1 and 2 at the exit of the amplifier:

$$g^{(2)}_{12}(\tau) = \frac{\langle \widehat{a}_1^\dagger \widehat{a}_2^\dagger \widehat{a}_2 \widehat{a}_1\rangle}{\langle \widehat{a}_1^\dagger \widehat{a}_1\rangle \langle \widehat{a}_2^\dagger \widehat{a}_2\rangle} \tag{2.29}$$

generally the mixed correlation function follows the Cauchy-Schwartz inequality:

$$\left[g^{(2)}_{12}(0)\right] \leq g^{(2)}_1(0) g^{(2)}_2(0) \tag{2.30}$$

in the quantum case a more strict inequality holds [WM94], which implies a greater correlation between the two spatial modes:

$$g^{(2)}_{12}(0) \leq g^{(2)}_1 + \frac{1}{\langle \widehat{a}_1^\dagger \widehat{a}_1\rangle} \tag{2.31}$$

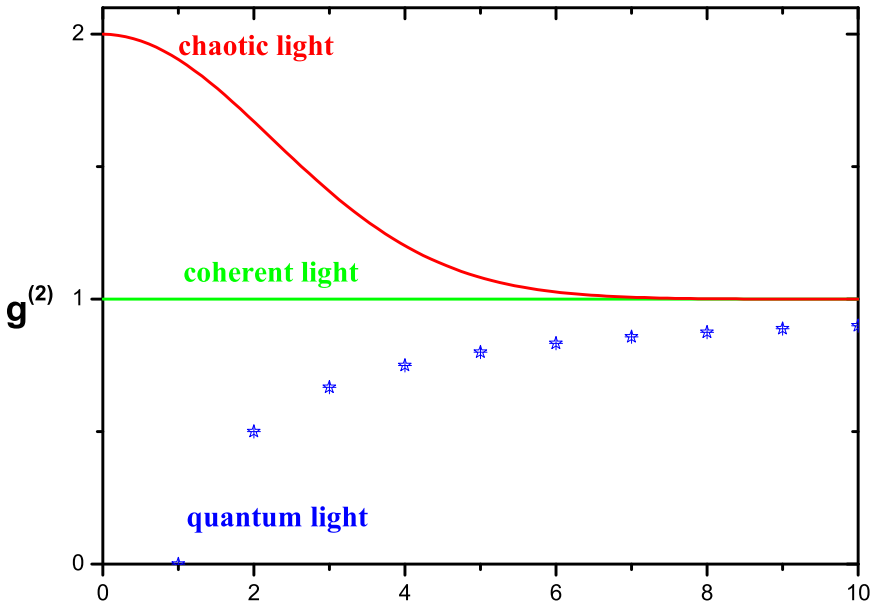

Figure 2.3: Second order correlation function for different light types: for number states $0 \leq g^{(2)} \leq 1$, which is a range forbidden to classical light, for increasing n number states behavior approaches to the coherent light one.

2.5 Phase Covariant parametric amplifier

Let us consider the experimental implementation of the collinear optical parametric amplifier, in which the output fields are on the same spatial mode $\overrightarrow{k}$ [De 98b].
The interaction Hamiltonian reads:

$$\mathscr{H}_{coll} = i\hbar\chi(\hat{a}_H^\dagger \hat{a}_V^\dagger) + h.c \tag{2.32}$$

where $\hat{a}_i^\dagger$, is the creation operator on mode $\overrightarrow{k}$ with polarization i, being $i = H,V$. The collinear Hamiltonian (2.32) has the property of invariance respect to $U(1)$ group, this allows to write it as a function of an equatorial polarization basis $\{\overrightarrow{\pi}, \overrightarrow{\pi^\perp}\}$:

$$\begin{aligned} \hat{a}_\pi^\dagger &= \frac{\hat{a}_H + e^{i\phi}\hat{a}_V}{\sqrt{2}} \\ \hat{a}_{\pi^\perp}^\dagger &= \frac{\hat{a}_H - e^{-i\phi}\hat{a}_V}{\sqrt{2}} \end{aligned} \tag{2.33}$$

as:

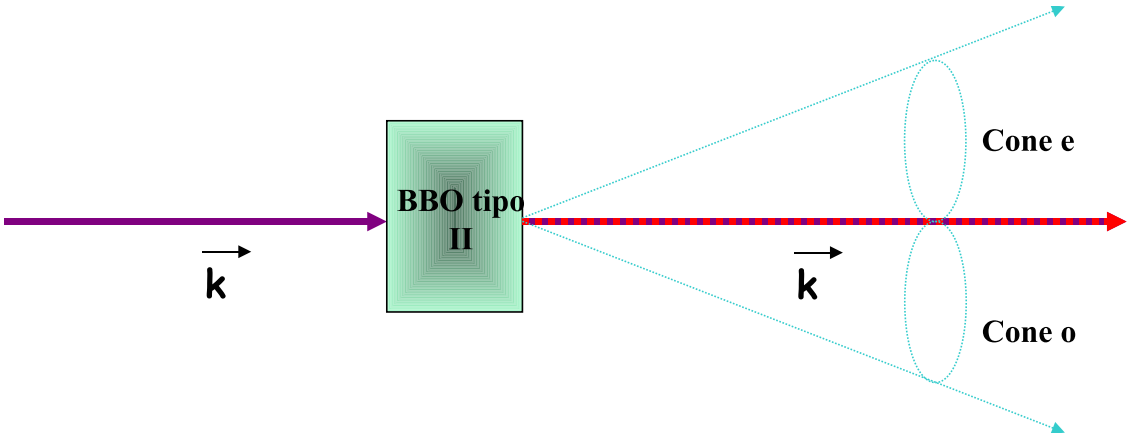

Figure 2.4: Degenerate optical parametric amplifier in collinear configuration: the pump beam on mode k at frequency 2ω interacts with a non linear crystal, cut for type II phase matching, and generates two fields at frequency ω, both on the same spatial mode k.

$$\mathscr{H}_{coll} = \frac{i\chi\hbar}{2} e^{-i\phi}((\hat{a}_{\pi}^{\dagger})^2 - e^{2i\phi}(\hat{a}_{\pi_\perp}^{\dagger})^2) + h.c. \tag{2.34}$$

this Hamiltonian can then be written as a sum of two independent amplifiers:

$$\mathscr{H}_{coll} = \mathscr{H}_{\pi} + \mathscr{H}_{\pi^\perp} \tag{2.35}$$

belonging to different polarization modes. This property is verified by each state belonging to the equatorial polarization plane of the Bolch sphere.
The operators evolution follows the Heisenberg relation:

$$i\hbar\frac{d\hat{a}_{\pi}}{dt} = [\hat{a}_{\pi}, \mathscr{H}_I] \tag{2.36}$$

the particular case in which the polarization basis is the 45° linear one, spanned by vectors $\overrightarrow{\pi}_+$ and $\overrightarrow{\pi}_-$ we have:

$$\begin{aligned} \hat{a}_+(t) &= \hat{a}_+(0)\cosh\chi t + \overrightarrow{a}_+^{\dagger}(0)\sinh\chi t \\ \hat{a}_-(t) &= \hat{a}_-(0)\cosh\chi t + \hat{a}_-^{\dagger}(0)\sinh\chi t \end{aligned} \tag{2.37}$$

The temporal evolution operator can be written as:

$$\hat{U} = \hat{U}_+\hat{U}_-, \quad con \quad \hat{U}_{\pm} = \exp\left(g\left(\left(\frac{\hat{a}_{\pm}^{\dagger}}{\sqrt{2}}\right)^2 - \left(\frac{\hat{a}_{\pm}}{\sqrt{2}}\right)^2\right)\right) \tag{2.38}$$

and by using the *disentangling theorem* we can write:

$$\widehat{U}_{\pm} = \exp\left[\pm\Gamma\left(\frac{\widehat{a}_{\pm}^{\dagger}}{\sqrt{2}}\right)^2\right]\exp\left[-\ln(\cosh(g))\left(\widehat{a}_{\pm}^{\dagger}\widehat{a}_{\pm}+1/2\right)\right]\exp\left[\pm\Gamma\left(\frac{\widehat{a}_{\pm}}{\sqrt{2}}\right)^2\right] \tag{2.39}$$

with $\Gamma = \tanh g$.

2.5.1 Single-photon amplification

When a quantum state is injected into the amplifier, we deal with *quantum injected optical parametric amplifier* (QIOPA).
In this work we are interested into the *phase covariant* cloning case, in which the injected state is an equatorial qubit:

$$|\phi\rangle_{in} = \frac{1}{\sqrt{2}}\left(|H\rangle + e^{i\phi}|V\rangle\right) = e^{i\phi/2}\left(\cos(\frac{\phi}{2})|1+,0-\rangle + i\sin(\frac{\phi}{2})|0+,1-\rangle\right) \tag{2.40}$$

the state will evolve according to equation (2.38) as:

$$|\Phi\rangle_{out} = \cos(\frac{\phi}{2})|\Phi^+\rangle_{out} + i\sin(\frac{\phi}{2})|\Phi^-\rangle_{out} \tag{2.41}$$

where:

$$|\Phi^+\rangle_{out} = \widehat{U}_+\widehat{U}_-|1+,0-\rangle = \frac{1}{\cosh^2 g}\sum_{ij}\left(\frac{-\Gamma}{2}\right)^j\left(\frac{\Gamma}{2}\right)^i\frac{\sqrt{(2j)!}}{j!}\frac{\sqrt{(2i+1)!}}{i!}|(2i+1)+,(2j)-\rangle \tag{2.42}$$

$$|\Phi^-\rangle_{out} = \widehat{U}_+\widehat{U}_-|0+,1-\rangle = \frac{1}{\cosh^2 g}\sum_{ij}\left(\frac{-\Gamma}{2}\right)^j\left(\frac{\Gamma}{2}\right)^i\frac{\sqrt{(2i)!}}{i!}\frac{\sqrt{(2j+1)!}}{j!}|(2i)+,(2j+1)-\rangle \tag{2.43}$$

If the single photon belongs to an entangled coupled:

$$|\psi^-\rangle_{1,2} = \frac{1}{\sqrt{2}}(|+\rangle_1|-\rangle_2 - |-\rangle_1|+\rangle_2) \tag{2.44}$$

where 1 and 2 refer to two different spatial modes, the overall state evolution is:

$$|\Sigma\rangle_{1,2} = (U_1\otimes I_2)|\psi^-\rangle_{1,2} = \frac{1}{\sqrt{2}}(|\Phi^+\rangle_1|-\rangle_2 - |\Phi^-\rangle_1|+\rangle_2) \tag{2.45}$$

the overall state preserve the singlet form, by keeping the correlation between spatial modes 1 (single photon state) and 2 (multi-photon state). The two mesoscopic states $|\Phi^+\rangle$

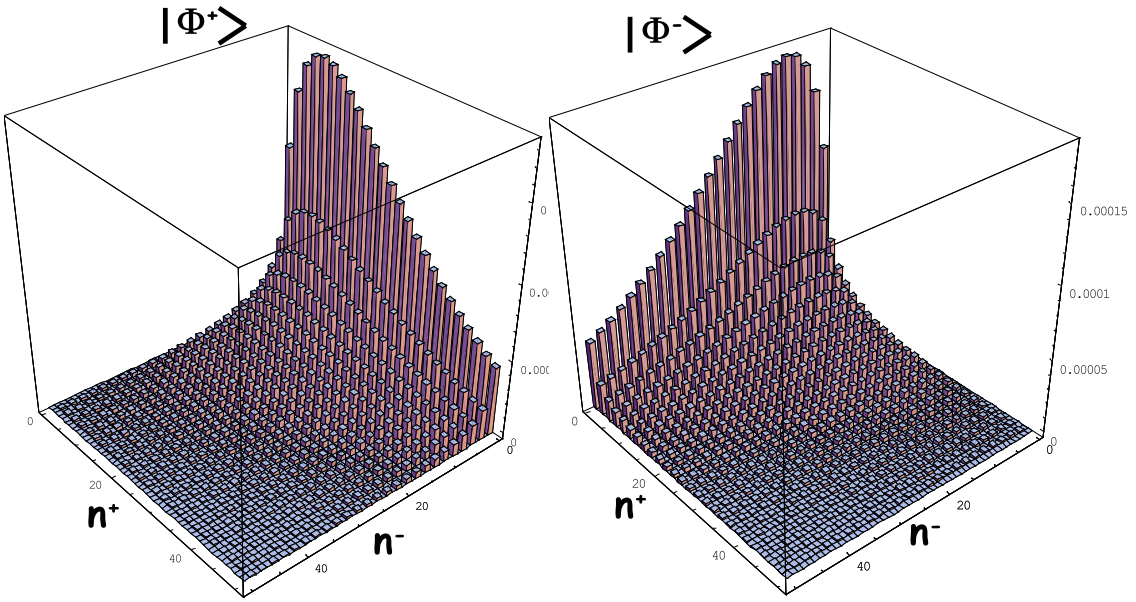

Figure 2.5: Probability distributions of the multi-photon states $|\Phi^+\rangle$ and $|\Phi^-\rangle$ show a macroscopically different trend as a function of photons polarized π_+ and π_-.

and $|\Phi^-\rangle$ are macroscopically different, due to the different shapes of their probability distributions as a function of the photons polarized $\overrightarrow{\pi_+}$, and $\overrightarrow{\pi_-}$: n_+ and n_- respectively. A discrimination between the two states could be achieved by counting the orthogonally polarized photons contained into each state. Experimental limitations don't allow this measurement procedure, but in the following chapter we will see how a probabilistic identification can be achieved by analyzing the macro-states probability distributions.

Analyzing figure 2.5, we observe that the probability distributions have long tails as a function of photons polarized as the injected qubit and a planckian distribution as a function of photons orthogonally polarized. This effect is due to the stimulated emission process and this feature holds for any equatorial polarization basis, where the cloning process is optimal. This unbalancement in the number of photons will be exploited in order to discriminate between orthogonal macrostates. The number of photons in a given polarization can indeed be estimated by measuring the intensity signal in a fixed polarization, the comparison between orthogonally polarized signals above a certain given threshold is able to identify the macro-state: namely if the number of photons N_+ exceed the number of photons N_- over a certain threshold k the state produced by the amplifier is with an higher probability Φ_+, otherwise Φ_-; when the two signals are not unbalanced nothing can be said about the nature of the output state.

2.5.2 Correlation functions

The study of macro-states generated by the optical parametric amplifier can be performed by the correlation functions of the output fields. In the equatorial qubit injection case $|\phi\rangle$(2.40), the mean number of generated photons with polarization $\overrightarrow{\pi}_+$ and $\overrightarrow{\pi}_-$, proportional to the first order correlation function, are:

$$G^{(1)}_{\pm\,(spin1/2)} = \langle N_\pm \rangle = \langle \phi | \widehat{a}^\dagger_\pm(t) \widehat{a}_\pm | \phi \rangle = \sinh^2 g + \frac{1}{2}(2\sinh^2 g + 1)(1 \pm \cos(\phi)) \quad (2.46)$$

Since the mean number of generated photons is $\overline{n} = \sinh^2 g$, we can write:

$$G^{(1)}_\pm = \overline{n} + \frac{1}{2}(2\overline{n}+1)(1 \pm \cos(\phi)) \quad (2.47)$$

The visibility of the interference fringe pattern is defined by:

$$\mathscr{V}^{th} = \frac{N_+(0) - N_-(0)}{N_+(0) + N_-(0)} \quad (2.48)$$

which gives:

$$\mathscr{V}^{th} = \frac{2\overline{n}+1}{4\overline{n}+1} \quad (2.49)$$

for increasing g, $g \to \infty$, the visibility tends to the asymptotic value:

$$\mathscr{V}^{th}_{spin1/2} \to \frac{1}{2} \quad (2.50)$$

In the high gain regime, we obtain that the visibility of the macro state correlation function is reduced to from 1 (single photon case) to $1/2$. The related fidelity $F = \frac{V+1/2}{2}$ is indeed $F = 3/4$ and coincides with the optimal phase covariant cloning faced in section 1.5.3.

2.6 Universal Cloning amplifier

The other class of macrostates that will be investigated in the next chapter is not obtained through an amplification process but is generated through the process of SPDC in a high gain regime. The annihilation of a pump photon produces a couple of photons on different spatial modes and with orthogonal polarizations. The interaction Hamiltonian reads:

$$\mathscr{H}_{int} = \imath\hbar\chi \left(\hat{a}_1{}^\dagger_\pi \hat{a}_2{}^\dagger_{\pi_\perp} - \hat{a}_1{}^\dagger_{\pi_\perp} \hat{a}_2{}^\dagger_\pi \right) + \text{H.c.} \quad (2.51)$$

where $\hat{a}_1{}^\dagger_\pi$ and $\hat{a}_2{}^\dagger_\pi$ are the creation operators corresponding to the generation of a π-polarized photon on spatial modes $\mathbf{k}_1$ and $\mathbf{k}_2$, as sketched in figure 2.6 and χ is the constant describing the strength of the interaction.

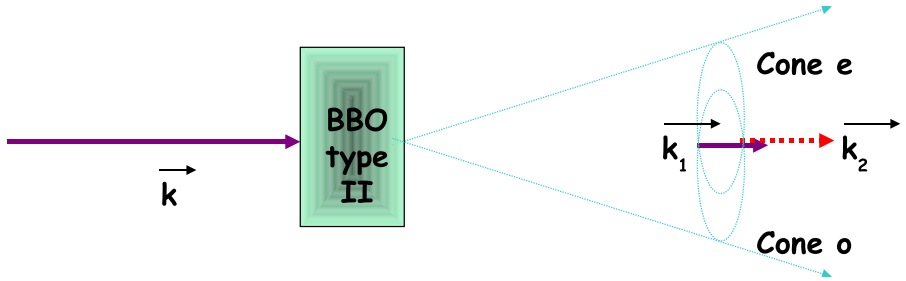

Figure 2.6: Optical parametric amplifier in a non-collinear configuration: the pump beam on mode k at frequency 2ω interacts with a non linear crystal, cut for type II phase matching, and generates two fields at frequency ω, on the same spatial modes k_1 and k_2.

The output state reads [EKD+04]:

$$|\Psi^-\rangle = \frac{1}{C^2}\sum_{n=0}^{\infty}\Gamma^n\sqrt{n+1}||\psi_n^-\rangle \tag{2.52}$$

$$|\psi_n^-\rangle = \frac{1}{\sqrt{n+1}}\sum_{m=0}^{n}(-1)^m|(n-m)\pi, m\pi_\perp\rangle_1|m\pi,(n-m)\pi_\perp\rangle_2 \tag{2.53}$$

where $\Gamma = \tanh g$ and $C = \cosh g$; $g = \chi t$ is the non-linear gain (NL) of the process. Hence, the output state can be written as the weighted coherent superposition of singlet spin-$\frac{n}{2}$ states $|\psi_n^-\rangle$. In this case both the state on mode k_1 and the one on mode k_2 contain an high number of photons, depending on the non linear gain of the amplifier. The correlation between the two macro-states could be exploited by measuring the exact number of photons on the orthogonal polarization components. As shown in figure 2.7 are reported

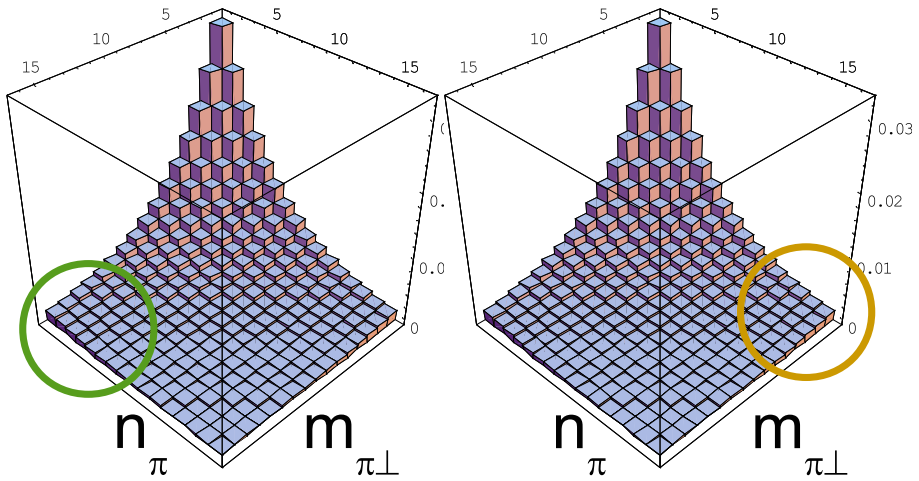

Figure 2.7: Probability distributions of the orthogonal multiphoton states on mode k_1 and k_2.

the two probability distributions as a function of orthogonally polarized photons numbers. Due to the correlations between the two spatial modes, an intensity measurement of the orthogonally polarized signals would find the two components unbalanced over a certain threshold as shown if figure 2.7: if on mode k_1 (left) a projective measurement finds the state into the green circle on the Fock space, the state on mode k_2 is with higher probability on the yellow region of the Fock space. This property can be used in order to discriminate between orthogonal macro states, but, as we will show in chapter 4, such a comparison measurement is not suitable in order to perform a non-locality test or to infer the entanglement of the macro-macroscopic state.

Part II

Generation of multiphoton quantum states

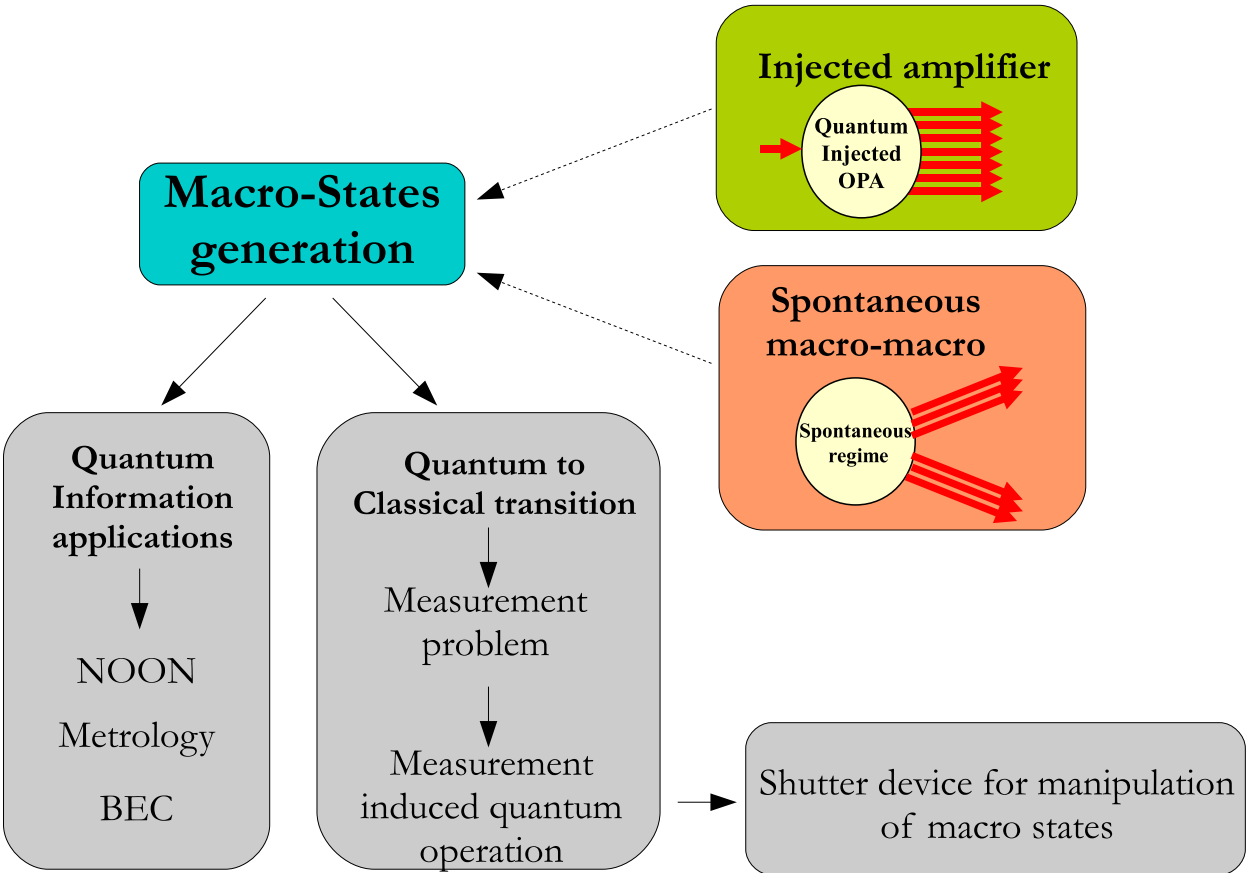

Figure 2.8: Conceptual scheme of the present work: in this part the colored boxes will be addressed. Two different schemes for the generation of multiphoton states are presented, one based on the optimal phase covariant cloning of an injected qubit and the other based on the spontaneous emission of an optimal parametric amplifier working in high gain regime.

In this part two different sources for the generation of multiphoton states are presented. In chapter 3 a micro-macroscopic system obtained by the phase covariant amplification of an entangled photon pair is studied. The quantum features of the overall state are investigated by performing a probabilistic measurement over the multiphoton state. A separability criterion is then violated requiring an auxiliary assumption. A different scheme for the generation of multiphoton quantum state is studied in chapter 4: there an optical parametric amplifier working in a non collinear geometry and in a high gain regime generates a macro-macroscopic entangled state, the possibility of observing the quantum features of such a quantum system of increasing size is studied. Different measurement strategies are investigated and the problem of decoherence is addressed.

Chapter 3

Experimental entanglement in a Micro-Macroscopic photon system

In this chapter a macro-state consisting of $\mathbf{N} \approx 3.5 \times 10^4$ photons in a quantum superposition and entangled with a far apart single-photon state (Micro-state) is generated. Precisely, an entangled photon pair is created by a nonlinear optical process, then one photon of the pair is injected into an optical parametric amplifier (OPA) operating for any input polarization state, i.e. into a phase-covariant cloning machine. Such transformation establishes a connection between the single photon and the multi particle fields. We demonstrate the non-separability of the bipartite system by adopting a local filtering technique within a positive operator valued measurement. We then discuss the auxiliary assumptions, related to the performed measurement, necessary to assess such a statement. At the end of the chapter a broader vision over the possible measurements on the micro-macro system are given and their reliability is discussed [DSV08].

3.1 From micro to macro

In recent years quantum entanglement has been demonstrated within a two photon system [KMW$^+$95], within a single photon and atomic ensemble [MCB$^+$05, dLC$^+$06] and within atomic ensembles [JKP01, MMO$^+$07, CdRF$^+$05]. The innovative character of the present work is enlightened by the diagrams reported in Figure 3.1. While, according to the 1935 proposal the nonlocal correlations were conceived to connect the dynamics of two "microscopic" objects, i.e. two spins within the well known EPR-Bohm scheme here represented by diagram (a)[KMW$^+$95], in the present work the entanglement is established between a "Microscopic" and a "Macroscopic", i.e. multi-particle quantum object, via cloning amplification: diagram (b). The amplification is achieved by adopting a high-gain nonlinear (NL) parametric amplifier acting on a single-photon input carrier of quantum information, i.e., a qubit state: $|\phi\rangle$. This process, referred to as "quantum injected optical parametric amplification" (QI-OPA) [De 98a] turned out to be particularly fruitful in the recent past to gain insight into several little explored albeit fundamental, modern aspects of quan-

tum information, as quantum cloning machines [PSS$^+$03, DS05], quantum U-NOT gate [DBSS02], quantum no-signaling [DNSD07]. Here, by exploiting the amplification process, we convert a single photon qubit into a Macro-qubit involving a large number of photons. The entanglement between the microscopic qubit and the macroscopic one obtained by the amplification process is achieved, under specific assumptions, performing a local dichotomic measurement on the multiphoton field.

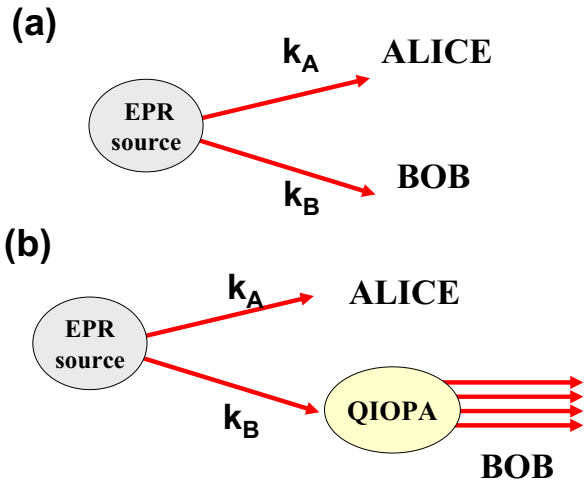

Figure 3.1: (a) Generation of an entangled photon pair by Spontaneous Parametric Down Conversion (SPDC) in a nonlinear (NL) crystal; (b) Schematic diagram showing the single photon Quantum-Injected Optical Parametric Amplification (QI-OPA).

3.2 Generation of the micro-macro state

An entangled pair of two photons in the singlet state

$$\left|\Psi^-\right\rangle_{A,B} = 2^{-\frac{1}{2}} \left(|H\rangle_A |V\rangle_B - |V\rangle_A |H\rangle_B\right) \tag{3.1}$$

was produced through a Spontaneous Parametric Down-Conversion (SPDC) by the NL crystal 1 (C1) pumped by a pulsed UV pump beam: Figure 7.13. There $|H\rangle$ and $|V\rangle$ stands, respectively, for a single photon with horizontal and vertical polarization while the labels A,B refer to particles associated respectively with the spatial modes $\mathbf{k}_A$ and $\mathbf{k}_B$. Precisely, A,B represent the two space-like separated Hilbert spaces coupled by the entanglement. The photon belonging to $\mathbf{k}_B$, together with a strong ultra-violet (UV) pump laser beam, was fed into an optical parametric amplifier consisting of a NL crystal 2 (C2) pumped by the beam $\mathbf{k}'_P$. A the exit of the amplifier a macro-qubit state is obtained from the single photon input qubit.

3.2.1 Generation of the single photon entangled state

The interaction hamiltonian of the first non linear crystal $C1$:

$$\widehat{H} = i\chi\hbar(\widehat{a}^{\dagger}_{AH}\widehat{a}^{\dagger}_{BV} - \widehat{a}^{\dagger}_{AV}\widehat{a}^{\dagger}_{BH}) + h.c. \tag{3.2}$$

where $\widehat{a}^{\dagger}_{i,j}$ con $i = A,B$ e $j = H,V$, are the creation operators on spatial mode i and polarization j. The treatment of the OPA in the non-degenerate regime, faced in paragraph 2.3.2, has then to be extended to the case in which the the Fock state at the exit of the amplifier is described by a tensorial product of four factors, relative to the four degrees of freedom of the generated photons. In this four dimensional space we can recognize two independent amplifiers acting on modes (AH,BV) and on modes (AV,BH), respectively. The evolution of the creation operators is then described by:

$$\begin{pmatrix} \widehat{a}_{AH}(t) \\ \widehat{a}^{\dagger}_{BV}(t) \end{pmatrix} = \begin{pmatrix} C & S \\ S & C \end{pmatrix} \begin{pmatrix} \widehat{a}_{AH}(0) \\ \widehat{a}^{\dagger}_{BV}(0) \end{pmatrix} \tag{3.3}$$

$$\begin{pmatrix} \widehat{a}_{AV}(t) \\ \widehat{a}^{\dagger}_{BH}(t) \end{pmatrix} = \begin{pmatrix} C & S \\ S & C \end{pmatrix} \begin{pmatrix} \widehat{a}_{AV}(0) \\ \widehat{a}^{\dagger}_{BH}(0) \end{pmatrix} \tag{3.4}$$

where $C = \cosh g_1$ e $S = \sinh g_1$, and $g_1 = \chi_1 t$ is the NL gain of the first non linear crystal. The generated state in the spontaneous emission regime is represented by the wavefunction:

$$|\psi\rangle = \frac{1}{\cosh^2(g_1)} \sum_{n=0}^{\infty} \sqrt{n+1}\tanh^2(g_1)|\psi_n^-\rangle \tag{3.5}$$

where:

$$|\psi_n^-\rangle = \frac{1}{\sqrt{n+1}} \sum_{m=0}^{n} (-1)^m |(n-m)H, mV\rangle_A |mH, (n-m)V\rangle_B \tag{3.6}$$

The first order term of the wavefunction (3.5) is indeed the singlet state:

$$|\psi^-\rangle_{A,B} = \frac{1}{\sqrt{2}}(|H\rangle_A|V\rangle_B - |V\rangle_A|H\rangle_B) \tag{3.7}$$

As said, the single photon on mode $\mathbf{k}_B$ was injected into the second crystal $C2$ in figure 7.13 and amplified, while the single photon on mode $\mathbf{k}_A$ was analyzed in polarization through a Babinet-Soleil phase-shifter (PS), i.e. a variable birefringent optical retarder, two waveplates $\left\{\frac{\lambda}{4}, \frac{\lambda}{2}\right\}$ and polarizing beam splitter (PBS). It was finally detected by two single-photon detectors D_A and D_A^* (ALICE box), realizing the trigger for the performed experiment.

3.2.2 Amplification of the entangled state

The crystal 2, cut for collinear operation, emitted over the two modes of linear polarization, respectively horizontal and vertical associated with $\mathbf{k}_B$. The interaction Hamiltonian

of the parametric amplification is:

$$\widehat{H} = i\chi\hbar\widehat{a}_H^{\dagger}\widehat{a}_V^{\dagger} + h.c. \tag{3.8}$$

and acts on the single spatial mode $\mathbf{k}_B$ where $\widehat{a}_{\pi}^{\dagger}$ is the one photon creation operator associated with the polarization $\overrightarrow{\pi}$. The main feature of this Hamiltonian is its property of "phase-covariance" for "equatorial" qubits $|\phi\rangle$, i.e. representing equatorial states of polarization, $\overrightarrow{\pi}_{\phi} = 2^{-1/2}\left(\overrightarrow{\pi}_H + e^{i\phi}\overrightarrow{\pi}_V\right)$, $\overrightarrow{\pi}_{\phi\perp} = \overrightarrow{\pi}_{\phi}^{\perp}$, in a Poincaré sphere representation having $\overrightarrow{\pi}_H$ and $\overrightarrow{\pi}_V$ as the opposite "poles" [NDSD07]. The equatorial qubits are expressed in terms of a single phase $\phi \in (0, 2\pi)$ in the basis $\{|H\rangle, |V\rangle\}$. The overall output state amplified by the OPA apparatus is expressed, in any polarization equatorial basis $\left\{\overrightarrow{\pi}_{\phi}, \overrightarrow{\pi}_{\phi\perp}\right\}$, by the Micro-Macro entangled state:

$$|\Sigma\rangle_{A,B} = 2^{-1/2}\left(\left|\Phi^{\phi}\right\rangle_B \left|1\phi^{\perp}\right\rangle_A - \left|\Phi^{\phi\perp}\right\rangle_B |1\phi\rangle_A\right) \tag{3.9}$$

where the mutually orthogonal multi-particle "Macro-states" are:

$$\begin{aligned} \left|\Phi^{\phi}\right\rangle_B &= \sum_{i,j=0}^{\infty} \gamma_{ij} \frac{\sqrt{(1+2i)!(2j)!}}{i!\,j!} \left|(2i+1)\phi; (2j)\phi^{\perp}\right\rangle_B \\ \left|\Phi^{\phi\perp}\right\rangle_B &= \sum_{i,j=0}^{\infty} \gamma_{ij} \frac{\sqrt{(1+2i)!(2j)!}}{i!\,j!} \left|(2j)\phi; (2i+1)\phi^{\perp}\right\rangle_B \end{aligned} \tag{3.10}$$

with $\gamma_{ij} \equiv C^{-2}(-\frac{\Gamma}{2})^i \frac{\Gamma}{2}^j$, $C \equiv \cosh g$, $\Gamma \equiv \tanh g$, being g the NL gain[DBSS02]. There $\left|p\phi; q\phi^{\perp}\right\rangle_B$ stands for a Fock state with p photons with polarization $\overrightarrow{\pi}_{\phi}$ and q photons with $\overrightarrow{\pi}_{\phi\perp}$ over the mode $\mathbf{k}_B$. Most important, any injected single-particle qubit $(\alpha|\phi\rangle_B + \beta\left|\phi^{\perp}\right\rangle_B)$ is transformed by the *information preserving* QI-OPA operation into a corresponding Macro-qubit $(\alpha\left|\Phi^{\phi}\right\rangle_B + \beta\left|\Phi^{\phi\perp}\right\rangle_B)$. The quantum states of Eq.(2-3) deserve some comments. The multi-particle states $\left|\Phi^{\phi}\right\rangle_B$, $\left|\Phi^{\phi\perp}\right\rangle_B$ are orthonormal and exhibit observables bearing macroscopically distinct average values. Precisely, for the polarization mode $\overrightarrow{\pi}_{\phi}$ the average number of photons is $\overline{m} = \sinh^2 g$ for $\left|\Phi^{\phi\perp}\right\rangle_B$, and $(3\overline{m}+1)$ for $\left|\Phi^{\phi}\right\rangle_B$. For the $\pi-$mode $\overrightarrow{\pi}_{\phi\perp}$ these values are interchanged among the two Macro-states. On the other hand, as shown by [De 98a], by changing the representation basis from $\left\{\overrightarrow{\pi}_{\phi}, \overrightarrow{\pi}_{\phi\perp}\right\}$ to $\left\{\overrightarrow{\pi}_H, \overrightarrow{\pi}_V\right\}$, the same Macro-states, $\left|\Phi^{\phi}\right\rangle_B$ or $\left|\Phi^{\phi\perp}\right\rangle_B$ are found to be quantum superpositions of two orthogonal states $\left|\Phi^{H}\right\rangle_B$, $\left|\Phi^{V}\right\rangle_B$ which differ by a single quantum. This unexpected and quite peculiar combination, i.e. a large difference of a measured observable when the states are expressed in one basis and a small Hilbert-Schmidt distance of the same states when expressed in another basis turned out to be a useful property since it rendered the coherence patterns of our system very robust toward coupling with environment, e.g. losses. This was verified experimentally. The decoherence the system was investigated theoretically in [DSS09a].

The multiphoton QI-OPA amplified field associated with the mode $\mathbf{k}_B$ was sent, through a single-mode optical fiber (SM), to a measurement apparatus consisting of a set of waveplates $\left\{\frac{\lambda}{4}, \frac{\lambda}{2}\right\}$, a (PBS) and two photomultipliers (PM) P_B and P_B^* (BOB box). The output

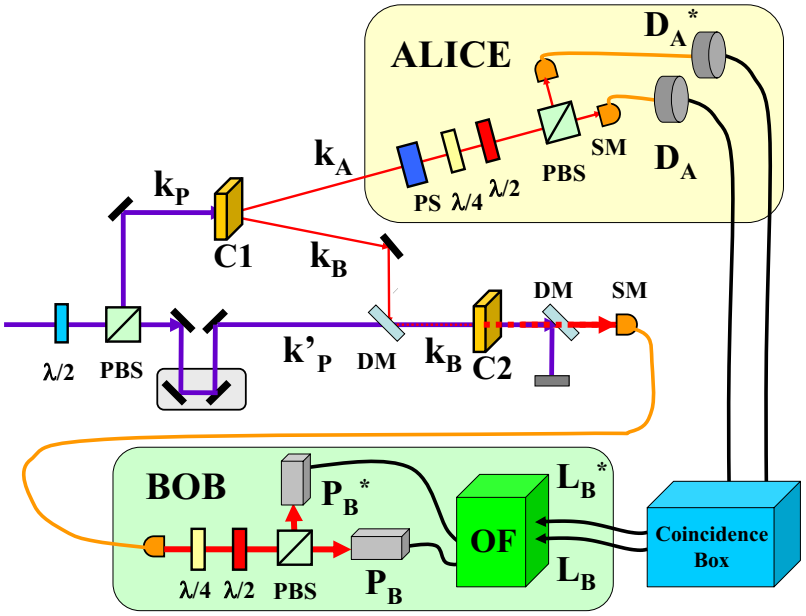

Figure 3.2: Optical configuration of the QI-OPA apparatus. The excitation source was a Ti:Sa Coherent MIRA mode-locked laser amplified by a Ti:Sa regenerative REGA device operating with repetition rate $250kHz$. The output beam, frequency-doubled by second-harmonic generation, provided the OPA excitation field beam at the UV wavelength (wl) $\lambda_P = 397.5nm$ with power: $750 \div 800mW$. A type II BBO crystal (crystal 1: C1) generates pair of photons with wavelength $\lambda = 2\lambda_p = 795nm$. C1 generates an average photon number per mode equal to about 0.35, while the overall detection efficiency of the trigger mode was estimated to be $\simeq 10\%$. The NL BBO crystal 2: C2, realizing the optical parametric amplification (OPA), is cut for collinear type II phase matching. Both crystals C1 and C2 are 1.5 mm thick. The fields are coupled to single mode (SM) fibers.

signals of the PM's were analyzed by an "orthogonality filter" (OF) that will be described in the following sections.

3.3 Demonstration of entanglement

We now investigate the bipartite entanglement between the modes $\mathbf{k}_A$ and $\mathbf{k}_B$. We define the $\frac{1}{2}-$spin Pauli operators for a single photon polarization state $\{\hat{\sigma}_i\}$ where the label $i = (1,2,3)$ refer to the polarization bases: $i = 1 \Longleftrightarrow \{\vec{\pi}_H, \vec{\pi}_V\}$, $i = 2 \Longleftrightarrow \{\vec{\pi}_R, \vec{\pi}_L\}$, $i = 3 \Longleftrightarrow \{\vec{\pi}_+, \vec{\pi}_-\}$. Here $\vec{\pi}_R = 2^{-1/2}(\vec{\pi}_H - i\vec{\pi}_V)$, $\vec{\pi}_L = \vec{\pi}_R^{\perp}$ are the right and left handed circular polarizations and $\vec{\pi}_\pm = 2^{-1/2}(\vec{\pi}_H \pm \vec{\pi}_V)$. It is found:

$$\hat{\sigma}_i = |\psi_i\rangle\langle\psi_i| - \left|\psi_i^{\perp}\right\rangle\left\langle\psi_i^{\perp}\right| \tag{3.11}$$

where $\{|\psi_i\rangle, |\psi_i^{\perp}\rangle\}$ are the two orthogonal qubits corresponding to the $\overrightarrow{\pi}_i$ basis, e.g., $\{|\psi_1\rangle, |\psi_1^{\perp}\rangle\} = \{|H\rangle, |V\rangle\}$, etc. By the QI-OPA unitary process the single-photon $\hat{\sigma}_i$ operators evolve into the "Macro-spin" operators:

$$\hat{\Sigma}_i = \hat{U}\hat{\sigma}_i\hat{U}^{\dagger} = |\Phi^{\psi i}\rangle\langle\Phi^{\psi i}| - |\Phi^{\psi i\perp}\rangle\langle\Phi^{\psi i\perp}| \tag{3.12}$$

Since the operators $\{\hat{\Sigma}_i\}$ are built from the unitary evolution of eigenstates of $\hat{\sigma}_i$, they satisfy the same commutation rules of the single particle $\frac{1}{2}-$spin: $[\hat{\Sigma}_i, \hat{\Sigma}_j] = \varepsilon_{ijk} 2i\hat{\Sigma}_k$ where ε_{ijk} is the Levi-Civita tensor density. The generic state $(\alpha |\Phi^H\rangle_B + \beta |\Phi^V\rangle_B)$ is a Macro-qubit in the Hilbert space B spanned by $\{|\Phi^H\rangle_B, |\Phi^V\rangle_B\}$, as said. To test whether the overall output state is entangled, one should measure the correlation between the single photon spin operator $\hat{\sigma}_i^A$ on the mode $\mathbf{k}_A$ and the Macro-spin operator $\widehat{\Sigma}_i^B$ on the mode $\mathbf{k}_B$. We then adopt the criteria for two qubit bipartite systems based on the spin-correlation. We define the "visibility" $V_i = \left|\left\langle \widehat{\Sigma}_i^B \otimes \widehat{\sigma}_i^A \right\rangle\right|$ a parameter which quantifies the correlation between the systems A and B. Precisely $V_i = \left|P(\psi_i, \Phi^{\psi i}) + P(\psi_i^{\perp}, \Phi^{\psi i\perp}) - P(\psi_i, \Phi^{\psi i\perp}) - P(\psi_i^{\perp}, \Phi^{\psi i})\right|$ where $P(\psi_i, \Phi^{\psi i})$ is the probability to detect the systems A and B in the states $|\psi_i\rangle_A$ and $|\Phi^{\psi i}\rangle_B$, respectively. The value $V_i = 1$ corresponds to perfect anti-correlation, while $V_i = 0$ expresses the absence of any correlation. The following upper bound criterion for a separable state holds [EKD$^+$04]:

$$S = (V_1 + V_2 + V_3) \leq 1 \tag{3.13}$$

In order to measure the expectation value of $\widehat{\Sigma}_i^B$ a discrimination among the pair of states $\{|\Phi^{\psi i}\rangle_B, |\Phi^{\psi i\perp}\rangle_B\}$ for the three different polarization bases $1,2,3$ is required. Consider the Macro-states $|\Phi^+\rangle_B$, $|\Phi^-\rangle_B$ expressed by Equations 3.10, for $\phi = 0$ and $\phi = \pi$. In principle, a perfect discrimination can be achieved by identifying whether the number of photons over the $\mathbf{k}_B$ mode with polarization $\overrightarrow{\pi}_+$ is even or odd, i.e. by measuring an appropriate "parity operator". This requires the detection of the macroscopic field by a perfect *photon-number resolving* detectors operating with an overall quantum efficiency $\eta \approx 1$, a device out of reach of the present technology.

It is nevertheless possible to exploit, by a somewhat sophisticated electronic device dubbed "Orthogonality Filter" (OF), the macroscopic difference existing between the functional characteristics of the probability distributions of the photon numbers associated with the quantum states $\{|\Phi^{\pm}\rangle_B\}$.

3.3.1 Orthogonality filter and probabilistic measurement

The measurement scheme works as follows: Figures 3.2 and 3.3. The multiphoton field is detected by two PM's (P_B, P_B^*) which provide the electronic signals (I_+, I_-) corresponding to the field intensity on the mode $\mathbf{k}_B$ associated with the $\pi-$components $(\overrightarrow{\pi}_+, \overrightarrow{\pi}_-)$, respectively. By (OF) the difference signals $\pm(I_+ - I_-)$ are compared with a threshold $\xi k > 0$. When the condition $(I_+ - I_-) > \xi k$ is satisfied, the detection of the state $|\Phi^+\rangle_B$

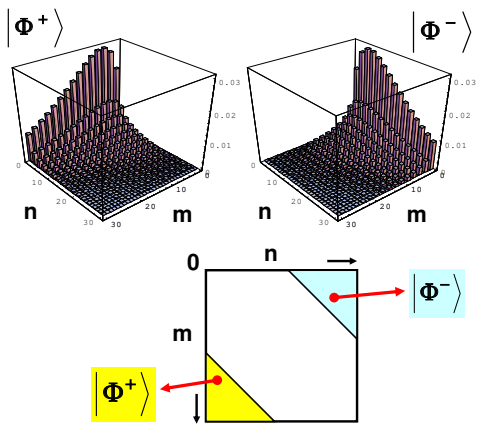

Figure 3.3: Theoretical probability distributions $P^{\pm}(m,n)$ of the number of photons associated with the Macro-states $|\Phi^{\pm}\rangle$ ($g = 1.6$). Probabilistic identification of the wave-functions $|\Phi^{\pm}\rangle$ by OF-filtering the $P^{\pm}(m,n)$ distributions over the photon number two-dimensional space $\{m,n\}$. The white section in the cartesian plane (m,n) corresponds to the "inconclusive events" of our POVM OF-filtering technique.

is inferred and a standard transistor-transistor-logic (TTL) electronic square-pulse L_B is realized at one of the two output ports of (OF). This corresponds to the measurement of the eigenvalue $+1$ of the operator $\widehat{\Sigma}_3^B$. Likewise, when the condition $(I_- - I_+) > \xi k$ is satisfied, the detection of the state $|\Phi^-\rangle_B$ is inferred, a TTL pulse is realized at other output port of (OF) and the eigenvalue of $\widehat{\Sigma}_3^B$ is -1. The PM output signals are discarded for $-\xi k < (I_+ - I_-) < \xi k$, i.e. in condition of low state discrimination. By increasing the value of the threshold k an increasingly better discrimination is obtained together with a decrease of detection efficiency. This "local distillation" procedure is conceptually justified by the following theorem: since entanglement cannot be created or enhanced by any "local" manipulation of the quantum state, the non-separability condition demonstrated for a "distilled" quantum system, e.g., after application of the OF-filtering procedure, fully applies to the same system in absence of distillation [EKD$^+$04]. This statement can be applied to the measurement of I_ϕ and $I_{\phi\perp}$ for any pair of quantum states $\{|\Phi^\phi\rangle_B, |\Phi^{\phi\perp}\rangle_B\}$. This method is but an application of a Positive Operator Value Measurement procedure (POVM) [Per95] by which a large discrimination between the two states $\{|\Phi^{\pm}\rangle_B\}$ is attained at the cost of a reduced probability of a successful detection.

The measurement scheme just described has been physically implemented by the OF shown in Figure 3.4, an electronic device by which the pulse heights of the couple of input signals (I_+, I_-) provided by two PM's (P_B, P_B^*) are summed with opposite signs by a balanced linear amplifier (LA) with "gain" G (chip National LM733). Each of the two signals $\pm[G(I_+ - I_-)] \equiv \pm[G\xi(m-n)]$ realized at the two symmetric outputs of (LA) feeds an independent electronic discriminator (AD9696) set at a common threshold level $G\xi k$. Owing to previous considerations the two discriminators never fire simultaneously and each of them provides, when activated, a standard transistor-transistor-logic (TTL) square signal at its output port. As said, when the condition $(I_+ - I_-) > \xi k$, i.e. $(m-n) > k$ is satisfied, a TTL signal L_B is generated and then the realization of the state $|\Phi^+\rangle_B$ is inferred. Likewise, when $(I_- - I_+) > \xi k$ a TTL signal L_B^* is generated and the realization of the state $|\Phi^-\rangle_B$ is inferred. The events that are discarded for: $-\xi k < (I_+ - I_-) < \xi k$

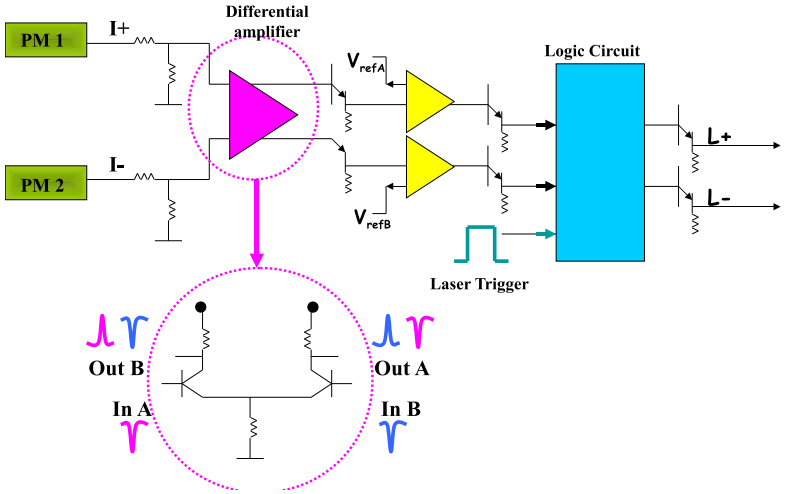

Figure 3.4: Electronic Orthogonality filter OF. The electronic signals (I_+, I_-) emitted simultaneously by two photomultipliers P_B and P_B^* feed a linear difference amplifier (National LM733). Each of the two output ports of the amplifier is con- nected to an electronic discriminator set at a threshold level $\xi k > 0$ equal for the two discriminators. Each discriminator emits a TTL electronic square signal if the threshold is overcome by the difference signals. Precisely, a TTL signal is realized at the port L_B when: $(I_+ - I_-) > \xi k$ or at the port L_B^* when $(I_- - I_+) > \xi k$. The two discriminators never fire si- multaneously. The rejected events, for $-\xi k < (I_+ - I_-) < \xi k$, correspond to the "inconclusive outcomes" of our generalized POVM measurement technique.

correspond to the "inconclusive" outcomes of any POVM [Per95].
The OF device has been tested and characterized in condition of spontaneous emission, i.e., in absence of any quantum injection into C2. In this condition the output TTL signals $L_B(L_B^*)$ were measured by sending only the signal $I_+(I_-)$ as input and by varying the threshold k. In this regime the number of photons generated per mode should exhibit a thermal probability distribution: $P(n) = \frac{\langle n \rangle^n}{(1+\langle n \rangle)^{n+1}}$ with $\langle n \rangle$ average photon number per mode. Hence the probability to detect a signal above the threshold k is: $\Pi(k) = \sum_{n=k}^{\infty} P(n) = \left(\frac{\langle n \rangle}{(1+\langle n \rangle)}\right)^k$. We have experimentally checked the dependence on the threshold k of the number of counts, which is expressed by $R \times \Pi(k)$, being R the repetition rate of the source. The experimental data shown by Figure 3.5 represent a fair support of the expected exponential behavior.

3.3.2 Experimental results

The present experiment was carried out with a gain value $g = 4.4$ leading to a number of output photons $N \approx 3 \times 10^4$, after OF filtering. In this case the probability of photon transmission through the OF filter was: $p \approx 10^{-4}$. In order to verify the correlations

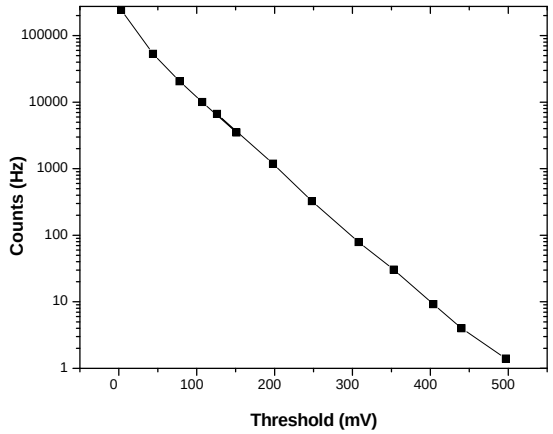

Figure 3.5: Count rates versus the threshold k. The measured average electronic signal was $\simeq 40mV$, while the repetition rate of the main laser source was 250 kHz.

existing between the single photon generated by the NL crystal 1 and the corresponding amplified Macro-state, we have recorded the coincidences between the single photon detector signal D_A (or D_A^*) and the TTL signal L_B (or L_B^*) both detected in the same $\pi-$basis $\left\{\overrightarrow{\pi}_+, \overrightarrow{\pi}_-\right\}$: Figure 3.2. This measurement has been repeated by adopting the common basis $\left\{\overrightarrow{\pi}_R, \overrightarrow{\pi_L}\right\}$. Since the filtering technique can hardly be applied to the $\left\{\overrightarrow{\pi}_H, \overrightarrow{\pi}_V\right\}$ basis, because of the lack of a broader $SU(2)$ covariance of the amplifier, the small quantity $V_1 > 0$ could not be precisely measured. The phase ϕ between the $\pi-$components $\overrightarrow{\pi}_H$ and $\overrightarrow{\pi}_V$ on mode $\mathbf{k}_A$ was determined by the Babinet-Soleil variable phase shifter (*PS*). Figure 3.3.2 shows the fringe patterns obtained by recording the rate of coincidences of the signals detected by the Alice's and Bob's measurement apparata, for different values of ϕ. These patterns were obtained by adopting the common analysis basis $\left\{\overrightarrow{\pi}_R, \overrightarrow{\pi}_L\right\}$ with a filtering probability $\simeq 10^{-4}$, corresponding to a threshold ξk about 8 times higher than the average photomultiplier signals I. In this case the average visibility has been found $V_2 = (54.0 \pm 0.7)\%$. A similar oscillation pattern has been obtained in the basis $\left\{\overrightarrow{\pi}_+, \overrightarrow{\pi}_-\right\}$ leading to: $V_3 = (55 \pm 1)\,\%$. Since always is $V_1 > 0$, our experimental result $S = V_2 + V_3 = (109.0 \pm 1.2)\%$ implies the violation of the separability criteria of Equation (3.13) and then demonstrates the non-separability of our Micro-Macro system belonging to the space-like separated Hilbert spaces A and B.

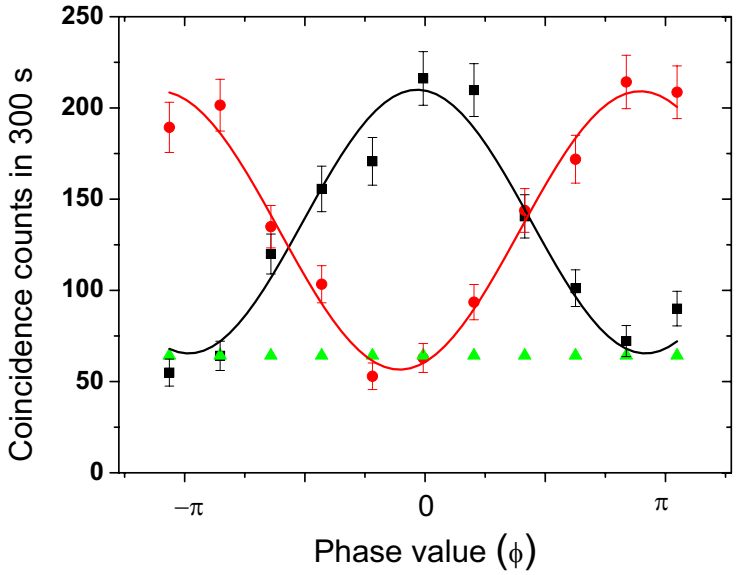

Figure 3.6: Coincidence counts versus the phase ϕ of the injected qubit for a common basis $\{\vec{\pi}_+, \vec{\pi}_-\}$: square data $[L_B, D_A]$, circle data $[L_B^*, D_A]$. The visibility of the fringe pattern is: $V \simeq 55\%$. Triangle data: noise due to accidental coincidences.

3.4 Entanglement tests

As said, the exploited entanglement criterion is an extension of the spin-based single-particle criterion of Ref.[EKD$^+$04]. Due to the presence of losses, such an extension requires a supplementary assumption which will be clarified in the remaining part of this chapter. We now focus on the conditions that are necessary in order to justify the exploited entanglement criterion. And finally, we perform a theoretical analysis of the micro-macro system based on the parametric amplification of an entangled pair. Several approaches for the verification of the entanglement property of the system will be addressed, showing that a substantial fraction ε of the original entanglement survives even in high losses condition.

3.4.1 Auxiliary assumptions

For a two-photon state $|\psi\rangle$, defined on two different modes a and b, the entanglement is demonstrated by applying the criterion in equation (3.18). More specifically, for any separable state, the following inequality holds [Dur04, EKD$^+$04]:

$$ {}_\psi\langle \hat{\sigma}_1^{(a)} \otimes \hat{\sigma}_1^{(b)} \rangle_\psi + {}_\psi\langle \hat{\sigma}_2^{(a)} \otimes \hat{\sigma}_2^{(b)} \rangle_\psi + {}_\psi\langle \hat{\sigma}_3^{(a)} \otimes \hat{\sigma}_3^{(b)} \rangle_\psi \leq 1 \qquad (3.14) $$

where $\hat{\sigma}_{1,2,3}$ are the Pauli operators and ${}_{\psi}\langle\cdot\rangle_{\psi}$ stands for the average on the state $|\psi\rangle$. The same criterion can be extended to a micro-macro scenario by measuring the pseudo spin operators $\hat{\Sigma}_i$ on the macro state, obtained through an unitary transformation upon the micro-micro state. Here, the $\hat{\Sigma}_i$ operators are the time evolution of the Pauli operators according to $\hat{\Sigma}_i = \hat{U}\hat{\sigma}_i\hat{U}^{\dagger}$, where $\hat{U}$ is the time evolution operator of the amplifier. The following inequality holds:

$$ {}_{\Psi}\langle\hat{\sigma}_1^{(a)} \otimes \hat{\Sigma}_1^{(b)}\rangle_{\Psi} + {}_{\Psi}\langle\hat{\sigma}_2^{(a)} \otimes \hat{\Sigma}_2^{(b)}\rangle_{\Psi} + {}_{\Psi}\langle\hat{\sigma}_3^{(a)} \otimes \hat{\Sigma}_3^{(b)}\rangle_{\Psi} \leq 1 \tag{3.15} $$

In the non ideal case the multiphoton state obtained after the amplification undergoes a decoherence process due to losses. In this case the macro-qubit $|\Phi^{\phi}\rangle$ transforms into a density matrix $\hat{\rho}_{\eta}^{\phi}$ that does not live anymore in a bidimensional Hilbert space and the macro-qubit formalism does not hold anymore. The measurement of the pseudo-Pauli operators requires the perfect discrimination of the number of photons present in the detected state. In order to implement such measurement, which is out of reach for the current technology, we have adopted the OF based strategy. The action of the O-Filter is described by the following measurement observables, applied on the multiphoton state *after* losses:

$$ \hat{\Pi}_i(k) = \sum_{n=k}^{\infty}\sum_{m=0}^{n-k} |n\vec{\pi}_i, m\vec{\pi}_i^{\perp}\rangle\langle n\vec{\pi}_i, m\vec{\pi}_i^{\perp}| - \tag{3.16} $$

$$ \sum_{m=k}^{\infty}\sum_{n=0}^{m-k} |n\vec{\pi}_i, m\vec{\pi}_i^{\perp}\rangle\langle n\vec{\pi}_i, m\vec{\pi}_i^{\perp}| \tag{3.17} $$

This probabilistic detection method allows us to infer the generation *before* losses of a $|\Phi^{\phi}\rangle$ or a $|\Phi^{\phi_{\perp}}\rangle$ state by exploiting the information encoded in the unbalancement of the number of photons present in the state.

An analogous measurement scheme is shown in Fig.3.7-(b). The field is analyzed in polarization, and each branch is equally divided among a set of single-photon detectors (APD). Coincidences between the output TTL signals are recorded for each analyzed polarization, and the (+1) or the (-1) outcomes are assigned depending on which of the two analyzed sets of APDs record the N-fold coincidence. If no N-fold coincidences are recorded, the (0) inconclusive outcome is assigned to the event. This scheme performs the measurement of the N-th order correlation function of the field, where N is the number of detectors. We note that the O-Filter based and the multi-detector based schemes select analogous regions of the Fock space.

On one side, we note that the measurement of the correlations for the entanglement test of Eq.(3.15), where the $\{\hat{\Sigma}\}$ operators must be replaced with the $\{\hat{\Pi}\}$ operators of the O-Filter, are performed in the same basis for Alice and Bob's sites. However, care should be taken when a filtering of the detected state is performed. As shown in Fig.3.7-(a), the O-filter detection scheme corresponds to a Fock space filtering of the output state. The measurements performed on different polarization basis select *different* regions of

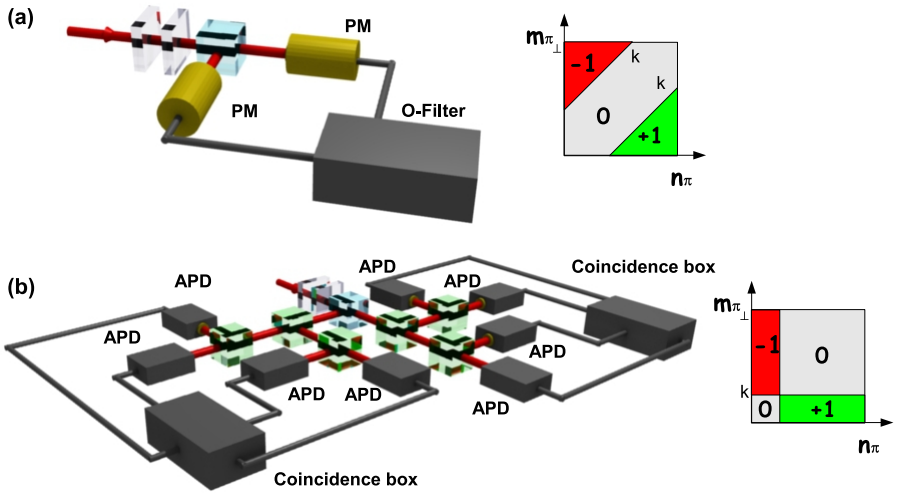

Figure 3.7: (a) O-Filter based detection apparatus. Right figure: selected Fock space region with the O-Filter measurement scheme. (b) Multi-detector measurement strategies. The field is detected by four APD: the coincidences between all four detectors trigger the successful events. Right figure: selected Fock space region with the multi-detector measurement scheme.

the Fock space, corresponding to different portions of the density matrix. This is shown in Fig.3.8, where the photon number distribution of a $|n+,0-\rangle$ Fock state with $n = 10$ in the $\{+,-\}$ and $\{R,L\}$ polarization bases is reported. When measured with the O-Filter device, such state generates a conclusive (+1) outcome in the $\{+,-\}$ basis, since a strong unbalancement is present between the two polarizations. On the contrary, in the $\{R,L\}$ basis with high probability the state generates an inconclusive outcome (0) and is filtered out. This feature has no counterpart in the micro-qubit formalism: indeed the Hilbert space of the original photon is only two-dimensional, so there is no risk of different subspaces being detected for different choices of measurement basis.

Without any specific assumption on the investigated system the inequality (3.15), in which the $\{\hat{\Sigma}_i\}$ operators must be replaced by the $\{\hat{\Pi}_i\}$ ones, does not represent anymore a bound for entangled states. It is satisfied by separable states of the form [SBB+09]:

$$\begin{aligned}\hat{\rho}_{sep} &= \frac{1}{2\pi}\int_0^{2\pi} d\phi \hat{U}(\phi)|1\pi_i, 0\pi_i^\perp\rangle_a|0\pi_i, N\pi_i^\perp\rangle_b \times \\ &\quad {}_a\langle 1\pi_i, 0\pi_i^\perp|_b\langle 0\pi_i, N\pi_i^\perp|\hat{U}(\phi)^\dagger \end{aligned} \tag{3.18}$$

where $\hat{U}(\phi)$ is a rotation of the whole system polarization around the z axis by an angle ϕ.

Despite the previous considerations, the OF based strategy allows us to discriminate between different macro states in a probabilistic way. When $k \to \infty$ the mean value of the $\{\hat{\Pi}_i\}$ operators, calculated over the real state $\mathrm{Tr}(\hat{\rho}_\eta^\phi \hat{\Pi}_i)$, tends to the mean value of the

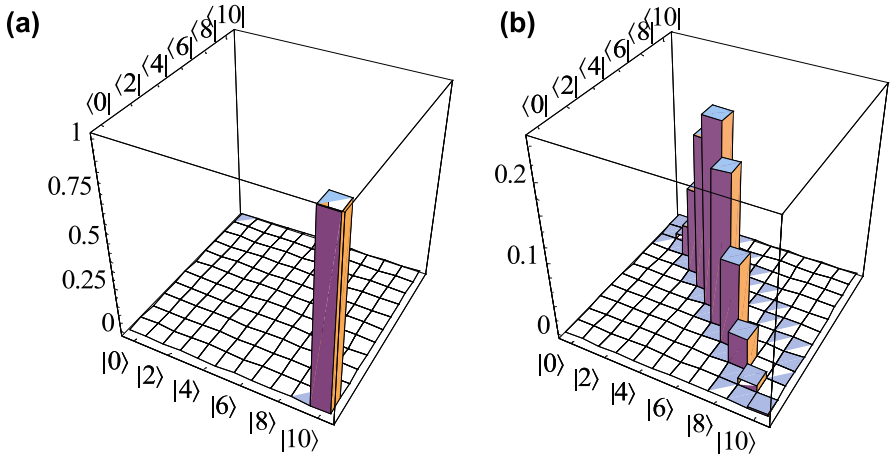

Figure 3.8: (a) Photon number distribution for a Fock state $|n+,0-\rangle$ with $n = 10$ in the $\{+,-\}$ polarization basis. (b) Photon number distribution for a Fock state $|n+,0-\rangle$ with $n = 10$ in the $\{R,L\}$ polarization basis.

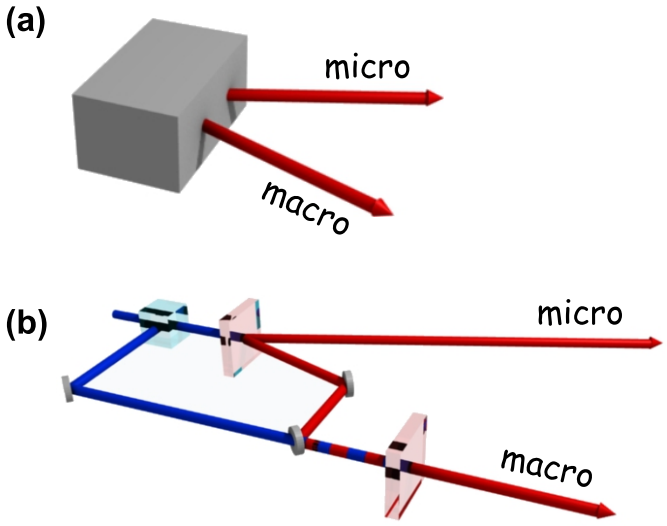

Figure 3.9: (a) Micro-macro system source in a black box configuration: no assumption is made about the source. (b) Micro-macro amplified system: the macroscopic state is generated by a coherent amplification process of a single photon, belonging to an EPR pair.

Pauli pseudo-spin operators, calculated over the ideal macro-qubit one $\langle\Phi^{\phi}|\hat{\Sigma}_i|\Phi^{\phi}\rangle$. Indeed, for asymptotically high values of the threshold $k \to \infty$, the measurement of the $\{\hat{\Pi}_i\}$ operators on the $\hat{\rho}_{\eta}^{\phi}$ allows perfect, although probabilistic in the POVM spirit, discrimination of orthogonal states, as the pseudo-spin operator does for the macro-qubits $|\Phi^{\phi}\rangle$. In other words, if the $|\Phi^{+}\rangle$ state is generated, the measurement with the $\{\hat{\Sigma}_i\}$ operator in the $\{+,-\}$ basis never leads to the (-1) outcome. At the same time, the measurement of the $\hat{\rho}_{\eta}^{+}$ state after losses with the $\{\hat{\Pi}_i\}$ operator in the $\{+,-\}$ basis does not generate the (-1) outcome if k is large enough. According to these considerations, we can infer the presence of the macro-qubit *before* losses and *after* the amplifier and then apply the

original micro-macro inequality of Eq.(3.15). This inference implies an assumption on the micro-macro system: the macro state has to be generated by an amplification process upon a micro-micro entangled pair. Therefore the entanglement test performed by the OF scheme allows us to infer the presence of entanglement *at least before* losses, and to demonstrate the capability of amplifying an entangled pair in a coherent way. Indeed the class of separable state in Eq.(3.18) cannot be generated by a coherent amplification process.

3.4.2 Different micro-macro entanglement tests

For a set $\{\hat{\Pi}_i\}$ of dichotomic operators, without making any supplementary assumptions, the bound to be violated in order to demonstrate the entanglement of the overall micro-macro system must be modified with respect to Eq.(2), and a necessary condition for separable states is given by the following inequality:

$$S = \langle \hat{\sigma}_1^{(a)} \otimes \hat{\Pi}_1^{(b)} \rangle_\Psi + \langle \hat{\sigma}_2^{(a)} \otimes \hat{\Pi}_2^{(b)} \rangle_\Psi + \langle \hat{\sigma}_3^{(a)} \otimes \hat{\Pi}_3^{(b)} \rangle_\Psi \leq \sqrt{3} \tag{3.19}$$

Such criterion presents the interesting feature of not requiring any knowledge of the Hilbert space where the analyzed states live. Indeed, in the derivation of the bound (3.19) the only necessary assumption concerns the measurement operators, which can have only two possible outcomes (± 1) . We then applied the obtained criterion to evaluate the quan-

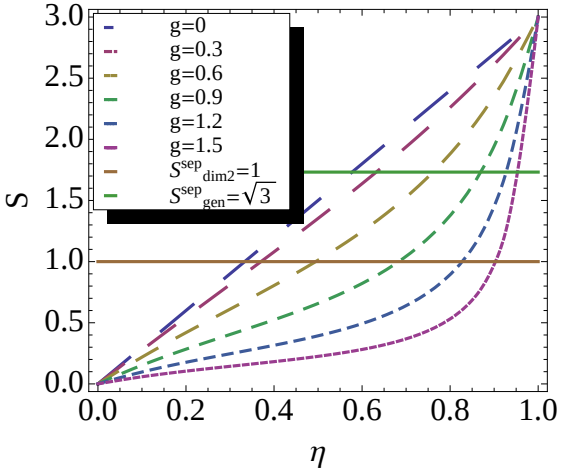

Figure 3.10: Numerical evaluation of the witness S for the specific choice of the Pauli pseudo-spin operators $\{\hat{\Sigma}_i\}$ as measurement operators $\{\hat{\Pi}_i\}$ as a function of the detection losses η, calculated for several values of the gain of the amplifier. The upper horizontal solid line corresponds to the bound for separables states of the general criterion (3.19), while the lower solid line corresponds to the bound for separable states (3.15) where a standard assumption on the Hilbert space is necessary.

tity S for the micro-macro state generated through the process of optical parametric amplification, for the specific choice of the Pauli pseudo-spin operators as the measurement

operators. More specifically, we evaluated the value of S as a function of the transmission efficiency η of the multiphoton mode $\mathbf{k}_B$ for several values of the gain g [Fig.3.10]. The value of S is then compared to the bound for separable states $S_{gen}^{sep} = \sqrt{3}$. We observe that this entanglement measure is fragile under losses, since the value of S falls below the bound for separable states when the number of lost photons is $R\langle n\rangle \sim 1$. Such result is expected since the Pauli operators allows to distinguish the $|\Phi^{\phi}\rangle$ states exploiting the well-defined parity in the number of photon generated by the amplifier depending on the polarization of the input states. In presence of losses, such well-defined parity is quickly cancelled, thus not allowing to discriminate among the macro-states with this kind of measurement. This feature of the macro-states generated through the process of optical parametric amplification is reported and discussed in Refs.[DSS09b, SVD^{+}09].

Entanglement detection in a highly attenuated scenario

An alternative approach can be used to demonstrate the presence of entanglement in our micro-macro configuration. The macroscopic field is deliberately attenuated up to the single-photon regime and detected through an APD. Such method has been exploited to demonstrate the entanglement up to 12 photons in a spontaneous parametric down conversion source [EKD^{+}04], or in a micro-macro configuration [DS05]. The average number of photons impinging onto the detector in this regime is then $\eta\langle n\rangle \leq 1$, where η is the overall quantum efficiency of the channel. The density matrix of the macroscopic state can be reduced to a 1-photon subspace, and the joint micro-macro system is defined in a 2×2 Hilbert space. The complete state $\hat{\rho}_{\eta}^{AB}$ reads:

$$\hat{\rho}_{\eta}^{AB} = \frac{1}{1+3t^2}\begin{pmatrix} t^2 & 0 & 0 & 0 \\ 0 & \frac{1}{2}\left(1+t^2\right) & -\frac{1}{2}\left(1+t^2\right) & 0 \\ 0 & -\frac{1}{2}\left(1+t^2\right) & \frac{1}{2}\left(1+t^2\right) & 0 \\ 0 & 0 & 0 & t^2 \end{pmatrix} \tag{3.20}$$

where:

$$t = (1-\eta)\Gamma \tag{3.21}$$

In Fig.3.11-(a) we show the density matrix of the joint micro-macro system for a value of $g = 3$ and $\eta = 10^{-4}$, showing the presence of the off-diagonal terms even in the high losses regime. This system is entangled for any value of the nonlinear gain g. This property can be tested by application of the Peres criterion or by direct calculation of the concurrence, which reads:

$$C(\hat{\rho}_{\eta}^{AB}) = \left(\frac{1-t^2}{1+3t^2}\right) > 0 \tag{3.22}$$

This quantity is always positive, as plotted in Fig.3.11-(b), showing the presence of entanglement for any value of the gain. Since no entanglement can be generated with local operations (such as a lossy process) [EKD^{+}04], the presence of entanglement in the

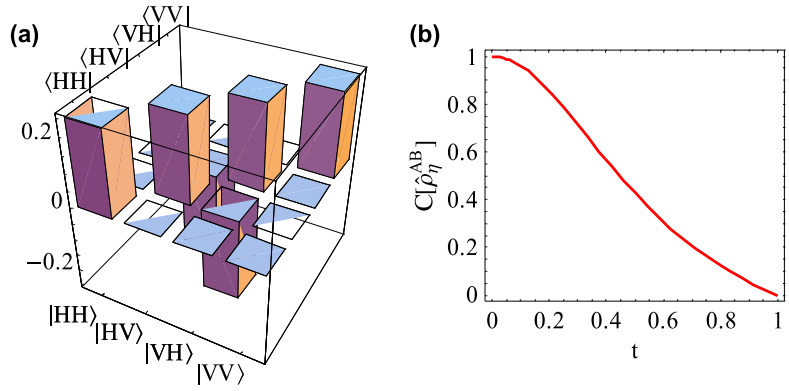

Figure 3.11: (a) Density matrix of joint micro-macro system in the high losses regime, for a gain value of $g = 3$ and a value of the losses parameter $\eta = 10^{-4}$. (b) Plot of the concurrence $C(\hat{\rho}_{\eta}^{AB})$ as a function of the parameter $t = \Gamma(1-\eta)$. We note the persistence of the off-diagonal terms and entanglement for all values of g and η.

highly attenuated regime is due to the presence of entanglement in the micro-macro system before losses.

This criterion allows us to discuss an important feature of the micro-macro system based on optical parametric amplification. The entanglement of this system is generated in the micro-micro source, where the singlet polarization state $|\psi^-\rangle$ is produced. The action of the amplifier is to broadcast the properties of the injected seed to the multiparticle state. In particular, the entanglement present in the original photon pair after the amplification process is transferred and shared among the generated particles (see Fig.3.12). If a certain amount of losses is introduced in the macro-state and ε is the percentage of photons that survive such decoherence process, the amount of entanglement detected after losses is reduced of a factor ε but drops to 0 only if all particles are lost.

To conclude these considerations, we extend the analysis of the micro-macro amplified system in this highly attenuated scenario to the case where the injection of the single-photon in the optical parametric amplifier occurs with a non unitary efficiency $p < 1$. In this case, the density matrix of the joint micro-macro system reads:

$$\hat{\rho}_{\eta,p}^{AB} = \mathscr{N}_{\eta,p}^{-1} \left\{ \frac{2p}{C^2} \frac{1}{1-t^2} \begin{pmatrix} t^2 & 0 & 0 & 0 \\ 0 & \frac{1}{2}(1+t^2) & -\frac{1}{2}(1+t^2) & 0 \\ 0 & -\frac{1}{2}(1+t^2) & \frac{1}{2}(1+t^2) & 0 \\ 0 & 0 & 0 & t^2 \end{pmatrix} + (1-p)\Gamma \begin{pmatrix} t & 0 & 0 & 0 \\ 0 & t & 0 & 0 \\ 0 & 0 & t & 0 \\ 0 & 0 & 0 & t \end{pmatrix} \right\} \tag{3.23}$$

where $\mathscr{N}_{\eta,p}$ is the opportune normalization constant. In Fig.3.13 (a)-(b) we show the density matrix for a gain value $g = 3$, for $\eta = 10^{-4}$ and injection probabilities of $p = 0.5$ and $p = 0.25$. The effect of a decreasing injection probability p is the reduction of the off-diagonal terms and hence of the coherence terms. The application of the Peres criterion

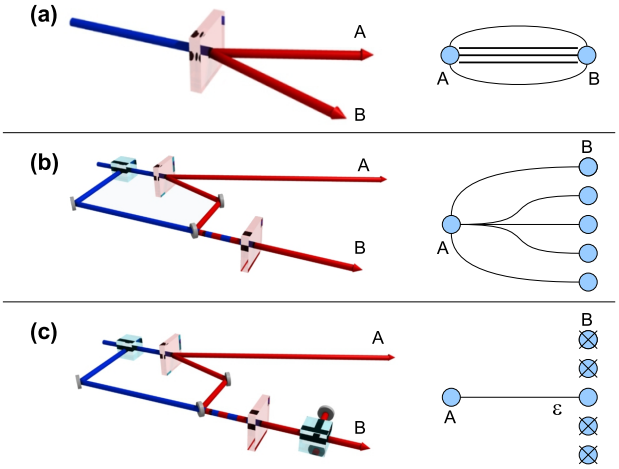

Figure 3.12: Diagramatic scheme of the entanglement broadcasting from the single photon pair to the multiparticle state. In presence of losses, the entanglement is reduced of a factor ε.

on this density matrix gives a critical value of the injection probability $p_{crit} = \frac{S^2(1-\eta)}{1+S^2(1-\eta)}$. For $p > p_{crit}$, the micro-macro system in this highly attenuated regime is entangled, while for $p \leq p_{crit}$ the system is separable. The same result is confirmed by the calculation of the concurrence, which reads:

$$C(\hat{\rho}^{AB}_{\eta,p}) = \begin{cases} \frac{p(1-t^2)-(1-p)tS^2(1-t^2)}{p(1+3t^2)+2(1-p)tS^2(1-t^2)} & \text{for } p > p_{crit} \\ 0 & \text{for } p \leq p_{crit} \end{cases} \tag{3.24}$$

In Fig.3.13 (c) we report the plot of the concurrence as a function of the gain g for several values of the injection probability p and $\eta = 10^{-4}$. For decreasing p, the concurrence drops to 0 for a lower value of the gain. Furthermore, in Fig.3.13 (d) we report the plot of the critical injection probability p_{crit} as a function of the gain g and the transmission efficiency η. As the gain g is increased, the value of the critical injection probability increases up to a value close to 1. This means that, for high values of the gain, an high injection efficiency is requested to detect the entanglement with such measurement strategy.

Spin-based entanglement criterion

Another approach for a micro-macro entanglement test is based on the detection of the quantum Stokes operators, defined as: $\hat{J}^B_{\vec{\pi}_i} = \hat{b}^\dagger_{\vec{\pi}_i}\hat{b}_{\vec{\pi}_i} - \hat{b}^\dagger_{\vec{\pi}_i^\perp}\hat{b}_{\vec{\pi}_i^\perp}$. For a micro-macro system, the following inequality, found by Simon et al. in Ref.[SB03], holds for any separable state:

$$|\langle \vec{\hat{\sigma}}^A \cdot \vec{\hat{J}}^B \rangle| - \langle \hat{N}^B \rangle \leq 0 \tag{3.25}$$

where $\hat{N}^B$ is the photon number operator. Both $\vec{\hat{\sigma}}^A$ and $\vec{\hat{J}}^B$ are vectors of the Pauli and Stokes operators respectively. For the micro-macro configuration under investigation, based on the amplification of a single-photon state, the following result [SBB$^+$09] holds:

$$|\langle \vec{\hat{\sigma}}^A \cdot \vec{\hat{J}}^B \rangle| - \langle \hat{N}^B \rangle = 2\eta \geq 0 \tag{3.26}$$

thus violating the bound for separable states. A more detailed discussion of this Stokes-based approach on the investigated micro-macro source is reported in Ref.[SSP+10]. Again, some entanglement survives for any value of the gain and of the losses parameter η. However such criterion is not feasible from an experimental point of view since the measurement of the Stokes operators requires perfect discrimination in the photon-number, as in the pseudo-Spin operator case.

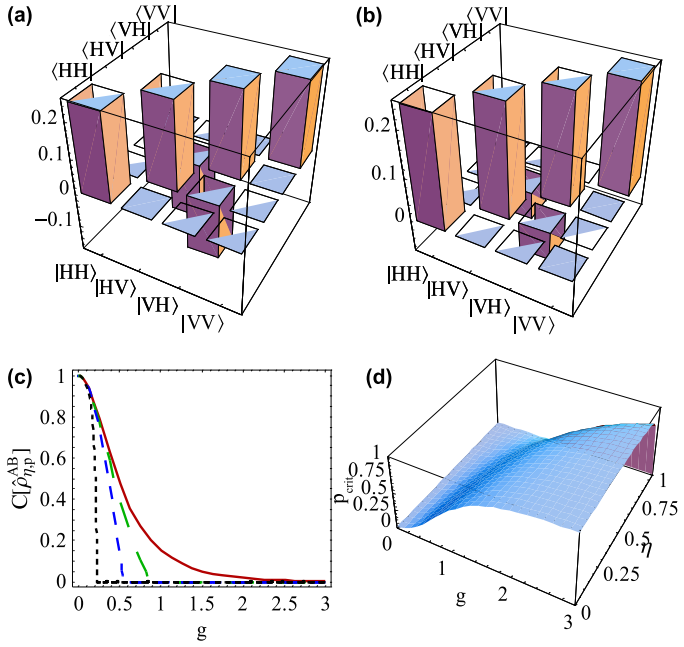

Figure 3.13: (a)-(b) Density matrix of the micro-macro system in the high losses regime, for a gain value of $g = 3$ and a value of the losses parameter $\eta = 10^{-4}$. (a) Injection probability $p = 0.5$ and (b) injection probability of $p = 0.15$. (c) Concurrence $C(\hat{\rho}^{AB}_{\eta,p})$ as a function of the gain g for $\eta = 10^{-4}$. Red solid line corresponds to an injection probability $p = 1$, green long dashed line to $p = 0.5$, blue short dashed line to $p = 0.25$ and black dotted line to $p = 0.05$. (d) 3-dimensional plot for the critical injection probability p_{crit} as a function of the gain g and the transmission coefficient η.

3.5 Observations and conclusions

In this chapter we have shown how to realize a multiphoton state consisting in thousands of photons through an amplification process performed over a single photon state belonging to an entangled pair. The micro-macro state so realized still shows quantum features, and it is found to be non-separable under specific assumptions. The adopted entanglement criterion in our experiment allowed indeed to infer the presence of entanglement after the amplification process but before losses in the detection apparatus. An a priori knowledge of the source is necessary in order to exclude a class of separable states that can reproduce the obtained experimental results. One of the reason for the necessity of this assumption is given by the exploited detection strategy, which presents the feature of a POVM with an in- conclusive outcome which depends on the measurement basis.

A more general analysis about the possibility of observing entanglement, even in presence of losses, in a micro-macroscopic state has been addressed at the end of the chapter: the spin formalism as well as the Stokes parameters one requires perfect discrimination in the photon-number, which is not a feasible requirement from an experimental point of view. A possible perspective for such an investigation field could then involve the analysis of the micro-macro system through the continuous variables formalism and the reconstruction of Wigner function for the overall state. An appropriate entanglement criterion in that case has then to be found.

Chapter 4

Macro-Macroscopic quantum systems based on high gain spontaneous parametric down-conversion

In this chapter we consider the high gain spontaneous parametric down-conversion in a non collinear geometry as a paradigmatic scenario to investigate the quantum-to-classical transition by increasing the pump power, that is, the average number of generated photons. The possibility of observing quantum correlations in such macroscopic quantum system through dichotomic measurement will be analyzed by addressing two different measurement schemes, based on different dichotomization processes. More specifically, we will investigate the persistence of non-locality in an increasing size $\frac{n}{2}$-spin singlet state by studying the change in the correlations form as n increases, both in the ideal case and in presence of losses. We observe a fast decrease in the amount of Bell's inequality violation for increasing system size. This theoretical analysis is supported by the experimental observation of macro-macro correlations with an average number of photons of about 10^3. Our results enlighten the practical extreme difficulty of observing non-locality by performing such a dichotomic fuzzy measurement.

4.1 Quantum to classical transition

For long time the investigation about entanglement and non-locality has been limited to quantum systems of small size [Bel64]. Theoretical and experimental works on Bell's inequalities have been devoted to the study of single particle states, in which dichotomic measurements have been performed [CHSH69]. Non-locality tests have been achieved with single photon states, produced by parametric down conversion, by detecting polarization correlations [AS98, OM88, KSSA98]. More recently the violation of Bell's inequality has been performed with a larger number of photons: on GHZ [CYZ$^+$06] and cluster states [WARZ05] up to 4 photons.
On the other hand, the possibility of observing quantum phenomena at a macroscopic

level seems to be in conflict with the classical description of our everyday world knowledge. The main problem for such observation arises from the experimental difficulty of sufficiently isolating a quantum system from its environment, i.e., from the decoherence process [Zur03]. An alterative approach to explain the quantum-to-classical transition, conceptually different from the decoherence program, has been given, very recently, by Kofler and Brukner, along the idea earlier discussed by Bell, Peres [Per95] and others. They have given a description of the emergence of macroscopic realism and classical physics in systems of increasing size *within quantum theory* [KB07]. They focused on the limits of the quantum effects observability in macroscopic objects, showing that, for large systems, macrorealism arises under coarse-grained measurements. More specifically they demonstrated that, while the evolution of a large spin cannot be described classically when sharp measurement are performed, a fuzzy measurement on a large spin system would induce the emergence of the Newtonian time evolution from a full quantum description of the spin state. However, some counterexamples to such modelization have been found later by the same authors: some non classical Hamiltonians violate macrorealism despite coarse-grained measurements [KB08]. One example is given by the time-dependent Schrödinger catlike superposition, which can violate macrorealism by adopting a suitable "which hemisphere" measurement. Therefore the measurement problem seems to be a key ingredient in the attempt of understanding the limits of the quantum behavior of physical systems and the quantum-to-classical transition question. As a further step, they also demonstrated [KBB09] that macrorealism does not imply a continuous spatiotemporal evolution. Indeed, they showed that the same Schrödinger catlike non-classical Hamiltonian, in contact with a dephasing environment does not violate any longer a Leggett-Garg inequality, while it still presents a non-classical time evolution. In a recent paper Jeong et al. [JPR09] contribute to the investigation about the possibility of observing the quantum features of a system when fuzzy measurement are performed on it, finding that extremely-coarse-grained measurements can still be useful to reveal the quantum world where local realism fails.

In this context, the possibility of obtaining macroscopic quantum systems in laboratory has raised the problem of investigating entanglement and non locality in systems in which single particles cannot be addressed singularly. As shown in Ref. [CPHZ02], the demonstration of non-locality in a multiphoton state produced by a non-degenerate optical parametric amplifier would require the experimental application of parity operators. On the other hand, the estimation of a coarse grained quantity, through collective measurements as the ones proposed in Ref. [PDS$^+$06], would miss the underlying quantum structure of the generated state, introducing elements of local realism even in presence of strong entanglement and in absence of decoherence. The theoretical investigation on a multiphoton system, obtained via parametric down conversion, has been also carried out by Reid et al. [RMD02]. They analyzed the possibility of obtaining the violation of Bell's inequality by performing dichotomic measurement on the multiparticle quantum state. More specifically, in analogy with the spin formalism, they proposed to compare the num-

ber of photons polarized "up" with the number of photons polarized "down" at the exit of the amplifier. The result of this comparison could be either (+1) or (-1) hence the measurement on the multiphoton state turned out to be dichotomic. In such a way Reid et al. revealed a small violation of the multiparticle Bell's inequality even in presence of losses and quantum inefficiency of detectors. It's worth nothing that this violation presents a fast decreasing behavior as a function of the generated photons number. In a recent paper, Bancal et al. [BBB$^+$08] have discussed different techniques for testing Bell's inequalities in multipair scenarios, in which either at Alice's and Bob's site a global measurement is performed. They distinguished between two cases: distinguishable, i.e. independent, and indistinguishable, i.e. belonging to the same spatial and temporal mode, photon pairs. They found that while the state of indistinguishable pairs results more entangled, the state of independent pairs appears to be more nonlocal.

In this chapter, we investigate the macroscopic-macroscopic state generated by high gain spontaneous parametric down-conversion. The possibility of observing quantum correlations in macroscopic quantum systems through dichotomic measurement will be analyzed, by addressing two different measurement schemes, based on different dichotomization processes. More specifically, we will investigate the persistence of non-locality in an increasing size $\frac{n}{2}$-spin singlet state by studying the change in the correlations form as n increases, both in the ideal case and in presence of losses. At last, experimental observation of macro-macro correlations will be reported. The results obtained enlighten that dichotomic fuzzy measurements lack of the necessary resolution to characterize such states and show the extreme difficulty to observe quantum non-locality in this experimental configuration.

4.2 Macroscopic quantum state based on high gain spontaneous parametric down-conversion

The investigation on the micro-macro transition will be performed on a paradigmatic physical system: the optical parametric amplifier working in a high gain regime. The quantum state produced in a low gain regime has been experimentally realized and deeply studied in the past few years [EKD$^+$04, CDP$^+$06]. We are now interested in analyzing the behavior of such quantum system when the number of photons is increased and it undergoes a fuzzy measurement, in which the generated particles cannot be addressed singularly, but a dichotomic measurement is performed on the overall state. More specifically, the radiation field under investigation is the quantum state obtained by spontaneous parametric down-conversion (SPDC) with an EPR type-II source [KMW$^+$95, EKD$^+$04], whose interaction Hamiltonian is: $\mathscr{H}_{int} = \imath\hbar\chi\left(\hat{a}^\dagger_\pi \hat{b}^\dagger_{\pi_\perp} - \hat{a}^\dagger_{\pi_\perp}\hat{b}^\dagger_\pi\right) + \text{H.c.}$ where $\hat{a}^\dagger_\pi$ and $\hat{b}^\dagger_\pi$ are the creation operators corresponding to the generation of a π-polarized photon on spatial modes $\mathbf{k}_A$ and $\mathbf{k}_B$, as sketched in Fig.4.1, and χ is the constant describing the strength of the interaction.

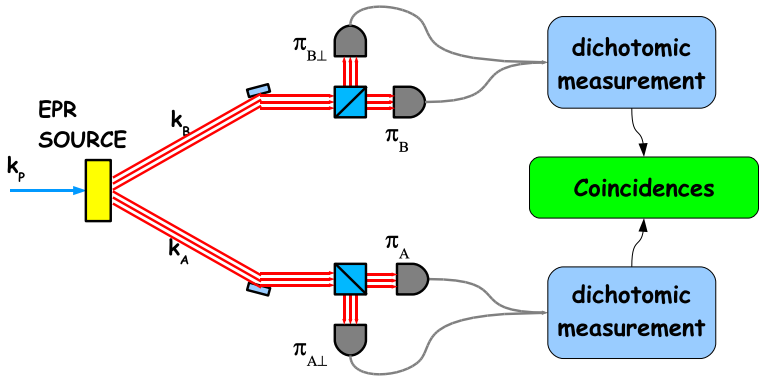

Figure 4.1: Conceptual scheme of the macroscopic-macroscopic source and of the detection apparatus. The multiphoton fields on the two spatial modes of an EPR source are analyzed in polarization with dichotomic measurements, where the $+1$ value is assigned if $n_\pi > n_{\pi_\perp}$, and -1 otherwise. Finally, coincidences between the two apparata are considered.

The output state reads [EKD+04]:

$$|\Psi^-\rangle = \frac{1}{C^2}\sum_{n=0}^{\infty}\Gamma^n\sqrt{n+1}\,|\psi_n^-\rangle \tag{4.1}$$

$$|\psi_n^-\rangle = \frac{1}{\sqrt{n+1}}\sum_{m=0}^{n}(-1)^m|(n-m)\pi, m\pi_\perp\rangle_A|m\pi,(n-m)\pi_\perp\rangle_B \tag{4.2}$$

where $\Gamma = \tanh g$ and $C = \cosh g$; $g = \chi t$ is the non-linear gain (NL) of the process. Hence, the output state can be written as the weighted coherent superposition of singlet spin-$\frac{n}{2}$ states $|\psi_n^-\rangle$.

As said, this EPR source has been already studied in different gain regimes. First, Kwiat et al. [KMW+95] exploited the polarization singlet-state emitted in the single-pair regime to obtain the violation of Bell's inequalities. Subsequent works studied the multi-photon states generated in a high gain SPDC source. Eibl. et al. [EGB+03] experimentally demonstrated four-photon entanglement in the second-order emission state of the SPDC source, by taking the four-fold coincidences after the two output modes of the source were splitted by 50-50 beam-splitters. A generalized non-locality test [WZ01] was also successfully performed in this configuration. A similar scheme was subsequently exploited by Wieczorek et al. [WSK+08] to experimentally generate an entire family of four-photon entangled states. The presence of polarization-entanglement in the multi-photon states up to 12 photons has been proved by studying the high losses regime where at most one photon per branch was detected [EKD+04]. The density matrix of this two-photons state was analytically derived and experimentally investigated in a more recent work [CDP+06], where it has been demonstrated that it coincides with the one of a Werner state (WS), i.e., a weighted superposition of a maximally entangled singlet state with a

fully mixed state. However, no experimental demonstration of entanglement and non-locality has been given in the multi-photon regime where the generated state does not undergo to a controlled lossy detection scheme.

4.3 Dichotomic measurements on macroscopic states

In the context of the investigation on entanglement and non-locality between macroscopic systems, Bell's inequalities have been generalized to many particle regimes. Among various strategies, several possible extensions of dichotomic measurements in the macroscopic regime have been presented [RMD02, BBB$^+$08]. By these methods, CHSH-type inequalities can be exploited in order to perform non-locality tests also in many-particle collective states.

In this section we analyze two possible kind of dichotomic measurements on macroscopic states, based on photon counting and signal processing techniques. The first technique is based on the Orthogonality-Filter (O-Filter) device [NDSD07, DSV08], which has already been introduced in the previous chapter to test experimentally the entanglement between a microscopic and a macroscopic field. This method has several analogies with the detection strategy presented in Ref. [SBB$^+$09] and attributed to a biological "human eye" detector. The second technique is a threshold dichotomic detection scheme, whose action is independent on the input state and hence can be exploited for a Bell's inequalities test.

4.3.1 Orthogonality Filtering

The first dichotomic measurement technique we analyze in this section is based on the O-Filter (OF) device introduced in the previous chapter. We utilize now this technique in a different experimental framework. Let us now give a formal description of this measurement technique in the POVM framework. First, the incident radiation is analyzed in polarization by a couple of photon-number resolving detectors on each spatial mode $\{\mathbf{k}_A, \mathbf{k}_B\}$. In the ideal case, this measurement corresponds to the projection of the impinging field onto the Von Neumann operators: $\hat{\Pi}_{n,m} = |n\pi, m\pi_\perp\rangle\langle n\pi, m\pi_\perp|$, where $|n\pi, m\pi_\perp\rangle$ represents a quantum state with n photons with polarization π and m photons with polarization $\pi_\perp$. Subsequently, the dichotomization of the measurement corresponds to assign the value (+1) if $n_\pi - m_{\pi_\perp} > k$, (-1) if $m_{\pi_\perp} - n_\pi > k$, and (0) otherwise (Fig.4.2-(a)). This choice of the detection scheme corresponds to the POVM operators:

$$\hat{F}^{(+1)}_{\pi,\pi_\perp}(k) = \sum_{n=k}^{\infty}\sum_{m=0}^{n-k}\hat{\Pi}_{n,m} \tag{4.3}$$

$$\hat{F}^{(-1)}_{\pi,\pi_\perp}(k) = \sum_{m=k}^{\infty}\sum_{n=0}^{m-k}\hat{\Pi}_{n,m} \tag{4.4}$$

$$\hat{F}^{(0)}_{\pi,\pi_\perp}(k) = \hat{I} - \hat{F}^{(+1)}_{\pi,\pi_\perp} - \hat{F}^{(-1)}_{\pi,\pi_\perp} \tag{4.5}$$

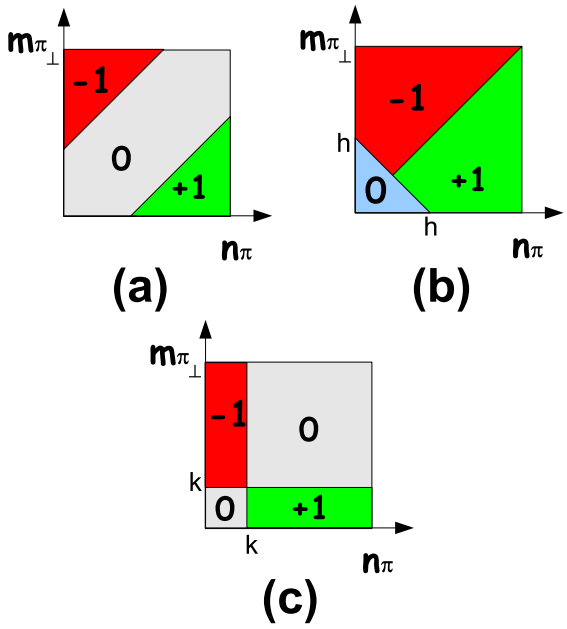

Figure 4.2: Selected regions of the Fock space for the two presented measurement schemes. Each diagram in this figure is referred to a single spatial mode. (a) O-Filtering technique representation in the bidimensional Fock-Space $\{n_\pi, m_{\pi_\perp}\}$. The (+1) and (-1) regions correspond to a difference in the detected photon numbers $|n_\pi - m_{\pi_\perp}| > k$. The (0) region corresponds to an inconclusive measurement. (b) Dichotomic threshold measurement representation in the bidimensional Fock-Space $\{n_\pi, m_{\pi_\perp}\}$. Only those pulses containing a sufficiently high photon number can be detected due to the threshold response of the apparatus. Then, a dichotomic assignment is performed on the measurement outcomes. (c) Response of "biological" detectors, which are sensible to the impinging field only if the photon number exceeds an intrinsic threshold k.

The discarded outcome (white region in Fig.4.2-(a)) turns out to be state dependent. This property, as we shall see later, renders this kind of dichotomic measurement unfeasible for applications in Bell's inequalities test.

4.3.2 Threshold detection

We now introduce a different dichotomic measurement method which is based on a threshold detection scheme. Let us consider the following apparatus. As in the OF case, the incident field is analyzed in polarization on each spatial mode by photon-counting detectors, and the Von Neumann operators that describe this intensity measurement are again the $\hat{\Pi}_{n,m}$ projectors. The dichotomization of the measurement then proceeds as follows (Fig. 4.2-(b)). The (+1) outcome is assigned when the threshold condition $n_\pi + m_{\pi_\perp} > h$ is satisfied and when $n_\pi > m_{\pi_\perp}$. Analogously, the (-1) outcome is assigned in the opposite case $n_\pi < m_{\pi_\perp}$ conditionally to the satisfaction of the threshold condition $n_\pi + m_{\pi_\perp} > h$. If $n_\pi = m_{\pi_\perp}$, one of the two outputs (± 1) is assigned with equal probability $p = 1/2$. The

POVM operators that describe the measurement can then be written in the form:

$$\hat{T}^{(+1)}_{\pi,\pi_\perp}(h) = \sum_{n=h}^{\infty} \sum_{m<\frac{n}{2}} \hat{\Pi}_{n-m,m} \tag{4.6}$$

$$\hat{T}^{(-1)}_{\pi,\pi_\perp}(h) = \sum_{n=h}^{\infty} \sum_{m>\frac{n}{2}} \hat{\Pi}_{n-m,m} \tag{4.7}$$

$$\hat{T}^{(0)}_{\pi,\pi_\perp}(h) = \hat{I} - \hat{T}^{(+1)}_{\pi,\pi_\perp} - \hat{T}^{(-1)}_{\pi,\pi_\perp} \tag{4.8}$$

We note that the choice of the threshold h is made independently on the input state, and it is an intrinsic property of the detection apparatus. Furthermore, this scheme has the peculiar property of selecting an invariant region of the Fock space with respect to rotations of the polarization basis. More specifically, let us consider the case in which the measurement is performed choosing a polarization basis $\pi, \pi_\perp$. With that choice, all the pulses for which $n_\pi + m_{\pi_\perp} \leq h$ are not detected. Rotating the basis to $\pi', \pi'_\perp$, the undetected part of the wave function still corresponds to the application of the same threshold condition in the new basis $n_{\pi'} + m'_{\pi_\perp} > h$. Hence, the filtered Fock-space region is independent on the choice of the polarization basis but is a function only of the threshold h, which is an intrinsic property of the detection apparatus. This feature is the main difference with the OF device discussed in previous section, and renders the TD based detection strategy feasible for its implementation in Bell's inequalities tests.

4.4 Bell's inequalities between macroscopic photonic states

In this section we perform a theoretical investigation on non-locality in a specific macroscopic quantum system analyzed with the threshold detection apparatus previously introduced. Specifically, we investigate the quantum correlations between the fields associated to modes $\mathbf{k}_A$ and $\mathbf{k}_B$ of the state of Eq.(4.1) by using the dichotomic measurements described in the previous section. More specifically, we derive the interference fringe pattern obtained by varying the polarization analysis basis on mode $\mathbf{k}_B$. As a first step, we consider individually the singlet spin-$\frac{n}{2}$ states (4.2), and we subsequently extend the results to the SPDC output superposition state of Eq. (4.1). To generalize the results to a realistic detection and transmission apparatus, we numerically simulate the effect of losses and non-unitary detection efficiency in the interference fringe pattern. Finally, we address the problem of non-locality by investigating a CHSH inequality for this detection apparatus, studying how the amount of violation is modified by the increase in the photon's number n.

4.4.1 Interference fringe pattern on singlet spin-$\frac{n}{2}$ states

We begin our analysis on the macroscopic-macroscopic state by evaluating the correlations existing between the two spatial modes of the spin-$\frac{n}{2}$ singlet states (Eq.(4.2)). We

use a pure dichotomic measurement scheme, where the (+1) and (-1) outcomes are assigned whether the difference in the number of photons with two orthogonal polarization is positive or negative. Finally, if the detected difference in the number of photons is 0, one of the (± 1) outcomes is randomly assigned to the event with equal probability $p = 1/2$. We note that this choice is a subcase of the threshold detection and O-filtering methods introduced in the previous Section, corresponding to the values $h = 0$ and $k = 0$.

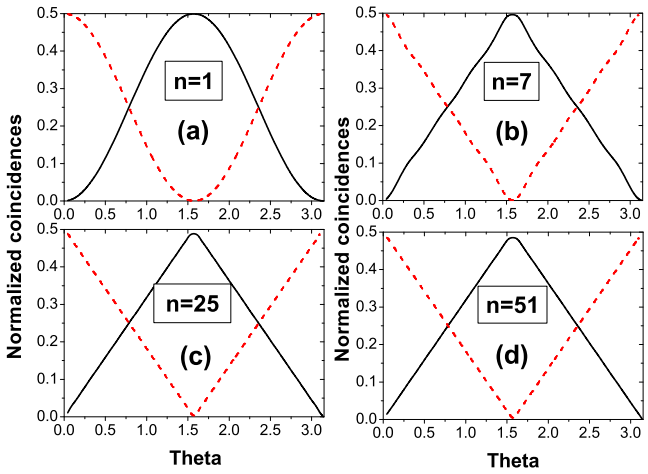

Figure 4.3: Theoretical interference fringe-patterns for singlet spin-$\frac{n}{2}$ states. The polarization basis on mode $\mathbf{k}_A$ is kept fixed while on mode $\mathbf{k}_B$ the basis is varied to obtain the fringe pattern. Figures correspond to values of (a) $n = 1$, (b) $n = 7$, (c) $n = 25$ and (d) $n = 51$. The sinusoidal pattern of the spin-$\frac{1}{2}$ progressively transforms into a linear pattern. In all figures, black continuous line corresponds to the coincidences of both the (+1,+1) and (-1,-1) outcome configurations, while red dashed line corresponds to the (+1,-1) and (-1,+1) outcomes on the two spatial mode. Note that the maximum for each fringe is 0.5, which is the probability to obtain one of the two possible anti-correlated outcomes $(\mp 1, \pm 1)$.

The scheme for evaluating the correlations is sketched in Fig. 4.1. The two spatial modes of the $|\psi_n^-\rangle$ are analyzed with the dichotomic measurement apparatus here described. The polarization's basis on mode $\mathbf{k}_A$ is fixed on $\{\vec{\pi}_+, \vec{\pi}_-\}$, while on mode $\mathbf{k}_B$ the analysis basis is varied over the Bloch sphere. In particular, due to the SU(2) symmetry of the emitted states, it is sufficient to consider only the linear polarizations case, defined by the rotation: $\vec{\pi}_\theta = \cos\theta\,\vec{\pi}_+ + \sin\theta\,\vec{\pi}_-$. The fringe patterns are then obtained by evaluating the coincidences between the outcomes of the two detection apparatus on modes $\mathbf{k}_A$ and

$\mathbf{k}_B$. More specifically, this measurement corresponds to the evaluation of the averages:

$$\begin{aligned} D^{(\pm1,\pm1)}_{|\psi_n^-\rangle}(\theta) &= \langle\psi_n^-|\left(\hat{T}^{(\pm1)}_{+,-}(0)\right)_A \otimes \left(\hat{T}^{(\pm1)}_{\theta,\theta_\perp}(0)\right)_B |\psi_n^-\rangle \\ &= \langle\psi_n^-|\left(\hat{F}^{(\pm1)}_{+,-}(0)\right)_A \otimes \left(\hat{F}^{(\pm1)}_{\theta,\theta_\perp}(0)\right)_B |\psi_n^-\rangle \end{aligned} \tag{4.9}$$

The calculation of this measurement has been analytically performed by expressing the singlet spin-$\frac{n}{2}$ states of eq.(4.2) in the analyzed polarization basis:

$$|\psi_n^-\rangle = \sum_{m=0}^{n}\sum_{p=0}^{n} \varepsilon^n_{m,p}(\theta)\,|(n-m)+,m-\rangle_A\,|p\theta,(n-p)\theta_\perp\rangle_B \tag{4.10}$$

where:

$$\begin{aligned} \varepsilon^n_{m,p}(\theta) = &\sum_{q(m,p)} (-1)^q \alpha_\theta^{m+p-2q}\beta_\theta^{n-m-p+2q} \\ &\left[C^{n-m}_{p-q}C^{n-p}_{m-q}C^m_q C^p_q\right]^{\frac{1}{2}} \end{aligned} \tag{4.11}$$

with $\alpha_\theta = \cos\theta$, $\beta_\theta = \sin\theta$ and $C^i_j = \frac{i!}{j!(i-j)!}$ is the binomial coefficient. The limits of the sum over q have an explicit dependence on the values of p and m and are not reported here. Finally, by direct application of the measurement operator, the interference fringe patterns are evaluated as:

$$D^{(\pm1,\pm1)}_{|\psi_n^-\rangle}(\theta) = \sum_{\{m,p\}} |\varepsilon^n_{m,p}(\theta)|^2 \tag{4.12}$$

The extension of the sums over m and p depends on the choice of the outcome on each spatial mode according to the definitions of Eqs.(4.3-4.5) and (4.6-4.8).

In Fig.4.3 we report the results obtained for different values of the number of photons n. The simplest case, corresponding to a spin-$\frac{1}{2}$ state, presents the well-known sinusoidal pattern, as shown in Fig. 4.3-(a). The sinusoidal pattern is responsible for the violation of Bell's inequalities as no classical system can present this dependence from the phase θ. For progressively higher values of n, as shown in Fig. 4.3-(b-d), the fringe pattern changes its dependence from the phase from a sinusoidal to a linear form. The latter represents the typical response of a pair of classically anti-correlated spin-**J** systems, analyzed through a dichotomic "which hemisphere" measurement [Red], i.e. the measurement of the angular momentum sign.

Such detection scheme is completely analogous to the dichotomic strategy analyzed in this section.

The transition with increasing n towards a classical response for the singlet spin-$\frac{n}{2}$ can be explained observing that the chosen dichotomic detection scheme is no more sufficient to fully characterize the singlet spin states of increasing size $n > 1$. This measurement lacks of the necessary resolution [CHRB] to observe the peculiar quantum properties of these states. In other words, this measurement scheme is not sufficient to fully extract the

information encoded in the polarization anti-correlation of the singlet spin states. Their characterization would require a more sophisticated detection apparatus able to discriminate the value m of the spin projection, i.e. in our case the difference in the orthogonally polarized photon number, and not only its sign. An example of such measurement [Per95] is given by the parity operator $\hat{P}_{\pi,\pi_\perp} = \sum_{m=0}^{n}(-1)^m |(n-m)\pi, m\pi_\perp\rangle\langle(n-m)\pi, m\pi_\perp|$.

The correlation between the two spatial modes of the singlet spin-$\frac{n}{2}$ states evaluated with this measurement operator leads to the following expression:

$$\begin{aligned} P_{|\psi_n^-\rangle}(\theta) &= \langle\psi_n^-| \left(\hat{P}_{+,-}\right)_A \otimes \left(\hat{P}_{\theta,\theta_\perp}\right)_B |\psi_n^-\rangle \\ &= (-1)^n \frac{\sin[(n+1)\theta]}{(n+1)\sin\theta} \end{aligned} \tag{4.13}$$

This correlation function violates a CHSH inequality of an amount $S_{CHSH} = 2.481 > 2$ [Per95] even in the asymptotic limit of large number of particle ($n \to \infty$). However, such scheme based on the parity operator requires a sharp photon number measurement in order to discriminate with unitary efficiency among contiguous values of the spin projection.

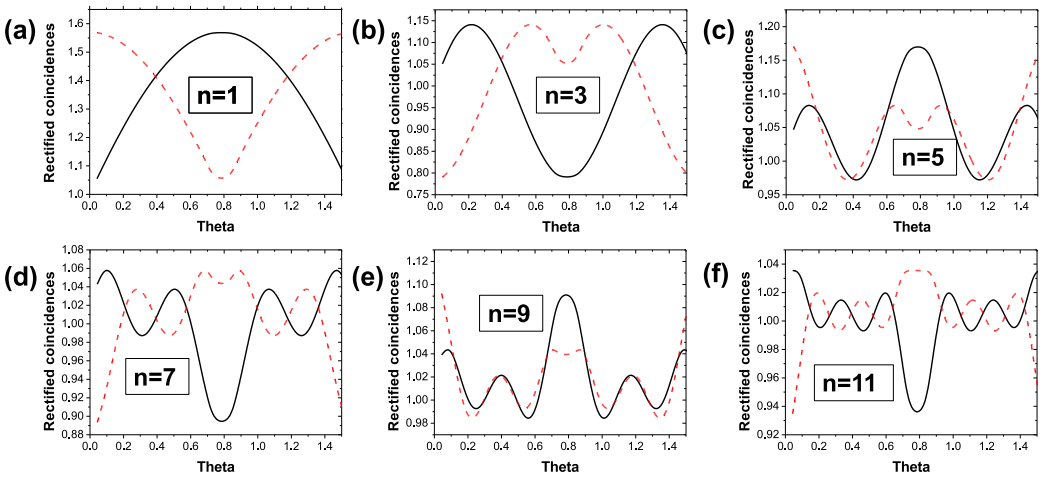

Figure 4.4: Plot of the interference fringe pattern $D^{(\pm1,\pm1)}_{|\psi_n^-\rangle}(\theta)$ for singlet spin- $\frac{n}{2}$ states divided by a linear function $L(\theta)$ corresponding to the behavior of two distinct classical macroscopic objects.

As a further analysis, let us plot (Fig.4.4) the function $D^{(\pm1,\pm1)}_{|\psi_-^n\rangle}(\theta)/L(\theta)$, which corresponds to the ratio between the interference fringe pattern of the macro-macro configuration and a linear function of θ. The choice of the curve $L(\theta)$ as a reference is motivated by the following consideration. The evaluation of the CHSH parameter in a system characterized by the linear response leads to the maximum value in a classical framework $S_{CHSH} = 2$. Hence, this function $L(\theta)$ can be considered as the boundary between the "classical" and the "quantum" regions, since it represents the response of two classical

anti-correlated systems to this test. In Fig.4.4, we note that the ratio $D^{(\pm1,\pm1)}_{|\psi^n_-\rangle}(\theta)/L(\theta)$ presents a number of intersections with the axis $y = 1$ (unitary ratio) proportional to the value of n. This depends on the explicit functional form of the interference fringe pattern of Eq.(4.12). Indeed, analyzing the explicit expression (Eq.(4.11)) of the coefficients $\varepsilon^n_{m,p}(\theta)$, we find a sum of terms $(\cos\theta)^{m+p-2q}\,(\sin\theta)^{n-m-p+2q}$, where the sum of the exponents is equal to the number of photons n. Hence, the fringe pattern $D^{(\pm1,\pm1)}_{|\psi^n_-\rangle}(\theta)$ (Eq.(4.12)) can be re-organized in a Fourier series expansion containing all the Harmonics up to $k = 2n$. With increasing n, the difference between $D^{(\pm1,\pm1)}_{|\psi^n_-\rangle}(\theta)$ and the linear function $L(\theta)$ is progressively reduced, since more harmonics are present in the Fourier expansion which asymptotically reaches the expansion of $L(\theta)$.

In conclusion, the increase in the number of photons renders the dichotomic measurement inefficient for the complete characterization of the state, and the decreased correlations become more similar to classical ones.

4.4.2 Propagation over a lossy channel

Decoherence in macroscopic systems represents the main cause for the impossibility of observing quantum phenomena in every-day life and for the realization of quantum experimental schemes. In the previous section we described a correlation experiment based on dichotomic detection in an ideal setup, where both the transmission channel and the detection apparatus possess unitary quantum efficiency. However, in real setups loss in both stages must be considered. Hence, the investigation on the effects of decoherence allows to understand both the transition from the quantum to the classical world and the feasibility of the schemes here presented in order to violate the Bell's inequalities.

To this end, we introduce a beam-splitter model [Lou00, Leo93] to simulate losses phenomena on the macroscopic field here analyzed. In particular, the analysis has been performed for any singlet spin-$\frac{n}{2}$ state which, in the decoherence-free case, exhibits the transition from a sinusoidal interference pattern ($n = 1$) to an asymptotic linear interference fringe pattern ($n \gg 1$). Again, the detection scheme used is a pure dichotomic measurement apparatus (corresponding to the threshold detector and a O-Filter with $h = k = 0$). As the measurement operators of Eqs. (4.3-4.8) are linear combination of Fock-state projectors, the lossy channel can be simulated numerically. More specifically, our calculation is divided in the following steps. First, for a set of angles θ of the analysis basis on spatial mode $\mathbf{k}_B$, we calculated the coefficients of the state $\varepsilon^n_{m,p}(\theta)$ defined in Eq.(4.11). As the measurement operators are diagonal in the Fock basis, the results of the measurement depend only on the diagonal part of the density matrix after losses. Furthermore, the map that describes the lossy process, i.e. $\mathscr{L}[\hat{\rho}] = \sum_k \gamma_k \hat{a}^k \hat{\rho} \hat{a}^{\dagger k} \gamma_k^\dagger$ where $\gamma_k = \frac{1}{\sqrt{k!}}(1-\eta)^{k/2}\eta^{(\hat{a}^\dagger\hat{a})/2}$, maps diagonal elements in diagonal elements of the density matrix. All these considerations allow us to focus our numerical analysis on the diagonal part of the density matrix. The numerical simulation proceeds as follows. Let us for example focus our attention on the (+1,+1) joint outcome. The coefficients of the

distribution $|\varepsilon^n_{m,p}(\theta)|^2$ are arranged in a matrix form, labeled by the row and column indexes (m,p). For each value of m and p, 4 binomial random number generators with average values respectively $\{(n-m)\eta, m\eta, p\eta, (n-p)\eta\}$ simulate a single shot passage of the $|(n-m)+,m-\rangle_A \otimes |p\theta,(n-p)\theta_\perp\rangle_B$ element through the lossy channel of efficiency η. Then, the output number of photons transmitted by the channel on each spatial mode are dichotomically compared, assigning 1 to the event if it belongs to the (+1,+1) joint outcome configuration and 0 otherwise. We then repeat this procedure N times, averaging the results of the simulation for each value m and p, thus generating a matrix $M^{(+1,+1)}_{m,p}$ containing both the transmission and the measurement processes. Finally, the point $D^{(+1,+1)}_{\hat{\rho}^-_{n,\eta}}(\theta)$ is reconstructed combining the matrix $M^{(+1,+1)}_{m,p}$ that describes the dynamical process and the original photon number distribution of the state in the chosen basis, according to:

$$D^{(+1,+1)}_{\hat{\rho}^-_{n,\eta}}(\theta) = \sum_{m,p=0}^{n} M^{(+1,+1)}_{m,p} |\varepsilon^n_{m,p}(\theta)|^2 \tag{4.14}$$

The same procedure is applied for the other three outcomes of the joint dichotomic measurements. The results of the simulation for different values of the channel transmittivity η are reported for a fixed value of $n = 51$ in Fig.4.5. As the efficiencies of the channel and the detection scheme decrease, the linear fringe patterns progressively evolve into sinusoidal ones, at the cost of a smaller value of the visibility.

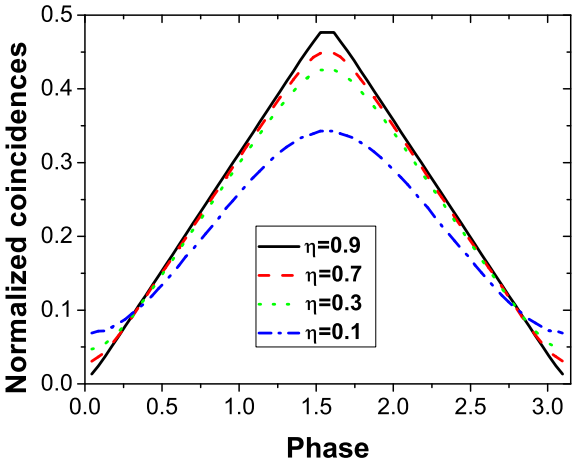

Figure 4.5: Interference fringe pattern in presence of losses for the singlet spin-$\frac{n}{2}$ state for $n = 51$. The effect of the lossy channel is the progressive lowering of the visibility, while the dependence on the phase changes from a linear to a sinusoidal pattern.

4.4.3 O-Filtering and Threshold detection in a lossy regime

The analysis performed on the correlations present in the singlet spin-$\frac{n}{2}$ states has been focused on the detection by a pure dichotomic scheme. We are now interested in observing the effects of more sophisticated POVM measurements, as the threshold detection or the O-filtering methods introduced in Section 4.3. In particular, we analyze how both the visibility and the form of the fringe pattern are modified exploiting this different measurement schemes. The main idea beyond this approach concerns the possibility of beating the losses effects on the macro-macro correlations, by using a more sophisticated measurement than a pure dichotomic one.

We first analyze the correlations obtained by the O-Filtering detection scheme, introduced in Section 4.3.1. The fringe pattern can be calculated by evaluating the average:

$$F^{(\pm 1,\pm 1)}_{|\psi_n^-\rangle}(\theta,h) = \left\langle \left(\hat{F}^{(\pm 1)}_{+,-}(h)\right)_A \otimes \left(\hat{F}^{(\pm 1)}_{\theta,\theta_\perp}(h)\right)_B \right\rangle \tag{4.15}$$

We performed a numerical simulation, in order to consider also the transmission over a lossy channel, with a procedure analogous to the one described in the previous section. We report in Fig.4.6 the fringe pattern obtained for the $n = 51$ singlet states for two values of the channel efficiency. We note that, as the OF threshold k is increased, the tails of the fringe pattern are damped, while the form of the fringe around the peaks remains unchanged. Furthermore, both the minimum and the maximum of the fringes are lowered by this filtering procedure. To understand the advantage of this measurement scheme with respect to the pure dichotomic case, we analyze in Fig.4.8 the trend of visibility of the fringe pattern as a function of the threshold. We note that, for increasing k, the visibility is increased by the filtering process. This advantage obtained by exploiting the O-filtering measurement can be explained by the following considerations. In absence of losses, the visibility of the fringe pattern is always unitary, as the analyzed state presents perfect polarization anti-correlations. After the transmission over a lossy channel, the binomial statistics added to the photon number distribution is responsible for the partial cancelation of this property. More precisely, if the difference between n_π and $m_{\pi_\perp}$ on any of the two spatial mode is little, losses may invert the outcome of a dichotomic measurement, i.e. for example the (+1) outcome may be converted to the (-1) outcome if unbalanced losses occur in that specific event. Such a process can generate the occurrence in the joint measurement of a result with positive correlations, i.e. (+1,+1) or (-1,-1), where in the decoherence-free case only anti-correlations are present. Thus, the visibility of the fringe pattern can be reduced by the presence of losses. However, to invert the outcome of matrix elements with $n_\pi - m_{\pi_\perp} = q \gg 0$, a strongly unbalanced losses in a single shot for the two polarization modes must occur. This event has a decreasing probability as the difference q becomes larger. Since the O-filter device selects these zones of the Fock space which present such unbalancement, the outcome inversion becomes practically negligible and the visibility of the fringe pattern progressively returns unitary as the threshold k is increased.

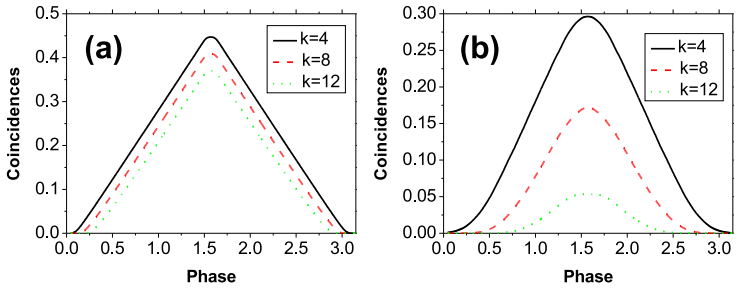

Figure 4.6: Effect of the O-Filtering detection technique on the fringe pattern of a $n = 51$ singlet state. (a) Transmittivity $\eta = 1$ and (b) transmittivity $\eta = 0.3$. As the threshold k is increased, the tails of the fringe pattern are rounded.

Let us now consider the second POVM dichotomic measurement under investigation, the threshold detection TD. The interference fringe pattern with this measurement scheme can be calculated as:

$$T^{(\pm1,\pm1)}_{|\psi_n^-\rangle}(\theta,k) = \left\langle \left(\hat{T}^{(\pm1)}_{+,-}(k)\right)_A \otimes \left(\hat{T}^{(\pm1)}_{\theta,\theta_\perp}(k)\right)_B \right\rangle \tag{4.16}$$

In this expression, as before, the average is evaluated over the density matrix of the state after the numerical simulation of the lossy channel. In Fig.4.7 we report the form of the fringe pattern for $n = 51$ and two different values of the transmittivity of the channel. As the threshold h is increased, we note that the TD device is responsible for the progressive return of the fringe patterns to their original form in absence of losses, i.e. for high values of n an approximately linear form. This behaviour can be explained as follows. While the original singlet-state has a well definite number of photons, the lossy channel reduces the number of photons to an average of $\eta\langle n\rangle$, with Poissonian fluctuations. At the measurement stage the threshold h in the TD device neglects (Fig.4.2-(b)) the sectors of the Fock-space corresponding to a low number of photons. As h approaches the value $h = n$, only the events in which the original singlet state travels undisturbed in the channel (with probability η^{2n}) are selected, thus restoring the original correlation. We then analyze the effects of this measurement scheme in the visibility of the fringe pattern in Fig.4.8. We note that this quantity increases with a slower rate with respect to the OF apparatus. Differently from the O-filtering case, on each spatial mode the zones of the Fock space in which $n_\pi - m_{\pi_\perp}$ is small are not filtered out, and the increase in the visibility is then much slower with the threshold h. However, also with the TD apparatus the visibility reaches asymptotically the unitary value, since as said for a threshold $h = n$ only the original singlet state, having unitary visibility, is detected.

The analysis carried in this section then shows that both the OF and the TD detection strategies can be used to enhance the fringe pattern visibility in lossy conditions for the singlet spin-$\frac{n}{2}$ states. A comparison between the two schemes shows the better enhancement achievable with the OF device. In Sec.4.4.4, we shall discuss in details the

feasibility of a CHSH test with such measurements.

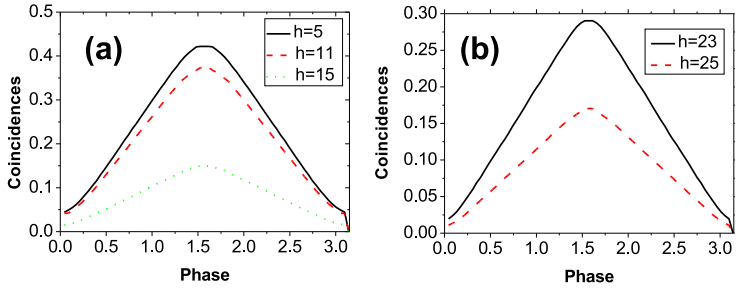

Figure 4.7: Effect of the Threshold detection technique on the fringe pattern for a $n = 51$ singlet state. (a) Transmittivity $\eta = 0.3$ and (b) transmittivity $\eta = 0.5$. As the threshold h on the total photon-number is increased, the fringe patterns progressively return to have approximately a linear dependence from the phase θ, as for the original $n = 51$ singlet state. The values of the thresholds are indicated in the figure.

4.4.4 Investigation of non-locality with a CHSH-type inequality

In the previous paragraphs of this Section we reported the interference fringe pattern obtained evaluating the correlations between singlet spin-$\frac{n}{2}$ states both in absence and in presence of experimental imperfections. The scheme here presented can be exploited to perform a CHSH test [CHSH69] to investigate non-local effects in these multiparticle states.

Let us briefly summarize in the light of a local hidden variable (LHV) theory the content of Bell inequalities for a set of dichotomic observables, by generalizing further the results already obtained by Reid *et al.* [RMD02]. Consider a quantum state described by the density matrix $\hat{\rho}$ defined in the Hilbert space $\mathscr{H}_1 \otimes \mathscr{H}_2$. Define $\hat{O}_a^i$ the positive operator acting on subspace $\mathscr{H}_1$, and the probability of finding the value i after the measurement a as given by $\mathrm{Tr}\left[\hat{\rho}(\hat{O}_a^i \otimes \hat{I})\right]$. The same relation holds for the positive operator $\hat{O}_b^j$ acting on subspace $\mathscr{H}_2$.

The existence of a LHV model implies that the expectation values of the a and b are predetermined by the value of the parameter λ: $\{X_a, X_{a'}, X_b, X_{b'}\}$, hence the product $a \cdot b$ is equal to $X_a(\lambda)X_n(\lambda)$. For a fixed value of λ the variables X_n with $n = \{a, b, a', b'\}$ take the values $-1, 1$ and satisfy the CHSH inequality:

$$X_a(\lambda)X_b(\lambda) + X_a(\lambda)X_{b'}(\lambda) + X_{a'}(\lambda)X_b(\lambda) - X_{a'}(\lambda)X_{b'}(\lambda) \leq 2 \tag{4.17}$$

The same inequality holds by integrating this equation on the space of the hidden variable (λ):

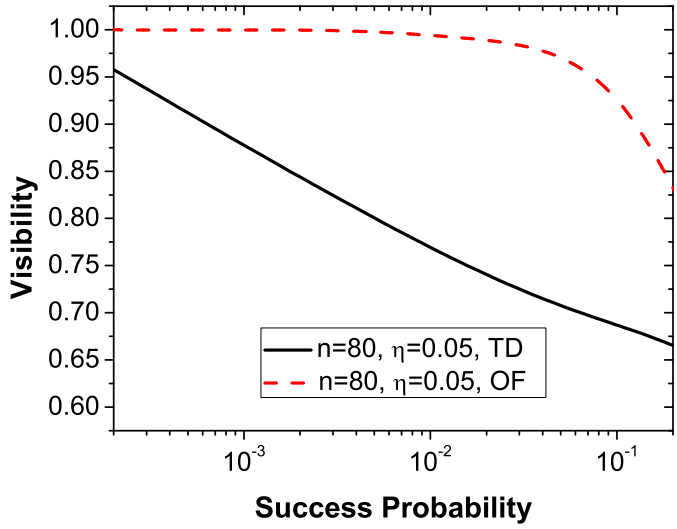

Figure 4.8: Trend of the visibility for the singlet spin states for $n = 80$ and $\eta = 0.05$. The black straight curve corresponds to the TD detection scheme, while the red dashed line to the OF apparatus. In both cases, the success probability is calculated as the sum of the rate for the two conclusive outcomes (+1) and (-1).

$$\int_{\Omega} d\mathbb{P}(\lambda) X_a(\lambda) X_b(\lambda) + \int_{\Omega} d\mathbb{P}(\lambda) X_a(\lambda) X_{b'}(\lambda) + \int_{\Omega} d\mathbb{P}(\lambda) X_{a'}(\lambda) X_b(\lambda) - \int_{\Omega} d\mathbb{P}(\lambda) X_{a'}(\lambda) X_{b'}(\lambda) \leq 2 \tag{4.18}$$

where $P(\lambda)$ is the measure of the λ probability space. If there is a local hidden variables model for quantum measurement taking values $[-1,+1]$, then the following inequality must be satisfied by the measured mean values:

$$S_{CHSH} = E^{\rho}(a,b) + E^{\rho}(a,b^{'}) + E^{\rho}(a^{'},b) - E^{\rho}(a^{'},b^{'}) \leq 2 \tag{4.19}$$

where $E^{\rho}(a,b)$ can be expressed as a function of the LHV as $E^{\rho}(a,b) = \int_{\Omega} X_a(\lambda) X_b(\lambda) d\mathbb{P}(\lambda)$. The violation of (6.23) proves that a LHV variables model for the considered experiment is impossible.

In our case, the positive operators $\hat{O}^{i}_{a(b)}$ are given by the dichotomic measurement operators $\left\{\hat{T}^{(\pm 1)}_{\pi,\pi_{\perp}}(0), \hat{F}^{(\pm 1)}_{\pi,\pi_{\perp}}(0)\right\}$. In order to theoretically investigate the feasibility of a CHSH test on the spin-$\frac{n}{2}$ states, we evaluated the S_{CHSH} parameter in such system. The value of the S_{CHSH} has been numerically maximized over the measurement angles

$\{\theta, \theta', \varphi, \varphi'\}$ of Alice's [$\mathbf{a}(\theta)$ or $\mathbf{a}'(\theta')$] and Bob's [$\mathbf{b}(\varphi)$ or $\mathbf{b}'(\varphi')$] the polarization basis. In Fig.4.9 we report the results obtained for different values of the number of photons, and hence the spin, of the analyzed state. We observe the decrease in the absolute value of $S_{CHSH}^{|\psi_n^-\rangle}$ analogously to what reported in [RMD02, BBB$^+$08] for an equivalent Bell's inequalities test. However, the asymptotic behavior for high n shows that the parameter S_{CHSH} never falls below the classical limit, but the amount of violation progressively becomes smaller and any decoherence process may forbid its experimental observation.

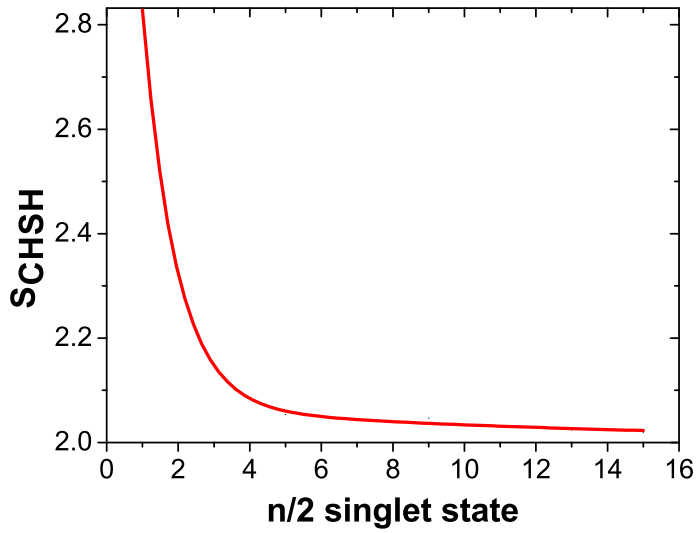

Figure 4.9: Value of the CHSH parameter $S_{CHSH}^{|\psi_n^-\rangle}$ for singlet spin-$\frac{n}{2}$ states for an optimal choice of the angle settings and the dichotomic "majority-voting" measurement. We observe the progressive decrease in the amount of violation for an increasing value of the number of photons present in the state.

We now discuss the feasibility of a Bell's inequality test when the OF and the TD detection methods are adopted in the context of Local Hidden Variables (LHV) models. This analysis is motivated by the increase in the visibility obtained with this measurement operators with respect to the pure dichotomic case. Both strategies present the POVM feature of having three possible outcomes $\{-1, 1, 0\}$, at variance with a genuine dichotomic measurement. In order to clarify the validity of a Bell test in presence of such kind of POVM's, let us consider the case in which at the A site a standard dichotomic measurement is performed, while at the B site a POVM measurement is carried out.

Consider the outcomes for which the Bob's results are different from 0. In this case the expectation value of the product of a and b is conditioned by the event: "outcome b

different from zero". In a LHV model these conditional expectations are represented by:

$$E^{\rho}(a\cdot b)=\int_{\Omega'}X_a(\lambda)X_b(\lambda)d\mathbb{P}'(\lambda) \tag{4.20}$$

where $\Omega^{'}$ is the hidden variable probability sub-space for which, for *any* $X_{b'}(\lambda)$, is $X_b(\lambda)\neq 0$ and $d\mathbb{P}'=d\mathbb{P}/\int_{\Omega'}d\mathbb{P}$. Similarly:

$$E^{\rho}(a\cdot b')=\int_{\Omega''}X_a(\lambda)X_b(\lambda)d\mathbb{P}''(\lambda) \tag{4.21}$$

where $\Omega^{''}$ is the hidden variable probability sub-space for which, for *any* $X_b(\lambda)$, is $X_{b'}(\lambda)\neq 0$ and $d\mathbb{P}''=d\mathbb{P}/\int_{\Omega''}d\mathbb{P}$. Since for different random variables X_b and $X_{b'}$ these conditional expectations values can in principle refer to different subensembles Ω' and Ω" of the original ensemble Ω, in general the equation (6.22) doesn't hold any more and the measured quantity, based on the detection of conditional values, is:

$$\begin{aligned}&\int_{\Omega'}d\mathbb{P}'(\lambda)X_a(\lambda)X_b(\lambda)+\int_{\Omega'}d\mathbb{P}'(\lambda)X_{a'}(\lambda)X_b(\lambda)+\\&\int_{\Omega''}d\mathbb{P}''(\lambda)X_a(\lambda)X_{b'}(\lambda)-\int_{\Omega''}d\mathbb{P}''(\lambda)X_{a'}(\lambda)X_{b'}(\lambda)\end{aligned} \tag{4.22}$$

Let us consider the class of LHV models such that, for a fixed value of λ, simultaneously is: $X_b(\lambda)\neq 0, X_{b'}(\lambda)\neq 0$. In this case the inequality (6.21) still holds since it becomes:

$$\begin{aligned}&\int_{\Omega*}d\mathbb{P}^*(\lambda)X_a(\lambda)X_b(\lambda)+\int_{\Omega*}d\mathbb{P}^*(\lambda)X_a(\lambda)X_{b'}(\lambda)+\\&\int_{\Omega*}d\mathbb{P}^*(\lambda)X_{a'}(\lambda)X_b(\lambda)-\int_{\Omega*}d\mathbb{P}^*(\lambda)X_{a'}(\lambda)X_{b'}(\lambda)\leq 2\end{aligned} \tag{4.23}$$

where Ω^* is the hidden variable probability common subspace for which $X_b(\lambda)\neq 0$ and $X_{b'}(\lambda)\neq 0$.
With reference to our experimental situation, let us now make an auxiliary assumption implying that the probability of rejecting a measurement does not depend on the hidden parameter λ and on the measurement settings, i.e. $\Omega'=\Omega''=\Omega^*$ [AK03]. In this case the experimentally observed quantity (4.22) will follow the LHV inequality (4.23), and its violation implies the non-locality of the considered system. While for what concerns the OF based strategy this assumption on the LHV is a strong one, in the TD case it is legitimated by the fact that the Hilbert subspace leading to a conclusive outcome is invariant under any rotation of the polarization basis since data are excluded depending only on the overall number of photons. In other words, when an event leads to a (± 1) outcome

for a specific choice of the measurement basis, it would correspond to a conclusive outcome if measured in another basis. This scenario is exactly the same encountered in any two-photon Bell inequality test and hence requires a fair sampling assumption.

To conclude the discussion, we briefly analyze the advantages of the two POVM schemes presented here in terms of the achievable violation of the CHSH inequality $S_{CHSH} - 2$. In the OF case, we expect that the fast increase in the visibility may lead to an increase in the amount of violation with respect to the pure dichotomic measurement. In the TD case, as already discussed in the previous section, the effect of the threshold h is the restoration of the original correlations present in the $|\psi_n^-\rangle$ state before the lossy channel. This means that the value of the S_{CHSH} parameter reaches for $h = n$ the maximum value $S_{CHSH}^{|\psi_n^-\rangle}$, reported in Fig.4.9, and the amount of achievable violation becomes practically negligible for large n.

4.4.5 Spontaneous Parametric Down Conversion: interference fringe pattern

The following step of our theoretical analysis is the investigation on the interference fringe pattern obtained by the process of spontaneous parametric down conversion exploiting the dichotomic measurement schemes presented in Sec.4.3. As already stressed in Eqs.(4.1-4.2), this optical source generates a quantum superposition of the singlet spin-$\frac{n}{2}$ states. We performed the same calculation of Sec.4.4.3 in order to analyze both the form of the interference fringe pattern and the trend of the visibility when the two dichotomic measurements (OF and TD) were exploited at the detection stage.

We then report in Fig.4.10 the form of the fringe pattern for the SPDC output state in presence of losses, with $g = 2.5$ and $\eta = 0.5$. Analogously to what observed for singlet spin states, the effect of the two measurement devices is different. On one side, the O-filtering technique is responsible for a smoothing of the fringe pattern tails, while on the other side, the Threshold Detector leaves the form of the fringe pattern unaltered.

To conclude the analysis of this section, we report in Fig.4.11 the trend of the visibility of the fringe pattern as a function of the success probability of the two dichotomic measurement devices. A comparison between the technique shows the faster increase of the visibility in the OF case (Fig.4.11-(a)) with respect to the TD one (Fig.4.11-(b)) The cost of this faster increase in the visibility is a loss in the universality of the device, since the Threshold Detector selects a regions of the Fock space which is invariant under rotations of the polarization basis, at variance with the O-filter.

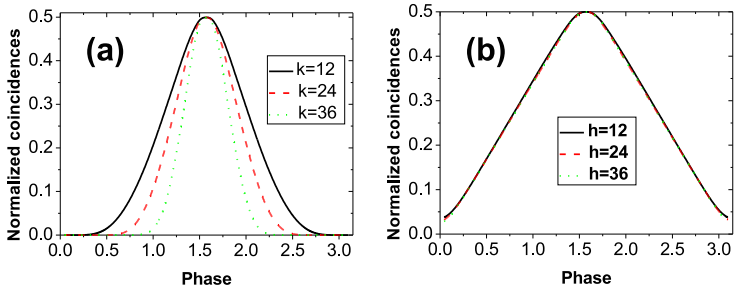

Figure 4.10: Fringe pattern in presence of losses for the SPDC output state with the two different analyzed dichotomic measurements. In all curves, $g = 2.5$ and $\eta = 0.5$. (a) Normalized fringe pattern with the O-filter device for different values of the threshold k. The three curves correspond to a filtering signal of $P(k = 12) = 0.116$ (black straight curve), $P(k = 24) = 0.014$ (red dashed curve) and $P(k = 36) = 2.07 \times 10^{-4}$ (green dotted curve). We note the increase in the smoothing of the minimum of the fringes. (b) Normalized fringe pattern with the TD device for different values of the threshold h. The three curves correspond to a filtered signal of $P(h = 12) = 0.328$ (black straight curve), $P(h = 24) = 0.068$ (red dashed curve) and $P(h = 36) = 1.07 \times 10^{-3}$ (green dotted curve). We note that the form of the normalized fringes is left unchanged by the TD device.

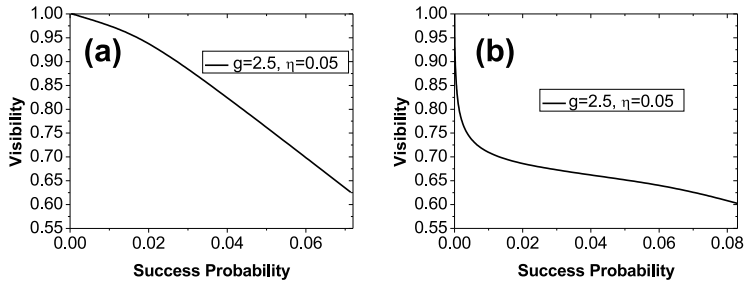

Figure 4.11: (a) Visibility of the fringe pattern as a function of the success probability $\langle \hat{F}^{(+1)}_{\pi,\pi_\perp}(k) \rangle + \langle \hat{F}^{(-1)}_{\pi,\pi_\perp}(k) \rangle$ for the SPDC states analyzed with the OF device. (b) Visibility of the fringe pattern as a function of the success probability $\langle \hat{T}^{(+1)}_{\pi,\pi_\perp}(h) \rangle + \langle \hat{T}^{(-1)}_{\pi,\pi_\perp}(h) \rangle$ for the SPDC states analyzed with the TD device. For both curves, $g = 2.5$ and $\eta = 0.05$.

4.5 Experimental observation of correlations in high gain SPDC

In order to complete our analysis on the correlations connecting a macro-macro state obtained via high gain optical parametric amplification, we have experimentally investigated the conceptual scheme presented in the previous sections. We have generated a multiphoton state through an EPR source and we have performed dichotomic measurement via O-Filter (OF) and Threshold Detector (TD) upon it. In this section we report the experimental interference fringe patterns observed for the spontaneous field generated by the high gain OPA working in a non collinear configuration. As a first step we shall characterize the OPA in a high gain regime, by evaluating the non linear gain of the amplifier and by reporting the generated field fringe pattern visibility as a function of the gain. Then, we shall investigate the features of the multiphoton field through the two measurement strategies studied in Sec. 4.3.

Let us now describe the experimental setup shown in Fig.4.12. The excitation source was a Ti:Sapphire Coherent Mira mode-locked laser amplified by a Ti:Sapphire regenerative RegA device operating with repetition rate 250 kHz. The output beam, frequency-doubled by second-harmonic generation, provided the OPA excitation field beam at the UV wave-length (wl) $\lambda = 397.5$ nm with power 600 mW on mode $\mathbf{k}_P$.The SPDC source was a BBO crystal cut for type-II phase-matching, working in a non-collinear configuration [KMW$^+$95], in a high gain regime. The evaluated non linear gain is $g = 3.49 \pm 0.05$ corresponding to the generation of an average number of photons per mode of $\overline{n} \approx 270$ per pulse, corresponding to an overall average value of $\langle n \rangle \approx 540$ on each spatial mode.

The multiphoton fields on modes $\mathbf{k}_A$ and $\mathbf{k}_B$ were filtered by 1.5 nm interferential filters (IF) and coupled by single mode fibers. The signals were then attenuated, analyzed in polarization and detected by single photon SPCM detectors (not shown in Fig.4.12).

In order to characterize the source, we performed a set of preliminary measurements exploiting a SPCM detector on both spatial modes, deliberately attenuating the generated in order to have only few photons incident on the detector. First, we measured the non-linear gain of the amplifier studying how the detected signal is increased by varying the power of the incident pump beam on the crystal. In Fig.4.13 we report the counts registered on mode $\mathbf{k}_A$ by a SPCM detector as a function of the normalized UV power signal. The evaluation of the NL-gain has been performed as shown in Ref.[EKD$^+$04], and, as said, we found $g = 3.49 \pm 0.05$. As a further investigation on the multiphoton field features, we registered the coincidences between the signals on mode $\mathbf{k}_A$ and $\mathbf{k}_B$, as a function of the phase φ, that represents the variation of the polarization analysis basis on Bob site, i.e. $\vec{\pi}_\varphi = \vec{\pi}_H + e^{i\varphi}\vec{\pi}_V$. Both fields are detected by two SPCM at Alice's and Bob's sites. Again, the signals were attenuated in order to have few photons incident on the detectors, in order to work in a linear response regime for the SPCM. The visibility of the obtained fringe patterns as a function the NL-gain is shown in Fig. 7.7. As stressed in [EKD$^+$04], the trend of visibility decreases as the gain increases, this is due to losses

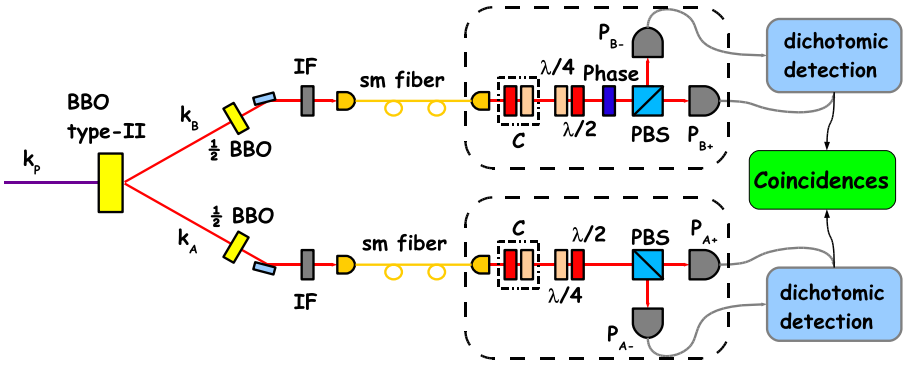

Figure 4.12: Experimental setup for the generation and detection of a bipartite macroscopic field. The high laser pulse on mode $\mathbf{k}_P$ excites a type-II EPR source in the high gain regime, i.e. $g = 3.5$. The two spatial mode $\mathbf{k}_A$ and $\mathbf{k}_B$ are spectrally and spatially selected by interference filters (IF) and single mode fibers. After fiber compensation C, the two modes are analyzed in polarization and detected by four photomultipliers (P_{A+},P_{A-},P_{B+},P_{B-}). The signals are then analyzed electronically to perform either the threshold dichotomic detection described in the paper or the Orthogonality filtering detection technique. Finally, the coincidences between the measurement outcomes are recorded to obtain the desired interference fringe patterns.

and to limited detectors photon number resolution. The decrease of visibility below the theoretical asymptotic value of 33% is due to the multimodal operation of the amplifier, although, differently from what is reported in [EKD$^+$04], we observe a value of visibility that remains above 15% as far as the NL-gain reaches the value of 3.5, while in [EKD$^+$04] the visibility seems to fall below 15% for gain values higher than 2.

4.5.1 Non-collinear SPDC analyzed with the Orthogonality Filter

In this Section we report the observation of the fringe patterns obtained by the O-Filtering measurement strategy illustrated in Sec.4.3-A.
The multiphoton fields at Alice's and Bob's site are analyzed in polarization and detected by two photomultipliers (PMs), (P_{A+},P_{A-}) and (P_{B+},P_{B-}) respectively. This devices produce on each pulse a macroscopic output electronic current, whose amplitude is linearly proportional to the number of incident photons.

Let us fix the polarization analysis basis at Bob's site: the PMs provide the electronic signals (I^B_+,I^B_-) corresponding to the field intensity on the mode $\mathbf{k}_B$ associated with the $\pi-$components $(\overrightarrow{\pi}_+,\overrightarrow{\pi}_-)$, respectively. By the OF, shot by shot the difference signals $\pm(I^B_+ - I^B_-)$ are compared with a threshold $\xi k > 0$, where ξ is a constant describing the response of the photomultipliers. When the condition $(I^B_+ - I^B_-) > \xi k$ is satisfied, a standard transistor-transistor-logic (TTL) electronic square-pulse L_B is realized at one of the two output ports of OF. Likewise, when the condition $(I^B_- - I^B_+) > \xi k$ is satisfied, a L^*_B TTL pulse is realized at other output port of OF. The PM output signals are discarded for

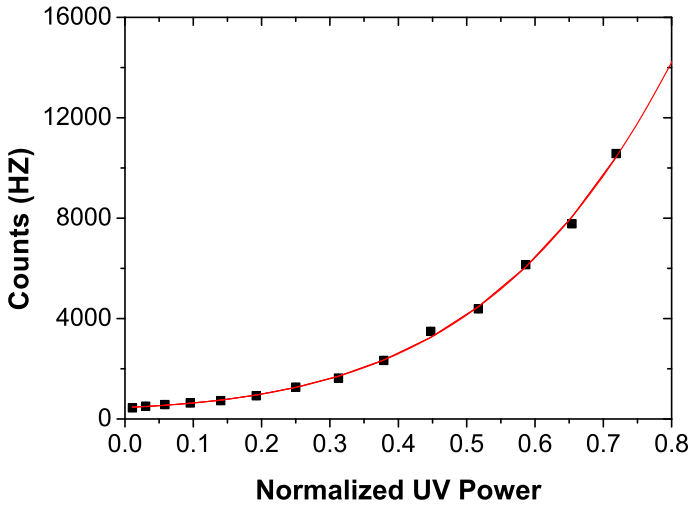

Figure 4.13: Experimental evaluation of the amplifier NL-gain: we report the counts of an SPCM detector on mode $\mathbf{k}_A$ versus the normalized UV power, defined as $I_{\text{in}}/I_{\text{max}}$. The red curve reproduces the best fit of the experimental data, the expected trend function is reported in [EKD$^+$04].

$-\xi k < (I_+^B - I_-^B) < \xi k$, i.e. in condition of low state discrimination. By increasing the value of the threshold k an increasingly better discrimination is obtained together with a decrease of the rate of successful detection. The same measurement strategy is adopted at Alice's site, where the output TTL signals (L_A, L_A^*) are generated. The fringe patterns are obtained by the following procedure: the analysis basis at Alice's site is kept fixed while the basis at Bob's site is varied through an adjustable phase delay given by a Babinet-Soleil compensator. Finally the coincidences between the TTL signals at Alice's and Bob's site are taken into account, namely $(L_A, L_B), (L_A, L_B^*), (L_A^*, L_B), (L_A^*, L_B^*)$. We report in figure 4.15 the corresponding fringe patterns obtained in the $\{\pi_+, \pi_-\}$ basis, analogous results are observed in the $\{\pi_R, \pi_L\}$ and $\{\pi_H, \pi_V\}$ basis, due to the irrotational invariance of the generated multiphoton state. The threshold k was set so that the percentage of data taken into account was 2×10^{-3} of the overall sample.

For sake of completeness we report the trend of visibility as a function of the OF counts in Fig.4.16. We observe an increase of visibility as the counts detected decrease. The highest visibility obtained is not enough to violate the CHSH inequality, due to the inefficiency of a dichotomic measurement performed on a multiphoton quantum state and to experimental imperfections. However, in accordance with theoretical predictions, we observe that the OF technique allows to minimize losses effects.

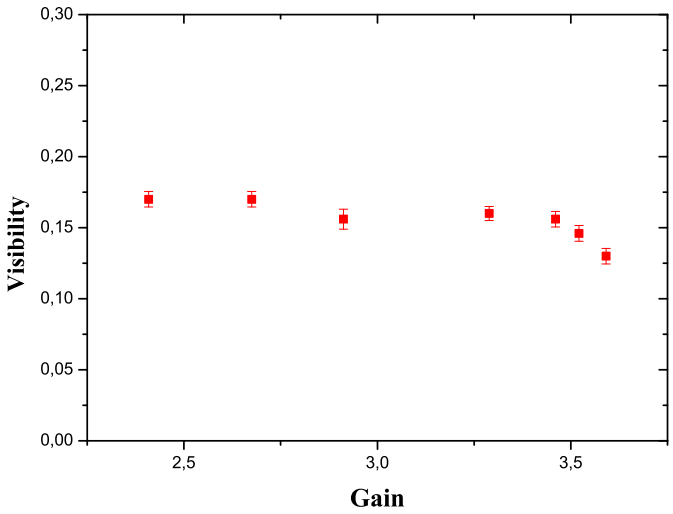

Figure 4.14: Experimental trend of the visibility as a function of the NL-gain.

4.5.2 Non-collinear SPDC analyzed with threshold detection

A further investigation on the macro-macro correlation has been carried out by performing another dichotomic measurement on the amplified states on modes $\mathbf{k}_A$ and $\mathbf{k}_B$. The signals detected by the photomultipliers (P_{A+}, P_{A-}) and (P_{B+}, P_{B-}) enter into two threshold detectors (TD), that performs the shot by shot measurement illustrated in Sec.4.3-B. Each TD works as follows: the PMs electronic signals (I^B_+, I^B_-) $((I^A_+, I^A_-))$ corresponding to the field intensity on the mode $\mathbf{k}_B$ $(\mathbf{k}_A)$, associated with the $\pi-$components $(\overrightarrow{\pi}_+, \overrightarrow{\pi}_-)$ respectively, enter into the TD. By it the sum signals $\pm(I^B_+ + I^B_-)$ $(\pm(I^A_+ + I^A_-))$ are compared with a threshold $\xi h > 0$. When the condition $(I^B_+ + I^B_-) > \xi h$ and $I^B_+ - I^B_- > 0$ $((I^A_+ + I^A_-) > \xi h$ and $I^A_+ - I^A_- > 0)$ is satisfied, a standard transistor-transistor-logic (TTL) electronic square-pulse J_B (J_A) is realized at one of the two output ports of TD. On the other hand when the condition $(I^B_+ + I^B_-) > \xi h$ and $I^B_- - I^B_+ > 0$ $((I^A_+ + I^A_-) > \xi h$ and $I^A_- - I^A_+ > 0)$ is satisfied, a standard transistor-transistor-logic (TTL) electronic square-pulse J^*_B (J^*_A) is realized at the other output ports of TD. Finally the coincidences between signals $(J_A, J_B), (J_A, J^*_B), (J^*_A, J_B), (J^*_A, J^*_B)$ are registered by a coincidences box. The obtained fringe patterns corresponding to a detection probability equal to $P = 1.6 \times 10^{-3}$ are shown in Fig.4.17. Finally, a study on the obtained visibility as a function of the fraction of considered data has been carried out. We report in Fig.4.18 the trend of visibility versus TDs counts.

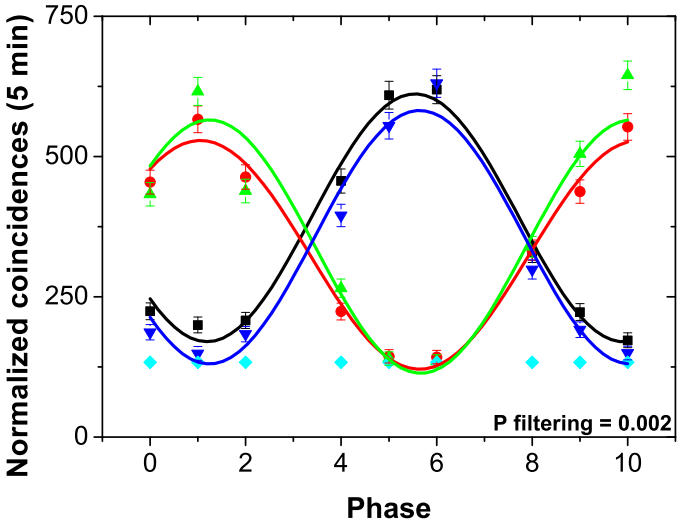

Figure 4.15: Fringe patterns obtained by filtering on the difference of the signals. The main visibility is 0.67 ± 0.02. Coincidences have been normalized to the product of the signals detected on each of the analyzed outcomes of the OF.

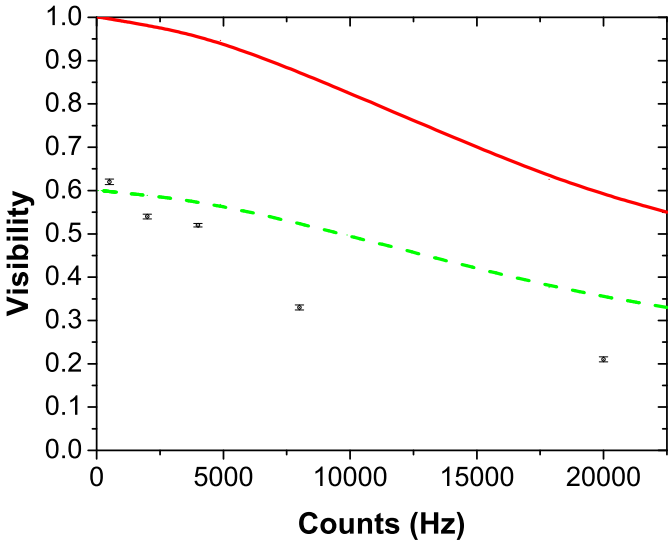

Figure 4.16: Trend of visibility versus OF counts. The theoretical predictions (continuous red line) has been renormalized (dotted green line) respect to the maximum reached visibility value.

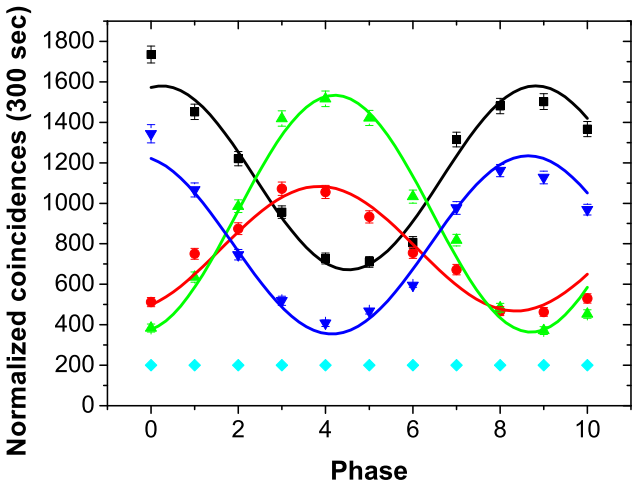

Figure 4.17: Fringe patterns obtained by filtering on the sum of the signals. The main visibility is 0.49 ± 0.02.

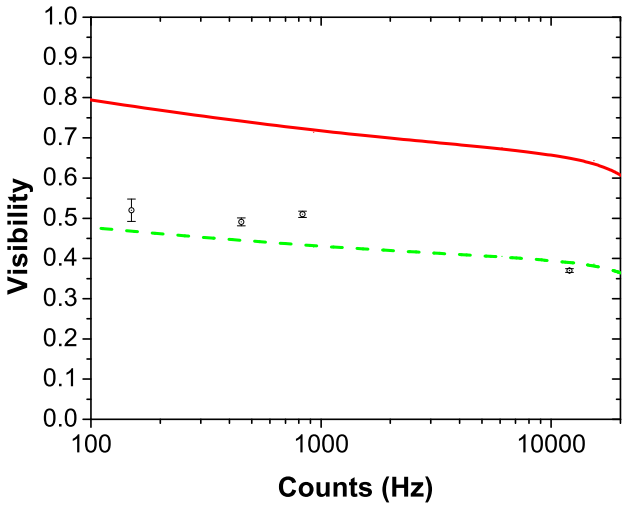

Figure 4.18: Visibility versus threshold detector counts.The theoretical predictions (continuous red line) has been renormalized (dotted green line) respect to the maximum reached visibility value.

4.6 Observations and conclusions

In this chapter we have reported a deep analysis on the possibility of observing quantum correlation on a multiphoton quantum system by performing probabilistic dichotomic measurements. We have addressed a specific class of multiphoton states: the ones obtained by the high gain optical parametric amplifier working in a non-collinear configuration. To this end we have introduced two kind of dichotomization processes, based on the O-Filtering procedure discussed in the previous chapter and on a threshold detection scheme. It has been demonstrated that these two detection schemes reduce to a simple dichotomic measurement when their characteristic thresholds are set to 0. We have shown that such dichotomic measurement when performed on $\frac{n}{2}$-spin states with increasing n, asymptotically allows in the ideal case the violation of CHSH Bell's inequality even for large n. The shape of correlation functions has been investigated, and we have shown that the sinusoidal correlation pattern, typical of an $\frac{1}{2}$-spin state, tends asymptotically to a triangular form, proper to classical correlations. When losses and decoherence are introduced the visibility of the correlation pattern is lowered and its shape turns out to be sinusoidal. In presence of losses, the violation of CHSH Bell's inequality is not allowed by a dichotomic measurement and more complicated detection schemes are required. We then discussed in terms of LHV models the feasibility of a CHSH test with the two probabilistic measurements presented in this chapter.

Finally, we have shown experimentally that the measurement performed by the probabilistic dichotomic schemes, the O-Filter and the Threshold Detector, allow to obtain higher visibility of correlation functions, not enough to violate CHSH Bell's inequality, but effective to reduce losses and decoherence effects. An open question concerns the existence of entanglement criteria able to demonstrate the presence of entanglement in a "macro-macro" scenario, and the possibility of adopting the measurement devices introduced in this paper within such context.

Part III

Manipulation of multiphoton quantum states

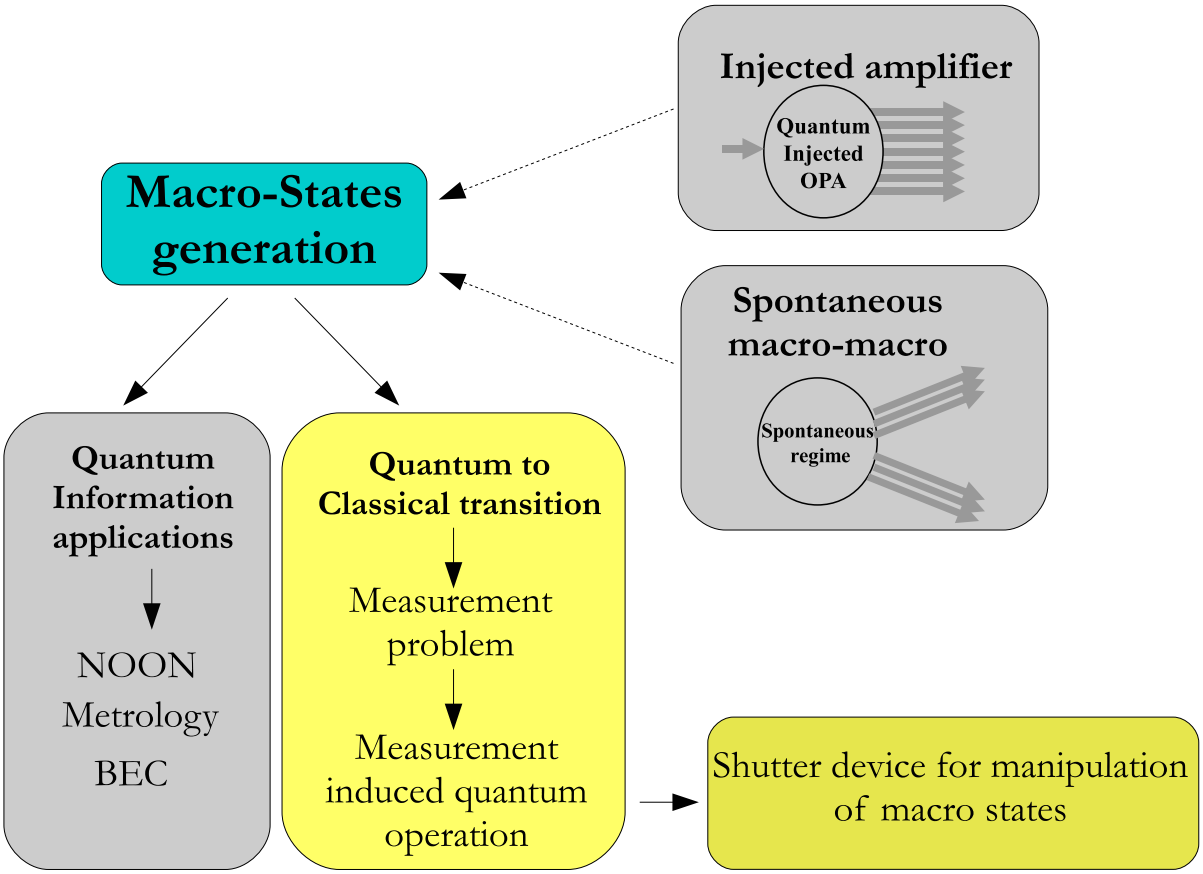

Figure 4.19: Conceptual scheme of the present work: in this part the colored boxes will be addressed. The problem of quantum-to-classical transition will be exploited in strict relation with the possible manipulation of multiphoton quantum states. This can be performed by an ultrafast optical shutter experimentally realized and tested on multiphoton coherent states.

In this part the quantum-to-classical investigation problem already mentioned in the second part will be addressed from a different point of view: from chapter 4 it turns out that the main problem of studying quantum properties of multiphoton state resides into the measurement process. In chapter 6 a possible manipulation of multiphoton states in order to extract the maximum available information about them will be investigated. The shown manipulation protocols make use of an ultrafast optical shutter experimentally realized and tested on multiphoton coherent states which will be addressed in chapter 5.

Chapter 5

Polarization preserving ultra fast optical shutter

In this chapter we present the realization of an ultra fast shutter for optical fields, which allows to preserve a generic polarization state, based on a self-stabilized interferometer. It exhibits high (or low) transmittivity when turned on (or inactive), while the fidelity of the polarization state is high. The shutter is realized through two beam displacing prisms and a longitudinal Pockels cell. This can represent a useful tool for controlling light-atom interfaces in quantum information processing, and can be used for the manipulation of the multiphoton states realized by optical parametric amplification processes, introduced in part II.

5.1 Optical shutters

In quantum information framework, the ability to perform fast-switching of an optical field can have different, useful applications. On one hand, preparation of multi-photon entangled states, as the ones addressed in the previous chapters, by optimized measurements and feed-forward operations can lead to innovative QIP protocols. On the other one, the coupling of mesoscopic field and Bose-Einstein condensate has been recently investigated [DSVC10], and, as we will see in the following part, requires the implementation of optical shutters able to switch in a very fast time,while preserving the quantum state and exhibiting a high extinction value. Since the content of information is usually encoded in the polarization degree of freedom of the field, the switching device should be able to preserve any polarization state of the incoming radiation. Hence a shutter device based on a fast-pockels cell, as the one developed by Ref.[GSLD02, PWT$^+$07, VPMM08], combined with a polarizing beamsplitter would destroy the carried information.
An alternative solution based on an acousto-optic modulator requires a longer activation time and leads to an intensity of the diffracted beam between 0% and 60%, while the zero order contribution is always higher than 15%. In this chapter we present the realization of an ultra-fast shutter for optical field, which preserves a generic polarization state and

exhibits a high transmittivity. The shutter, based on a self-stabilized interferometer, is realized through two beam displacing prisms and a longitudinal Pockels cell (PC). This can represent a useful tool for controlling light-atom interfaces in quantum information processing, and to manipulate the multiphoton quantum states introduced in the first part of this thesis, as we will explain in the following chapter.

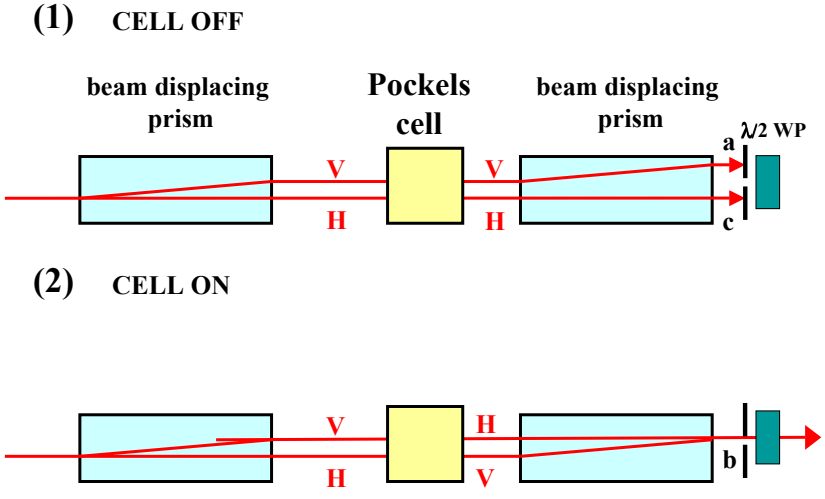

Figure 5.1: Experimental scheme of the shutter: (1) when the shutter is off the two beams separated by the two calcites are stopped by the pin-hole (modes **a** and **c**). (2) On the contrary when the shutter is on the two beams are recombined on the second calcite and the resulting beam (mode **b**) passes through the pin-hole.

5.2 Shutter working principles

Let us sketch the working details. Calcite beam displacing prism is used to separate an input beam into two orthogonally polarized output beams. Before passing through a second calcite prism these are manipulated in a PC with optical axis oriented at 45°(Fig. 5.1). When the PC is off (Fig. 5.1-(1)) it leaves the polarization state unperturbed and the beams are further separated in the second calcite . In this situation the shutter is off, and the output beams on modes **a** and **c** are stopped by a pin-hole. On the other hand, when the cell is on, the PC driving voltage is set to induce a $\lambda/2$ phase shift between the ordinary and extraordinary components and it can be activated in a short time ($t < 10ns$) by an external TTL signal. In this way the transformation $\overrightarrow{\pi_H} \Leftrightarrow \overrightarrow{\pi_V}$ is implemented. Then the two orthogonally beams are recombined spatially and temporally in the second calcite, Fig. 5.1-(2). In this situation the output field emerges on mode **b**. At the end of the stage a $\lambda/2$ waveplate at 45° flips the polarization of the output beam to restore its initial state. It's worth noting that the temporal overlap between the two beams is automatically ensured

by the symmetry of the device: the $\overrightarrow{\pi_H}$ polarization component of the input beam goes through the first calcite on a straight path whereas the $\overrightarrow{\pi_V}$ component's path is deviated. At the exit of the first calcite the two orthogonal polarization components are separated by a distance $d = 4mm$, the PC exchanges them and in the second calcite they are recombined by virtue of the fact that they have experienced the same overall path deviation.
The present device can be adopted with ultra short pulses ($200fs$). We note that this system is also stable in phase. Indeed the two orthogonally polarized beams are subjected to the same phase fluctuations since they propagate along parallel optical paths and share the same optical mounts. The phase difference between the two beams can be finally controlled by tilting the second calcite [OPW$^+$03].

Let us now analyze the action of the shutter on an input quantum state $|\varphi\rangle$ with generic polarization $\overrightarrow{\pi}_\varphi = \alpha\overrightarrow{\pi}_H + \beta\overrightarrow{\pi}_V$, where (α,β) are complex numbers satisfying $|\alpha|^2 + |\beta|^2 = 1$ and $\vec{\pi}_H$ and $\vec{\pi}_V$ stand for horizontal and vertical polarization, respectively. The evolution of $|\varphi\rangle$ is investigated by looking to the Heisenberg dynamic of the creation operator associated to the spatial mode $\mathbf{c}$ with polarization $\overrightarrow{\pi}_\varphi : \widehat{c}^\dagger_\varphi = \alpha\widehat{c}^\dagger_H + \beta\widehat{c}^\dagger_V$. After the first calcite the operator becomes $(e^{i\chi_1}\alpha\widehat{c}^\dagger_H + e^{i\chi_2}\beta\widehat{b}^\dagger_V)$, where χ_1 and χ_2 are the phase-shifts induced on the two orthogonal polarizations due to their different optical paths. When the Pockels cell is switched, the operator evolves into : $(e^{i\chi_1}\alpha\widehat{c}^\dagger_V + e^{i\chi_2}\beta\widehat{b}^\dagger_H)$, and the output state results after the recombination in the second calcite: $e^{i\chi}(\alpha\widehat{b}^\dagger_V + \beta\widehat{b}^\dagger_H)$, where $\chi = \chi_1 + \chi_2$. Finally, after the $\frac{\lambda}{2}-$waveplate, we obtain the same polarization state as the input one $\alpha\widehat{b}^\dagger_H + \beta\widehat{b}^\dagger_V$. On the contrary, if the cell is off, the total operator becomes $(e^{i2\chi_1}\alpha\widehat{c}^\dagger_H + e^{i2\chi_2}\beta\widehat{a}^\dagger_V)$, and, in this case, the initial polarization state is lost. We note that this scheme can be adopted in all the visible range by changing the PC voltage and by exploiting the spectral operating range (from $350nm$ to $2.3\mu m$) of the optical grade calcite of the displacers.

The adopted electro optic cell, Lasermetrics Series 1042, was composed by the series of two longitudinal PC of same length $35mm$, powered by a high voltage of $3200V$ to produce a $\lambda/2$ shift on the incident polarization and driven by the circuit reported in Fig.5.2. The problem of realizing a fast electronic circuit transforming a TTL signal into a calibrated fast pulse in the kV range was solved by a solid state switch HTS 50-08-UF, characterized by a very low jitter and a lifetime typical of semiconductor devices. The switch is triggered by a positive going pulse of 2 to 10 volts amplitude and generates the signal shown in Fig.5.3. The pulse remains constant for a time window of almost $10ns$ and decays exponentially within $500ns$.

The time duration of the driver pulse has been chosen to satisfy two criteria: (a) reduced low-frequency components and (b) suitable activation time window. (a) The KD*P crystal suffers the piezoelectric effect: when excited by a long high voltage pulse an effective coupling is introduced between the corresponding low frequency spectral components and the acoustic phononic modes of the crystal. The corresponding strain causes a mechanical damped oscillation of the crystal for a time duration longer than the ultra fast activation time of the shutter. This effect due to the polarizability of the Pockels cell

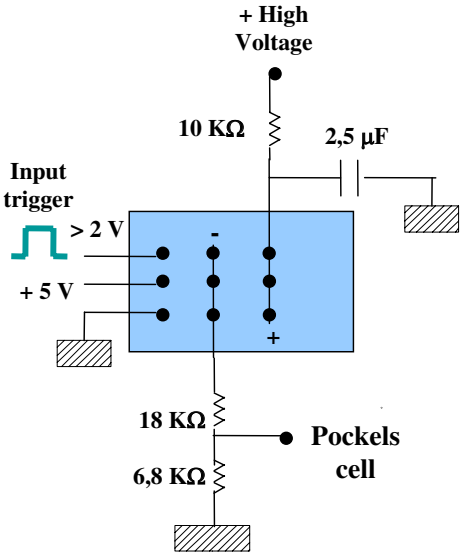

Figure 5.2: Electronic driver of the Pockels cell. When the signal of the trigger is on the PC is activated.

is harmonically modulated. Hence, the shutter is periodically reactivated and several subsequent pulses are partially transmitted. In order to eliminate this effect an ultra-short activation pulse is required [BB06]. (b) The electronic jitter of the driver circuit, almost $1-2ns$, gives a lower limit to the time activation window.

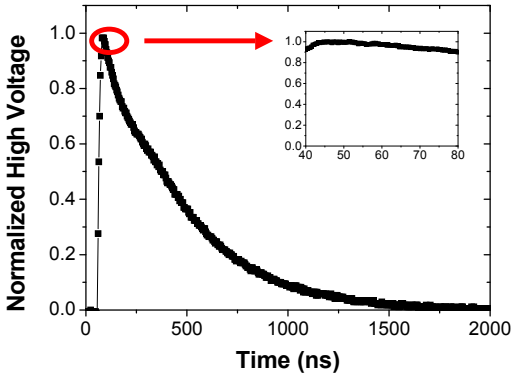

Figure 5.3: Trend of the high voltage signal as function of time. Inset: the trigger signal remain constant for almost $10ns$.

5.3 Experimental Characterization

We describe now the experimental characterization of the shutter device. We used a pulsed laser source centered at $800nm$ with a repetition rate of $250kHz$ and a bandwidth of $1.5nm$, selected before the shutter by two interferential filters . A $\lambda/2$ waveplate (WP) and a polarizing beam splitter (PBS) allowed to vary the polarization of the input beam on the first calcite (fig. 5.4). A second $\frac{\lambda}{2}$-WP and a PBS realized the polarization analysis of the output beam, which was detected by a photodiode (PD).

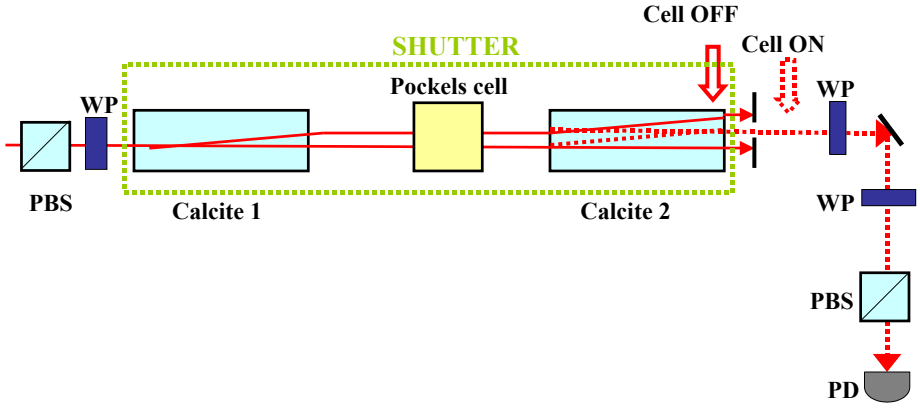

Figure 5.4: Experimental setup. A PBS and a $\lambda/2$ waveplate allow to vary the polarization of the input beam. A second PBS and $\lambda/2$ waveplate analyze the polarization state of the output beam **b**. The signal is detected by a photodiode (PD).

The PC was activated via the circuit above described (fig. 5.2). For different values of the frequency of the TTL trigger signal, we measured the fidelity $\mathscr{F}_{ON}$ of the polarization state when the PC was on, the transmittivity $\mathscr{T}_{ON}$ and the transmittivity $\mathscr{T}_{OFF}$ when the shutter was on and off respectively:

$$\mathscr{F}_{ON} = \frac{I_i^{ON}}{I_i^{ON} + I_{i^\perp}^{ON}} \tag{5.1}$$

$$\mathscr{T}_{ON} = \frac{I_i^{ON} + I_{i^\perp}^{ON}}{I_{IN}} \tag{5.2}$$

$$\mathscr{T}_{OFF} = \frac{I_i^{OFF} + I_{i^\perp}^{OFF}}{I_{IN}} \tag{5.3}$$

where I_i^{ON} (I_i^{OFF}) stands for the measured intensity on spatial mode **b** with polarization state π_i equal to the input one when the PC is (is not) activated. $I_{i^\perp}^{ON}$ ($I_{i^\perp}^{OFF}$) stands for the measured intensity of the analyzed polarization state $\overrightarrow{\pi}_i^\perp$ perpendicular to the input one $\overrightarrow{\pi}_i$. I_{IN} stands for the incident intensity on the shutter. For a trigger signal frequency equal to $1kHz$ we found the following results:

Polarization	$\mathscr{F}_{\mathbf{ON}}$ (± 0.001)	$\mathscr{T}_{\mathbf{ON}}$ (± 0.001)	$\mathscr{T}_{\mathbf{OFF}}$ (± 0.001)
$\overrightarrow{\pi_+}$	0.956	0.991	0.0025
$\overrightarrow{\pi_-}$	0.956	0.991	0.0025
$\overrightarrow{\pi_H}$	0.998	0.991	0.0050
$\overrightarrow{\pi_V}$	0.998	0.991	0.0020

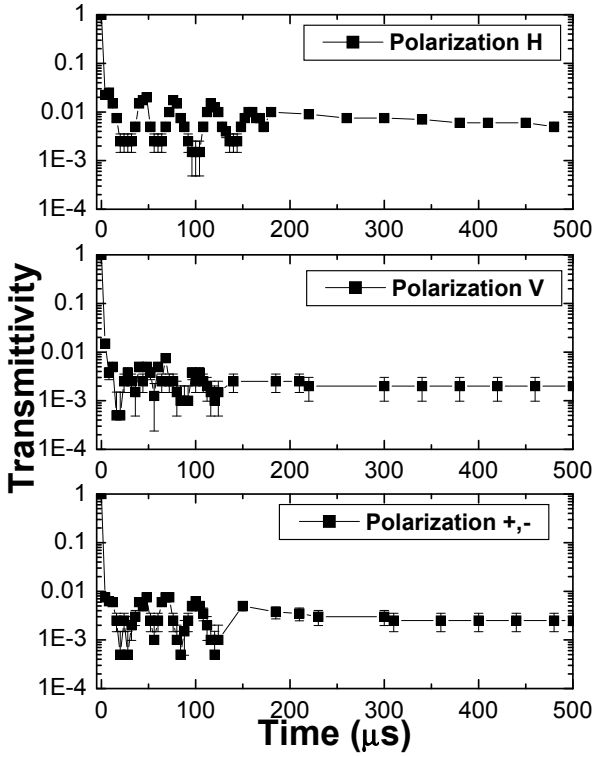

Figure 5.5: Transmittivity for an input state with polarization $\{\pi_+, \pi_-\}$ and $\{\pi_H, \pi_V\}$ measured with a frequency of the trigger equal to 1 kHz.

The transmittivity obtained with the shutter off gives an estimation of the extinction power of the shutter. The mean transmittivity in this case was $\mathscr{T}_{OFF} = 0.003$. In order to verify the absence of the piezoelectric ringing effect we report in Fig.5.5 the transmittivity of the shutter as a function of time. After few μs the transmitted signal is reduced by a factor of 100, leading to the transmission of one pulse once activated and the extinction of the subsequent pulses. When the shutter was on we obtained a mean fidelity $\mathscr{F}_{ON} = 0.998$ for $\overrightarrow{\pi_H}$ and $\overrightarrow{\pi_V}$ polarizations, and $\mathscr{F}_{ON} = 0.956$ for $\overrightarrow{\pi_+}$ and $\overrightarrow{\pi_-}$ polarizations.

We observe at last that the increase of the repetition rate causes an increase of transmittivity $\mathscr{T}_{\mathbf{OFF}}$ and a decrease of fidelity $\mathscr{F}_{\mathbf{ON}}$ (fig.5.6). Indeed for high repetition rate

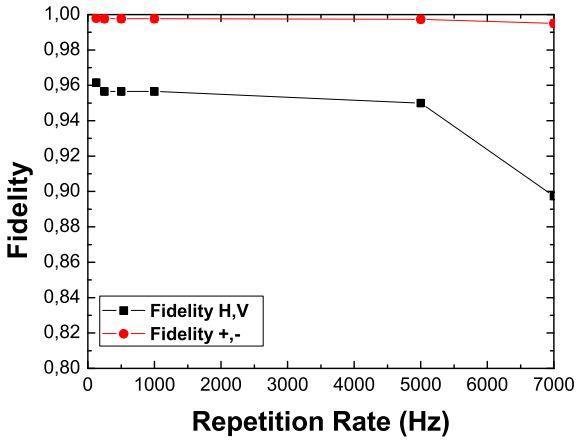

Figure 5.6: Fidelity of the polarization state in the $\{\pi_+, \pi_-\}$ and the $\{\pi_H, \pi_V\}$ basis versus the frequency of the trigger signal.

values, the time interval between two following trigger signals is shorter than the PC recovery time. By varying the frequency of the trigger signal, we have at last studied the fidelity in the two polarization basis: $\{\overrightarrow{\pi_H}, \overrightarrow{\pi_V}\}$ and $\{\overrightarrow{\pi_+}, \overrightarrow{\pi_-}\}$. We report the experimental results in fig. 5.6. The fidelity values for the states $(\overrightarrow{\pi}_+, \overrightarrow{\pi}_-)$ are lower due to the interferometric feature of the device, however an average fidelity value as high as 97% has been observed with the present scheme.

5.4 Observation and conclusions

In conclusion, we reported the experimental realization and characterization of a ultra fast shutter for optical field, based on a self-stabilized interferometer, which preserves a generic polarization state with high fidelity and exhibits a high contrast operation. This device can have direct applications in the context of measurement induced quantum operations.
In next chapter its action will be exploited for the theoretical analysis of conditional measurements performed on multiphoton states. In that context the shutter activation will be driven by a measurement performed over a small portion of the overall macro state.

Chapter 6

Measurement induced quantum operations on multiphoton states

In this chapter we investigate how multiphoton quantum states obtained through optical parametric amplification can be manipulated by performing a measurement on a small portion of the output light field. We study in details how the macro-qubit features are modified by varying the amount of extracted information and the strategy adopted at the final measurement stage. At last the obtained results are employed to investigate the possibility of performing a micro-macro non-locality test free from auxiliary assumptions.

6.1 Measurements induced protocols with multiphoton states

The possibility of performing quantum operations in order to tailor quantum states of light on demand has been widely investigated in the last few years. Several fields of research have been found to benefit from the capability of generating fields possessing the desired quantum properties. Non-classical states of light, such as sub-Poissonian light [Fiu01], squeezed light [HMD$^+$06, GAF$^+$06] or the quantum superposition of coherent states [OJTBG07a, OFTBG09], have been generated in a conditional fashion. In this context, continuous variables (CV) quantum information represents one of the most promising fields where conditional and measurement-induced non-Gaussian operations can find application. To this end, quantum interactions can be induced by exploiting linear optics, detection processes and ancillary states [FMA05]. For example, the process of coherent photon-subtraction has been exploited to increase the entanglement present in Gaussian states [KTSC06, OJTBG07b] and to engineer quantum operations in traveling light beams [Fiu09]. Finally, very recently conditional operations lead to the realization of different schemes for the implementation of the probabilistic noiseless amplifier [FBB$^+$10, XRL$^+$10, ZFB10], which can find interesting application within the context of quantum phase estimation [UMW$^+$10].

Strictly related to the problem of engineering quantum states of light for applications to Quantum Information, there is the one of beating the decoherence due to losses which affect quantum resources interacting with an external environment. In the last few years a large investigation effort has been devoted to the decoherence process and the robustness of increasing size quantum fields, realized by non linear optical methods [DS05, NDSD07, DSV08, DSS09a]. Recently quantum phenomena generated in the microscopic world and then transferred to the macroscopic one via parametric amplification have been experimentally investigated. In Ref.[DSV08] it has been reported the realization of a resilient to decoherence multiphoton quantum superposition (MQS) [DSS09b] involving a large number of photons and obtained by parametric amplification of a single photon belonging to a microscopic entangled pair: $|\psi^-\rangle = \frac{1}{\sqrt{2}}(|H\rangle_A|V\rangle_B - |V\rangle_A|H\rangle_B)$, where A,B refer to spatial modes $\mathbf{k_A},\mathbf{k_B}$ and the kets refer to single photon polarization states $\vec{\pi}$ ($\pi = H,V$). This process has been realized through a non linear crystal pumped by a UV high power beam acting as a parametric amplifier on the single entangled injected photon, i.e. the qubit $|\phi\rangle_B$ on spatial mode $\mathbf{k_B}$. In virtue of the unitarity of the optical parametric amplifier (OPA), the generated state was found to keep the same superposition character and the interfering properties of the injected qubit [De 98a, DS05, NDSD07] and, by exploiting the amplification process, the single photon qubit has been converted into a macro-qubit involving a large number of photons.

In this chapter we consider several strategies for the realization of measurement-induced quantum operations on these multiphoton states, generated thought the process of optical parametric amplification. We investigate theoretically how the measurement strategies, applied on a part of the multiphoton state before the final identification measurement, affect the distinguishability of orthogonal macro-qubits. Such measurements based on the discrimination of multiphoton probability distributions combine features of both continuous and discrete variables techniques. The interest in improving the capability of identifying the state generated by the quantum injected optical parametric amplifier (QIOPA) system mainly relies in two motivations: the first one concerns the development of a discrimination method able to increase the transmission fidelity of the state after the propagation over a lossy channel, and hence to overcome the imperfections related to the practical implementation. Such increased discrimination capability in lossy conditions could find applications within the quantum communication context. The second reason concerns the scenario in which an appropriate pre-selection of the macro-qubits could be adopted to demonstrate the micro-macro non-locality, free from the auxiliary assumptions requested if the filtering procedure was applied at the final measurement stage. In chapter 3 a probabilistic discrimination method, the orthogonality-filter (OF), has been introduced and it has been successfully applied [NDSD07, DSV08] to an entanglement test in a microscopic-macroscopic bipartite system. The application of the OF strategy, acting at the measurement stage, is indeed not suitable for the demonstration of loophole-free micro-macro non-locality because of the presence of inconclusive results [VST$^+$10a]. These correspond to the selection of different sub-ensembles of data, depending on the

choice of the measurement basis. As shown by Popescu in [Pop95], the pre-selection of data before the final measurement could encompass this problem.

Both the tasks determined above could exploit the capability to obtain at the output of the parametric amplifier a quantum state of large size, since this scheme allows to act on a small portion of the field in order to modify the features of the remaining part by a suitable selection. We consider the particular case in which a macro-state generated by the QIOPA is split by an unbalanced beam splitter (UBS) and manipulated by measuring the state on the reflected mode. The conceptual scheme underlying the present investigation is shown in figure 6.1-(b): a part of the wave-function is measured and the results of the measurement are exploited to conditionally activate an optical shutter placed in the transmitted part. Such shutter, whose realization has been recently reported in Ref.[SVG$^+$08], is used to allow the transmission of the optical beam only in presence of a trigger event, i.e. in this case the results of the measurement performed in the reflected part of the state. Several detection schemes will be investigated in this chapter. In fig.6.2-I is reported the distillation method based on the intensity pre-selection. As analyzed in more details in section 6.2, the signal of the reflected part of the macro state is analyzed by a threshold detector. If the measured intensity value is above a certain threshold, the shutter on the transmitted mode is activated. This strategy allows to overcome the experimental imperfection related to the vacuum injection into the amplifier, and hence to distillate the macro state from the noise belonging to the crystal spontaneous emission. In fig6.2-II is reported the strategy illustrated in section 6.3, based on a probabilistic discrimination of the reflected macro-qubit part performed by the OF device. By changing the polarization analysis basis on the reflected mode, we have investigated how the macro-state visibility obtained by a dichotomic measurement of the transmitted state is affected. In fig.6.2-III is illustrated the measurement procedure described in section 6.4, in which both the reflected and the transmitted mode are analyzed by a probabilistic OF-based measurement. At last, section 6.5 addresses the case in which the reflected macro qubit part is measured in two different polarization basis, as shown in figure 6.2-IV, and the final measurement is purely dichotomic. This measurement strategy is aimed at the realization of a non-locality test on the micro-macro photon state, without any auxiliary assumption. However, we show that such scheme does not allow to obtain a violation of a Bell's inequality since the analyzed strategy has the effect of increasing the correlations present in the micro-macro system only in a specific polarization basis while suppressing the correlations in the other basis.

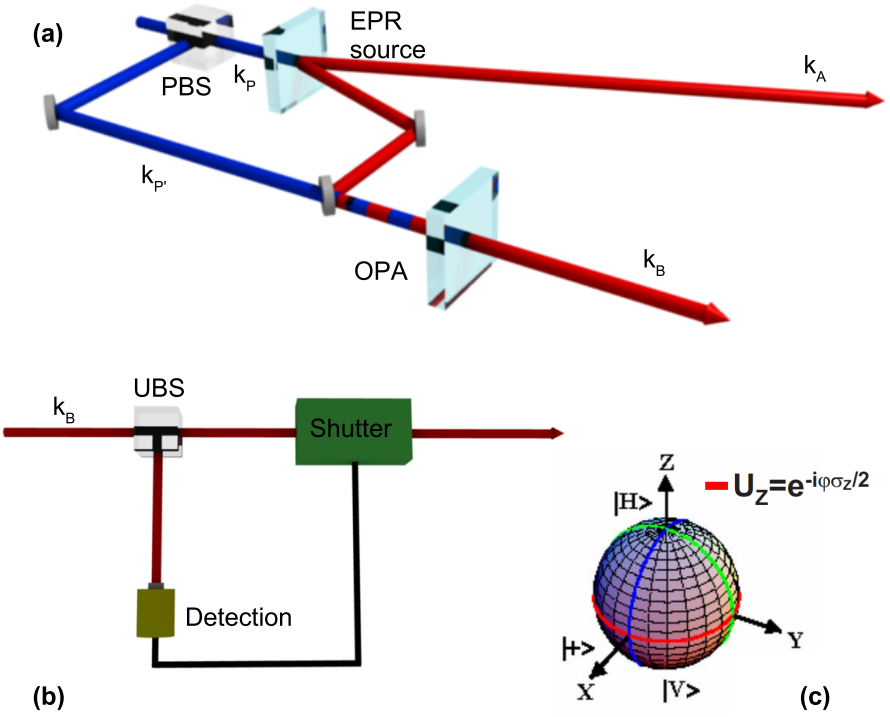

Figure 6.1: (a) Quantum injected optical parametric amplifier (QIOPA) scheme: an entangled photon pair is generated through spontaneous parametric down conversion (SPDC). One of the two photon is amplified by a non linear crystal, realizing the optimal phase covariant cloning of the injected qubit. (b) Scheme of the measurement-induced quantum operation process. The field is split by an unbalanced beam splitter (UBS), and reflected portion is measured to conditionally active the optical shutter placed in the path of the transmitted portion of the field. (c) Schematic view of the single photon Bloch sphere. The QIOPA device performs the optimal phase covariant process, hence amplifying equally all photons belonging to the equator of the sphere (red line), with polarization $\vec{\pi}_\phi = 2^{-1/2}(\vec{\pi}_H + e^{\imath\phi}\vec{\pi}_V)$.

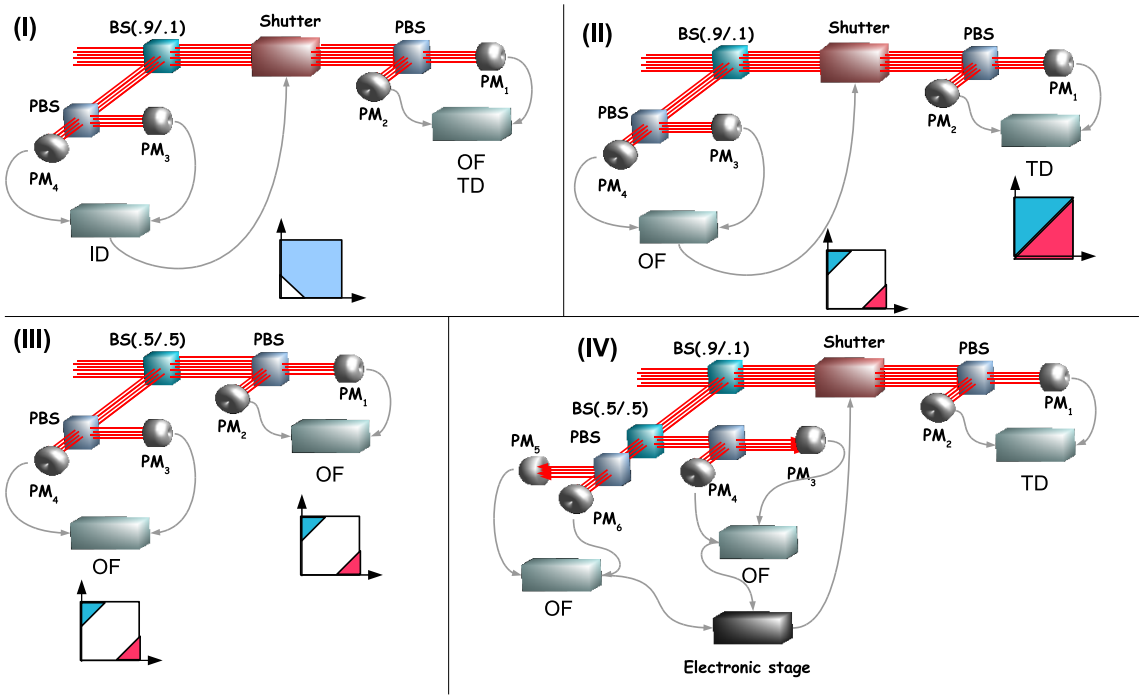

Figure 6.2: Measurement strategies devoted to the distillation of the macro-qubit state: (I) the shutter activation is conditioned to an intensity measurement on the reflected portion of the macro state; (II) the small reflected part of the macro state is analyzed in polarization and detected through an OF based measurement strategy; (III) the macro state is split in two equal parts, and both the reflected and the transmitted components are detected through an OF device; (IV) a double basis measurement is performed on the small reflected portion of the macro qubit.

6.2 Distillation of the macro-qubit

In this section we discuss the distillation method sketched in Fig. 6.2-(I). One of the main experimental challenge for the realization of the micro-macro system of Fig.6.1 is the achievement of spectral, spatial and temporal matching between the optical mode of the injected single photon state and the optical mode of the amplifier. In realistic conditions, the injected micro-macro system is given by: $\hat{\rho}_{\psi^-} = p|\psi^-\rangle_{AB}\langle\psi^-| + (1-p)/2\hat{I}_A \otimes |0\rangle_B\langle 0|$, where $|\psi^-\rangle_{AB} = \frac{1}{\sqrt{2}}(|H\rangle_A|V\rangle_B - |V\rangle_A|H\rangle_B)$ is the entangled singlet state connecting the spatial modes A and B, generated by the EPR source in figure 6.1, and the parameter p expresses the amount of mode-matching between the seed and the amplifier. Then in the expression of the number of photons $N_{\pi_\pm}(\varphi)$ generated by the amplifier when a single photon with equatorial [Fig.6.1-(c)] polarization state $|\phi\rangle$ is injected, the spontaneous emission has to be taken into account: $N_{\pi_\pm}(\varphi) = p[\bar{m} + \frac{1}{2}(2\bar{m}+1)(1 \pm \cos(\varphi))] + (1-p)\bar{m}$. When the single photon is injected correctly in the OPA, a pulse with a higher photon number is generated since stimulated emission processes occur in the amplifier. The distillation method here presented exploits this feature to reduce the noise introduced by the spontaneous emission of the amplifier.

Let us now discuss the propagation of the multiphoton field produced by the amplifier and the distillation procedure obtained through an intensity threshold detector (ID) and the shutter device. As shown in fig.6.2-I, the amplified state is split by an unbalanced beam splitter (UBS) $0.90 - 0.10$ in two parts: the smaller portion on mode $\mathbf{k}_D$ is analyzed by the ID, and the larger one on mode $\mathbf{k}_C$ is conditionally pushed through a polarization preserving shutter [SVG$^+$08], and measured in polarization by a dichotomic measurement. The ID based distillation strategy allows then to obtain a better discrimination between

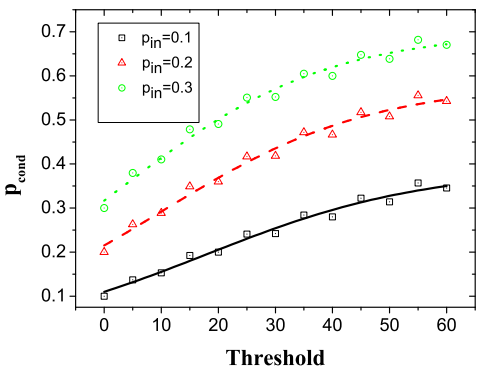

Figure 6.3: Trend of the injection probability as a function of the ID threshold, for different initial values of p.

the orthogonal macro states, by minimizing the noise related to the vacuum injection into the amplifier. It's worth nothing that, at variance with the techniques which will be introduced in the following sections, the ID action is invariant for rotation on the Fock space. It indeed selects the same region of the macro-qubit either in the $\{\vec{\pi}_+, \vec{\pi}_-\}$ basis either in the $\{\vec{\pi}_R, \vec{\pi}_L\}$ one. The action of the ID on mode $\mathbf{k}_D$ and of the shutter on mode $\mathbf{k}_C$ allows to

distill the macro-qubit from the noise generated by the amplifier and related to the spontaneous emission of the crystal. In the ideal case, this measurement corresponds to the projection of the impinging field onto the subspace: $\hat{\Pi}_k = \sum_{m+n>h} |n\pi, m\pi_\perp\rangle \langle n\pi, m\pi_\perp|$, where $|n\pi, m\pi_\perp\rangle$ represents a quantum state with n photons with polarization π and m photons with polarization $\pi_\perp$. The measurement method is hence based on a threshold detection scheme, in which the ID clicks only if $n_\pi + m_{\pi_\perp} > h$, where h is a threshold conveniently selected. This click activates the shutter on the transmitted UBS mode, ensuring the presence of the higher, i.e. correctly injected, pulses. This scheme has the peculiar property of selecting an invariant region of the Fock space with respect to rotations of the polarization basis. As said, the action of the ID device allows to decrease the noise due to the vacuum injection into the amplifier since it preserves only the higher pulses, and hence the ones that, with an higher probability, belong to the amplification process. These considerations can be quantified in the following way. The parameter of interest is the conditional injection probability, i.e. the injection probability conditioned to the activation of the shutter given by the threshold condition of the ID. We then evaluated numerically this quantity for several values of the un-conditioned injection probability p. It turns out that the value of p_{cond} is increased as shown in Fig.6.3, in which we report the trend of the conditional injection probability p_{cond} as a function of the ID threshold h.

6.3 Deterministic transmitted state identification

In this section we are interested in exploiting the action of a different pre-selection strategy, no more based on the intensity filtering but on a comparison between orthogonally polarized signals. This configuration is illustrated in fig.6.2-II and is based on a peculiar feature of the equatorial macro states. Indeed, any macro-qubit belonging to the injection of an equatorial qubit, due to the phase covariance of the amplifier, can be discriminated through a measurement based on a comparison. Precisely, we can measure the intensity signals belonging to orthogonal polarization components of the same macro-state and subsequently compare them above a certain threshold k. If analyzed in the same polarization basis of the injected qubit, the two signals will be unbalanced with an high probability. This can be explained by analyzing the probability distribution of the amplified states, reported in figure 6.5: (b) in the same basis as the injected qubit one and (a) in the mutually unbiased equatorial polarization basis.

We will address two cases in which the state generated by the amplifier is either $|\Phi^+\rangle$ or $|\Phi^R\rangle$, obtained by the amplification of a single photon polarized $\vec{\pi}_+ = \frac{\vec{\pi}_H + \vec{\pi}_V}{\sqrt{2}}$ and $\vec{\pi}_R = \frac{\vec{\pi}_H + i\vec{\pi}_V}{\sqrt{2}}$, respectively. In both cases the analysis basis corresponding to the UBS reflected mode is fixed to $\{\vec{\pi}_+, \vec{\pi}_-\}$, while the transmitted mode is analyzed in the same basis in which the injected qubit has been encoded. Let us discuss the experimental setup shown in Figure 6.2-II. The macro-state $|\Phi^+\rangle$ (or $|\Phi^R\rangle$) generated by the QIOPA impinges on the UBS. A small portion of the field is reflected on mode $\mathbf{k}_D$ and measured on the $\{\vec{\pi}_+, \vec{\pi}_-\}$

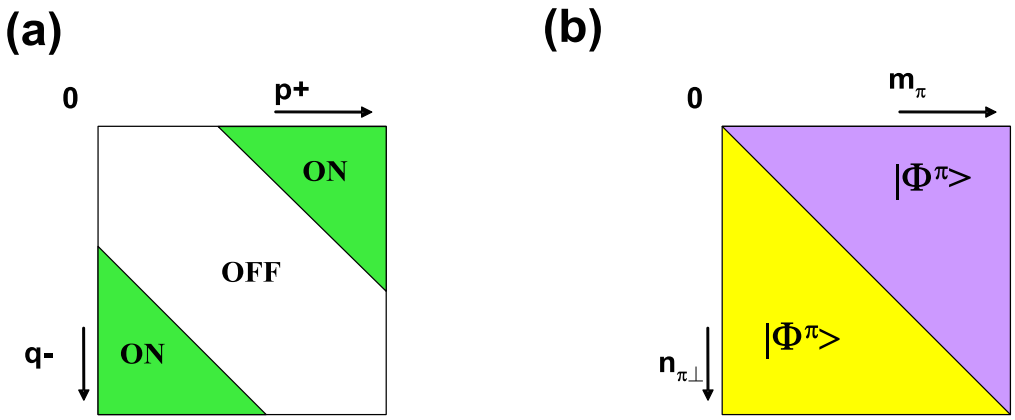

Figure 6.4: (a) Measurement scheme adopted for the conditional activation of the shutter: if the OF, on the reflected mode, measures the state on the green regions, the shutter, on the transmitted mode, is conditionally activated. The green regions correspond to the state for which the signals belonging to orthogonal polarizations are unbalanced over a certain threshold k, i.e. $|p-q| \geq k$. (b) Scheme for the final detection of the output state: Conditioned on a measurement result in the ON region on the reflected mode, the transmitted mode is identified by a dichotomic measurement in the $\{\pi, \pi_\perp\}$ basis. The diagonal contribution to the quantum state is assigned randomly to the state $|\Phi^\pi\rangle$ or $|\Phi^{\pi_\perp}\rangle$.

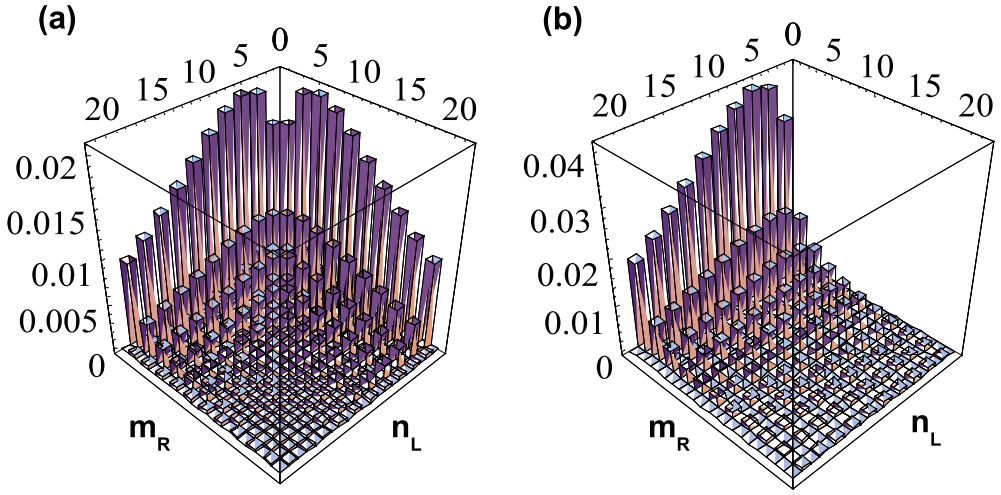

Figure 6.5: (a) Probability distribution of the state $|\Phi^R\rangle$ as a function of the number of photons $\{\vec{\pi}_+, \vec{\pi}_-\}$. (b) Probability distribution of the state $|\Phi^R\rangle$ as a function of the number of photons $\{\vec{\pi}_R, \vec{\pi}_L\}$.

basis. The two signals belonging to orthogonal polarizations are then compared by an orthogonality filter (OF). When the two signals are unbalanced, i.e. $|p-q| > k$, being p, q

the number of photons $\vec{\pi}_+, \vec{\pi}_-$ polarized and k an appropriate threshold, the shutter on mode $\mathbf{k}_C$ is activated and the field on that mode is conditionally transmitted (see Fig.6.4). The macro-state $|\Phi^+\rangle$ ($|\Phi^R\rangle$) is then analyzed in the $\{\vec{\pi}_+, \vec{\pi}_-\}$ (or $\{\vec{\pi}_R, \vec{\pi}_L\}$) basis. In the following sections we will address the problem of discriminating the final macro-state, given the acquired information on the small portion of the reflected field.

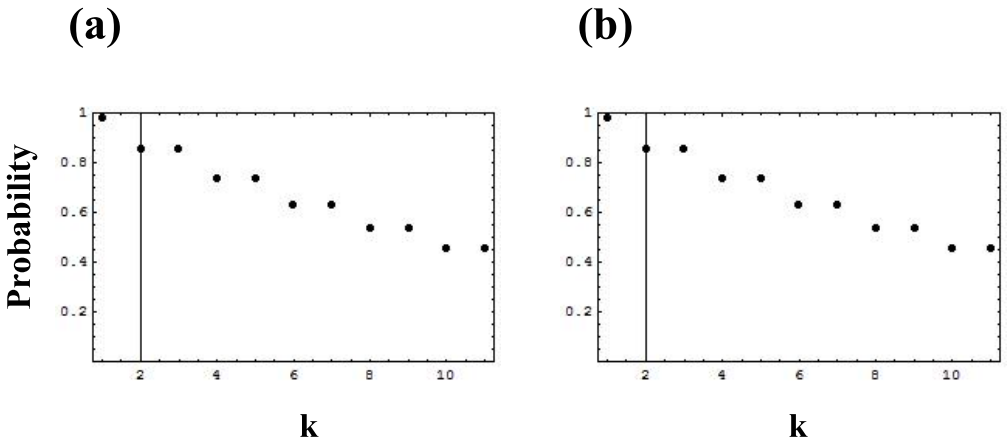

Figure 6.6: (a) Probability of activating the shutter when the state $|\Phi^R\rangle$ is analyzed in the $\{\vec{\pi}_+, \vec{\pi}_-\}$ basis versus the threshold k of the OF. (b) Probability of activating the shutter when the state $|\Phi^+\rangle$ is analyzed on the $\{\vec{\pi}_+, \vec{\pi}_-\}$ basis.

6.3.1 Probability of shutter activation

Let us first evaluate the probability P of activating the shutter when the impinging state is detected on the $\{\vec{\pi}_+, \vec{\pi}_-\}$ basis, depending on the value of k, with an OF technique. As shown in figure 6.6, the probability of activating the shutter is the same for the two output fields $|\Phi^+\rangle$ and $|\Phi^R\rangle$. This result can be explained by considering the probability distributions of the state $|\Phi^R\rangle$ in the two mutually unbiased equatorial bases shown in figure 6.5. Due to the linearity of the quantum mechanics, the state $|\Phi^R\rangle$ can be written as $|\Phi^R\rangle = \frac{1}{\sqrt{2}}(|\Phi^+\rangle + i|\Phi^-\rangle)$. Hence, due to the peculiar features of the two macro-states $|\Phi^\pm\rangle$, that have non-zero contributions for terms with different parity, the probability distribution of the macro-state $|\Phi^R\rangle$ in the $\{\vec{\pi}_+, \vec{\pi}_-\}$ basis is given as the sum of the two probability distributions of the states $|\Phi^+\rangle$ and $|\Phi^-\rangle$ in the same basis. Since shot by shot the OF identifies the state $|\Phi^+\rangle$ or $|\Phi^-\rangle$ with the same probability, the activation of the shutter has the same probability of occurrence for any linear combination of $|\Phi^R\rangle$ and $|\Phi^+\rangle$ impinging on the BS.

6.3.2 Analysis of the Macro-state $|\Phi^+\rangle$

Let us analyze the evolution of the state $|\Phi^+\rangle$ passing through an unbalanced beam-splitter (UBS). We start with the expression of the macro-qubit:

$$\begin{aligned}|\Phi^+\rangle &= \frac{1}{C^2}\sum_{ij}^{\infty}\left(\frac{-\Gamma}{2}\right)^j\left(\frac{\Gamma}{2}\right)^i\frac{\sqrt{(2j)!(2i+1)!}}{j!i!}\\ &\times|(2i+1)+,2j-\rangle_b = \\ &= \frac{1}{C^2}\sum_{ij}^{\infty}\left(\frac{-\Gamma}{2}\right)^j\left(\frac{\Gamma}{2}\right)^i\frac{(\mathbf{b}_+^\dagger)^{\mathbf{2i+1}}}{j!}\frac{(\mathbf{b}_-^\dagger)^{\mathbf{2j}}}{i!}|0\rangle\end{aligned} \tag{6.1}$$

The UBS transformation equations for the creation operators on spatial mode **b** read:

$$\mathbf{b}_\pm = \sqrt{\tau}\mathbf{c}_\pm + i\sqrt{1-\tau}\,\mathbf{d}_\pm \tag{6.2}$$

where the subscript $\pm$ refers to the polarization modes $\vec{\pi}_\pm = \frac{\vec{\pi}_H \pm \vec{\pi}_V}{2}$, and $\mathbf{c}^\dagger$ and $\mathbf{d}^\dagger$ refer to the creation operators on the spatial modes transmitted and reflected by the UBS. Hence after the UBS the output state becomes:

$$\begin{aligned}|\Phi^+\rangle^{out} = \frac{1}{C^2}\sum_{ij}^{\infty}\sum_{k}^{2i+1}\sum_{l}^{2j}&\binom{2i+1}{k}\binom{2j}{l}\left(\frac{-\Gamma}{2}\right)^j\\ &\left(\frac{\Gamma}{2}\right)^i\frac{1}{j!}\frac{1}{i!}\left(\sqrt{\tau}\mathbf{c}_+^\dagger\right)^k\left(i\sqrt{1-\tau}\mathbf{d}_+^\dagger\right)^{2i+1-k}\\ &\left(\sqrt{\tau}\mathbf{c}_-^\dagger\right)^l\left(i\sqrt{1-\tau}\mathbf{d}_-^\dagger\right)^{2j-l}|0\rangle\end{aligned} \tag{6.3}$$

By applying the creation operators to the vacuum state the output state reads:

$$\begin{aligned}|\Phi^+\rangle^{out} = \frac{1}{C^2}\sum_{ij}^{\infty}\sum_{k}^{2i+1}\sum_{l}^{2j}&\left(\frac{-\Gamma}{2}\right)^j\left(\frac{\Gamma}{2}\right)^i\frac{1}{j!}\frac{1}{i!}\frac{\sqrt{\tau}^{k+l}}{\sqrt{k!}}\\ &\frac{(2i+1)!(2j)!}{\sqrt{(2i+1-k)!(2j-l)!}}\frac{(i\sqrt{1-\tau})^{2i+1+2j-k-l}}{\sqrt{l!}}\\ &|k+,l-\rangle_d|(2i+1-k)+,(2j-l)-\rangle_c\end{aligned} \tag{6.4}$$

Let us now consider the case in which the reflected mode by the UBS is measured on the $\{\vec{\pi}_+,\vec{\pi}_-\}$ basis. The state $|p+,q-\rangle_d$ is detected on the reflected mode, the transmitted state then reads:

$$
\begin{aligned}
|\Phi^+\rangle^{meas} &= \frac{1}{C^2}\sum_{ij}^{\infty}\left(\frac{-\Gamma}{2}\right)^j\left(\frac{\Gamma}{2}\right)^i\frac{\sqrt{\tau}^{2i+1+2j-p-q}}{j!} \\
&\quad \frac{(i\sqrt{1-\tau})^{p+q}}{i!}\frac{(2i+1)!(2j)!}{\sqrt{p!q!(2i+1-p)!(2j-q)}} \\
&\quad |(2i+1-p)+,(2j-q)-\rangle_c
\end{aligned} \tag{6.5}
$$

Our scope is to investigate the visibility of the transmitted mode as a function of the unbalancement between $\vec{\pi}_+$ and $\vec{\pi}_-$ photons, detected on the reflected mode. Namely, if $|p-q|>k$ on mode $\mathbf{k}_D$, what is the visibility of the state $|\Phi^+\rangle^{meas}$ on mode $\mathbf{k}_C$?
This quantity can be quantified in the following way. Due to the peculiar shape of the photon number probability distribution (figure 6.5-(b)), the identification of the state $|\Phi^+\rangle$ can be performed by discriminating between the number of photons $\vec{\pi}_+$ and $\vec{\pi}_-$ polarized. Let us define the following quantities: $P^+(m,n|p,q)$ is the probability that, if the state $|p+,q-\rangle_d$ is detected on spatial mode $\mathbf{k}_D$, $m>n$ is obtained on spatial mode $\mathbf{k}_C$, and hence the macro-state $|\Phi^+\rangle$ is identified (m,n being the number of photons $\vec{\pi}_+$ and $\vec{\pi}_-$ polarized). On the contrary $P^-(m,n|p,q)$ is the probability that, given the detection of the state $|p+,q-\rangle_d$ on spatial mode $\mathbf{k}_D$, $n>m$ is obtained on spatial mode $\mathbf{k}_C$, and hence the macro-state $|\Phi^-\rangle$ is identified, even if the initial state impinging on the UBS was $|\Phi^+\rangle$. We can then derive the visibility as a function of the threshold k such that $|p-q|>k$:

$$
V(k)=\frac{\sum_{m,n}\sum_{p,q}\left(P_{m,n}^{p,q\,+}(k)-P_{m,n}^{p,q\,+}(k)\right)}{\sum_{m,n}\sum_{p,q}\left(P_{m,n}^{p,q\,+}(k)+P_{m,n}^{p,q\,-}(k)\right)} \tag{6.6}
$$

where $P_{m,n}^{p,q\,\pm}(k)=P^{\pm}(m,n||p-q|>k)$. The trend of visibility as a function of k is reported on Figure 6.7-(a). We observe that, increasing the value of k, hence detecting a higher unbalancement between $\vec{\pi}_+$ and $\vec{\pi}_-$ photons on mode $\mathbf{k}_D$, we obtain an higher visibility of the state on mode $\mathbf{k}_C$.

6.3.3 Analysis of the Macro-state $|\Phi^R\rangle$

Let us consider the case in which the state $|\Phi^R\rangle$ impinges on the UBS:

$$
\begin{aligned}
|\Phi^R\rangle &= \frac{1}{C^2}\sum_{ij}^{\infty}\left(\frac{i\Gamma}{2}\right)^j\left(\frac{i\Gamma}{2}\right)^i\frac{\sqrt{(2j)!}}{j!}\frac{\sqrt{(2i+1)!}}{i!} \\
&\quad \times|(2i+1)R,(2j)L\rangle_b = \\
&= \frac{1}{C^2}\sum_{ij}^{\infty}\left(\frac{i\Gamma}{2}\right)^j\left(\frac{i\Gamma}{2}\right)^i\frac{(\mathbf{b_R^\dagger})^{\mathbf{2i+1}}}{j!}\frac{(\mathbf{b_L^\dagger})^{\mathbf{2j}}}{i!}|0\rangle
\end{aligned} \tag{6.7}
$$

After the UBS the state can be written as:

$$|\Phi^R\rangle^{out} = \frac{1}{C^2}\sum_{ij}^{\infty}\sum_{k}^{2i+1}\sum_{l}^{2j}\left(\frac{i\Gamma}{2}\right)^j\left(\frac{i\Gamma}{2}\right)^i\frac{1}{j!}\frac{1}{i!}\frac{\sqrt{\tau}^{k+l}}{\sqrt{k!}} \\ \frac{(2i+1)!(2j)!}{\sqrt{(2i+1-k)!(2j-l)!}}\frac{(i\sqrt{1-\tau})^{2i+1+2j-k-l}}{\sqrt{l!}} \\ |kR,lL\rangle_c|(2i+1-k)R,(2j-l)L\rangle_d \tag{6.8}$$

The state on mode $\mathbf{k}_D$ is then measured in the $\{\vec{\pi}_+,\vec{\pi}_-\}$ basis. The state $|(2i+1-k)R,(2j-l)L\rangle_d$ can then be rewritten as:

$$|(2i+1-k)R,(2j-l)L\rangle = \sum_{r}^{2i+1-k}\sum_{s}^{2j-l}\frac{1}{\sqrt{2}^{2i+1+2j-k-l}} \\ \frac{1}{\sqrt{(2i+1-k)!}}\frac{1}{\sqrt{(2j-l)}}\binom{2i+1-k}{s}\binom{2j-l}{s}\times \\ \sqrt{(s+r)!(2i+1+2j-k-l-s-r)!}i^{2i+1-k-r}i^{2j-l-s} \\ |(r+s)+,(2i+1+2j-k-l-r-s)-\rangle_d \tag{6.9}$$

and the overall state reads:

$$|\Phi^R\rangle^{out} = \frac{1}{C^2}\sum_{ij}^{\infty}\sum_{k}^{2i+1}\sum_{l}^{2j}\sum_{r}^{2i+1-k}\sum_{s}^{2j-l}\left(\frac{i\Gamma}{2}\right)^j\left(\frac{i\Gamma}{2}\right)^i\frac{1}{i!}\frac{1}{j!}\frac{(2i+1)!(2j)!i^{2i+1-k-r}(-\imath)^{2j-l-s}}{\sqrt{(2i+1-k)!(2j-l)!k!l!}} \\ \frac{\sqrt{\tau}^{k+l}\sqrt{i(1-\tau)}^{2i+1+2j-k-l}}{\sqrt{2}^{2i+1+2j-k-l}}\frac{\sqrt{(r+s)!}\sqrt{(2i+1+2j-k-l-r-s)!}}{\sqrt{(2i+1-k)!(2j-l)!}}\binom{2i+1-k}{r}\binom{2j-l}{s} \\ |(r+s)+,(2i+1+2j-k-l-r-s)-\rangle_d|kR,lL\rangle_c \tag{6.10}$$

If the state on mode $\mathbf{k}_D$ is detected : $|(r+s)+,(2i+1+2j-k-l-r-s)-\rangle_d = |p+,q-\rangle_d$, the state on mode $\mathbf{k}_C$ is:

$$|\Phi^R\rangle^{meas} = \frac{1}{C^2}\sum_{ij}^{\infty}\sum_{l}^{2j}\sum_{s}^{2j-l}\left(\frac{i\Gamma}{2}\right)^j\left(\frac{i\Gamma}{2}\right)^i\frac{1}{i!}\frac{1}{j!}\frac{(2i+1)!(2j)!}{\sqrt{(l+p+q-2j)!(2j-l)!}} \\ \frac{\sqrt{\tau}^{2i+2j+1-p-q}}{\sqrt{(2i+1+2j-l-p-q)!l!}}\frac{\sqrt{p!q!}}{\sqrt{2}^{p+q}}\frac{\sqrt{i(1-\tau)}^{p+q}}{\sqrt{(l+p+q-2j)!(2j-l)!}}\binom{l+p+q-2j}{p-s}\binom{2j-l}{s} \\ \imath^{l+q-2j}(-\imath)^{2j-l-s}|(2i+1+2j-l-p-q)R,lL\rangle_c \tag{6.11}$$

where the following conditions have to be satisfied:

$$\begin{aligned} p &> s \\ 2i+1+2j &> l+p+q \\ 2j &< l+p+q \end{aligned} \tag{6.12}$$

If the state (6.11) is measured in the polarization basis $\{\vec{\pi}_R, \vec{\pi}_L\}$ obtaining a state $|mR, nL\rangle_c$, the corresponding probability amplitude is:

$$\begin{aligned} &\frac{1}{C^2}\sum_{j}^{\infty}\sum_{s}^{2j-n}\left(\frac{i\Gamma}{2}\right)^{j}\left(\frac{i\Gamma}{2}\right)^{(-2j+m+n+p+q-1)/2}\frac{(-i)^{2j-n-s}}{\sqrt{m!n!}} \\ &\frac{1}{j!}\frac{1}{\left(\frac{-2j+m+n+p+q-1}{2}\right)!}\frac{(-2j+p+q+m+n)!(2j)!}{\sqrt{(n+q-2j+s)!(p-s)!}} \\ &\frac{\sqrt{p!q!}}{(2j-n-s)!s!}\sqrt{\tau}^{m+n}(i\sqrt{1-\tau})^{p+q}\frac{1}{\sqrt{2}^{p+q}}i^{n+p+q-2j-r} \end{aligned} \tag{6.13}$$

and the probability of measuring the state $|mR, nL\rangle_c$ is given by:

$$\begin{aligned} P(m,n|p,q) = &\frac{1}{C^4}\sum_{j=0}^{\infty}\sum_{s}^{2j-n}\sum_{i}^{\infty}\sum_{r}^{2i-n}\frac{1}{C^4}\left(\frac{\Gamma}{2}\right)^{m+n+p+q-1} \\ &\frac{p!q!}{m!n!}\frac{(-1)^{r-s}}{2^{p+q}}\frac{\tau^{m+n}(1-\tau)^{p+q}}{\left(\frac{p+q+m+n-2j-1}{2}\right)!j!}\frac{1}{\left(\frac{p+q+m+n-2i-1}{2}\right)!i!} \\ &\frac{(p+q+m+n-2j)!(2j)!}{(n+q+s-2j)!s!(2j-n-s)!(p-s)!}\times \\ &\frac{(p+q+m+n-2i)!(2i)!}{(q+n+r-2i)!r!(2i-n-r)!(p-r)!} \end{aligned} \tag{6.14}$$

The visibility of the macro-state reads:

$$V(k) = \frac{\sum_{m,n}\sum_{p,q}\left(P_{m,n}^{p,q\,+}(k) - P_{m,n}^{p,q\,+}(k)\right)}{\sum_{m,n}\sum_{p,q}\left(P_{m,n}^{p,q\,+}(k) + P_{m,n}^{p,q\,-}(k)\right)} \tag{6.15}$$

where $P_{m,n}^{p,q\,\pm}(k) = P^{\pm}(m,n||p-q|>k)$. Here, $P^R(m,n||p-q|>k)$ is the probability that, given the detection of the state $|p+,q-\rangle_d$ on mode $\mathbf{k}_C$, $n>m$ is obtained on mode $\mathbf{k}_D$ ($m(n)$, number of photons polarized $\vec{\pi}_+(\vec{\pi}_-)$). In this case the state $|\Phi^R\rangle$ is identified; conversely the state $|\Phi^L\rangle$ is detected even if the the state $|\Phi^R\rangle$ impinged on the UBS.

We observe that the visibility of the state $|\Phi^R\rangle$ in the case in which a small portion of the overall state is measured on the $\{\vec{\pi}_+, \vec{\pi}_-\}$ polarization basis, is a decreasing function of the threshold k ($|p-q|>k$). This trend is shown in figure 6.7-(c). The decreasing trend of visibility can be explained by considering that the measurements in the two polarization basis correspond to two non-commuting operators acting on the same initial

state. Indeed, for asymptotically high values of the threshold $k \to \infty$, the measurement of the $\hat{\Pi}_i$ operators that describe the OF tends to the measurement of the pseudo-spin operators $\hat{\Sigma}_i$: i.e $\hat{\Sigma}_1 = |\Phi^+\rangle\langle\Phi^+| - |\Phi^-\rangle\langle\Phi^-|$ or $\hat{\Sigma}_2 = |\Phi^R\rangle\langle\Phi^R| - |\Phi^L\rangle\langle\Phi^L|$. In view of this consideration, the measurement on the $\mathbf{k}_C$ mode corresponds to the measurement of the $\hat{\Sigma}_i$ operators. The information gained on this mode about one of the two pseudo-spin operator acting on the macro qubit does not allow to gain information about orthogonal pseudo-spin operator. As a further remark, let us stress that this feature of the OF measurement is related to the filtering of different regions of the Fock space depending on the analyzed basis. The portion of the state that survives the action of the OF is indeed different if measured on the $\{\vec{\pi}_+, \vec{\pi}_-\}$ basis or in the $\{\vec{\pi}_R, \vec{\pi}_L\}$ one and is shown in figure 6.8.

6.4 Probabilistic transmitted state identification

In the previous sections we have shown how the visibility of the macro qubit obtained by a pure dichotomic measurement can be modified if a small portion of the beam is identified by a probabilistic measurement strategy.

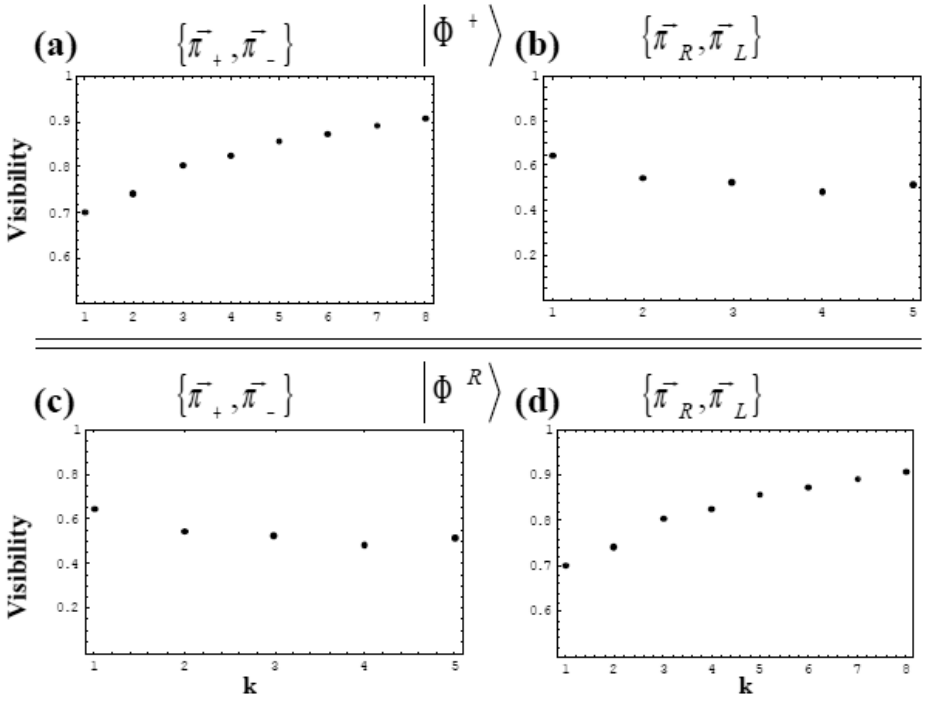

Figure 6.7: (a)-(b)Trend of the visibility of the state $|\Phi^+\rangle$ measured in the basis $\{\vec{\pi}_+, \vec{\pi}_-\}$ as a function of the threshold k. (c)-(d) Trend of the visibility of the state $|\Phi^R\rangle$ measured in the basis $\{\vec{\pi}_+, \vec{\pi}_-\}$ as a function of the threshold k. The numerical results have been obtained for the value of the gain parameter $g = 1.1$.

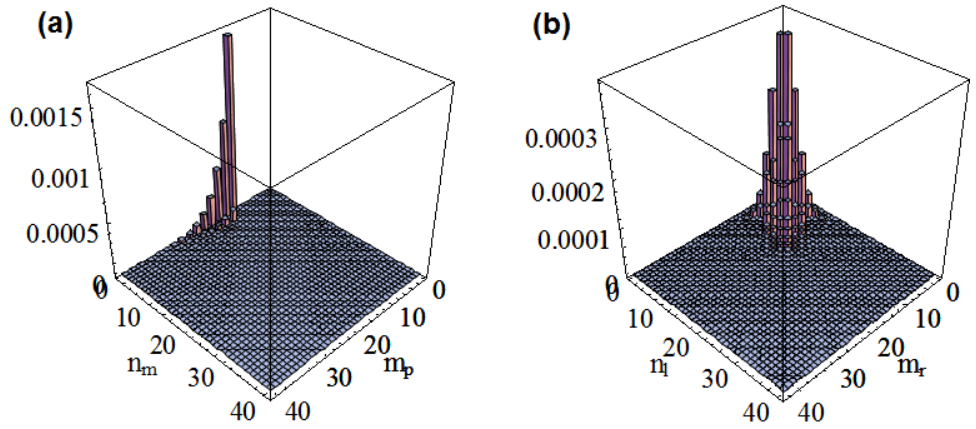

Figure 6.8: Selected region for the $|\Phi^+\rangle$ state after the measurement with an OF in the $\{\vec{\pi}_+, \vec{\pi}_-\}$ basis. (a) Photon number distribution in the $\{\vec{\pi}_+, \vec{\pi}_-\}$ basis. (b) Photon number distribution in the $\{\vec{\pi}_R, \vec{\pi}_L\}$ basis.

This section addresses the trend of the macro-states visibility when the field is split in two equal parts by a $0.5/0.5$ beam-splitter and both the reflected and the transmitted states are detected through the OF device. In this case the measurement schemes are shown in figures 6.2-(III) and 6.9: the OF technique is applied in order to extract the maximum information available from the two measured states.

We consider the case in which the portion on the reflected mode is analyzed in the polarization basis orthogonal to the codification one. In figure 6.10 is reported the trend of visibility as a function of the threshold k on the transmitted mode, and h on the reflected one. The two polarization analysis basis are chosen to be mutually unbiased. It can be seen that for equal values of the two thresholds $h = k$ the visibility reaches a value around 0.64, the same obtained through a pure dichotomic measurement, without any pre-selection procedure on the macro-state. In figure 6.11 is reported the trend of the visibility as a function of the threshold on the reflected mode, keeping fixed the value of the threshold on the transmitted one. We can see that the visibility of the transmitted state decreases when the threshold on the reflected mode increases. If the threshold on the transmitted mode is greater than the one on the reflected mode, the visibility results to be higher than 0.64, as expected by the action of the OF, which allows a better discrimination of the macro-state, measured in the codification polarization basis. Otherwise it can be seen how, increasing the threshold k above the threshold h, the visibility decreases below the "no filtering value".

From the analysis performed in this chapter we can conclude that the macro states are not suitable for secure communication. The action on a portion of the state can indeed be seen as an eavesdropping attack. If the state is measured in the codification basis, the visibility of the final state results to increase as shown in figure 6.7-(a)-(d). This

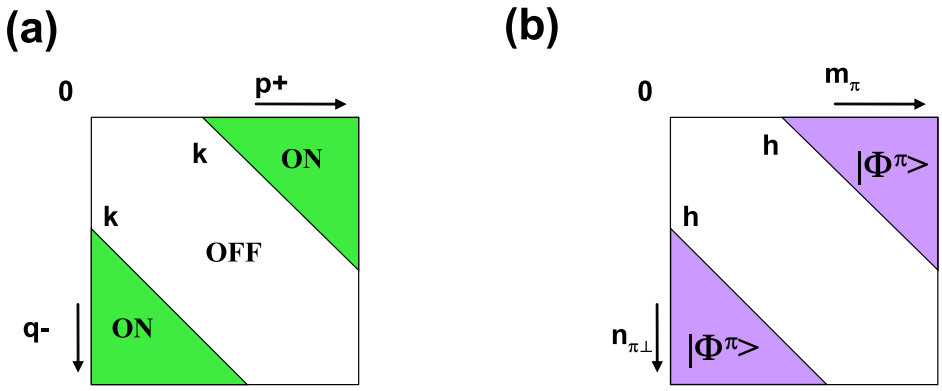

Figure 6.9: (a) Conditional activation of the shutter: if the OF acting on the reflected mode measures the state on the green regions, the shutter, on the transmitted mode, is conditionally activated. The green regions correspond to the state for which the signals belonging to orthogonal polarizations are unbalanced over a certain threshold k, i.e. $|p-q| \geq k$. (b) Corresponding to the ON region on the reflected mode, the transmitted mode is identified by a probabilistic measurement in the $\{\pi, \pi_\perp\}$ basis. The identification condition is $|m-n| \geq h$.

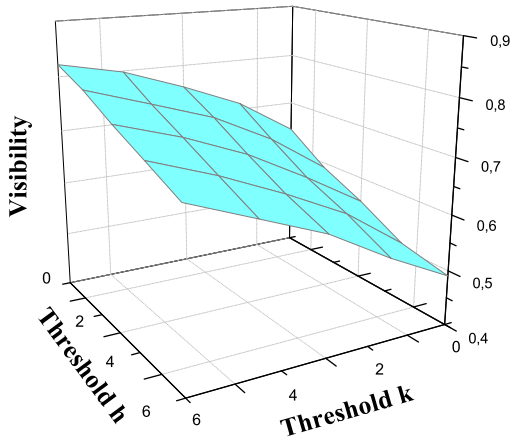

Figure 6.10: Trend of the visibility of the state $|\Phi^R\rangle$ for different values of the threshold k on the transmitted mode and of the threshold h on the reflected one. The numerical result has been obtained for a value of the parameter $g = 1.2$.

means that the conclusive results for the eavesdropper would coincide with the conclusive results for the receiver, and the eavesdropper can gain information on the macrostates without introducing noise. Otherwise if the state is measured by the eavesdropper in the wrong basis, the visibility at the receiver is not affected if the state is measured above a certain filtering threshold. According to these considerations, an eavesdropper could then develop a strategy in which he measures its part of the transmitted state in two bases. With this approach he could gain information on the transmitted signal by considering only the measurement outcome in the right basis, and only a small amount of noise is introduced by keeping the filtering thresholds above a certain value. Related to the security of the

macro-states is the possibility of performing a non-locality tests upon them. We will address this problem in the following section.

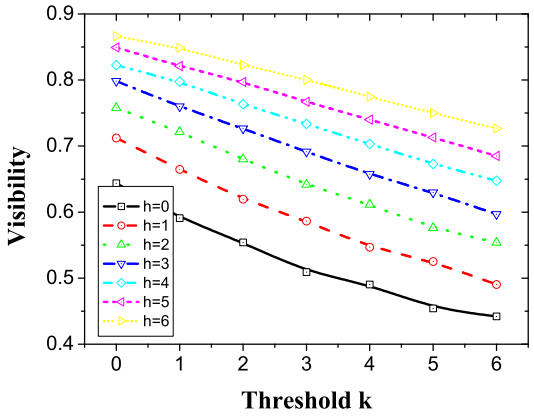

Figure 6.11: Trend of the macro-state visibility as a function of the threshold k on the reflected mode, fixed the threshold k on the transmitted one.

6.5 Pre-selection for entanglement and non-locality tests

In this section we shall investigate a pre-selection scheme based on a conditional operation driven by the measurement of a portion of the multiphoton state in two different polarization basis. The setup of this pre-selection scheme is reported in fig.6.2-IV. A small portion of the generated multiphoton state is reflected by an unbalanced beam-splitter of transmittivity $T = 0.9$ and subsequently split by a 50/50 beam-splitter in two equal parts. One of the two parts is measured in an equatorial $\{\vec{\pi}_\beta, \vec{\pi}_{\beta_\perp}\}$ basis by two photomultipliers, and the photocurrents $\{I_\beta, I_{\beta_\perp}\}$ are analyzed by an O-Filter device [Fig.6.4]. The other part undergoes the same measurement process in a different equatorial basis $\{\vec{\pi}_{\beta'}, \vec{\pi}_{\beta'_\perp}\}$.

When the threshold condition $|I_\pi - I_{\pi_\perp}| > k$ [Fig.6.4] is realized in both branches, measured respectively in the polarization basis $\{\vec{\pi}_\beta, \vec{\pi}_{\beta_\perp}\}$ and $\{\vec{\pi}_{\beta'}, \vec{\pi}_{\beta'_\perp}\}$, a TTL electronic signal is sent to conditionally activate the optical shutter placed in the optical path of the remaining part of the multiphoton state. Then, the field is analyzed at the measurement stage with the dichotomic strategy discussed in the previous paragraphs. For this pre-selection method, the relevant parameter is the angle ϕ between the two bases $\{\vec{\pi}_\beta, \vec{\pi}_{\beta_\perp}\}$ and $\{\vec{\pi}_{\beta'}, \vec{\pi}_{\beta'_\perp}\}$ in which the small portion of the beam is analyzed. The angle ϕ is defined according to the relations between the two polarization bases:

$$\vec{\pi}_{\beta'} = e^{\imath\frac{\phi}{2}}\left[\cos\left(\frac{\phi}{2}\right)\vec{\pi}_\beta - \imath\sin\left(\frac{\phi}{2}\right)\vec{\pi}_{\beta_\perp}\right] \tag{6.16}$$

$$\vec{\pi}_{\beta'_\perp} = e^{\imath\frac{\phi}{2}}\left[-\imath\sin\left(\frac{\phi}{2}\right)\vec{\pi}_\beta + \cos\left(\frac{\phi}{2}\right)\vec{\pi}_{\beta_\perp}\right] \tag{6.17}$$

Let us begin by analyzing the trend of the visibility of the fringe pattern obtained by varying the equatorial polarization $\vec{\pi}_\alpha$ of the injected single-photon state in the amplifier. More specifically, we analyze how the visibility changes as a function of the angle ϕ between the two bases of the pre-selection branch. In Fig.6.12 we show the numerical results obtained by calculating the visibility according to the standard definition $V = \frac{I_{max}-I_{min}}{I_{max}+I_{min}}$. In this case, the visibility is evaluated according to the following expression:

$$V(k) = \frac{\sum_{m>n} P_{\overline{\alpha}}\left[m,n\middle|(|I_\beta - I_{\beta_\perp}|>k)\cap(|I_{\beta'} - I_{\beta'_\perp}|>k)\right] - \sum_{m<n} P_{\overline{\alpha}}\left[m,n\middle|(|I_\beta - I_{\beta_\perp}|>k)\cap(|I_{\beta'} - I_{\beta'_\perp}|>k)\right]}{\sum_{m>n} P_{\overline{\alpha}}\left[m,n\middle|(|I_\beta - I_{\beta_\perp}|>k)\cap(|I_{\beta'} - I_{\beta'_\perp}|>k)\right] - \sum_{m<n} P_{\overline{\alpha}}\left[m,n\middle|(|I_\beta - I_{\beta_\perp}|>k)\cap(|I_{\beta'} - I_{\beta'_\perp}|>k)\right]} \tag{6.18}$$

Here $P_{\overline{\alpha}}\left[m,n\middle|(|I_\beta - I_{\beta_\perp}|>k)\cap(|I_{\beta'} - I_{\beta'_\perp}|>k)\right]$ is the photon-number distribution of the state $|\Phi^{\overline{\alpha}}\rangle$ after the pre-selection stage. More specifically, the value of $\overline{\alpha}$ is chosen in order to maximize the contribution of the $\sum_{m>n}$ term and minimize the contribution of the $\sum_{m<n}$ term:

$$I_{max} = \sum_{m>n} P_{\overline{\alpha}}\left[m,n\middle|(|I_\beta - I_{\beta_\perp}|>k)\cap(|I_{\beta'} - I_{\beta'_\perp}|>k)\right] \tag{6.19}$$

$$I_{min} = \sum_{m<n} P_{\overline{\alpha}}\left[m,n\middle|(|I_\beta - I_{\beta_\perp}|>k)\cap(|I_{\beta'} - I_{\beta'_\perp}|>k)\right] \tag{6.20}$$

Eq.(6.18) then coincides with the usual definition of visibility. We note that the visibility is higher for smaller angles ϕ, since in that case a strong projection of the state is performed in two close bases. This condition is equivalent to the scheme of Fig.6.2-(II), where the O-Filter measurement performed in one basis allows to obtain a better discrimination of the detected state only in the polarization basis of the pre-selection measurement [Fig.6.7 (a)-(b)]. When ϕ is high, a lower visibility can be achieved since the projection of the macrostate occurs in two distant bases. In this case, the increasing effect of the pre-selection in one basis on the visibility is in contrast with the decreasing effect of the pre-selection in the other basis, as shown in Sec.III.

We conclude this section by discussing the feasibility of a non-locality test by exploiting the proposed pre-selection method. We consider the case of a CHSH inequality [CHSH69]. Let us briefly summarize in the light of a local hidden variable (LHV) theory the content of Bell's inequalities for a set of dichotomic observables. Consider a quantum state described by the density matrix $\hat{\rho}$ defined in the Hilbert space $\mathscr{H}_1 \otimes \mathscr{H}_2$. Define $\hat{O}^i_a$ the positive operator acting on subspace $\mathscr{H}_1$, and the probability of finding the value i after the measurement a as given by $\mathrm{Tr}\left[\hat{\rho}(\hat{O}^i_a \otimes \hat{I})\right]$. The same relation holds for the positive operator $\hat{O}^j_b$ acting on subspace $\mathscr{H}_2$.

The existence of a LHV model implies that the expectation values of the a and b observables are predetermined by the value of the parameter λ: $\{X_a)(\lambda), X_{a'}(\lambda), X_b(\lambda), X_{b'}(\lambda)\}$, hence the product $a \cdot b$ is equal to $X_a(\lambda)X_n(\lambda)$. For a fixed value of λ the variables X_n with $n = \{a, b, a', b'\}$ take the values $-1, 1$ and satisfy the CHSH inequality:

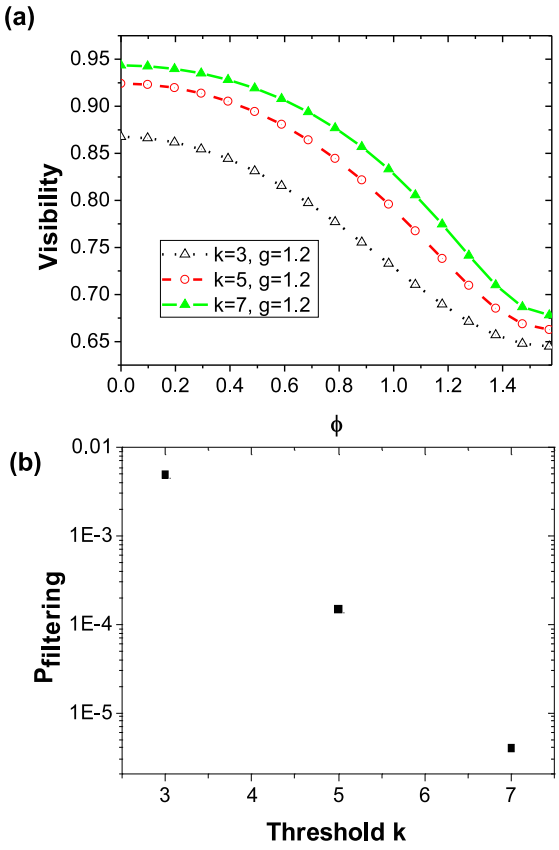

Figure 6.12: (a) Trend of the visibility for the double-filtering technique as a function of the angle ϕ between the two polarization bases $\{\vec{\pi}_\beta, \vec{\pi}_{\beta_\perp}\}$ and $\{\vec{\pi}_{\beta'}, \vec{\pi}_{\beta'_\perp}\}$ of the pre-selection measurement. Square black points correspond to $k = 3$, circular red points to $k = 5$ and triangular green points to $k = 7$. (b) Filtering probability of the scheme as a function of the threshold k at the pre-selection measurement stage. All graphs correspond to $g = 1.2$.

$$X_a(\lambda)X_b(\lambda) + X_a(\lambda)X_{b'}(\lambda) + X_{a'}(\lambda)X_b(\lambda) - X_{a'}(\lambda)X_{b'}(\lambda) \leq 2 \tag{6.21}$$

The same inequality holds by integrating this equation on the space of the hidden variable (λ):

$$\begin{aligned} &\int_\Omega d\mathbb{P}(\lambda)X_a(\lambda)X_b(\lambda) + \int_\Omega d\mathbb{P}(\lambda)X_a(\lambda)X_{b'}(\lambda) + \\ &\int_\Omega d\mathbb{P}(\lambda)X_{a'}(\lambda)X_b(\lambda) - \int_\Omega d\mathbb{P}(\lambda)X_{a'}(\lambda)X_{b'}(\lambda) \leq 2 \end{aligned} \tag{6.22}$$

where $P(\lambda)$ is the measure of the λ probability space. If there is a local hidden variables model for quantum measurement taking values $[-1,+1]$, then the following inequality must be satisfied:

$$S_{CHSH} = E^\rho(a,b) + E^\rho(a,b') + E^\rho(a',b) - E^\rho(a',b') \leq 2 \tag{6.23}$$

where $E^\rho(a,b) = \int_\Omega X_a(\lambda)X_b(\lambda)d\mathbb{P}(\lambda)$. The violation of (6.23) proves that a LHV variables model for the considered experiment is impossible.

We consider the case in which the angle ϕ between the two bases $\{\vec{\pi}_\beta, \vec{\pi}_{\beta_\perp}\}$ and $\{\vec{\pi}_{\beta'}, \vec{\pi}_{\beta'_\perp}\}$ is set at $\phi = \pi/4$. This choice is motivated by the following considerations. On one side, low values of ϕ would lead to a micro-macro state possessing strong correlations only in one polarization basis, thus not allowing to violate a Bell's inequality. On the other side, high values of ϕ does not allow to obtain the necessary enhancement in the correlations of the micro-macro system to violate a Bell's inequality. The obtained fringe patterns for the chosen case are reported in Fig.6.13 and corresponds to the following conditions. The $(+1)$ outcome of the dichotomic measurement is recorded as a function of the polarization $\vec{\pi}_\alpha$ of the injected single photon state. In particular, the two chosen equatorial polarization bases $\{\vec{\pi}_\beta, \vec{\pi}_{\beta_\perp}\}$ and $\{\vec{\pi}_{\beta'}, \vec{\pi}_{\beta'_\perp}\}$ corresponds to $\beta = 0$ and $\beta' = \frac{\pi}{4}$. We then analyzed three different choices for the threshold k at the pre-selection stage. When the threshold k is set to 0, the fringe pattern corresponding to the two basis $\beta = 0$ and $\beta = \frac{\pi}{4}$ are mutually shifted of an angle $\frac{\pi}{4}$, since no filtering and no pre-selection is performed on the state. When the threshold k is increased, the mutual shift between the fringe pattern is progressively reduced and canceled, since a strong filtering of the state is performed. In particular, the maximum of both the fringe pattern in the $\beta = 0$ and $\beta = \frac{\pi}{4}$ bases is obtained for the $|\Phi^{\overline{\alpha}}\rangle$ state with $\overline{\alpha} = \frac{\pi}{8}$. This means that this pre-selection strategy for sufficiently high value of k enhances the correlations in the micro-macro system in a specific polarization basis and suppresses the correlations in the other bases. For this reason, the proposed strategy does not allow to observe the violation of a Bell's inequality in the micro-macro system here analyzed. The enhanced value of the visibility could nevertheless be employed in quantum lithography and quantum metrology schemes, in which high visibility correlations pattern and high photon number regimes are required. Recently it has indeed been shown how the amplification process of a single photon probe can beat the detrimental effect of losses which happen in the transmission and detection stages [VST$^+$10b]. Such a scheme for non invasive quantum metrology could benefits from the presented filtering procedures in order to improve the visibility value of the interference fringe pattern.

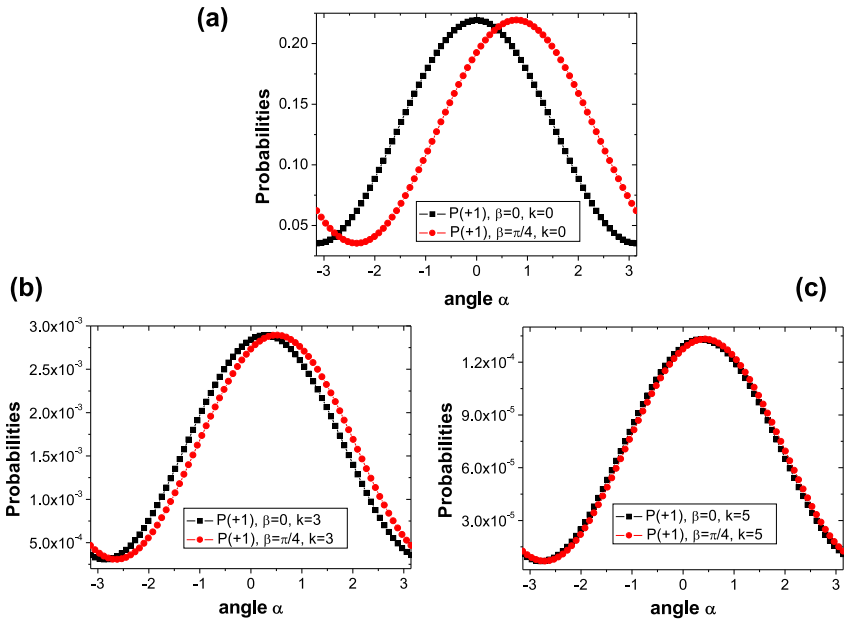

Figure 6.13: Fringe pattern as a function of the angle α of the polarization basis at the single-photon site. The angle ϕ between the two bases of the pre-selection stage is set at $\phi = \pi/4$. (a) Threshold $k = 0$. (b) Threshold $k = 3$. (c) Threshold $k = 5$. Square black points: fringe patterns obtained by recording the $(+1)$ outcome at the measurement stage, where the measurement basis $\{\vec{\pi}_\beta, \vec{\pi}_{\beta_\perp}\}$ is set at $\beta = 0$. Circle red points: fringe patterns obtained by recording the $(+1)$ outcome at the measurement stage, where the measurement basis $\{\vec{\pi}_\beta, \vec{\pi}_{\beta_\perp}\}$ is set at $\beta = \frac{\pi}{4}$.

6.6 Observations and Conclusions

In this chapter we have analyzed the properties of the macro states obtained by a quantum injected amplification process, by addressing the behavior of the indistinguishability between orthogonal macro-states when a filtering process is applied over a portion of them. More specifically, we analyzed theoretically in details several schemes for the realization of conditional measurement-induced operations. All these strategies are aimed at the manipulation and distillation of the macro-states for their applications in different contexts, such as the realization of a non-locality test or quantum communication.

We have identified a strategy, based on the ID device, able to minimize the effects of the noise due to the vacuum injection into the amplifier. The ID based filtering procedure is independent on the analysis basis and selects the same portion of the state when the measurement is performed in any equatorial polarization basis.

A different filtering procedure, based on the OF device, has been deeply studied: it turned out that when a small portion of the state is analyzed through the OF, the visibility of the overall state, relative to a dichotomic measurement, is affected in a different way

depending on the polarization basis in which the small portion has been measured. If the polarization basis is the same of the macro qubit codification, the final visibility increases with the increase of the filtering threshold, otherwise it decreases. This behavior is related with the impossibility of measuring non commuting operators on the same quantum state, as explained in Section III.

We have further addressed in Sec.IV the trend of the macro state visibility when an OF discrimination system is used even at the transmitted state detection stage. In this case, the two OF apparatus in both transmitted and reflected branches play an opposing role in increasing or decreasing the visibility of the fringe-pattern obtained in a micro-macro configuration. Such analysis shows that the macro-states generated by optical parametric amplification of a single-photon state are not suitable for quantum cryptography, since they are not robust under an eavesdropping attack.

Finally, in Sec.V we addressed a pre-selection scheme for the realization of a Bell's inequality test which do not suffer the same detection loopholes of the one based on post-selection strategies [VST$^+$10a]. The proposed method, based on the measurement of the reflected part of the wave-function in two different bases, does not allow to violate a Bell's inequality, since it induces the collapse of the correlations present in the macro-states in only a single polarization basis.

Several open points remain to be investigated. The measurement-induced operations analyzed in this chapter are all based on dichotomic detection schemes. Other approaches, such as the ones based on continuous variables measurements or on the processes of coherent photon-addition and photon-subtraction, can lead to a different manipulation of the QIOPA multiphoton states. Systems with different properties from the one analyzed in this chapter could be obtained with these methods.

Part IV

Applications

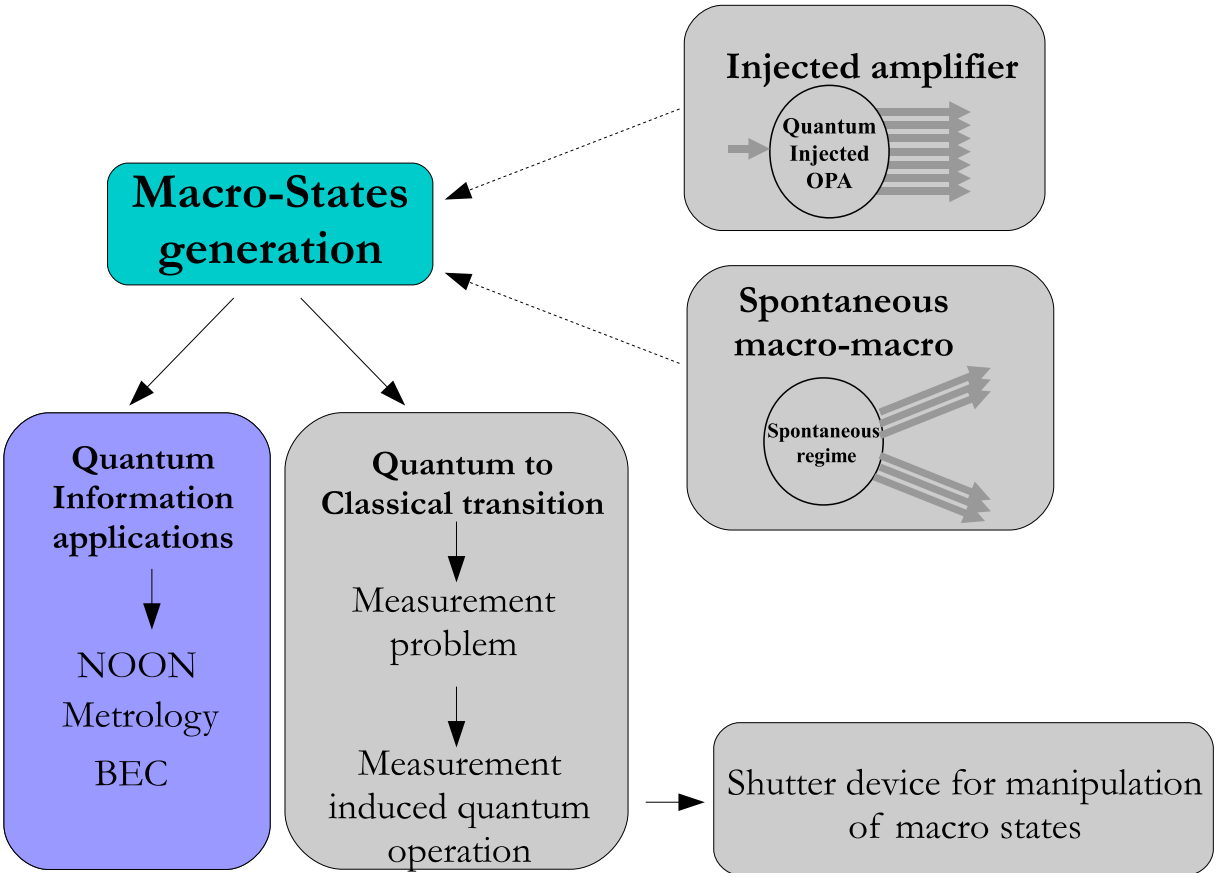

Figure 6.14: Conceptual scheme of the present work: in this part the colored boxes will be addressed. Different application to quantum information protocols are addressed.

In this part different applications of multiphoton states to quantum information problems are investigated. A first application is related with quantum metrology: the use of multiphoton quantum states can indeed be exploited in order to obtain a greater sensitivity for the estimation of a physical parameter of interest such as, in our case, a phase. In chapter 7 it is shown that a scaling factor in the available sensitivity in an interferometrical experiment can be observed when instead of a coherent state a multiphoton state, generated by a collinear source, is used. The analysis is then enlarged to the case in which a 2-photon NOON state is injected into the amplifier. In that case the scaling factor in the sensitivity goes with an increase in the detected signal respect to the spontaneous emission case. In chapter 8 the minimally invasive metrology scenario is addressed. In that case the amplification of a single photon probe, used to estimate a phase, results into an enhancement in the sensitivity, which is no more related with a scaling factor, but turns out to be a constant factor depending on the non linear gain of the amplifier and on the losses regime. This protocols works well in the high losses regime, in which dominant losses happen after the amplification, at the detection stage. The high resilience to losses of multiphoton states, obtained by an amplification process of single photon states, is then

addressed in chapter 9, where the non resonant interaction between the QIOPA field and a BEC system is investigated.

Chapter 7

Optical Parametric Amplifier and NOON states

NOON states are path entangled states which can be exploited to enhance phase resolution in interferometric measurements. In this chapter we will show that the output of a high-gain optical parametric amplifier can be intense yet exhibits quantum features, namely, sub- Rayleigh fringes, such as the ones shown by the few photons NOON states. We will investigate multiphoton states generated by a high-gain optical parametric amplifier operating with a quantum vacuum input for a gain values up to 2.5 [SVD$^+$08]. And then we will analyze the quantum states obtained by optical parametric amplification of polarization NOON states [GCD$^+$08, VSSD09]. Finally, we will compare the stimulated emission regime with the spontaneous one, finding comparable visibilities between the two cases but an enhancement of the signal in the stimulated case.

As a final step, we will show that the collinear amplifier cannot be successfully used for amplifying N-photon states with N>2 due to the intrinsic $\frac{\lambda}{4}$ oscillation pattern of the crystal. To overcome this limitation, we propose to adopt a scheme for the amplification of a generic state based on a non-collinear QIOPA and we show that the state obtained by the amplification process preserves the $\frac{\lambda}{N}$ feature and exhibits a high resilience to losses. Furthermore, an asymptotic unitary visibility can be obtained when correlation functions with sufficiently high order M are analyzed.

7.1 NOON states features

NOON states are path entangled states of the form:

$$|\psi\rangle = \frac{1}{\sqrt{2}}(|N\rangle_{k_1}|0\rangle_{k_2} + |0\rangle_{k_1}|N\rangle_{k_2}) \tag{7.1}$$

where k_1 and k_2 stand for the spatial modes. A phase shift ϕ introduced onto the single photon path, induces a shift between the two components equal to $N\phi$, this allows to observe a sub Rayleigh resolution in interferometric measurements which scales as $\frac{\lambda}{2N}$, λ

being the wavelength of the field [DCS01]. NOON states are then quite useful in quantum lithography applications, in which a resolution greater than the one imposed by Rayleigh $\frac{\lambda}{2}$ is required [BKA$^+$00].
In the context of classical interferometry the intensity generated by the interference of two field impinging on a screen is proportional to $\Delta(x) = 1+\cos(kx) = 1+\cos(\varphi)$, with $k = \frac{2\pi}{\lambda}$ and $\varphi = kx$ representing the phase difference associated with the path difference x. The Rayleigh criterion imposes that the minimal spatial resolution that can be achieved corresponds to the minimum distance between a maximum and a minimum of the resulting fringe pattern: $\varphi^{min} = \pi$, from which $x^{min} = \frac{\lambda}{2}$. This limit can be overcome by using NOON states in a quantum lithography experiment. Let us analyze a simple interferometric setup, shown in figure 7.1:

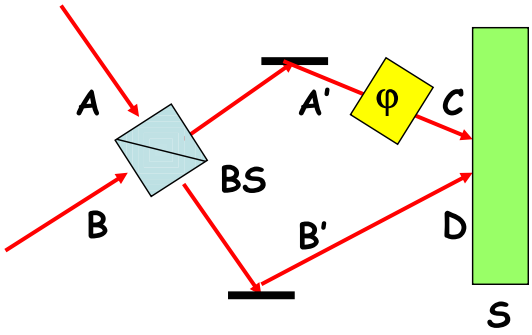

Figure 7.1: Interferometric scheme used in quantum lithography experiment.

A symmetric BS is placed on the two beams path, which enter by the input ports A and B. The output fields are reflected by two mirrors and represent the path C and D of the interferometer. The phase shift associated with the path difference between the two arms is simulated by dephasing medium which induces a a difference φ on the upper arm of the interferometer. The two input ports A and B can be identified by the creation operators $\widehat{a}$ and $\widehat{b}$ which satisfy the usual commutation relations: $\left[\widehat{a},\widehat{a}^\dagger\right] = \left[\widehat{b},\widehat{b}^\dagger\right] = 1$ and $\left[\widehat{a},\widehat{b}\right] = 0$. We can then consider the impinging field on plane S proportional to the sum of the operators $\widehat{c}$ and $\widehat{d}$ associated with the arms C and D of the interferometer. The fields $\widehat{c}$ and $\widehat{d}$ are connected with the fields $\widehat{a}$ and $\widehat{b}$ from the relation: $\widehat{\mathbf{T}}\begin{bmatrix}\widehat{a}\\ \widehat{b}\end{bmatrix} = \begin{bmatrix}\widehat{c}\\ \widehat{d}\end{bmatrix}$, the matrix $\widehat{\mathbf{T}}$ is the transfer matrix, which in our case is given by the product between matrices: $\widehat{\mathbf{B}} = \frac{1}{\sqrt{2}}\begin{pmatrix}-1 & i\\ i & -1\end{pmatrix}$, $\widehat{\mathbf{R}} = \begin{pmatrix}-1 & 0\\ 0 & -1\end{pmatrix}$, and $\widehat{\mathbf{P}} = \begin{pmatrix}e^{i\varphi} & 0\\ 0 & 1\end{pmatrix}$, which represent the action of the *BS*, mirror and dephasing medium, respectively. It turns out that: $\widehat{\mathbf{T}} = \widehat{\mathbf{P}}\widehat{\mathbf{R}}\widehat{\mathbf{B}}$. The output fields, expressed as a function of the input fields are: $\widehat{c} = (\widehat{a} - i\widehat{b})e^{i\varphi}/\sqrt{2}$ and $\widehat{d} = (-i\widehat{a}+\widehat{b})/\sqrt{2}$. The total electric field, impinging on the screen S is then: $\widehat{e} = \widehat{c}+\widehat{d} = \frac{1}{\sqrt{2}}\left[(e^{i\varphi}+i)\widehat{a}+(1-ie^{i\varphi})\widehat{b}\right]$. The absorption rate of the N photons onto the screen S is then proportional to the operator $\widehat{\delta}_N \equiv (\widehat{e}^\dagger)^N(\widehat{e})^N/N!$, and it can take different form depending on the input state into the interferometer. If we consider as input in the inter-

ferometer the single photon state $|\psi_I\rangle = |1\rangle_A|0\rangle_B$, we obtain:

$$\Delta_1(\varphi) = \langle\psi_I|\widehat{\delta_1}|\psi_I\rangle = 1 - \sin\varphi \tag{7.2}$$

if at the input there is a classical state, it turns out that:

$$\Delta_2^c(\varphi) = \langle\psi_{II}^c|\widehat{\delta_2}|\psi_{II}^c\rangle = \frac{3}{2} - 2\sin(\varphi) - \frac{1}{2}\cos(2\varphi) \tag{7.3}$$

in which the term $\cos(2\varphi)$, which presents a sub-Rayleigh resolution, appears. If the input state is given by a quantum state such as $|\psi_2^q\rangle = |1\rangle_A|1\rangle_B$ the two photon absorption rate takes the form:

$$\Delta_2^q(\varphi) = \langle\psi_{II}^q|\widehat{\delta_2}|\psi_{II}^q\rangle = 1 + \cos(2\varphi) \tag{7.4}$$

this interference pattern allows to obtain a resolution equal to $x_2^{min} = \lambda/4$.
The state $|\psi_{II}^q\rangle = |1\rangle_A|1\rangle_B$ in input into the BS, becomes at the exit an entangled state: $|\psi_E\rangle = \left(|0\rangle_{A'}|2\rangle_{B'} + |2\rangle_{A'}|0\rangle_{B'}\right)/\sqrt{2}$. After the phase φ the state reads:
$|\psi_E(\varphi)\rangle = \left(|0\rangle_C|2\rangle_D + e^{2i\varphi}|2\rangle_C|0\rangle_D\right)/\sqrt{2}$.
This result can be extended to the N-photons NOON case as follows: for an impinging state equal to: $|\psi_E\rangle = \left(|0\rangle_{A'}|N\rangle_{B'} + |N\rangle_{A'}|0\rangle_{B'}\right)/\sqrt{2}$ at the exit of the BS, we would obtain: $|\psi_E(\varphi)\rangle = \left(|0\rangle_C|N\rangle_D + e^{Ni\varphi}|N\rangle_C|0\rangle_D\right)/\sqrt{2}$, and the resulting interference pattern would be: $\Delta_N^q(\varphi) = \langle\psi_N^q|\widehat{\delta_2}|\psi_N^q\rangle = 1 + \cos(N\varphi)$ which allows to obtain a resolution equal to $\lambda/2N$. The generation of NOON state with increasing N can in principle be obtained by using materials with non-linear suscettivity $\chi^{(N)}$ [PST98], in which the interaction of the field with the crystal produces N photons by spontaneous parametric down conversion. Another approach exploits the adoption of $(N-1)$ crystals with non-linear suscettivity $\chi^{(2)}$ [PST98]. These proposals are nevertheless difficult to realize experimentally, and up to now, quantum lithography experiments have involved up to four-photons NOON states [MLS04, NDSD07].

7.1.1 Interferometrical pattern and decoherence

In this section we recall the interferometrical pattern of the NOON state looking at how the state features are affected by losses.
We begin with the polarization entangled NOON state $|\psi^N\rangle_1 = \frac{1}{\sqrt{2}}\left(|N+\rangle - |N-\rangle\right)_1$. In this case the N-photon state is entangled in the polarization degree of freedom and belongs to the spatial mode $\mathbf{k}_1$. Introducing a phase shift φ between the two orthogonal polarizations, the state reads $|\psi_\varphi^N\rangle_1 = \frac{1}{\sqrt{2}}\left(|N+\rangle - e^{\imath N\varphi}|N-\rangle\right)_1$, where $|p\xi\rangle$ refers to the quantum state with p photons polarized $\overrightarrow{\pi}_\xi$. The M-th order correlation function $\mathscr{G}_{seed}^{(M)} = \langle\psi_\varphi^N|\hat{a}_H^{\dagger M}\hat{a}_H^M|\psi_\varphi^N\rangle$ reads, for M=N:

$$\mathscr{G}_{seed}^{(N)} = \frac{N!}{2^N}\left[1 + (-1)^{N+1}\cos(N\varphi)\right] \tag{7.5}$$

while for $M < N$ all the functions do not exhibit any oscillation behaviour and have the expression:

$$\mathscr{G}^{(M)}_{seed} = \frac{N!}{2^M (N-M)!} \tag{7.6}$$

In order to simulate losses in the transmission path and non unitary detection efficiency, we now introduce a Beam Splitter (BS) of transmittivity η, as shown in Fig.7.2.

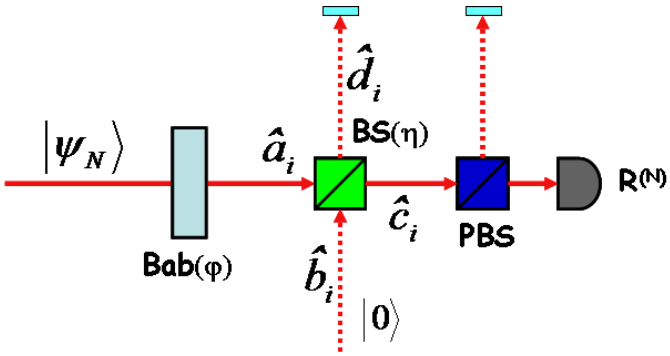

Figure 7.2: Decoherence model of the interferometric process. The phase shift in the NOON state $|\psi^N\rangle$ is inserted by a Babinet compensator, while the BS with efficiency η models the decoherence process. The signal is then analyzed in polarization by the PBS and the N photons absorbing device $R^{(N)}$.

The density matrix after the decoherence process, obtained by the insertion of the I/O BS relations and by tracing on the unrevealed reflected mode, becomes:

$$\hat{\rho}_{loss} = \eta^N \hat{\rho}_{NOON} + \sum_{i=0}^{N-1} \binom{N}{i} \eta^i (1-\eta)^{N-i} \hat{\rho}_i \tag{7.7}$$

where $\hat{\rho}_{NOON} = |\psi^N_\varphi\rangle\langle\psi^N_\varphi|$ is the density matrix of a pure NOON state, and $\hat{\rho}_i = \frac{1}{2}\left[|i+,0-\rangle\langle i+,0-| + |0+,i-\rangle\langle 0+,i-|\right]$ is the density matrix of a mixed i photons state. Only the first part of this quantum state contributes to the N-th order correlation function, and the successful events rate is reduced by a factor η^N. We finally obtain that the correlation function after losses reads:

$$\mathscr{G}^{(N)}_{loss} = \eta^N \mathscr{G}^{(N)}_{seed} \tag{7.8}$$

We propose in the following sections to exploit an amplification process in order to improve the robustness to losses of these states without losing their $\frac{\lambda}{N}$ sub-Rayleigh feature.

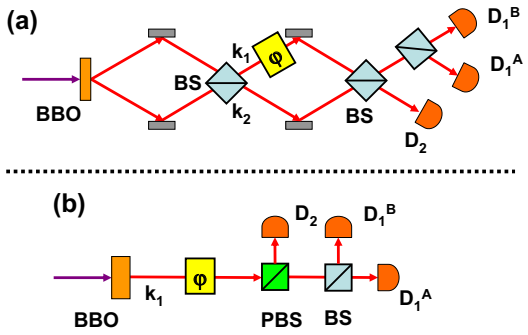

Figure 7.3: (a) Experimental scheme for quantum lithography based on spontaneous parametric down-conversion. The 2-photon absorption is simulated through a 2-photon coincidence detection. (b) Configuration based on polarization entangled beams.

7.2 Sub-Rayleigh resolution by an unseeded high-gain optical parametric amplifier

In the section we experimentally investigate the properties of the optical parametric amplifier (OPA) operating in the high gain regime. Instead of dealing with path entangled states, we consider the generation of entangled states over the same mode but with orthogonal polarizations, respectively, horizontal ($\overrightarrow{\pi}_H$) and vertical ($\overrightarrow{\pi}_V$). The scheme is shown in Fig.7.3. The non-linear crystal (BBO) is pumped by a high-power laser. The first order contribution to the output field is the twin photons state over the same mode: $2^{-1/2}\left(|2\rangle_+|0\rangle_- + |0\rangle_+|2\rangle_-\right) = |1\rangle_H|1\rangle_V$, with $\overrightarrow{\pi}_\pm = 2^{-1/2}(\overrightarrow{\pi}_H \pm \overrightarrow{\pi}_V)$. Such polarization-entangled photons can be easily converted to path entangled via an additional polarizing BS. The PBS of Fig.7.3-(b) mixes the two polarization components $\overrightarrow{\pi}_+$ and $\overrightarrow{\pi}_-$ as the second BS of Fig.7.3-(a) mixes the two different path modes, similar arrangements of polarization NOON were adopted in Ref.[MLS04, WPA$^+$04].

Let us introduce the generic quantum states generated by the OPA acting on the vacuum fields $|0\rangle_H|0\rangle_V$. The interaction Hamiltonian of the optical parametric amplification $\widehat{H}_{coll} = i\chi\hbar\widehat{a}_H^\dagger\widehat{a}_V^\dagger + h.c.$ acts on the single spatial mode $\mathbf{k}_1$. A fundamental physical property of $\widehat{H}_{coll}$ consists of its expression for any polarization basis belonging to the equatorial basis. Indeed $\widehat{H}_{coll}$ can be written as $\frac{1}{2}i\chi\hbar\left(\widehat{a}_+^{\dagger 2} + \widehat{a}_-^{\dagger 2}\right) + h.c.$ where $\widehat{a}_\pm^\dagger$ are the creation operators for the $\overrightarrow{\pi}_\pm$ polarization modes, respectively. The output state over the mode $\mathbf{k}_1$ of the unseeded optical parametric amplifier is found to be:

$$|\Phi\rangle = \frac{1}{C}\sum_{n=0}^{+\infty}\Gamma^n|n\rangle_H|n\rangle_V = \frac{1}{C}\sum_{i,j=0}^{+\infty}\Gamma^{i+j}|2i\rangle_+|2j\rangle_- \tag{7.9}$$

with $C \equiv \cosh g$, $\Gamma \equiv \tanh g$, being g the non linear (NL) gain [DS05]. This state is usually called a two-mode squeezed state. The average photon number created per polarization mode is equal to $\overline{n} = \sinh^2 g$. In the interferometric setup the output state is shifted by a phase φ in the basis $\{\overrightarrow{\pi}_+, \overrightarrow{\pi}_-\}$. Hence the output state is detected in the basis $\{\overrightarrow{\pi}_H, \overrightarrow{\pi}_V\}$; adopting a polarizing beam splitter (PBS). For different values of the phase φ, the quantum state $|\Phi\rangle$ is analyzed through two different second-

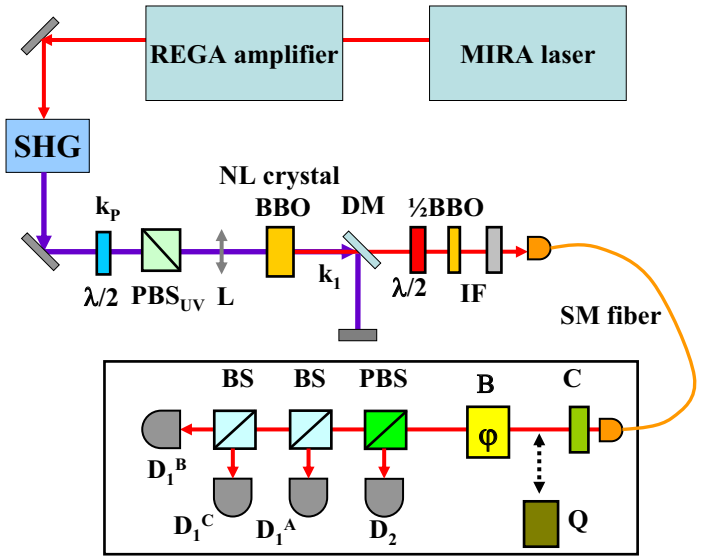

Figure 7.4: Experimental layout. The radiation generated in the NL crystal is spectrally filtered by an interferential filter (IF) with bandwidth equal to 3nm and spatially selected adopting a single mode (SM) fiber.

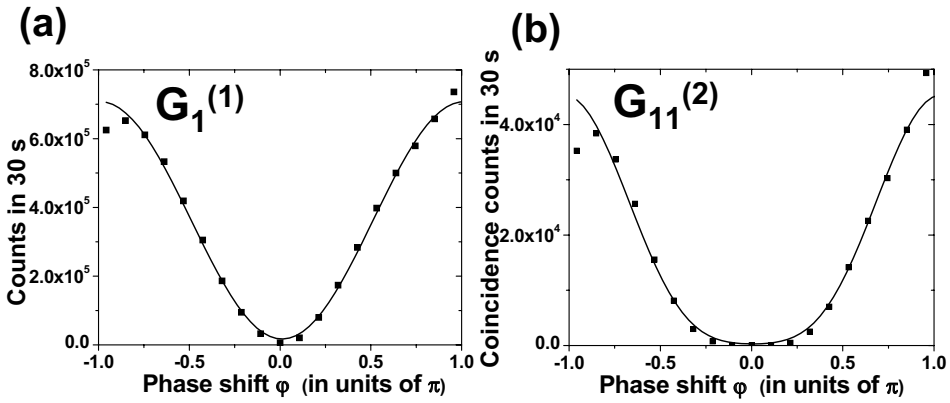

Figure 7.5: Coherent state as input field. (a) $G_1^{(1)}$: Count rates D_1^A versus the phase φ. (b) $G_{11}^{(2)}$: Coincidence counts $[D_1^A, D_1^B]$ versus the phase φ.

order correlation functions $G_{12}^{(2)} = \langle\Phi| c_1^\dagger c_2^\dagger c_2 c_1 |\Phi\rangle$ and $G_{11}^{(2)} = \langle\Phi| c_1^\dagger c_1^\dagger c_1 c_1 |\Phi\rangle$ where $\{c_1^\dagger = \left(\cos\frac{\varphi}{2}\hat{a}_H^\dagger - i\sin\frac{\varphi}{2}\hat{a}_V^\dagger\right)e^{i\frac{\varphi}{2}}, c_2^\dagger = \left(-i\sin\frac{\varphi}{2}\hat{a}_H^\dagger + \cos\frac{\varphi}{2}\hat{a}_V^\dagger\right)e^{i\frac{\varphi}{2}}\}$ are the output modes of the PBS. By tuning φ it is found $G_{12}^{(2)}(\varphi) = \overline{n}^2 + \frac{1}{2}(\overline{n}^2 + \overline{n})(1 + \cos 2\varphi)$ and $G_{11}^{(2)}(\varphi) = 2\overline{n}^2 + \frac{1}{2}(\overline{n}^2 + \overline{n})(1 - \cos 2\varphi)$ [NBBA01]. The corresponding visibilities of the obtained

fringe patterns read $V_1^{(2)} = \frac{\bar{n}+1}{5\bar{n}+1}$ and $V_{12}^{(2)} = \frac{\bar{n}+1}{3\bar{n}+1}$. We observe that a non-vanishing visibility is found for any value of g : $V_1^{(2)}(g \to \infty) = \frac{1}{5}$ and $V_{12}^{(2)}(g \to \infty) = \frac{1}{3}$. The two fringe patterns exhibit a dependence on 2φ and hence a period equal to $\frac{\lambda}{2}$. This feature can be exploited to carry out interferometry with sub-Rayleigh resolution, i.e., with fringe period lower than λ, in a higher flux regime compared to the two photon configurations.

7.2.1 Experimental setup and results

We now briefly describe the experimental configuration: Fig.7.4. The excitation source was a Ti:Sa Coherent MIRA mode-locked laser further amplified by a Ti:Sa regenerative REGA device operating with pulse duration 180fs at a repetition rate of 250kHz. The output beam, frequency-doubled by second harmonic generation, provided the excitation beam of UV wavelength $\lambda_P = 397.5$nm and power 300mW. The horizontally polarized UV beam was then adopted to pump a non-linear BBO crystal, which generated pairs of photons with polarization $\vec{\pi}_H$ and $\vec{\pi}_V$ over the modes k_1 with same wavelength $\lambda = 2\lambda_P$. This source allows us to obtain a high value of the gain g, which depends on the pumping power: $g \propto \sqrt{P_{UV}}$. Compared to conventional pulsed sources used to pump SPDC process, which achieve $g \simeq 0.1$, the energy per pulse is enhanced by a factor $\simeq 400$, leading to an increase of the gain value in the range of $20-40$ depending on the focal length of the UV beam. The pumping power could be tuned adopting a half-wave plate and a polarizing beam splitter (PBS_{UV}). The output state of BBO crystal with wavelength λ was spatially separated by the fundamental UV beam through a dichroic mirror (DM), then

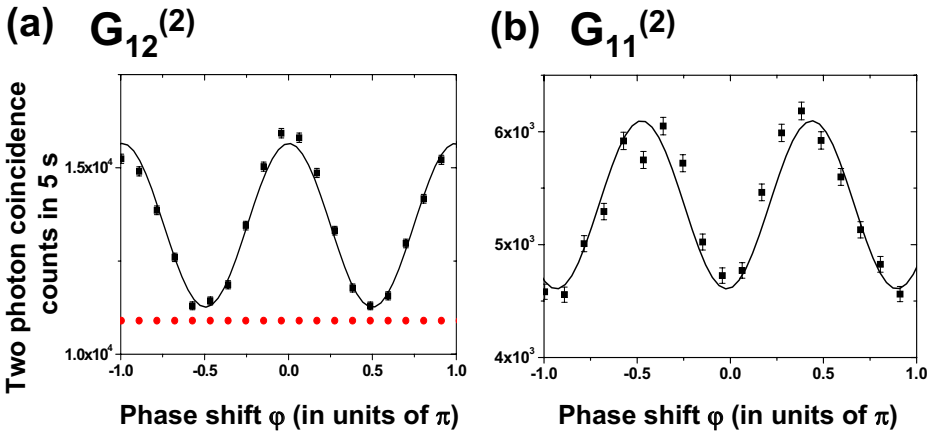

Figure 7.6: (a) $G_{12}^{(2)}$: two-photon coincidence counts $[D_1^A, D_2]$ versus the phase φ introduced by the Soleil-Babinet compensator ($g = 1.4$). Circle data: expected accidental (without correlations) coincidence rates. (b) $G_{11}^{(2)}$: two-photon coincidence counts $[D_1^A, D_1^B]$ versus the phase φ ($g = 1.4$). Variations of the detectors signal ($\sim 10\%$) due to different couplings of polarizations $\vec{\pi}_H$ and $\vec{\pi}_V$ with fiber have been corrected by normalizing coincidence counts with signal rates.

spectrally filtered adopting an interferential filter (IF) with bandwidth equal to 3nm and then coupled to a single mode fiber in order to select spatially a single mode of emission. A $\lambda/2$ waveplate and a BBO with thickness of 0.75mm provided the compensation of walk-off effects. At the output of the fiber, after compensation (C) of the polarization rotation induced by the fiber, a phase shifting φ was introduced adopting a Soleil-Babinet compensator (B). The output radiation was then analyzed through a polarizing beam splitter (PBS) and detected adopting single photon detectors SPCM-AQR14 (D_1^A, D_1^B, D_1^C, D_2). To characterize the detection apparatus, a coherent state with wavelength λ and polarization $\vec{\pi}_H$ was fed into the mode k_1. The count rates D_1^A and the coincidence rates $[D_1^A, D_1^B]$ were measured versus the phase φ: Fig.7.5. High visibility patterns have been observed with a period equal to λ

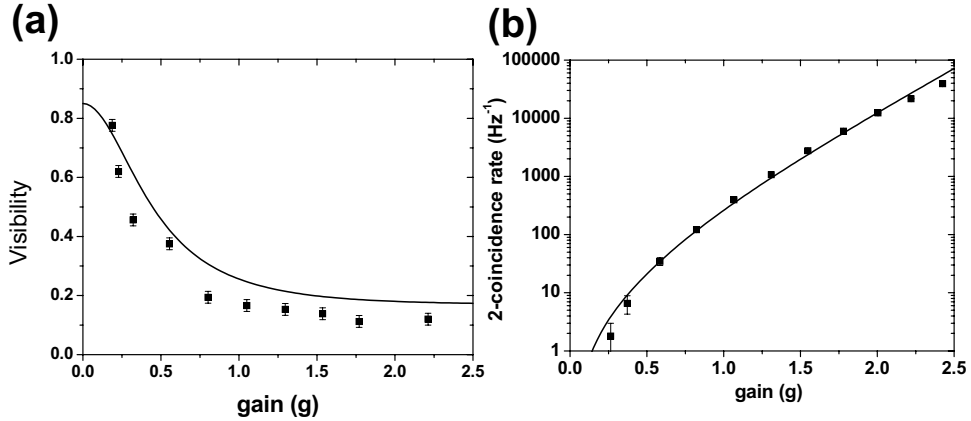

Figure 7.7: (a) Visibility versus non-linear gain. The continuous line corresponds to the function $V_{\max} \times V_1^{(2)}(g)$. (b) Excitation rate versus non-linear gain. The continuous line corresponds to the function $\overline{R}^{(2)}(\alpha g)$ where the parameter α has been optimized by fitting the data and reads 0.85.

As a first experimental step we have characterized the two-photon state generated by SPDC in the low gain regime. The visibilities have been found $V_{12}^{(2)} = (85 \pm 2)\%$ and $V_1^{(2)} = (80 \pm 1)\%$. The discrepancy with the expected values $V = 1$ is attributed to double-pair emission and to experimental imperfections. The same measurement has been carried out increasing the UV pump beam in order to measure the fringe patterns for different gain values. The gain has been estimated with the method introduced in Ref. [EKD$^+$04, CDP$^+$06]. Fig.7.6 refers to the configuration $g = 1.4$. The visibilities have been found to be $V_{12}^{(2)} = (16.8 \pm 0.6)\%$ and $V_1^{(2)} = (15 \pm 1)\%$. The sub Rayleigh resolution is clearly shown by the experimental data of Fig.7.6. For the sake of completeness the value of $V_1^{(2)}$ has been measured for different gains: Fig.7.7-(a). The continuous line shows the expected theoretical function $V_1^{(2)}(g)$ multiplied by the extrapolated visibilities for $g \to 0 : V_{\max} = 0.85$. We attribute the discrepancy between experimental and theoretical visibilities to partial multimode operation of the optical parametric amplifier

[TR04].

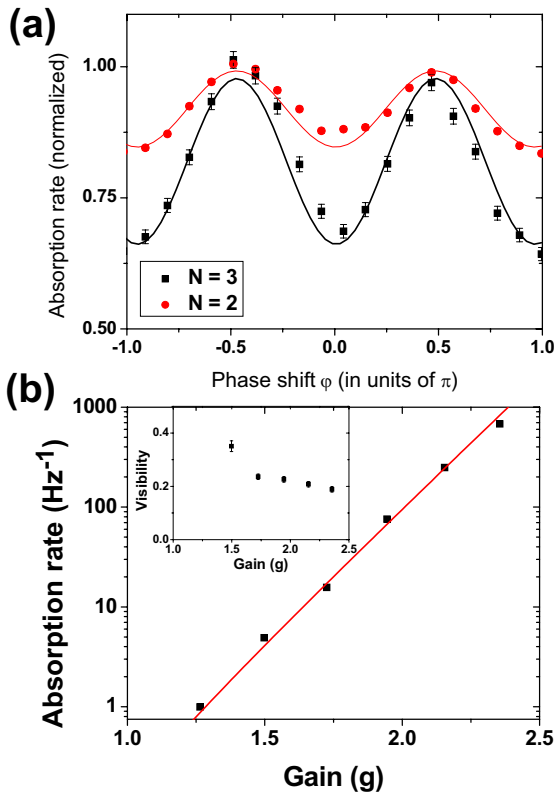

Figure 7.8: (a) Circle data: $G_1^{(2)}$ (two-photon coincidences $[D_1^A, D_1^B]$) versus the phase φ; Square data: $G_1^{(3)}$ (three-photon coincidences $[D_1^A, D_1^B, D_1^C]$) versus the phase φ ($g = 2.4$) (b) Excitation rate versus non-linear gain. The continuous line corresponds to the function $\overline{R}^{(3)}(g)$. Inset: visibility $V_1^{(3)}$ versus non-linear gain.

To estimate the dependence of the excitation rate from the NL gain g, the maxima and the minima of the fringes have been measured versus the pumping power. The average data are reported in Fig.7.7-(b). Our experiment validates the result found by Agarwal et al. [ACB$^+$07] showing an exponential dependence on the parameter g. The expected two-photon excitation rate reads $\overline{R}^{(2)} = 2\sigma^{(2)}(\overline{n} + 5\overline{n}^2)$ where $\sigma^{(2)}$ is a generalized two-photon excitation cross section [ACB$^+$07]. Fig.7.7-(b) shows how the excitation efficiency scales quadratically with the light intensity, in contrast with the two-photon SPDC regime; which leads to a linear dependence [JG90, PST98].

As further demonstration of the potentialities of the present approach, the simultaneous detection of three photons over the same mode has been investigated. The average three photon excitation rate reads $\overline{R}^{(3)} = 12\sigma^{(3)}(7\overline{n}^3 + 3\overline{n}^2)$ where $\sigma^{(3)}$ is a generalized three-photon excitation cross section and the visibility of the fringes is theoretically found as $V_1^{(3)} = \frac{3\overline{n}+3}{7\overline{n}+3}$ [ACB$^+$07]. Again a non-vanishing value of $V_1^{(3)}$ is found for any value of $g : V_1^{(3)}(g \to \infty) = \frac{3}{7}$ and the patterns exhibit a period equal to $\frac{\lambda}{2}$. Furthermore an increase of visibility is expected $V_1^{(3)} > V_1^{(2)}$. To demonstrate such a feature the three-photon coincidence rate $G_1^{(3)}$ has been measured versus the phase φ: Fig.7.8-(a). An increase of the visibility has been found $V_1^{(3)} = (21.6 \pm 0.6)\%$, the experimental dependencies of the three photon absorption rates and visibilities are shown in Fig.7.8-(b).

In order to investigate the connection between the quantum feature of the state and the visibility of the fringe pattern, we have introduced a decoherence between the two polarization components $\{\vec{\pi}_H, \vec{\pi}_V\}$ or $\{\vec{\pi}_+, \vec{\pi}_-\}$ with a quartz crystal (Q) with a length equal to 20mm. This device introduces a temporal delay higher than the coherence time of the multiphoton fields. The $G_1^{(2)}$ has been first measured without the quartz: Fig.7.9. When the decoherence affects the $\{\vec{\pi}_H, \vec{\pi}_V\}$ components, we observe a reduction of visibility down to $(4.8 \pm 0.6)\%$; on the other hand when the decoherence involves the $\{\vec{\pi}_+, \vec{\pi}_-\}$ we observe the disappearance of the fringe patterns. The inversion of the maxima and minima of the square data compared to the circle data, a phenomenon not expected in the single-pair regime, is due to the reduction of the bunching effect among photons detected on the same polarization mode when decoherence is introduced.

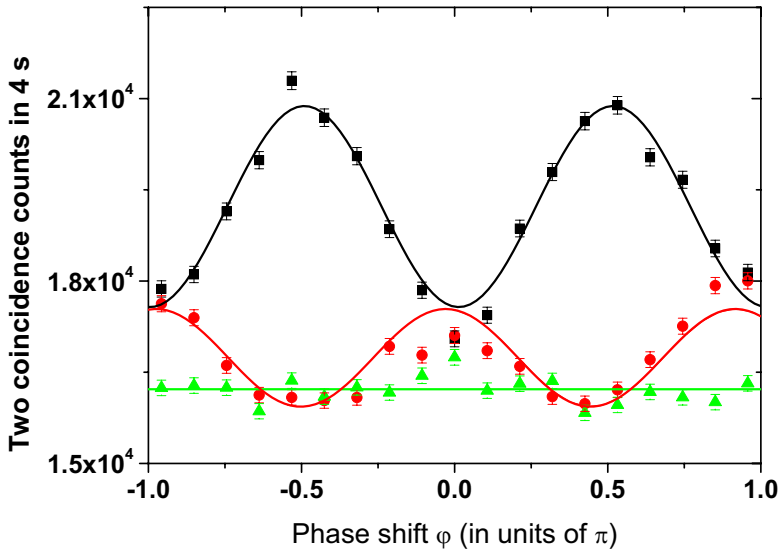

Figure 7.9: Effects of coherence on fringe visibility. Square data: 2-photon coincidences counts versus the phase φ without introducing decoherence. Circle data: decoherence introduced between the polarization components$\{\vec{\pi}_H, \vec{\pi}_V\}$. Triangle data: decoherence introduced between $\{\vec{\pi}_+, \vec{\pi}_-\}$.

7.3 Amplification of NOON states

We have seen that the weak value of the generated number of photons in a NOON state strongly limits the potential applications to quantum lithography and quantum metrology. Furthermore a NOON state, as any superposition of macroscopic states, is "supersensitive" to losses. Hence for a N-photon state a fractional loss $\frac{1}{N}$ would destroy the quantum effect responsible for the phase resolution improvement.
A natural approach to increase the number of photons and to minimize the effect of losses

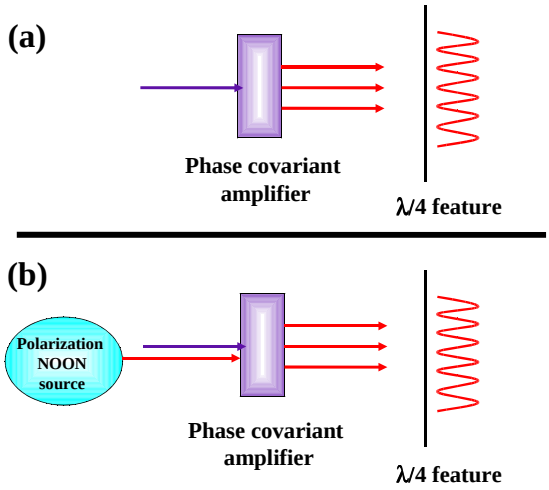

Figure 7.10: (a)Unseeded optical parametric amplifier . (b) Amplification of a polarization entangled NOON state.

is to exploit the process of stimulated emission.
In the previous sections we have seen how the output radiation of an unseeded optical parametric amplifier (OPA) can be exploited to show the typical $\lambda/4$ feature [DSV08] Fig.7.10-(a). In the present section we investigate the task of the amplification of photonic NOON states by two different devices, both based on a quantum injected optical parametric amplifier (QIOPA). In Sec.7.4 we study both theoretically and experimentally the amplification of a 2 photon state by a collinear QIOPA, as shown schematically in Fig.7.10-(b), investigating how the features of the state are modified when the entanglement is broadcasted via amplification over a large number of particles. An experimental comparison with the spontaneous field Fig.7.10-(a) of the collinear OPA, that intrinsically has a $\frac{\lambda}{4}$ feature [DSV08], shows that the visibilities in the two regimes are comparable, while the injected case manifests an increase of the signal due to the stimulated emission process. We then show that this device cannot be successfully used to amplify a generic N-photon state since the typical $\frac{\lambda}{2N}$ feature of the seed is lost. Finally, in Sec.7.5, we propose to exploit a non-collinear QIOPA in order to amplify a generic state maintaining the interference pattern of the seed, showing that significant value of the visibilities can be achieved by investigating high-order correlation functions. Finally, the effects of losses are investigated, demonstrating that the amplified field exhibits a higher resilience to losses with respect to a pure NOON state.

7.4 Collinear amplification of a 2 photon NOON state

In this section we study, both theoretically and experimentally, the amplification of a two-photons polarization-entangled NOON state exploiting an optical parametric amplifier working in a collinear configuration. It will be shown that this device cannot be used to amplify a generic N-photons state as its $\frac{\lambda}{2N}$ oscillation pattern is masked by the intrinsic oscillation of the amplification crystal.

7.4.1 Theoretical approach

As a first step we consider the generation of a two photon NOON state by spontaneous parametric down conversion in a first crystal over the two polarization mode $\overrightarrow{\pi}_+$ and $\overrightarrow{\pi}_-$, on the same spatial mode $\mathbf{k_1}$. The state generated is $|\psi^2\rangle_1 = \frac{1}{\sqrt{2}}(|2+\rangle - |2-\rangle)_1 = |1H;1V\rangle_1$, where $|p+;q-\rangle$ stands for the quantum state of p photons polarized $\overrightarrow{\pi}_+$ and q photons polarized $\overrightarrow{\pi}_-$.

The amplification of the state $|\psi^2\rangle_1$ is realized by injecting the quantum state into a QIOPA acting on the input field $\mathbf{k_1}$. The interaction Hamiltonian of the optical parametric amplification $\widehat{H}_{coll} = i\chi\hbar\widehat{a}^\dagger_{1H}\widehat{a}^\dagger_{1V} + h.c.$ acts on the spatial mode $\mathbf{k_1}$. The output state over the mode $\mathbf{k_1}$ is:

$$|\Phi^2\rangle_1 = \frac{1}{C}\sum_{n=0}^{\infty}\Gamma^{n-1}\left(\frac{n}{C^2} - \Gamma^2\right)|nH;nV\rangle_1 \tag{7.10}$$

with $C = \cosh g$, $\Gamma = \tanh g$, being g the non-linear gain of the amplification process [DS05].

The peculiar $\lambda/4$ interference path feature of a two photon NOON state, can be investigated by performing an interferometric measurement on the amplified field. To this end a phase shift θ is introduced, after the amplification stage, in the $\{\overrightarrow{\pi}_+, \overrightarrow{\pi}_-\}$ basis, corresponding to a rotation of an angle $\theta/2$ in the basis $\{\overrightarrow{\pi}_H, \overrightarrow{\pi}_V\}$. The state is then analyzed in polarization and detected adopting single photon detectors. The amplified signal can be evaluated by the first order correlation function $\mathscr{G}^{(1)}_{N=2} = {}_1\langle\Phi^2|\widehat{c}^\dagger_1\widehat{c}_1|\Phi^2\rangle_1$, where $\widehat{c}^\dagger_1 = \left(\cos\theta/2\widehat{a}^\dagger_{1H} - \sin\theta/2\widehat{a}^\dagger_{1V}\right)$ is the transmitted mode of a polarizing beam splitter (PBS). We find that $\mathscr{G}^{(1)}_{N=2} = 3\overline{n}+1$, independently of the phase value θ, with $\overline{n} = \sinh^2 g$. The state generated by the amplifier is then investigated through the second order correlation function $\mathscr{G}^{(2)}_{N=2} = {}_1\langle\Phi^2|\widehat{c}^\dagger_1\widehat{c}^\dagger_1\widehat{c}_1\widehat{c}_1|\Phi^2\rangle_1$. By tuning the phase shift θ, we find that the expression of the second order correlation function is:

$$\mathscr{G}^{(2)}_{N=2} = 2\overline{n}(4+7\overline{n}) + \frac{1}{2}(7\overline{n}^2 + 7\overline{n} + 1)(1-\cos(2\theta)) \tag{7.11}$$

The corresponding visibility of the obtained fringe pattern is calculated accordingly to the general definition:

$$\mathscr{V}^{(M)}_N = \frac{\mathscr{G}^{(M)}_N(max) - \mathscr{G}^{(M)}_N(min)}{\mathscr{G}^{(M)}_N(max) + \mathscr{G}^{(M)}_N(min)} \tag{7.12}$$

where M is the order of the correlation and N is the number of photon of the injected seed. In the case of eq.(7.11) the visibility reads:

$$\mathscr{V}^{(2)}_{N=2} = \frac{7\overline{n}^2 + 7\overline{n} + 1}{35\overline{n}^2 + 23\overline{n} + 1} \tag{7.13}$$

We observe that a non-vanishing visibility is found for any value of g : $\mathscr{V}^{(2)}_{N=2}(g \to \infty) = \frac{1}{5}$. The fringe pattern exhibits a dependence on 2θ and hence a period equal to

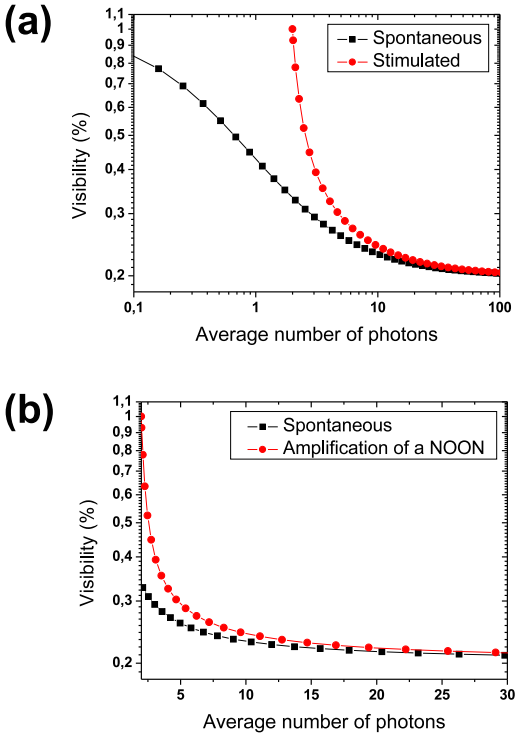

Figure 7.11: Theoretical trend of the visibility in function of the number of photons generated by the amplification in the two cases: spontaneous and stimulated.

$\frac{\lambda}{2}$. This feature can be exploited to carry out interferometry with sub-Rayleigh resolution, i.e., with fringe period lower than λ, in a higher flux regime compared to the two photon configurations. The interest in amplifying a NOON state belongs to the trend of visibility as a function of the number of generated photons. Recently, as said, it has been demonstrated [DSV08] that the output field of a collinear parametric amplifier working in spontaneous emission regime shows a $\lambda/4$ feature. There an unseeded optical parametric amplifier working in collinear regime was pumped by an UV beam. The output radiation, after a phase shifter, was analyzed in polarization. The fringe pattern visibility in that case was $\mathscr{V}^{(2)}_{N=0} = \frac{\bar{n}+1}{5\bar{n}+1}$. The asymptotical values of visibilities in the two regimes, spontaneous and stimulated, are equal; on the contrary for an intermediate number of generated photons the visibility in the amplified regime is higher than that in the spontaneous one as shown in Fig. 7.11-(a). Hence, the injection of a seed with theoretical visibility equal to 1 leads to an advantage in the visibility for the amplified field with respect to the case of spontaneous emission. We note that the same average number of photons in the two regimes is achieved for different values of the gain. In the spontaneous regime the average photons number generated by the amplifier is $\langle \hat{n} \rangle_{sp} = 2\sinh^2 g$, on the contrary, for the same gain value, in the stimulated regime we have: $\langle \hat{n} \rangle_{stim} = 2 + 6\sinh^2 g$. For a value of the gain $g = 0$ the number of photons in the stimulated case is $\langle \hat{n} \rangle_{stim} = 2$, unlike the spontaneous case in which $\langle \hat{n} \rangle_{sp} = 0$. In both cases the value of visibility tends to 1 for $g \to 0$. By analyzing the trends of visibilities in Fig.7.11-(b) we see that the advantage

of amplifying a NOON state holds until $\langle \hat{n} \rangle \simeq 30$.

An enhancement of the fringe pattern can be obtained by evaluating the M-th order visibility $\mathscr{V}_{N=2}^{(M)}$, with $M > 2$, corresponding to the M-th order correlation function at time t: $\mathscr{G}_{N=2}^{(M)} = {}_1\langle \psi^2 | [\hat{c}_1^\dagger(t)]^M [\hat{c}_1(t)]^M | \psi^2 \rangle_1$. This calculation have been performed in the Heisenberg picture, where the field operator $\hat{c}_1^\dagger(t)$ is the time evolution of the analyzed field $\hat{c}_1^\dagger$ solving the Heisenberg equations for the collinear OPA. We calculated the first 6 orders correlation functions, obtaining the following visibilities:

$$\mathscr{V}_{N=2}^{(2)} = \frac{1+7\overline{n}+7\overline{n}^2}{1+25\overline{n}+35\overline{n}^2} \tag{7.14}$$

$$\mathscr{V}_{N=2}^{(3)} = \frac{12+48\overline{n}+39\overline{n}^2}{12+84\overline{n}+91\overline{n}^2} \tag{7.15}$$

$$\mathscr{V}_{N=2}^{(4)} = \frac{12+291\overline{n}+822\overline{n}^2+567\overline{n}^3}{12+291\overline{n}+1078\overline{n}^2+903\overline{n}^3} \tag{7.16}$$

$$\mathscr{V}_{N=2}^{(5)} = \frac{135+1315\overline{n}+2845\overline{n}^2+1705\overline{n}^3}{135+1315\overline{n}+3245\overline{n}^2+2201\overline{n}^3} \tag{7.17}$$

$$\mathscr{V}_{N=2}^{(6)} = \frac{45+1745\overline{n}+10080\overline{n}^2+17507\overline{n}^3+9245\overline{n}^4}{45+1745\overline{n}+10080\overline{n}^2+18657\overline{n}^3+10621\overline{n}^4} \tag{7.18}$$

The theoretical plots of the visibilities are reported in Fig.7.12. We observe that an increasing trend is obtained by exploiting correlation functions with higher order M. This means that analyzing a higher order absorption process the contrast of the fringe pattern is enhanced. This feature was also predicted in the spontaneous emission regime in [ACB$^+$07], and experimentally observed in [DSV08].

7.4.2 Experimental verification

The previous theoretical results have been experimentally verified adopting an injected high-gain optical parametric amplifier. The experimental setup is sketched in Fig 7.13.

The excitation source was a Ti:Sa Coherent MIRA mode-locked laser amplified by a Ti:Sa regenerative REGA device operating with pulse duration 180fs at a repetition rate of 250kHz. The output beam, frequency-doubled by second harmonic generation, provided the excitation beam of UV wavelength (wl) $\lambda_P = 397.5$nm and power 750mW. The UV beam was split in two beams through a $\lambda/2$ waveplate and a polarizing beam splitter (PBS) and excited two BBO (β-barium borate) NL crystals cut for type II phase-matching. The pump power of beam $\mathbf{k}_P$ was set in order to have a negligible probability to generate three couples of photons ($< 10\%$). Let us describe how the 2-photon state $|\psi^2\rangle_1 = 2^{-1/2}(|2+\rangle - |2-\rangle)_1 = |1H;1V\rangle_1$ was conditionally generated on mode $\mathbf{k}_1$. We adopted the scheme demonstrated by Eisenberg et al [EKD$^+$04]: Crystal 1, excited by the beam $\mathbf{k}_P$, is the spontaneous parametric down-conversion (SPDC) source of entangled photons of wavelength $\lambda = 2\lambda_P$, emitted over the two output modes $\mathbf{k}_i$

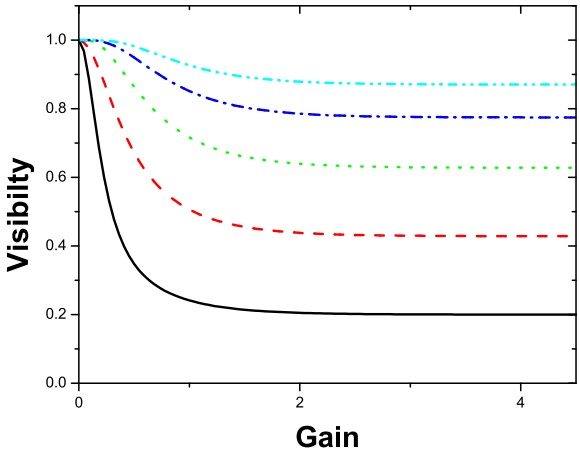

Figure 7.12: Plot of the visibilities $\mathscr{V}_{N=2}^{(M)}$ with $2 \leq M \leq 6$ for the collinear QIOPA in stimulated emission with the injection of a 2-photon NOON state as a function of the nonlinear gain g. Straight line corresponds to $\mathscr{V}_{N=2}^{(2)}$, dashed line to $\mathscr{V}_{N=2}^{(3)}$, dotted line to $\mathscr{V}_{N=2}^{(4)}$, dash-dotted line do $\mathscr{V}_{N=2}^{(5)}$ and short dash-dotted line to $\mathscr{V}_{N=2}^{(6)}$.

$(i = 1, T)$, where T stands for the trigger mode, in the state $|\Psi_2^-\rangle_{1T} = \frac{1}{\sqrt{3}}(|2H\rangle_1|2V\rangle_T - |1H;1V\rangle_1|1H;1V\rangle_T + |2V\rangle_1|2H\rangle_T)$. The two photons associated to mode $\mathbf{k}_T$ were coupled into a single mode fiber and excited two single photon counting module (SPCM) $\{D_T, D_T^*\}$. The state $|1H;1V\rangle_T$ was detected on mode $\mathbf{k_T}$ by measuring the coincidences between detectors $\{D_T, D_T^*\}$ in the $\{\overrightarrow{\pi}_H, \overrightarrow{\pi}_V\}$ polarization basis on mode $\mathbf{k}_T$ leading to the conditional preparation of the state $|1H;1V\rangle_1$ on mode $\mathbf{k}_1$.

The amplification of the injected 2-photon state was achieved by superimposing the pump beam on mode $\mathbf{k_p^{'}}$ and the field on mode $\mathbf{k_1}$ on crystal II exploiting a dichroic mirror (*DM*) with high reflectivity at λ and high transmittivity at λ_p. The output radiation was then analyzed through a polarizing beam splitter (PBS) and detected adopting single photon detectors SPCM-AQR14 $(\mathrm{D}_1^A, \mathrm{D}_1^B, \mathrm{D}_1)$.
In order to characterize the state produced by the first crystal, a measurement of the second order correlation function of the injected field, without the contribution of the UV pump beam on crystal 2, was carried out. The typical $\lambda/4$ fringe pattern was measured by the fourfold coincidences between detectors $\{D_1, D_1^B, D_T, D_T^*\}$, through evaluation of the second order correlation function $G_{seed}^{(2)} = {}_1\langle\psi^2|\hat{c}_1^\dagger\hat{c}_2^\dagger\hat{c}_2\hat{c}_1|\psi^2\rangle_1$, where $\hat{c}_2^\dagger = \left(\sin\theta/2\hat{a}_{1H}^\dagger + \cos\theta/2\hat{a}_{1V}^\dagger\right) = \hat{c}_{1^\perp}^\dagger$. The obtained visibility $\mathscr{V}_{seed}^{(2)} = (63 \pm 4)\%$ is lower than the expected one, due to the experimental imperfections and to the emission of higher number of photons by the first crystal. In Fig.7.14 we report the oscillation of the injected field with (Fig.7.14-(b)) and without (Fig.7.14-(a)) the conditional generation of the two

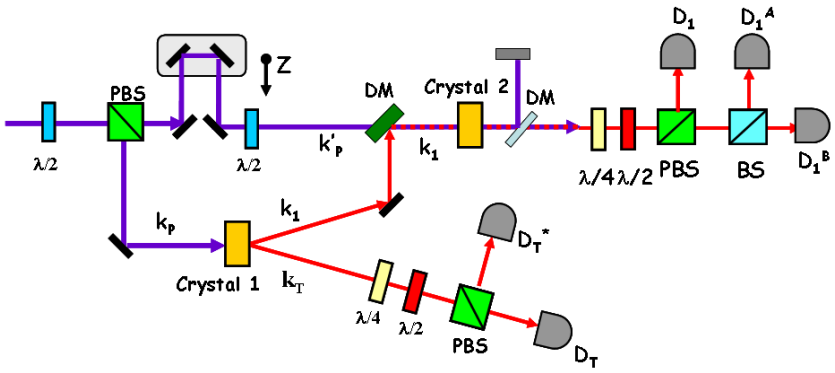

Figure 7.13: Experimental scheme adopted to amplify a 2-photon state.By measuring coincidences between detector $\{D_T, D_T^*\}$ on spatial mode $\mathbf{k_T}$, the state on spatial mode $\mathbf{k_1}$ is prepared in the two-photon NOON state $|\psi^2\rangle_1$.The rate of the trigger signal was around $10{\cdot}000Hz$ and the rate of coincidences between (D_T, D_T^*) was around $400Hz$.

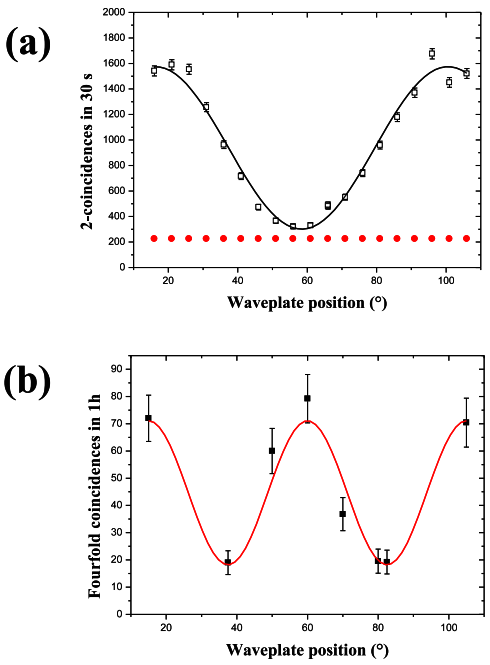

Figure 7.14: (a)Fringe pattern of the two-fold-coincidences between detectors $\{D_1^B, D_T\}$ (b) Fringe pattern of the four-fold-coincidences between detectors $\{D_1, D_1^B, D_T, D_T^*\}$.

photon NOON state by the first crystal. As shown, the two-fold coincidences present a λ period and the $\lambda/4$ feature is displayed only by the fourfold coincidences Fig.7.14-(b).

We characterized then the state generated by the second crystal by evaluating the correlation function $\mathscr{G}^{(2)}$ in the spontaneous, by detecting coincidences between detectors $\{D_1^A, D_1^B, D_T\}$, and stimulated regime, by detecting coincidences between detectors $\{D_1^A, D_1^B, D_T, D_T^*\}$, for a value of the NL gain $g = 2$ [EKD$^+$04, CDP$^+$06]. We observed that the $\lambda/2$ period has been preserved by the amplification process Fig.7.15-(a). The

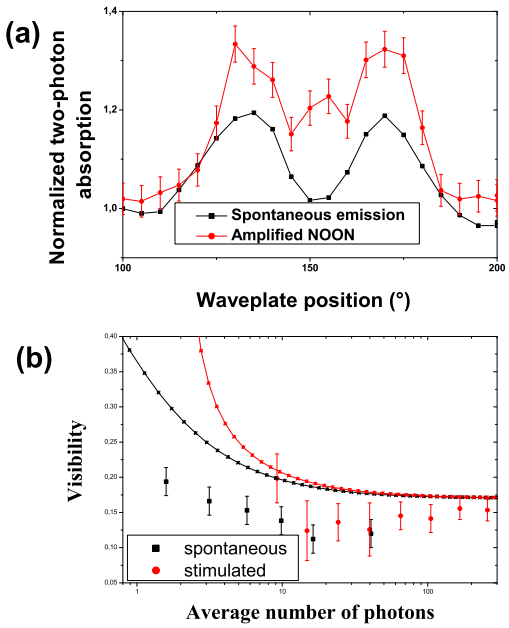

Figure 7.15: (a) Oscillation fringe patterns in the stimulated and spontaneous regimes. The unbalanced minima are due to a different coupling of the $\vec{\pi}_H$ and $\vec{\pi}_V$ polarized signals with the single mode fiber. (b) Visibility value $\mathscr{V}^{(2)}_{N=2}$ as a function of NL gain g in the spontaneous (triangular dots) and stimulated case (circular dots). Experimental (points) and theoretical trend of visibility in the stimulated regime (curve) are shown. The theoretical curve used are: $V_{sp} = 0.85\,\mathscr{V}^{(2)}_{N=0}$ and $V_{stim} = 0.85\,\mathscr{V}^{(2)}_{N=2}$. The factor 0.85 has been inserted to consider experimental imperfections. The curves are parametric plotted as a function of the respective number of generated photons, which are $\langle\hat{n}\rangle_{sp} = 2\sinh^2 g$ and $\langle\hat{n}\rangle_{stim} = 2 + 6\sinh^2 g$. Data in the spontaneous regime refer to work [DSV08].

minima, at 105° and 150°, correspond to polarizations $\vec{\pi}_H$ and $\vec{\pi}_V$. The unbalancing between the two values of the absorption rate is due to a different coupling of the two orthogonal linear polarizations with the single mode fiber. This effect is related with the distinguishability, i.e spectral difference, between the ordinary and extraordinary wave vectors cones generated by the second crystal during the amplification process. The visibility has been evaluated through the definition $\mathscr{V} = \frac{C^{(4)}_{max} - C^{(4)}_{min}}{C^{(4)}_{max} + C^{(4)}_{min}}$, where $C^{(4)}$ is the value of the fourfold coincidences. In particular, only a portion of the global fringe pattern of Fig.7.15 has been used to calculate the visibility. Only the maximum and the adjacent minimum which exhibit the higher contrast were considered, as a $\frac{\pi}{N}$ interval of the fringe pattern, showing a $\frac{\lambda}{2N}$ resolution, is necessary for quantum lithographic applications. By the same measurement we observe the fringe patterns for different gain values by increasing the UV pump beam. We report in Fig. 7.15-(b) the trend of visibility as a function of the number of photons generated: the spontaneous visibilities have been taken from [DSV08]. The experimental data are compared with theoretical predictions in both regimes: spontaneous and stimulated. The theoretical trends have been scaled by a factor 0.85, that was the asymptotical visibility obtained in the spontaneous case in [DSV08], due to experimental imperfections. In the amplified case the experimental asymptotical visibility is affected both by experimental imperfections and by the emission of higher

number of photons by the first crystal. We observe that both the data points for increasing gain values move away from the theoretical trends. This can be due to a partial multimode operation of the parametric amplifier [TR04]. We conclude that the value of visibility in the two regime is almost the same, but an enhancement of the signal in the stimulated case has been observed. Indeed the probability of observing a sub-Rayleigh phenomenon is proportional to the second order correlation function $\mathscr{G}^{(2)}$ in both regimes. By the theory, the stimulated signal is seven time higher than the spontaneous one: $\frac{\mathscr{G}^{(2)}_{N=2}}{\mathscr{G}^{(2)}_{N=0}} = 7$. Experimentally we can evaluate this ratio by the following method: the probability of detecting coincidences in the spontaneous case is $P_{sp} = \frac{C^{(2)}}{R}$, where $C^{(2)}$ are coincidences between detectors $\{D_1^A, D_1^B\}$ and R is the repetition rate. In the stimulated case it reads : $P_{stim} = \frac{C^{(4)}}{\Xi}$, where $C^{(4)}$ are coincidences between detectors $\{D_T, D_T^*, D_1^A, D_1^B\}$, and Ξ are coincidences between detectors $\{D_T, D_T^*\}$ on trigger mode, that is the rate of injection of the two photon NOON state in the QIOPA per second. Hence the ratio between the two probabilities is : $\frac{P_{stim}}{P_{sp}} = (6.21 \pm 0.8)$.

7.4.3 Amplification of $N > 2$ states

As last step, we investigate the amplification of N-photon NOON states with N>2 with the same device. The injection of a 3-photon state $|\psi^3\rangle_1 = 2^{-1/2}\left(|3+\rangle - |3-\rangle\right)_1$ leads to an amplified wave function of the form:

$$|\Phi^3\rangle = \frac{1}{\sqrt{12}C^4}\sum_{i,j=0}^{\infty}\frac{\left(\frac{\Gamma}{2}\right)^i\left(-\frac{\Gamma}{2}\right)^j}{i!\,j!}\left\{\sqrt{(2i+3)!2j!}|(2i+3)+,(2j)-\rangle - \sqrt{2i!(2j+3)!}|(2i)+,(2j+3)-\rangle\right\} +$$
$$-\frac{\Gamma\sqrt{3}}{2C^2}\sum_{i,j=0}^{\infty}\frac{\left(\frac{\Gamma}{2}\right)^i\left(-\frac{\Gamma}{2}\right)^j}{i!\,j!}\left\{\sqrt{(2i+1)!2j!}|(2i+1)+,(2j)-\rangle + \sqrt{2i!(2j+1)!}|(2i)+,(2j+1)-\rangle\right\} \tag{7.19}$$

Let us analyze the expression of the quantum state in equation (7.19). We expect the third order correlation function to have oscillation in all the three harmonics θ, 2θ and 3θ. In fact, the first part of the wave function contains the sum of quantum states of the form $|2i+3, 2j\rangle - |2i, 2j+3\rangle$. These are analogous to 3 photons NOON states with a common background $2i, 2j$ generated by the crystal, thus leading to a $\frac{\lambda}{3}$ period. The same argument holds for the second part of eq.(7.19), as the unbalancement of only 1 photon determines a λ period. We finally expect the presence of a $\frac{\lambda}{2}$ period due to the couple emission of photons by the crystal.
Explicit calculation of the third order correlation function gives the result:

$$\mathscr{G}^{(3)}_{N=3} = a(\overline{n}) + b(\overline{n})\cos(\theta) + c(\overline{n})\cos(2\theta) + d(\overline{n})\cos(3\theta) \tag{7.20}$$

where $a(\overline{n}) = 6 + 342\overline{n} + 1782\overline{n}^2 + 1824\overline{n}^3$ and $c(\overline{n}) = \frac{1}{2}\left[81\overline{n} + 369\overline{n}^2 + 288\overline{n}^3\right]$ are third degree polynomial in $\overline{n}$, while $b(\overline{n}) = \frac{3}{2}\left[3\overline{n}^2 + 3\overline{n} + 1\right]$ and $d(\overline{n}) = -\frac{27}{2}\left[\overline{n} + \overline{n}^2\right]$ are second degree polynomial in $\overline{n}$. We find, as said, the presence of oscillating terms at the three

fundamental harmonics in θ, 2θ and 3θ. The term in 2θ is dominant for high gain values, and the intrinsic oscillation of the crystal with period $\frac{\lambda}{2}$ suppresses the amplitude of the oscillations with $\frac{\lambda}{3}$ period. Hence this apparatus based on the collinear QIOPA device cannot be used for the amplification of a generic state, as the interference pattern of the seed is masked during the amplification process.
Hence in order to preserve the $\frac{\lambda}{2N}$ phase oscillation after the amplification process, a different amplifier device, not containing an intrinsic phase oscillation, has to be employed.

7.5 Non collinear amplifier

In this section we study the amplification of NOON states exploiting an Optical Parametric Amplifier working in a non-collinear configuration. The interaction Hamiltonian of this device is [DS05]:

$$\hat{\mathscr{H}}_{int} = \imath\hbar\chi\left(\hat{a}^{\dagger}_{1\pi}\hat{a}^{\dagger}_{2\pi_{\perp}} - \hat{a}^{\dagger}_{1\pi_{\perp}}\hat{a}^{\dagger}_{2\pi}\right) + \text{h.c.} \tag{7.21}$$

where $\pi, \pi_{\perp}$ stand for any two orthogonal polarizations, as this configuration is invariant under SU(2) rotations.
The proposed scheme is shown in Fig.7.16.

After the preparation of the seed, the state is injected on mode $\mathbf{k}_1$ in the amplifier together with the pump beam $\mathbf{k}_p$ to obtain the amplification process. A phase shift θ is then introduced between the two polarization $\vec{\pi}_+, \vec{\pi}_-$ and the M-th order absorption process is performed in $R^{(M)}$. An unbalanced BS with transmittivity η will be subsequently introduced in Sec.7.5.4 to simulate losses and non unitary efficiency of detection. This scheme corresponds to evaluating the M-th order correlation defined by the operator $\hat{G}^{(M)} = [\hat{c}^{\dagger}_1(t)]^M[\hat{c}_1(t)]^M$, where $\hat{c}^{\dagger}_1$ is the creation operator associated to the revealed mode correspondind to the Heisenberg evolution of the field operator $\hat{a}_{1H}$:

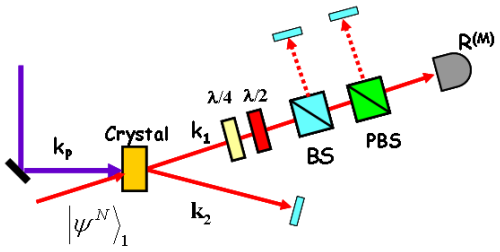

Figure 7.16: Experimental setup for the amplification of a NOON state by a non-collinear amplifier, implemented by a type-II cut BBO crystal in non collinear configuration. The state $|\psi^N\rangle_1$ is injected into the input mode $\mathbf{k}_1$. The BS is inserted in order to simulate losses.

$$\hat{c}_1^\dagger(t) = \frac{1}{\sqrt{2}}\left[\hat{a}_{1+}^\dagger(t) - e^{\imath\theta}\hat{a}_{1-}^\dagger(t)\right] \tag{7.22}$$

The time evolution of the field operators in the crystal is derived from the interaction Hamiltonian of the non-collinear OPA (7.21). The Heisenberg equations gives:

$$\hat{a}_{1+}^\dagger(t) = \hat{a}_{1+}^\dagger \cosh(g) + \hat{a}_{2-} \sinh(g) \tag{7.23}$$

$$\hat{a}_{1-}^\dagger(t) = \hat{a}_{1-}^\dagger \cosh(g) + \hat{a}_{2+} \sinh(g) \tag{7.24}$$

where $g = \chi t_{int}$ is the non-linear gain of the process.

7.5.1 Spontaneous emission

Let us study the interferometrical feature of this device in the spontaneous emission case. It will be shown that the spontaneous emitted field does not show any oscillation patterns for any orders of correlation.
The unitary time evolution operator in the interaction picture for the non-collinear OPA can be written in the form [DS05]:

$$\begin{aligned}\hat{U} = e^{\Gamma\left(\hat{a}_{1+}^\dagger \hat{a}_{2-}^\dagger - \hat{a}_{1-}^\dagger \hat{a}_{2+}^\dagger\right)} e^{-\ln C(1+\hat{n}_{1+}+\hat{n}_{1-}+\hat{n}_{2+}+\hat{n}_{2-})} \\ e^{\Gamma(\hat{a}_{1-}\hat{a}_{2+} - \hat{a}_{1+}\hat{a}_{2-})}\end{aligned} \tag{7.25}$$

where $C = \cosh(g)$ and $\Gamma = \tanh(g)$. Applying this operator to the input vacuum state we obtain:

$$|\Phi\rangle = \frac{1}{C}\sum_{n=0}^{\infty} \Gamma^n \sum_{m=0}^{n} |(n-m)+, m-\rangle_1 |m+, (n-m)-\rangle_2 \tag{7.26}$$

The M-th order correlation function, calculated in the Heisenberg picture shows that there is no oscillation pattern in the spontaneous radiation. Let us ignore for now the effects of losses, and evaluate $\mathscr{G}_0^{(M)} = \langle 0|\hat{G}^{(M)}|0\rangle$. The M-th order correlation operator reads:

$$\begin{aligned}\hat{G}^{(M)} = \frac{1}{2^M}\left[\hat{a}_{1+}^\dagger C + \hat{a}_{2-} S - e^{\imath\theta}\hat{a}_{1-}^\dagger C - e^{\imath\theta}\hat{a}_{2+} S\right]^M \times \\ \times \left[\hat{a}_{1+} C + \hat{a}_{2-}^\dagger S - e^{-\imath\theta}\hat{a}_{1-} C - e^{-\imath\theta}\hat{a}_{2+}^\dagger S\right]^M\end{aligned} \tag{7.27}$$

where $S = \sinh(g)$. This operator can be written, using the multinomial expansion, as:

$$\begin{aligned}\hat{G}^{(M)} = \frac{1}{2^M}\left(\sum_{i,j,k} g_{ijk} (\hat{a}_{1+}^\dagger)^{M-i-j-k} (\hat{a}_{2-})^i (\hat{a}_{1-}^\dagger)^j (\hat{a}_{2+})^k\right) \\ \times \left(\sum_{l,m,n} g_{lmn}^* (\hat{a}_{1+}^\dagger)^{M-i-j-k} (\hat{a}_{2-})^i (\hat{a}_{1-}^\dagger)^j (\hat{a}_{2+})^k\right)\end{aligned} \tag{7.28}$$

where:

$$g_{ijk} = \left(\frac{1}{\sqrt{2}}\right)^M \binom{M}{i,j,k} (-1)^{j+k} \left(e^{\imath\theta}\right)^{j+k} C^{M-i-k} S^{i+k} \tag{7.29}$$

and the sums are extended as $\sum_{i=0}^{M}\sum_{j=0}^{M-i}\sum_{k=0}^{M-i-j}$.
The average of $\widehat{G}^{(M)}$ on the vacuum input state gives:

$$\mathscr{G}_0^{(M)} = M!\, S^{2M} \tag{7.30}$$

This expression is independent on the phase for any order of the correlation. Thus, no intrinsic phase oscillation pattern is present in the radiation emitted in the spontaneous regime by the non collinear OPA, as expected from the form of the interaction Hamiltonian of eq.(7.21).

7.5.2 Amplified NOON quantum state

First we calculate the quantum state in the interaction picture. The amplified field is obtained, with a procedure completely analogous to the spontaneous emission case calculated in Sec.7.5.1, by applying the operator (7.25) to the injected state: $|\Phi^N\rangle = \hat{U}|\psi^N\rangle_1$. The output state reads:

$$\begin{aligned}|\Phi^N\rangle = &\frac{1}{\sqrt{2}\sqrt{N!}C^{N+1}} \sum_{n=0}^{\infty} \Gamma^n \sum_{m=0}^{n} (-1)^m \times \\ &\times \left[\sqrt{\frac{(n-m+N)!}{(n-m)!}}|(n-m+N)+,m-\rangle_1 - \sqrt{\frac{(m+N)!}{m!}}|(n-m)+,(m+N)-\rangle_1\right] |m+,(n-m)-\rangle_2\end{aligned} \tag{7.31}$$

Let us analyze the expression (7.31): the N-photons in excess on the two polarization modes with respect to the spontaneous emission case of eq.(7.26) are responsible for the $\frac{\lambda}{2N}$ fringe pattern. Hence the original N photons in the injected state are added to a background field emitted by the crystal.

7.5.3 M-th order correlation function

We now calculate the generic M-th order correlation function with the injection of a NOON state defined by the average $\mathscr{G}_N^{(M)} = {}_1\langle\psi^N|\hat{G}^{(M)}|\psi^N\rangle_1$. It will be shown that the original features of the injected seed will be maintained. It will be explicitly demonstrated that the correlation functions of order $M < N$ do not have any oscillation patterns, while the ones with $M \geq N$ exhibit sub-Rayleigh $\frac{\lambda}{2N}$ feature.
The value of the correlation functions can be calculated in the Heisenberg picture analogously to the spontaneous case of Sec.7.5.1. We obtain the following expression for $\mathscr{G}_N^{(M)}$:

$$\mathscr{G}_N^{(M)} = \frac{M!}{2^M}\left\{\sum_{i=0}^{M-N}\sum_{j=0}^{N} C^{2j}S^{2(M-j)}\binom{N}{j}\binom{M}{i,j} + \right.$$
$$+\sum_{i=M-N+1}^{M}\sum_{j=0}^{M-i} C^{2j}S^{2(M-j)}\binom{N}{j}\binom{M}{i,j} + \tag{7.32}$$
$$\left.-(-1)^M C^{2N}S^{2(M-N)}\left[\sum_{i=0}^{M-N}\binom{M}{i,N}\right]\cos(N\theta)\right\}$$

for $M \geq N$, while for $M < N$ we obtain:

$$\mathscr{G}_N^{(M)} = \frac{M!}{2^M}\sum_{i=0}^{M}\sum_{j=0}^{M-i} C^{2j}S^{2(M-j)}\binom{M}{i,j}\binom{N}{j} \tag{7.33}$$

The form of eq.(7.32) explicitly shows the $\frac{\lambda}{N}$ period of the emitted radiation, as only constant or oscillating terms in $N\theta$ are present.

7.5.4 Losses and decoherence effects

We are now interested in studying the effects of losses and of non unitary efficiency of detection on the amplified field. We introduce an unbalanced BS of transmittivity η in spatial mode $\mathbf{k}_1$ (Fig. 7.16). The two BS input modes are labelled by $\hat{b}_1^\dagger(t)$ and $\hat{c}_1^\dagger(t)$, where the second one is the OPA output mode and the first one is the vacuum input lossy channel. The revealed output mode corresponds to the field operator:

$$\hat{d}_1^\dagger(t) = \sqrt{\eta}\,\hat{c}_1^\dagger(t) + \imath\sqrt{1-\eta}\,\hat{b}_1^\dagger(t) \tag{7.34}$$

where the BS I/O relations have been used. The M-th order correlation function $\widetilde{\mathscr{G}}_N^{(M)} = {}_{b_1}\langle 0|_{c_1}\langle\psi^N|\left\{[\hat{d}_1^\dagger(t)]^M[\hat{d}_1(t)]^M\right\}|\psi^N\rangle_{c_1}|0\rangle_{b_1}$ reads:

$$\widetilde{\mathscr{G}}_N^{(M)} = \sum_{i,j=0}^{M}(\sqrt{\eta})^{i+j}\left(\imath\sqrt{1-\eta}\right)^{2M-i-j}(-1)^{M-j}\times$$
$$_{b_1}\langle 0|_{c_1}\langle\psi^N|\left\{[\hat{c}_1^\dagger(t)]^i[\hat{b}_1^\dagger]^{M-i}[\hat{c}_1(t)]^j[\hat{b}_1]^{M-j}\right\}|\psi^N\rangle_{c_1}|0\rangle_{b_1} \tag{7.35}$$

The input vacuum field on mode $\hat{b}_1$ imposes the constraints $i = M$ and $j = M$ when we evaluate the average. The correlation function $\widetilde{\mathscr{G}}_N^{(M)}$ then reads:

$$\widetilde{\mathscr{G}}_N^{(M)} = \eta^M\,{}_{c_1}\langle\psi^N|[\hat{c}_1^\dagger(t)]^M[\hat{c}_1(t)]^M|\psi^N\rangle_{c_1} = \eta^M\mathscr{G}_N^{(M)} \tag{7.36}$$

Hence, the presence of losses and of the non unitary efficiency of detection do not change the oscillation pattern of the amplified field, but only reduce the efficiency of the process by a factor η^N. The main difference between the pure NOON state and the amplified field is in their resilience to losses. For the injected state, as explained in Sec.7.1.1,

the loss of just a single photon cancels the $\frac{\lambda}{N}$ behaviour of the field and only a fraction η^N contributes to the successful events rate. On the contrary, for the amplified field the non-linear gain of the process can be chosen so that $\eta^M \overline{n} \gg 1$. In this condition, the large majority of the pulses give contribution to the M-th order correlation and the successful events rate is substantially not reduced.

7.5.5 Asymptotical visibilities

Knowing the correlation function, we can calculate the visibilities associated to this M-photon absorption processes. We can see by the form of eq.(7.36) that the visibility associated to the M-th order correlation function is not affected by losses and by non unitary detection efficiency. Restricting our attentions to the asymptotical visibilities, corresponding to $g \to \infty$ and hence to an ideal infinite number of photons in the emitted field, we obtain for a NOON state with N=2,3,4 the following expressions:

$$\widetilde{\mathscr{V}}^{(M)}_{N=2}(\overline{n} \to \infty) = \frac{M^2 - M}{M^2 + 7M + 8} \tag{7.37}$$

$$\widetilde{\mathscr{V}}^{(M)}_{N=3}(\overline{n} \to \infty) = \frac{M^3 - 3M^2 + 2M}{M^3 + 15M^2 + 56M + 48} \tag{7.38}$$

$$\widetilde{\mathscr{V}}^{(M)}_{N=4}(\overline{n} \to \infty) = \frac{M^4 - 6M^3 + 11M^2 - 6M}{M^4 + 26M^3 + 203M^2 + 538M + 384} \tag{7.39}$$

The plot of these three functions are reported in Fig.7.17. We observe that the values

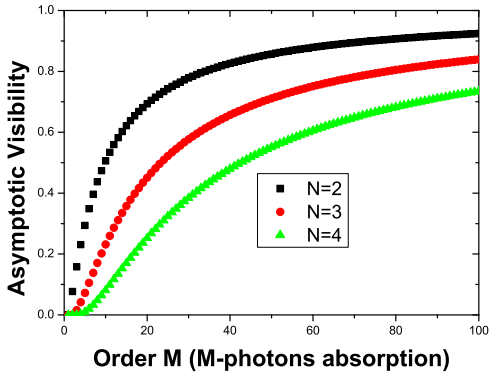

Figure 7.17: Plot of the asymptotic ($g \to \infty$ and $\overline{n} \to \infty$) M-th order correlation function as a function of the order M in three cases. The square data corresponds to the injection of a 2-photons state, the circular data to a 3-photons state and the triangular data to a 4-photons state.

of the visibilities grow with the order of correlation M and decrease as the number of

photons of the injected states increases. This is due to the characteristic of the N-photon NOON seed, which implies an increase of both the minimum and the maximum of the fringe pattern proportional to the number of photons N.

7.6 Observations and Conclusions

In this chapter we investigated the features of the field produced by an optical parametric amplifier working both in a spontaneous and in a stimulated regime. We have shown that in both cases the oscillation patterns of the generated field presents a sub Rayleigh feature, typical of two photons NOON states. The amplification of a two photons NOON state using two different scheme both based on the process of optical parametric amplification has then be addressed. We proposed to use a collinear optical parametric parametric amplifier to amplify a 2-photon entangled state, maintaining in the output field the $\frac{\lambda}{4}$ pattern of the injected seed. We analyzed the problem theoretically and experimentally , comparing the amplified with the spontaneous emission regime analyzed in [DSV08]. We found experimentally that the two regimes have comparable visibilities, while the advantage of the stimulated case is a significant increase of the number of photons in the emitted radiation. We then showed that this device, due to the intrinsic $\frac{\lambda}{4}$ oscillation of the radiation emitted by the crystal, cannot be used to amplify a generic N photon states. We then proposed to use a non-collinear optical parametric amplifier to amplify a generic NOON state. We showed that the oscillation period of the seed is maintained during the amplification process and the visibility reaches an asymptotical unitary value when the M-th order correlation function with sufficiently high value of M is analyzed. Furthermore, we showed that the amplified field exhibits a high resilience to losses with respect to the extreme sensitivity of the NOON states.

Chapter 8

Enhanced resolution of lossy interferometry by coherent amplification of single photons

In the quantum sensing context most of the efforts to design novel quantum techniques of sensing has been constrained to idealized, noise-free scenarios, in which effects of environmental disturbances could be neglected. In the present work, we propose to exploit optical parametric amplification to boost interferometry sensitivity in the presence of losses in a minimally invasive scenario. By performing the amplification process on the microscopic probe after the interaction with the sample, we can beat the losses detrimental effect on the phase measurement which affects the single photon state after its interaction with the sample, and thus improve the achievable sensitivity [VST$^+$10b].

8.1 Quantum sensing

The aim of quantum sensing is to develop quantum methods to extract the maximum amount of information from a system with minimal disturbance upon it. Indeed, the possibility of performing precision measurements by adopting quantum resources can increase the achievable precision going beyond the semiclassical regime of operation [GLM04, GLM06]. The employ of a quantum probe and entangled measurement schemes in order to estimate a classical parameter can beat the standard quantum limit imposed on the accuracy of the measurement [Hel76]. In the case of interferometry, this can be achieved by the use of the so-called N00N states, which are quantum mechanical superpositions of just two terms, corresponding to all the available photons N placed in either the signal arm or the reference arm. The use of N00N states can enhance the precision in phase estimation to 1/N, thus improving the scaling of the achievable precision with respect to the employed resources [BKA$^+$00, Dow08]. This approach can have wide applications for minimally invasive sensing methods in order to extract the maximum amount of information from a system with minimal disturbance. Imaging of

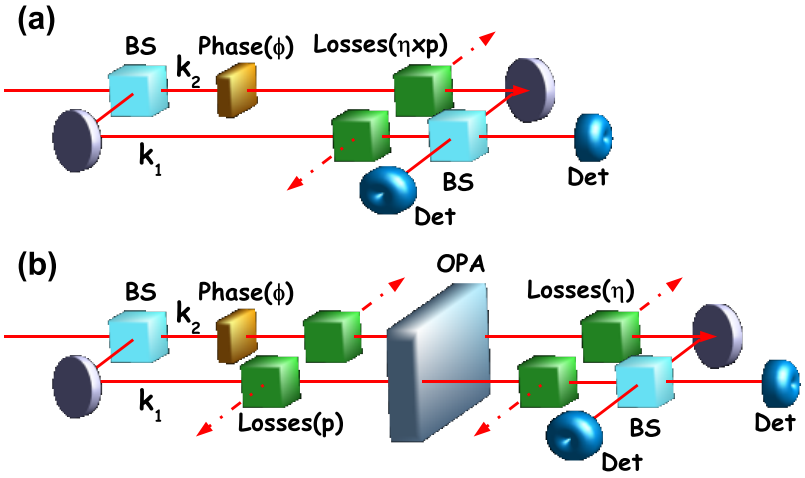

Figure 8.1: Scheme for the phase measurement. (a) Interferometric scheme adopted to estimate the phase (ϕ) introduced in the mode k_2. (b) Interferometric scheme adopting a single photon and the optical parametric amplifier: the amplification of the single photon state is performed before dominant losses.

biological samples and of an ancient artifact are examples of situations where it is clearly beneficial to use as weak light as necessary to achieve a desired level of measurement precision. In the quantum domain there is an even stronger motivation for minimally invasive measurements since the back action of the measurement actually changes the state of the quantum system under investigation. The experimental realization of protocols involving N00N states containing up to 4 photons have been realized in the last few years [DCS01, WPA$^+$04, MLS04, EHKB05, NOO$^+$07]. However these quantum states, suitable for quantum metrology protocols, result extremely fragile under losses and decoherence, unavoidable in experimental implementations. A sample, whose phase shift is to be measured, may at the same time introduce high attenuation. Because quantum-enhanced modes of operations exploit fragile quantum mechanical features, such as entanglement, the impact of these environmental effects can be much more deleterious than in semiclassical schemes, destroying completely quantum benefits [RK07, SC07]. This scenario puts the beating of realistic, noisy environments as the main challenge in developing quantum sensing. Very recently, the theoretical and experimental investigations of quantum states of light has attracted much attention, leading to the best possible precision in optical two-mode interferometry, even in presence of experimental imperfections [HWD08, DDDS$^+$09b, MD09, DDDS$^+$09a, KDDW$^+$09, LHL$^+$09].

In this chapter, we adopt an hybrid approach based on a high gain optical parametric amplifier operating for any polarization state in order to transfer quantum properties of different microscopic quantum states in the macroscopic regime [De 98a, De 98b]. By performing the amplification process of the microscopic probe after the interaction with the sample we can beat the losses detrimental effect on the phase measurement which

affects the single photon state after the sample. The effect of losses on the macroscopic field consists in the reduction of the detected signal and not in the complete cancellation of the phase information as would happen in the single photon probe case, thus improving the achievable sensitivity.

8.1.1 Evaluation of a phase φ with single photons

Let us review the adoption of single photons in order to evaluate the unknown phase φ, Fig.1-(a). The phase φ introduced in the path k_2 is probed by sending to the sample N input photons, each one in the state $2^{-1/2}(|1\rangle_{k1}+|1\rangle_{k2})$. After the propagation, the sample introduces a phase φ on the probe beam and each photon is found in the state: $\frac{1}{\sqrt{2}}\left(|1\rangle_{k1}+e^{i\varphi}|1\rangle_{k2}\right)$. The two modes k_1 and k_2 are then combined on a beamsplitter (BS) and detected by (D_1',D_2') with an overall detection efficiency equal to t. N performed experiments leads to an output signal equal to $I=I(D_1')-I(D_2')=tN\cos\varphi$, whose fluctuations are given by $\sigma=(tN)^{1/2}$. The uncertainty on the phase measurement around the value $\frac{\pi}{2}$ can hence be estimated as $\Delta\varphi=\left(\frac{\partial I}{\partial\varphi}\right)^{-1}\triangle I=\frac{1}{\sqrt{tN}}$, the semi-classical shot noise limit, and the sensitivity of the interferometer can be evaluated as $S_{1\text{phot.}}=\frac{1}{\Delta\varphi}=\sqrt{tN}$.

8.2 Sensitivity improvement by single photons probe amplification

In order to avoid the detrimental effect of a low value of t, our strategy involves the amplification of the single photon probe, Fig.1-(b). In the theory and experiment here described, the two modes k_1 and k_2 correspond to two orthogonal polarizations modes: horizontal (H) and vertical (V) associated to the same longitudinal spatial mode k. The input single-photon is prepared in the polarization state: $|+\rangle=\frac{1}{\sqrt{2}}(|H\rangle+|V\rangle)$. After the propagation over the interferometer, the photon acquires the unknown phase φ: $|\varphi\rangle=\frac{1}{\sqrt{2}}(|H\rangle+e^{\imath\varphi}|V\rangle)$. The amplification performed by the optical parametric device generates the output state $|\Phi^{\varphi}\rangle=\widehat{U}_{OPA}|\varphi\rangle=\cos\frac{\varphi}{2}|\Phi^{+}\rangle+\imath\sin\frac{\varphi}{2}|\Phi^{-}\rangle$, where $|\Phi^{+,-}\rangle$ are the wavefunctions described in Ref. [DSV08]. Precisely, the state $|\Phi^{+}\rangle$ ($|\Phi^{-}\rangle$) presents a Planckian probability distribution as a function of photons polarized $\vec{\pi}_{-}$ ($\vec{\pi}_{+}$) and a long tail distribution as a function of photons polarized $\vec{\pi}_{+}$ ($\vec{\pi}_{-}$). The two distributions belonging to the state $|\Phi^{+}\rangle$ and $|\Phi^{-}\rangle$ partially overlap, but become distinct on the border of the Fock states plane [NDSD07]. For the state $|\Phi^{\varphi}\rangle$, the average number of photons emitted over the polarization mode $\vec{\pi}_{+}$ is equal to $\langle n_{+}\rangle=\overline{n}+\sin^2\frac{\varphi}{2}(3\overline{n}+1)$ with $\overline{n}=\sinh^2 g$ and g the gain of the amplifier, while the average number of photons emitted over the polarization mode $\vec{\pi}_{-}$ is equal to $\langle n_{-}\rangle=\overline{n}+\cos^2\frac{\varphi}{2}(3\overline{n}+1)$. The previous expressions lead to a phase-dependent intensity with a visibility $V=\frac{\langle n_{+}\rangle-\langle n_{-}\rangle}{\langle n_{+}\rangle+\langle n_{-}\rangle}\rightarrow 0.50$ for $g\rightarrow\infty$. The resilience to losses of such multiphoton fields [DSS09a] renders them suitable for the

implementation of quantum information applications in which noisy channels and low detection efficiency are involved. We consider the case in which the losses are unavoidable during the detection process, and happen after the single photon amplification (Fig.8.1). After the propagation over a lossy channel, the state evolves from $|\Phi^{\varphi}\rangle\langle\Phi^{\varphi}|$ into a mixed state $\hat{\rho}_{\eta}^{\varphi}$. For details on the explicit expressions of the coefficients of the density matrix $\hat{\rho}_{\eta}^{\varphi}$ refer to [DSS09a].

8.2.1 SPCM measurement strategy

After the amplification stage and the transmission losses, the received field is analyzed through single photon detectors (D_1', D_2') in the $\{\vec{\pi}_+, \vec{\pi}_-\}$ polarization basis. Our aim is to compare the achievable sensitivity *with* and *without* the optical amplifier ($g = 0$). To take into account experimental imperfections, we divide the losses t in two contributions: the first one includes all the losses between the sample and the optical amplifier (p), while the second parameter takes into account all the inefficiencies up to the detection stage (η): $t = p \times \eta$. Our strategy cannot compensate for losses that occur before the amplifier (p), but can compensate for large (even very large, if the gain is high enough) losses after the amplification (η). A first insight on this property of the optical parametric amplifier has been given in Ref.[LBL$^+$] by analyzing the signal-to-noise of the amplification of a coherent state signal in lossy conditions. The sensitivity $S_{ampl.}$, obtained by measuring the difference $\langle D\rangle = \langle n_+\rangle - \langle n_-\rangle$ intensity signals provided by the detectors around the phase value $\varphi = \frac{\pi}{2}$, is found to be:

$$S_{ampl.} = \frac{\sqrt{N}p\eta c}{\left\{\eta^2\left[p\overline{n}(4c+2)+2\overline{n}c\right]+\eta\left[pc+2\overline{n}\right]\right\}^{1/2}} \tag{8.1}$$

with $c = 2\overline{n}+1$.

Let us first consider the case $p = 1$: figure 2-(a) reports the logarithm of the enhancement of the squared sensitivity $E = \left(\frac{S_{\text{ampl.}}}{S_{\text{1phot.}}}\right)^2$ versus g and η. E represents the reduction factor in the number of photons sent onto the sample in order to obtain the same information on the phase φ, by exploiting the amplification strategy with respect to the single-photon probe scheme. As it can be observed in figure 2-(a), a large improvement can be obtained in the regime of high losses and large gain of the amplifier. The motivation of such behaviour is the following: the present approach allows to increase the number of detected photons by a factor $4\overline{n}$ with respect to the single photon case keeping a visibility of the fringe patterns reduced only to 50% (for $g \to \infty$). In figure 2-(b) we report the trend of the enhancement as a function of the non linear gain g, for different values of the detection efficiency $\eta = 0.05$ (green continuous line) and $\eta = 0.1$ (black dashed line). We observe that, even for high value of η, an enhancement greater that 1 can be obtained.

Consider now the case $p \neq 1$. For large values of the gain g the enhancement saturates to the value: $E_{lim} = \frac{p}{\eta(2p+1)}$ (contour plot in figure 2-(c)), we can then identify a critical value of p above which the enhancement is greater than 1 : $p_{crit} = \frac{\eta}{1-2\eta}$. For $\eta \geq 0.33$ no

enhancement can be achieved by exploiting the amplification strategy (see figure 2-(d)).

Experimental implementation

The previous theoretical predictions have been experimentally tested by adopting a high gain optical parametric amplifier with a maximum gain $g = 4.5$, see figure 8.3. The single photon probe is generated by a BBO non linear crystal (C1) on spatial mode k_1 together with an entangled photon on spatial mode k_T. The overall singlet state produced by $C1$ is obtained through the spontaneous parametric amplification process, consisting in the annihilation of a pump photon at wavelength (wl) $\lambda_p = 397.5nm$ followed by the creation of twin photons, orthogonally polarized, at wl $\lambda = 795nm$. The overall pump beam is

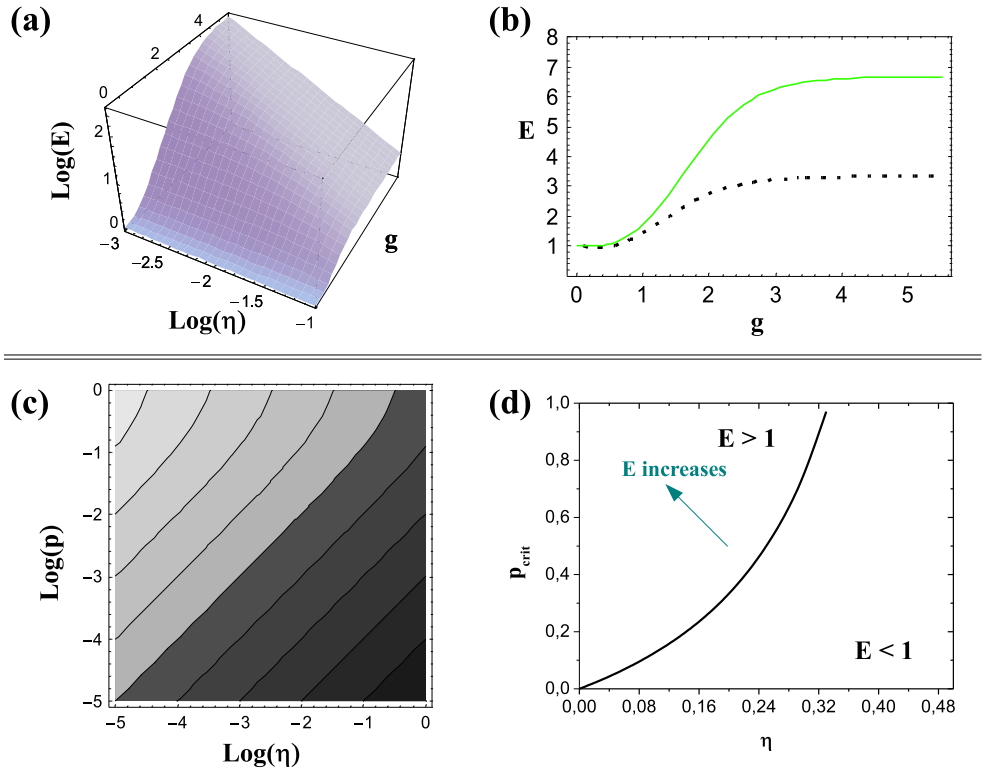

Figure 8.2: **(a)** Logarithm of the enhancement versus the non-linear gain g and the transmittivity of the lossy channel η in the perfect case, in which the losses between the phase-shifter and the amplifier are neglected ($p = 1$). **(b)** Trend of E as a function of the non linear gain for different values of the efficiency $\eta = 0.1$ (green continous line) and $\eta = 0.05$ (black dashed line), in both cases $p = 1$. **(c)** Contour plot of the enhancement as a fuction of the logarithm of p and η. The lighter region corresponds to $E > 1$, the darker one to $E < 1$. **(d)** Non ideal case $p \neq 1$: trend of the injection probability critical value for which $E > 1$ as a function of the detection efficiency.

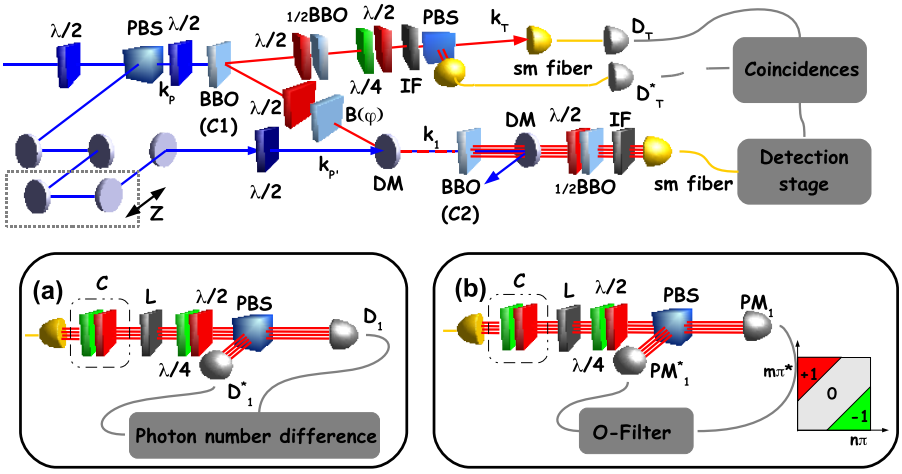

Figure 8.3: Experimental setup of the QI-OPA based interferometric scheme. An intense pulsed pump beam of $P = 750$mW and $\lambda = 397.5$nm is generated by a Ti:Sa laser system. The pump beam is split between modes $\mathbf{k}_p$ and $\mathbf{k}'_p$. In the first BBO crystal (C1), a single photon state in the $|+\rangle_1$ is prepared upon detection on mode $\mathbf{k}_T$ with a single-photon SPCM-AQR14 detector (D_T). Then, the phase φ is introduced through a Babinet-Soleil compensator (B) and the probe state $|\varphi\rangle$ after the interaction is then injected in the QI-OPA and superimposed with the pump beam on mode $\mathbf{k}'_p$. Spatial and temporal matching are obtained through an adjustable delay line (Z). (a) Measurement scheme based on detection of the average of the photon number difference $\hat{D} = \hat{n}_+ - \hat{n}_-$. After fiber polarization compensation (C), the output field undergoes controlled losses throughout a tunable attenuator (L). Then, the field is analyzed in polarization and detected with two SPCM-AQR14 detectors (D_1, D_1^*) (b) O-Filter based detection scheme. After fiber polarization compensation (C), the output field undergoes controlled losses throughout a tunable attenuator (L). Then, the field is analyzed in polarization and detected with two photomultipiers (PM_1, PM_1^*). The photocurrents are shot-by-shot processed by an electronic device (O-Filter), whose action is described in the text and in Ref.[DSV08].

generated by a Ti:Sa laser system, consisting in a Ti:Sa modelocked MIRA900, pumped by a Verdi V5 Nd:Yag solid state laser. The output beam from the MIRA900 is injected into the Ti:Sa REGA900 amplifier, pumped by a Verdi V18. The overall laser system allows to obtain a $1.5W$ output beam at wavelength $\lambda = 795nm$, that, after a a double harmonic generation process, generates the experiment pump beam at wl $\lambda_p = 397.5nm$ of power $P = 750W$. This beam is split into two parts, a smaller one impinges into $C1$ and the higher one is directed towards the amplifier crystal $C2$ superimposed spatially and temporally with the single photon probe after the interaction with the sample (simulated by the babinet $B(\varphi)$ in figure 8.3). The number of photons generated in the amplification process, as said, depends exponentially on the non linear of the amplifier g. The maximum value of g experimentally found is $g_{max} = 4.5$.

The output radiation was then coupled with a single mode fiber and detected with

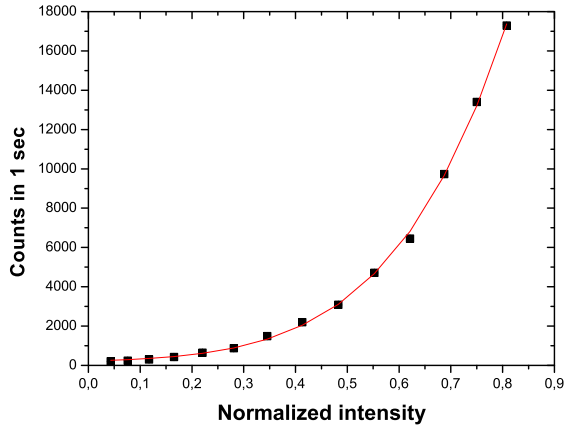

Figure 8.4: Trend of counts detected by D_1, D_1^* as a function of the normalized intensity signal impinging o the amplifier, working in a spontaneous (not-injected) configuration.

single photon detectors. Additional controlled losses were introduced by adopting neutral optical filters. The amplified state is then analyzed in polarization and detected by two single photon counting modules SPCM, D_1 and D_1^* in figure 8.3-(a). The resulting signals, triggered by the click of detectors D_T, D_T^* on mode k_T, are hence subtracted and the difference in the number of photons $\hat{D}$ is recorded as a function of the phase φ, varied by the Soleil-Babinet compensator $B(\varphi)$ on the probe path.

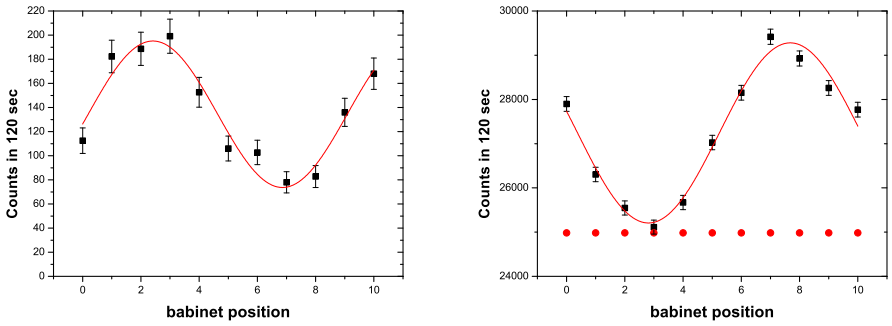

Figure 8.5: Experimental fringe pattern for the single photon probe (left) and for the amplified beam (right).

For the sake of simplicity we consider to work in the single photon counting regime; in order to describe the detection apparatus in a linear regime, the following condition for the average number of detected photons must be satisfied $\eta \langle n_{\pm} \rangle << 1$. We found experimentally a value of p equal to 0.15 due to spatial and spectral mismatch between the injected single photon and the ultraviolet pump beam (k_p'). The output fringe patterns

have been recorded for different values of the gain g and hence of the generated number of photon in the amplifier. In the extreme condition with $\eta = 3 * 10^{-4}$ and $g = 4.5$ we observed an enhancement of a factor ~ 210, as shown in figure 8.6, in which is reported the trend of E as a function of the amplifier gain, compared with the theoretical prediction.

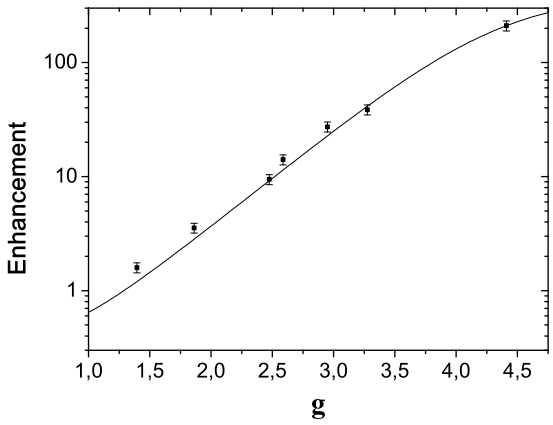

Figure 8.6: Experimental results of the enhancement E versus the non-linear gain. Continuous line: theoretical prediction for the expected enhancement with $\eta = 3 * 10^{-4}, p = 0.15$

Fisher Information and optimality of the performed measurement

We now discuss the optimality of the measurements performed on the multiphoton state, in order to extract the maximum information about the phase φ codified in the optical field. This quantity is expressed by the quantum Fisher Information [Hel76, Par09], defined as $H(\varphi) = \mathrm{Tr}[\hat{\rho}^{\varphi}\hat{L}_{\varphi}]$, where $\hat{L}_{\varphi}$ is the symmetric logarithmic derivative $\partial_{\varphi}\hat{\rho}^{\varphi} = \frac{\hat{L}_{\varphi}\hat{\rho}^{\varphi}+\hat{\rho}^{\varphi}\hat{L}_{\varphi}}{2}$ and $\hat{\rho}^{\varphi}$ is the density matrix of the state in which the phase is codified. The quantum Cramer-Rao bound [Hel76] quantifies the maximum precision achievable on the estimation of the phase φ optimized over all possible measurements as: $\Delta^2\varphi \geq 1/H(\varphi)$. In the high lossy regime $\eta\langle n_{\pm}\rangle \ll 1$, the single photon amplified states lead to a quantum Fisher Information equal to $H_{ampl}(\varphi) \approx 2\overline{n}\eta p(1+p^{-1})^{-1}$, to be compared with the single photon case, which gives $H_{1phot}(\varphi) = \eta p$. This result allows to investigate the optimality of the counting measurement strategy. The sensitivity achieved with this scheme, given by Eq.(8.1), can be written in the high lossy regime as $S^2_{ampl} = (\Delta^2\varphi)^{-1} \approx 2\overline{n}\eta p(1+p^{-1})^{-1}$, thus saturating the Cramer-Rao bound and ensuring the optimality of this scheme in the high lossy regime.

8.2.2 OF measurement strategy

As more sophisticated strategy, it is possible to elaborate an approach which leads to higher visibility of the detected fringe patterns at the cost of a reduced detection rate of the signal: the output radiation is measured in polarization with two linear detectors, for instance photomultipliers. The intensity signals generated by the detectors proportional to the orthogonally polarized number of photons, are compared shot-by-shot by the orthogonality-filter (OF) electronic device introduced in Ref. [DSV08]. When the number of photons m_φ, detected in the $\vec{\pi}_\varphi$ polarization, exceeds $n_{\varphi_\perp}$, detected in the $\vec{\pi}_{\varphi\perp}$ polarization, over a certain adjustable threshold k, i.e. $m_\varphi - n_{\varphi_\perp} > k$, the (+1) outcome is assigned to the event and the state $|\Phi^\varphi\rangle$ is detected. On the contrary, when the condition $n_{\varphi_\perp} - m_\varphi > k$ is satisfied, the (-1) outcome is assigned and the state $|\Phi^{\varphi\perp}\rangle$ is detected. Finally, an inconclusive result (0) is obtained when the unbalance between detected pulses does not exceed the threshold k. As the gain is increased, the number of transmitted photons $\eta\langle n\rangle$ becomes sufficient to detect all the N repeated trials. In the high losses regime, at variance with the single-photon case, all pulses can be exploited to extract information about the phase φ. The action of the OF is then to select those events which can be discriminated with higher fidelity, leading to an increase in the visibility, at the cost of discarding part of the data. According to these considerations, the "detection"

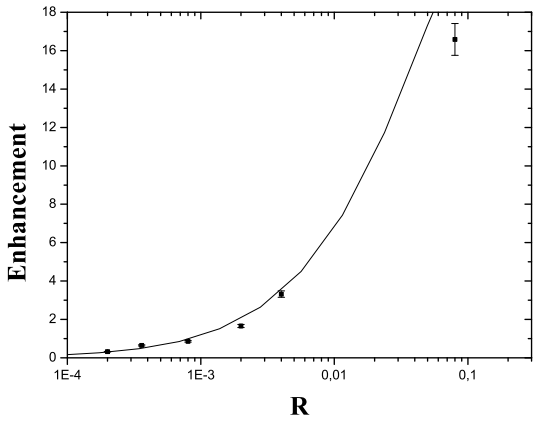

Figure 8.7: Experimental results of the enhancement E versus the signal rate, the continuous line reports the theoretical prediction for $p = 0.14$, $\eta = 0.005$.

efficiency of the scheme, i.e. the percentage of detected events, is given by the average signal $\overline{\eta} = R_{mean}(k)$ filtered by the OF device. This parameter $\overline{\eta}$ corresponds to the overall efficiency of the amplification-OF-based detection scheme. We calculated the phase measurement uncertainty through the standard definition $\Delta\varphi_{OF} = \Delta R_{OF}(\varphi)\left|\frac{\partial R_{OF}(\varphi)}{\partial\varphi}\right|^{-1}$. The minimum uncertainty is achieved for $\varphi = \frac{\pi}{2}$. The resulting sensitivity averaged over N trials is thus $S_{OF} = V\sqrt{R_{mean}}\sqrt{N}$. This expression shows that the phase fluctuations

no more depend on the efficiency η of the channel, but only on the average percentage of detected pulses R_{mean}.

We have experimentally tested the enhancement obtained by the OF strategy. We report in Fig. 8.7 the experimental trend of the enhancement as a function of the signal rate compared with the expected theoretical trend ($p = 0.14, \eta = 0.005$). In the adopted apparatus the single photon fringe pattern shows a visibility $\sim 50\%$ due to the generation of more than a single photon pair by the first non linear crystal adopted as the heralded single photon source. This seed visibility value is also responsible for a reduction of the amplified state visibility and has been taken into account in the comparison between the two strategies. By comparing the enhancement obtained through the counting and the OF based detection methods we can conclude that the first one allows to achieve an higher enhancement.

Chapter 9

Interaction between the QIOPA field and a Bragg BEC Mirror

In this chapter we address the adoption of the multiphoton states produced by the optical parametric amplifier for the implementation of a light-atom interaction protocol. It exploits the process of nonresonant scattering by a properly shaped Bose–Einstein condensate (BEC)[IWS99] of an externally generated multi-particle quantum photon state, a "macro-state" $|\Phi\rangle$, in order to create a joint atom-photon macro-state entangled by momentum conservation.
Light scattering from BEC structures has been used so far to enhance their non–linear macroscopic properties in super–radiance experiments [ICSK$^+$99], to show the possibility of matter wave amplification [MKTS$^+$99] and non-linear wave mixing [DHW$^+$99]. In the present chapter we intend to discuss the linear *coherent scattering, i.e.* the *reflection* by a multilayered BEC of a large assembly of nearly monochromatic photons generated by a high-gain "quantum-injected" Optical Parametric Amplifier (QI-OPA) in a Einstein-Podolsky-Rosen (EPR) configuration [De 98a, DS05]. In chapter 3 it has been demonstrated experimentally that the optical macrostate $|\Phi\rangle$ generated by the QI-OPA can be entangled with, i.e. non-separable from, a far apart single photon state belonging to the injected EPR pair [DSV08], thus resulting highly resilient to the decoherence due to losses [DSS09a]. In this chapter we address the possibility of extending this condition to the mechanical motion of an atomic assembly by making the photonic macrostate $|\Phi\rangle$ to exchange linear momentum with a high reflectivity BEC optical mirror, here referred to as a *"Mirror-BEC"* (M-BEC).

9.1 Bose Einstein Condensate (BEC)

Bose Einstein Condensate (BEC), whose concept can be dated back to the works of Bose and Einstein in 1924 [Bos24, Ein24], has been first observed in laboratory by Anderson et al. [AEM$^+$95] and Davis et al. [DMA$^+$95] in 1995. In both cases the systems under investigation were vapors of alkalis atoms, rubidium and sodium respectively, whose

characteristic features made them suitable for optical laser-based manipulation methods. Indeed laser cooling and trapping techniques had been developed during the 1980s and became the key point for the preparation of BEC systems. By combining laser and evaporative cooling for alkalis atoms the required density and temperature for observing the BEC transition can be reached. In these condition the BEC system is in a metastable state, whose lifetime is sufficiently long because the three-body collisions can be considered negligible in dilute and cold gases.
The trapped Bose gases are inhomogeneous and finite size systems, whose number of atoms ranges between few thousands and several millions. In most cases the confining traps are well approximated by harmonic potentials, whose trapping frequency ω_{ho} gives the characteristic length for the system $a_{ho} = (\hbar/(m\omega_{ho}))^2$. An important property of these systems is the big variation that occurs on this scale and that renders them highly inhomogeneous. The inhomogeneity of BEC systems is responsible for different consequences. Firstly the BEC shows up not only in *momentum* space but also in *coordinate* space. Another consequence is the role played by two-body interactions: despite the dilute nature of the condensate, the atom-atom interactions are enhanced on the measurable quantity, such as the condensate density, by the combination of the BEC and the harmonic trapping potential.
The behavior of BEC systems can be described by the Gross-Pitaevskii theory, which is a mean-field approach for the order parameter associated with the condensate that reproduces the typical properties exhibited by the superfluid systems (propagation of collective excitations, interference effects originated by the phase of the order parameter).

9.1.1 The ideal gas of non-interacting bosons

The magnetic traps for alkalis atoms act as confining potentials which can be safely approximated with quadratic form:

$$V_{ext}(r) = \frac{m}{2}\left(\omega_x^2 x^2 + \omega_y^2 y^2 + \omega_z^2 z^2\right) \tag{9.1}$$

If we neglect the atom atom interactions, the many-body Hamiltonian is the sum of single particles harmonic oscillator Hamiltonians, whore eigenvalues have the following form:

$$\varepsilon_{n_x n_y n_z} = \left(n_x + \frac{1}{2}\right)\hbar\omega_x + \left(n_y + \frac{1}{2}\right)\hbar\omega_y + \left(n_z + \frac{1}{2}\right)\hbar\omega_z \tag{9.2}$$

where $\{n_x, n_y, n_z\}$ are non-negative integers. The ground state of such a system correspond to the product of the N single particle states in the lowest accessible energy level ($n_x = n_y = n_z = 0$): $\phi(\mathbf{r_1}, \mathbf{r_2}...\mathbf{r_N}) = \prod_i \varphi_0(\mathbf{r_i})$ where

$$\varphi_0(\mathbf{r}) = \left(\frac{m\omega_{ho}}{\pi\hbar}\right)^{3/4} \exp\left[-\frac{m}{2\hbar}(\omega_x x^2 + \omega_y y^2 + \omega_z z^2)\right] \tag{9.3}$$

being $\omega_{ho} = (\omega_x\omega_y\omega_z)^{1/3}$. The density of the condensate can then be written as $n(\mathbf{r}) = N|\varphi_0(\mathbf{r})|^2$, and its value grows with N, while the the condensate dimension is independent

of N and is fixed by the harmonic oscillator length $a_{ho} = \left(\frac{\hbar}{m\omega_{ho}}\right)$. The typical experimental value of a_{ho} is about $1\mu m$, resulting in a typical size of the trapped condensate smaller than the thermal atoms one. At finite temperature part of the atoms will also be thermally distributed in the excited states at higher energy, as said the radius of the thermal cloud is larger than a_{ho}. It can be estimated by assuming $k_B T \gg \hbar\omega_{ho}$ and approximating the density of the thermal cloud with the Boltzmann distribution $n_{th} \propto \exp[-V_{ext}(r)/k_B T]$, where $V_{ext} = 1/2m\omega_{ho}^2 r^2$; the width of the gaussian is then $R_T = a_{ho}\left(\frac{k_B T}{\hbar\omega_{ho}}\right)^{1/2}$ and hence larger than a_{ho}. The above discussion shows that the Bose Einstein Condensation shows up with the appearance of a sharp peak in the central region of the density distribution.
It's worth noting that the Fourier transform of the ground state wavefunction is still a gaussian centered at zero momentum and whose width is proportional to a_{ho}^{-1}. Analogously the thermal distribution in the momentum space results broader and its width is proportional to $(k_B T)^{1/2}$. The appearance of a narrow peak both in the coordinate and in the momentum space is a peculiar feature of a trapped Bose gas, in contrast with what happens in the uniform gas case, in which the condensate cannot be revealed in coordinate space since the condensed and non condensed particles fill the same volume. In order to observe the condensate experimentally both the spatial and the velocity distribution can be determined by dispersive imaging [AMv$^+$96] and absorption methods [AEM$^+$95] respectively.
The symmetry of the condensate is fixed by the shape of the confining field. In the case of an axially symmetric trap, one can define an axial coordinate z and a radial one $r_\perp = (x^2 + y^2)^{1/2}$, with the relative frequencies: ω_z and $\omega_\perp = \omega_x = \omega_y$. The asymmetry of the trap is fixed by the ratio $\lambda = \frac{\omega_z}{\omega_\perp}$, for $\lambda < 1$ the shape of the trap is a cigar, otherwise it is a disk. In this case the ground state of the noninteracting bosons can be written as:

$$\varphi_0(\mathbf{r}) = \frac{\lambda^{1/4}}{\pi^{3/4} a_\perp^{3/2}} exp\left\{-\frac{1}{2a_\perp^2}(r_\perp^2 + \lambda z^2)\right\} \tag{9.4}$$

where $a_\perp = \left(\frac{\hbar}{m\omega_\perp}\right)^{1/2}$ is the harmonic oscillator length in the xy plane and $\omega_\perp = \lambda^{-1/3}\omega_{ho}$. The use of an axially symmetric trap allows to observe an important signature of BEC systems. Indeed in this case the *aspect ratio* is:

$$\sqrt{\frac{\langle p_z^2 \rangle}{\langle p_z^\perp \rangle}} = \sqrt{\lambda} \tag{9.5}$$

resulting fixed by the asymmetry parameter of the trap. This means that during the expansion the condensate cloud becomes an ellipse, while if the atoms were in a thermal state the shape of the cloud would be isotropic in momentum space. The occurrence of an isotropy in the the condensate peak has then been interpreted as a signature of BEC [AEM$^+$95, DMA$^+$95].

9.1.2 Trapped bosons at finite temperature

At finite temperature the total number of particles and the total energy of the bosons system are given by:

$$N = \sum_{n_x,n_y,n_z} \left\{\exp(\beta(\varepsilon_{n_x n_y n_z} - \mu)) - 1\right\}^{-1} \tag{9.6}$$

$$E = \sum_{n_x,n_y,n_z} \varepsilon_{n_x n_y n_z} \left\{\exp(\beta(\varepsilon_{n_x n_y n_z} - \mu)) - 1\right\}^{-1} \tag{9.7}$$

where μ is the chemical potential and $\beta = \frac{1}{k_B T}$. The number of condensed particles N_0 becomes macroscopic, i.e. of the order of the total number of particles N when the chemical potential becomes equal to the energy of the lowest state: $\mu \to \mu_c = \frac{3}{2}\hbar\overline{\omega}$, being $\overline{\omega} = (\omega_x + \omega_y + \omega_z)/3$. In this case the number of atoms in the excited states can be written as:

$$N - N_0 = \sum_{n_x,n_y,n_z} \frac{1}{\exp(\beta\hbar(\omega_x n_x + \omega_y n_y + \omega_z n_z)) - 1} \tag{9.8}$$

Assuming that the level spacing becomes smaller and smaller when $N \to \infty$, the sum can be replaced by the integral:

$$N - N_0 = \int_0^\infty \frac{dn_x dn_y dn_z}{\exp(\beta\hbar(\omega_x n_x + \omega_y n_y + \omega_z n_z)) - 1} \tag{9.9}$$

this approximation is supposed to be good when the number of trapped atoms is large and $k_B T >> \hbar\omega_{ho}$. In this way it is found:

$$N - N_0 = \zeta(3)\left(\frac{k_B T}{\hbar\omega_{ho}}\right)^3 \tag{9.10}$$

where $\zeta(n)$ is the Riemann function. By imposing $N_0 \to 0$ at the transition, it can be found the expression for the critical temperature T_c^0:

$$k_B T_c^0 = \hbar\omega_{ho}\left(\frac{N}{\zeta(3)}\right)^{1/3} = 0.94\hbar\omega_{ho}N^{1/3} \tag{9.11}$$

The T dependance of the condensate fraction for $T < T_c^0$ is then:

$$\frac{N_0}{N} = 1 - \left(\frac{T}{T_c^0}\right)^3 \tag{9.12}$$

From the previous analysis it turns out the existence of two relevant scales of energy for the ideal gas: the transition temperature $k_B T_c^0$ and the average level spacing $\hbar\omega_{ho}$. The former can be greater than the second, from 20 and 200 times larger depending on the number of total atoms. The frequency of the trapping potential $\omega_{ho}/2\pi$ is fixed by the trapping potential and ranges typically from tens to hundreds of Hertz. This gives $\hbar\omega_{ho}$ of the order of few nK.

9.1.3 Effects of interaction: the Gross-Pitaevskii equation

The many body hamiltonian describing N interacting bosons reads:

$$\hat{H} = \int d\mathbf{r}\hat{\Psi}^{\dagger}(\mathbf{r})\left[-\frac{\hbar^2}{2m}\nabla^2 + V_{ext}(\mathbf{r})\right]\hat{\Psi}(\mathbf{r}) + \frac{1}{2}\int d\mathbf{r}d\mathbf{r}'\hat{\Psi}^{\dagger}(\mathbf{r})\hat{\Psi}^{\dagger}(\mathbf{r}')V(\mathbf{r}-\mathbf{r}')\hat{\Psi}(\mathbf{r}')\hat{\Psi}(\mathbf{r}) \tag{9.13}$$

where V_{ext} is is the confining potential, $V(\mathbf{r}-\mathbf{r}')$ is the two-body interatomic potential, and $\hat{\Psi}(\mathbf{r}), \hat{\Psi}^{\dagger}(\mathbf{r})$ are the annihilation and creation bosons field operators. This hamiltonian can be treated in the mean field approach, under the approximation of dilute gas. The key point consists in separating out the condensate contribution to the bosonic field operator: $\hat{\Psi}(\mathbf{r}) = \sum_{\alpha}\Psi_{\alpha}(\mathbf{r})a_{\alpha}$, where$\Psi_{\alpha}(\mathbf{r})$ is the single-particle wavefunctions and a_{α} are the corresponding annihilation operators, defined in the Fock space as:

$$a_{\alpha}^{\dagger}|n_0, n_1, ...n_{\alpha}, ...\rangle = \sqrt{n_{\alpha}+1}|n_0, n_1, ..., n_{\alpha}+1, ...\rangle \tag{9.14}$$

$$a_{\alpha}|n_0, n_1, ...n_{\alpha}, ...\rangle = \sqrt{n_{\alpha}}|n_0, n_1, ..., n_{\alpha}-1, ...\rangle \tag{9.15}$$

$$\tag{9.16}$$

and for which the usual commutation rules hold:

$$[a_{\alpha}, a_{\beta}^{\dagger}] = \delta_{\alpha,\beta}, \quad [a_{\alpha}, a_{\beta}] = 0, \quad [a_{\alpha}^{\dagger}, a_{\beta}^{\dagger}] = 0 \tag{9.17}$$

Bose Einstein condensation occurs when the number of particles in a particular single-particle state becomes macroscopic $n_0 \equiv N_0 >> 1$, and the ration N_0/N remains finite when $N \to \infty$. In this limit the states that differ for one particle become indistinguishable and correspond to the same physical configuration, the operators a_0 and $a_0^{\dagger}$ can then be treated as numbers $a_0 = a_0^{\dagger} = \sqrt{N_0}$. For a uniform gas in a volume V, BEC occurs in the single particle state $\Psi_0 = 1/\sqrt{V}$ having zero momentum, and the field operator can be decomposed: $\hat{\Psi}^{\dagger}(\mathbf{r}) = \sqrt{N_0/V} + \hat{\Psi}'(\mathbf{r})$. By treating $\hat{\Psi}'$ as a small perturbation, Bogoliubov developed the first order theory for the excitations of interacting Bose gases.
The generalization for the non-uniform and time dependent configuration is given by:

$$\hat{\Psi}(\mathbf{r},t) = \Phi(\mathbf{r},t) + \hat{\Psi}'(\mathbf{r},t) \tag{9.18}$$

where $\Phi(\mathbf{r},t)$ is a complex function defined as the expectation value of the field operator: $\Phi(\mathbf{r},t) \equiv \langle\hat{\Psi}(\mathbf{r},t)\rangle$. The condensate density is given by $n_0(\mathbf{r},t) = |\Phi(\mathbf{r},t)|^2$. The function $\Phi(\mathbf{r},t)$ has the meaning of an "order parameter" and is called "wave function of the condensate".
In order to derive the equation for the condensate wave function, one has to write the time evolution of the field operator $\hat{\Psi}(\mathbf{r},t)$:

$$i\hbar\frac{\partial}{t}\hat{\Psi}(\mathbf{r},t) \equiv [\hat{\Psi}, \hat{H}] = \left[-\frac{\hbar^2\nabla^2}{2m} + V_{ext}(\mathbf{r}) + \int d\mathbf{r}'\hat{\Psi}^{\dagger}(\mathbf{r}',t)\times V(\mathbf{r}'-\mathbf{r})\hat{\Psi}(\mathbf{r}',t)\right]\hat{\Psi}(\mathbf{r},t) \tag{9.19}$$

By substituting the operator $\hat{\Psi}$ by the classical field Φ and by observing that in dilute cold gases only binary collision at low energy are relevant and are characterized by a single parameter (the s-wave scattering length a) $V(\mathbf{r}'-\mathbf{r}) = g\delta(\mathbf{r}'-\mathbf{r})$, one can write the Gross-Pitaevskii (GP) equation:

$$i\hbar\frac{\partial}{\partial t}\Phi(\mathbf{r},t) = \left(-\frac{\hbar^2\nabla^2}{2m} + V_{ext}(\mathbf{r}) + g\left|\Phi(\mathbf{r},t)\right|^2\right)\Phi(\mathbf{r},t) \tag{9.20}$$

where g is related to a through:

$$g = \frac{4\pi\hbar^2 a}{2m} \tag{9.21}$$

The validity of the GP-equation is based on the condition that the s-wave scattering length is much smaller than the average distance between atoms and that the number of atoms in the condensate is much larger than 1. These conditions can be parameterized by the relation $\overline{n}|a|^3 << 1$, where $\overline{n}$ is the average density of the gas. In this case the system is said dilute or weakly interacting. It's worth noting that the weakness of the interaction is not directly connected with the one of the effects. Indeed the effects have to be compared with the kinetic energy of the atoms in the trap. The interaction energy on the ground state of the harmonic oscillator is given by $E_{int} = gN\overline{n} \propto N^2\frac{|a|}{a_{ho}}$, on the other hand the kinetic energy is of the order of $N\hbar\omega_{ho}$, then the parameter expressing the ratio between the atom-atom interaction respect to the kinetic energy is:

$$\frac{E_{int}}{E_{kin}} \propto \frac{N|a|}{a_{ho}} \tag{9.22}$$

This expression can be larger than 1 even if $\overline{n}|a|^3 << 1$, so that also very dilute gases can exhibit a non-ideal behavior.

9.2 BEC in an optical lattice

In order to trap a condensate in a periodic rather than a harmonic potential, the interference pattern created by two overlapping beams can be exploited [MO06].
Optical lattices as optical traps are based on the Stark shift effect: when an atom is placed in a light field, the oscillating electric field of the latter induces an electric dipole moment on the atom, whose interaction with the field itself leads to an energy shift of the atomic level $\Delta E = -\frac{1}{2}\alpha(\omega)\left\langle E^2(t)\right\rangle$, where $\alpha(\omega)$ with $\omega = \omega_{res}+\Delta$ is the dynamic polarizability of the atomic level, exhibiting a resonance at ω_{res}. Δ is the detuning of the light field from the resonance and if $\Delta < 0$ (red detuning) the induced dipole $D = \alpha(\omega)E$ will be in phase with the electric field. This means that the resulting potential energy will be such that its gradient points in the direction of increasing field. A stable optical trap can then be obtained by simply focusing a laser beam to a waist of size w. If the cross section of

the beam is gaussian, the resulting position dependent Stark shift and the corresponding atom's potential will be:

$$\Delta E(r,z,) = V(r,z) = V_0 \exp\left(-\frac{2r^2}{w[z]^2}\right) \tag{9.23}$$

$$w[z] = w_0\sqrt{1+\left(\frac{z}{z_R}\right)^2} \tag{9.24}$$

where $V_0 \propto I_p/\Delta$ is the trap depth, with I_p the peak intensity of the beam, and w_0 and $z_R = w_0^2\pi/\lambda_L$ are the spot size and Rayleigh length of the Gaussian beam.
If we take two identical laser beams of peak intensity I_p counter-propagating with parallel polarizations, they will create an interference pattern with a distance $\lambda_L/2$ between the two maxima or minima of the resulting light intensity. The potential seen by the atoms is then:

$$V(x) = V_0 cos^2(\pi x/d) \tag{9.25}$$

where the lattice spacing is $d = \lambda_L/2$ and V_0 is the lattice depth, which is often measured in units of the recoil energy $E_R = \frac{\hbar^2\pi^2}{2md^2}$ by using the dimensionless parameter $s = V_0/E_R$.

9.3 Interaction between the QIOPA e the BEC-Mirror

Let us address now the experiment proposal for a light-atom interaction protocol, involving the QIOPA field and a BEC shaped as a Bragg mirror. The multiphoton nature and the high resilience to losses of the states introduced in chapter 3 can indeed be exploited for an efficient coupling with the atomic system.

The layout of the proposed experiment is then reported in Figure 9.1, and shows the QIOPA setup interacting with the mirror BEC. Let us recall briefly the features of the QIOPA setup: an EPR optical parametric amplifier, provided by Crystal 1, of a polarization entangled ($\pi-$entangled) pair of photons launched towards two distant measurement stations, here referred to as *Alice* (A) and *Bob* (B) [DSV08, NDSD07]. One of the EPR photons emitted towards the Bob's site is injected into the QIOPA which generates a corresponding macrostate $|\Phi\rangle$. The device operates in the collinear regime and amplifies with a large "gain" any injected single photon in a quantum superposition, i.e. a *qubit* $|\varphi\rangle_{k1}$ into a large number of photons, $\mathscr{N} \approx 10^5$, associated with a corresponding macro-qubit $|\Phi^{\varphi}\rangle_{k1}$ emitted over the same injection mode $\mathbf{k}_1$. These macrostates are then selected by a polarizing beam splitter (PBS) and drive the mechanical motion of the Mirror-BEC. Since these states are found to be entangled with the far part single-photon emitted over the mode $\mathbf{k}_2$ and detected by Alice, the same entanglement property is then transferred to the position-macrostate of the optically-driven Mirror-BEC (TR inset).

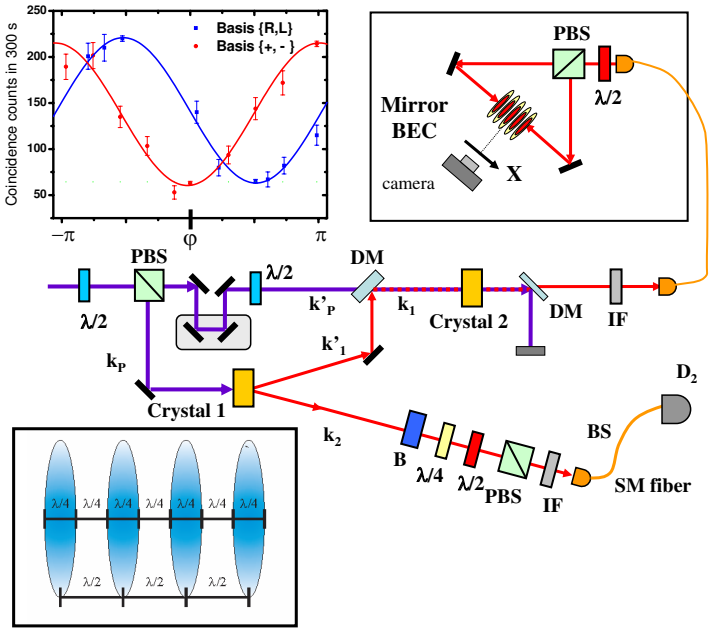

Figure 9.1: Layout of the QI-OPA + Mirror BEC experimental apparatus. The upper left (UL) Inset shows the interference patterns detected at the output of the PBS shown in the UR-Inset for two different measurement basis $\{+,-\}$ and $\{L,R\}$. Alternating slabs of condensate and vacuum are shown in the lower left (LL) Inset. A more detailed account of the Inset UR is given in Fig.3.

9.3.1 BEC mirror via Bragg reflection

Let us now describe the structure of the M-BEC and its interaction with light. The dynamics of a BEC loaded in a trap formed by a cylindrically symmetric harmonic potential (either an optical trap or a magnetic trap) with an optical standing - wave (SW) aligned along the symmetry axis, may be described by the Gross-Pitaevskii equation [Dal99]. If the trap is very elongated the ground state consists of an array of disks spaced by half the wavelength λ with a longitudinal size $R_l \propto \lambda/s^{-1/4}$ with s being an adimensional parameter describing the height of the optical lattice in terms of the recoil energy $E_R = h^2/2m\lambda^2$. The transverse size $R_\perp$ is dictated by the strength of the magnetic trap and by the number of atoms in the condensate N_{at} [PPS$^+$01]. The number N_D of the disks is also fixed by the strength of the magnetic trap in the longitudinal direction and by N_{at}. Typical numbers are $N_D \sim 200$, $N_{at} \sim 10^6$ with $R_\perp \sim 10\mu$m [MO06]. By choosing s it is then possible to prepare an array of disks with a longitudinal size of $R_l = \frac{\lambda}{4}$ spaced by $\frac{\lambda}{2}$: Figure 9.1 (Inset LL).

Releasing the condensate from the combined trap, the spatial periodic structure is initially preserved as long as the spreading disks do not start to overlap and interfere, and eventually leads for longer expansion times to a structure that reflects the momentum distribution of the condensate. Both regimes are fundamental to our proposal. If we expose

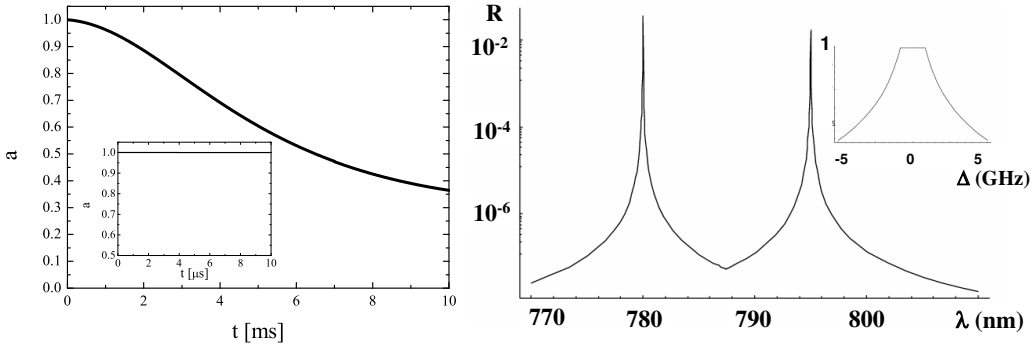

Figure 9.2: (**a**)Normalized amplitude of the beam reflected by the *Mirror BEC* in the proposed experimental conditions. In the inset it is shown the normalized amplitude in the first 10 μs. **b**)Reflectivity of a patterned BEC as a function of wavelength. In the inset is shown the reflectivity around resonance

the expanding condensate aligned along the symmetry axis of the harmonic trap to an optical beam with frequency $\omega - \omega_0 = \Delta$ largely detuned from the atomic resonance ω_0, the dominant scattering mechanism is Rayleigh scattering [ICSK$^+$99]. The dynamic evolution of the system in this regime is described by the 1-D CARL-BEC i.e. Gross-Pitaevskii, model generalized to include the self-consistent evolution of the scattered radiation amplitude [BCC$^+$04, DSB$^+$06, MZM99]:

$$i\frac{\partial \Psi}{\partial t} = -\frac{\hbar^2}{2m}\frac{\partial^2 \Psi}{\partial x^2} + ig\left\{a^* e^{i(2kx-\delta t)} - \text{c.c.}\right\}\Psi \tag{9.26}$$

$$\frac{da}{dt} = gN\int dx|\Psi|^2 e^{i(2kx-\delta t)} - \kappa a. \tag{9.27}$$

with $a = (\varepsilon_0 V/2\hbar\omega_s)^{1/2}E_s$ the dimensionless electric field amplitude of the reflected beam with frequency ω_s, $g = (\Omega/2\Delta)(\omega d^2/2\hbar\varepsilon_0 V)^{1/2}$ the coupling constant, and Ω the Rabi frequency modulation of the optical beam, $d = \hat{\varepsilon}\cdot\vec{d}$ is the electric dipole moment of the atom along the polarization direction $\vec{\varepsilon}$ of the laser, V is the volume of the condensate, N is the total number of atoms in the condensate and $\delta = \omega - \omega_s$. The last term in right-hand side of Eq.(9.26) represents the self-consistent optical wave grating while the first term in the right-hand side of Eq.(9.27) represents the self-consistent matter-wave grating. Eq.(9.27) has been written in the "mean-field" limit, which models the propagation effects by a damping term where $\kappa \approx c/2L$ and L is the length of the condensate. Let us focus on the amplitude of the reflected beam. We have integrated numerically the Equations (9.26,9.27) with the experimental parameters (given above) of a typical condensate and with the optical parameters for the output of the QI-OPA. As shown by Figure 2, the amplitude of the reflected optical beam drops as the matter wave grating is deteriorated by the interaction with the light beam. However, during the time duration of a QI-OPA pulse (typically 1 ps) no significant reduction is observed (inset of fig.9.2-(**a**)).

The above result leading to the dependence on ω of the M-BEC reflectivity has been found consistent with a less sophisticated model of the process based on a classical model for a Bragg mirror. The reflectivity of this one composed by $2N_D$ alternating layers with refraction index $n_B \sim (1+\varepsilon)$ is: $R = \left(\frac{n_B^{2N_D}-1}{n_B^{2N_D}+1}\right)^2 \sim N_D^2\varepsilon^2$.For a 2–level atom $\varepsilon = \frac{3\pi}{2}\mathscr{M}4\frac{\Gamma}{\Delta}\frac{1}{1+\left(2\frac{\Delta}{\Gamma}\right)^2}$ being $\mathscr{M} = \left(\frac{\lambda}{2\pi}\right)^3\frac{N}{V}$ is the rescaled density, Γ the atomic linewidth and Δ the detuning from resonance. In a rubidium BEC: $\Gamma \simeq 6$ MHz and typical densities are $\frac{N}{V} = 10^{14}\text{cm}^{-3}$. Combining all the previous equations and assumptions we obtain the graph Fig:2-(**b**). The inset of this Figure shows that around the atomic resonance with a bandwidth $\Delta\nu_a \simeq 8GHz$ the reflectivity of the patterned BEC is essentially unity, a more careful model should take into account a quasi sinusoidal modulation of the refractive index due to the atomic density distribution in the Thomas–Fermi approximation. This bandwidth, three orders of magnitude larger than in other proposals [AL06] is instrumental to the proposed experiment sketched in the right inset of Fig.1. A first estimate of the experimental parameters of the QIOPA system results in a NL gain $g = 6-7$ corresponding to a number of generated photons $\sim 10^5 - 10^6$. Since the spectral width of the QI-OPA generated beams is $\Delta\lambda \sim 0.75nm$, corresponding to a linewidth $\Delta\nu \sim 350GHz$, about the 3% of the incoming photon beams will be totally reflected by M-BEC. This will corresponds to a number of active photons $N'_{\pm}(\varphi) = (\Delta\nu_a/\Delta\nu) \times N_{\pm}(\varphi)$ in the range $(10^3 - 10^4)$. The ratio between the linewidths relative to the absorption (few MHz) and to the reflection process is $\simeq 0.1\%$ hence the mean number of absorbed photons is about one per pulse, it follows that the excitation of atoms can be considered negligible during the interaction process. At last, in the future we plan to use a different laser source with a longer pulse duration followed by a periodically-poled crystal amplifier. In such a way, it would be possible to obtain a high NL gain value and radiation fields with a bandwidth of $\sim 10GHz$.

9.3.2 Measurement of nonlocal correlations.

In order to observe the recoil effects of the *M-BEC*, the condensate has to be released from the optical lattice that shapes it. This can easily be done by shutting off the lasers light that provides the SW. Typical expansion velocities for a BEC are of the order of 1 nm/μs which leaves at least 50 μs before the pattern gets significantly spoiled. Let's investigate the different evolution of the BEC motions relative to the impinging field. Consider the case in which the multiphoton field is prepared in the state $|\Phi^+\rangle$ (or, alternatively: $|\Phi^-\rangle$) on the spatial mode $\mathbf{k}_1$. The state can be written as: $|\Phi^+\rangle_1 = |\phi^+\rangle_1|\xi^-\rangle_1$ ($|\Phi^-\rangle_1 = |\phi^-\rangle_1|\xi^+\rangle_1$), where $|\phi^+\rangle$ ($|\phi^-\rangle$) is the wavefunction contribution with polarization $\vec{\pi}_+(\vec{\pi}_-)$ and $|\xi\rangle^-(|\xi\rangle^+)$ is the contribution with polarization $\vec{\pi}_-(\vec{\pi}_+)$. The number of photons associated to $|\phi\rangle$ is dominant over the one associated to $|\xi\rangle$, as said,. The multiphoton state $|\Phi^+\rangle_1$ ($|\Phi^-\rangle_1$) is sent, through a single mode fiber, toward the BEC condensate. There, a $\lambda/2$ waveplate and a polarizing beam splitter direct the two polar-

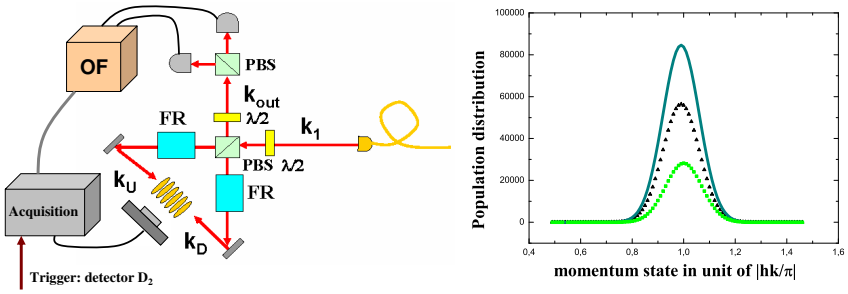

Figure 9.3: **Left**:Interaction between the amplified field and the Bragg Mirror BEC. The Faraday Rotators (FR) allows the recombination the reflected field on mode k_{out}. Indeed the field with polarization π_H transmitted by the PBS on mode k_U, passing through the first FR at 22.5°, becomes π_+ polarized. After the reflection by the Bragg Mirror its polarization is again rotated and becomes π_V: the field exits on mode k_{out}. A similar argumentation holds for the field polarized π_V. **Right:**comparison between the expected populations of the first order momentum peak (around 1% of total atoms) and the minus one momentum state after the interaction. The dotted (triangles) line represents the profile of the $+2\hbar k$ momentum state before interaction with the QIOPA pulse, continuous line and dotted (circles) line the $+2\hbar k$ and $-2\hbar k$ momentum state profiles after interaction, respectively. Both heating and collisional effects have been neglected (see text).

ization components $\vec{\pi}_+$ and $\vec{\pi}_-$ over the two spatial modes $\mathbf{k_U}$ and $\mathbf{k_D}$: the macrostate $|\Phi^+\rangle_1$ ($|\Phi^-\rangle_1$) evolves into $|\phi^+\rangle_U|\xi^-\rangle_D$ ($|\xi^+\rangle_U|\phi^-\rangle_D$): Figure 3. Then, the two counter-propagating fields are focused on the opposed sides of the cigar-shaped M-BEC. Thanks to the large reflectivity of the Bragg structure, an efficient coupling is achieved between the multiphoton fields and the atomic cloud. While the back-scattered light pulse changes direction of propagation ($U \Rightarrow D, D \Rightarrow U$), the M-BEC acquires a momentum kick in the opposite direction to the major photons contribution $|\phi^+\rangle_D$ ($|\phi^-\rangle_D$). Hence, after the interaction the overall light-matter state can be written as: $|\phi^+\rangle_D|\xi^-\rangle_U|\Psi^U\rangle_{BEC}$ ($|\xi^+\rangle_D|\phi^-\rangle_U|\Psi^D\rangle_{BEC}$) where $|\Psi^U\rangle_{BEC}$ ($|\Psi^D\rangle_{BEC}$) stands for the BEC that recoils in the direction $\mathbf{k_U}$ ($\mathbf{k_D}$). Two Faraday rotators inserted into the Sagnac-like interferometer allow the recombination of both the reflected fields $\{|\phi^+\rangle_D, |\xi^-\rangle_U\}$ ($\{|\xi^+\rangle_D, |\phi^-\rangle_U\}$) on the mode $\mathbf{k_{OUT}}$ leading to the output state $|\Phi^+\rangle_{OUT}|\Psi^U\rangle_{BEC}$ ($|\Phi^-\rangle_{OUT}|\Psi^D\rangle_{BEC}$).

In the analysis above, $|\Psi\rangle_{BEC}$ represents the state of the interacting portion rather than of the overall BEC system. Indeed the interaction with the QI-OPA pulse does not shift the BEC as a whole but only the atoms which get the momentum kick by the impinging photons. This mechanism of momentum transfer between light and atoms has been experimentally investigated in different works [CLM$^+$05, ARC$^+$06]. For a generic input photon macro-state $|\Phi^\varphi\rangle$, the resulting momentum exchange due to any elementary interaction will cause the spatial "displacement" of the M-BEC depending on the phase φ encoded in the far apart Alice's qubit, Since the spatial displacement of the M-BEC after the interaction with the QI-OPA pulse is too small to be directly detected, a stan-

dard "*expansion imaging*" technique will be adopted [IWS99]. The velocity acquired by the M-BEC is $\frac{N'}{N_{at}} v_r$, where v_r is the condensate recoil velocity of rubidium (in this case around 5 mm/s). This is visible during expansion where, due to the quantized nature of the momentum transfer, it appears as a transfer of atoms from the lower momentum state to a higher momentum state. Precisely, the normal momentum distribution of the M-BEC is made of sharp peaks centered around zero. Because of the photon-atom collisions a large number of atoms, for a total $N'_{\pm}(\varphi)$, will be transferred from the generic momentum state $n2h/\lambda$ to the successive state $(n \pm 1)2h/\lambda$. The momentum state distribution then becomes asymmetric as reported in Fig. 3-(Right). There we show the result of a numerical simulation of the population transfer from the zero momentum to the fist order momentum state, and we compare the population distributions after the interaction relative to the $-2\hbar k$ and $+\hbar k$ momentum states. A preliminary experimental test on a sample M-BEC with a classical light beam indeed showed a marked shift of the atomic momentum distribution due to light collision and a reflectivity in the range $0.5 - 0.9$. As a further improvement to this scenario, in the experiment only the largest, most efficient optical pulses could be singled out by a ultra-fast electro-optical switch placed at the output of the QI-OPA [SVG$^+$08].

9.4 Observations and Conclusions

In conclusion, the entanglement structure of $|\Sigma\rangle_{k1,k2}$ will imply the coherent displacement of the M-BEC system, depending on the phase φ of the single photon-measured by the far apart Alice's apparatus. The correlation measurements could be carried out by detecting the reflected light in different polarization basis and by observing the momentum distribution of the atomic cloud. In addition, the reflection process effect could be repeated several times by one or several external mirrors reflecting back the optical beams to the M-BEC after the first interaction, leading an optical *cavity* structure, e.g. a Fabry-Perot interferometer, by which the BEC displacing effect could be enhanced by a "quality factor" $Q >> 1$. Note also that the reflected photons, trapped in any *M-BEC* cavity or interferometer structure, will be themselves entangled with the atomic condensate.

Conclusions

In the context of QI the observation of quantum phenomena, such as quantum entanglement, has been mainly limited to systems of only few particles. One of the main open challenge for an experimental test in systems of large size is the construction of suitable criteria for the detection of entanglement in bipartite macroscopic systems. The possibility of observing quantum phenomena at a macroscopic level seems to be in conflict with the classical description of our everyday world knowledge. The main problem for such observation arises from the experimental difficulty of sufficiently isolating a quantum system from its environment, i.e., from the decoherence process.
The possibility of generating multiphoton states of light resilient to losses with the methods of quantum optics is then at the basis of this thesis. The multiphoton states can be generated through two different amplification schemes. In both cases the measurement problem is a key ingredient for the observation of quantum properties. The macro-states can then be studied as a paradigmatic example for the quantum to classical transition investigation. On the other hand the interest in investigating macroscopic states of light concerns the implementation of quantum information protocols related to quantum metrology and light atom efficient interactions.
The research work carried out within this thesis has then been focused onto the study of multiphoton states of light, obtained by non linear optics tools. We have investigated the quantum features of states produced by an amplification process and by a spontaneous emission of an optical parametric amplifier. In both cases the quantum features of increasing size quantum systems have been addressed. We have demonstrated the survival of entanglement after the amplification performed over an entangled pair by making auxiliary assumptions respect to the exploited entanglement criterion [DSV08]. Due to the probabilistic nature of the performed measurement, based on a local filtering of the macroscopic state, the microscopic-macroscopic entanglement has indeed been demonstrated by generalizing an entanglement criterion previously formulated for single-photon qubits [EKD$^+$04] with an auxiliary assumption about the presence of the amplifier acting upon the single photon state belonging to an EPR couple. We then discussed different entanglement criteria which do not require any supplementary assumption on the source, and applied these approaches to the micro-macro system based on optical parametric amplification. It turns out that these methods require an high detection efficiency in order to identify the macro-states and this requirement is not available with the present technology.

A second type of macro states, generated by a non-collinear optical parametric amplifier, working in a spontaneous emission regime, has been then investigated [VSSD09] . In this case a fuzzy measurement based on two different dichotomization procedures has been performed over the macro states. We observed that the amount of entanglement detected by this type of measurement decreases with the increase of the system's size. Our results enlighten the practical extreme difficulty of observing non-locality by performing such a dichotomic fuzzy measurement.
The problem of measurement on the multiphoton states has then been investigated in relation with the possibility of engineering the state of the system: the behavior of the indistinguishability between orthogonal macro-states when a filtering process is applied over a portion of them has been exploited. More specifically, we analyzed theoretically in details several schemes for the realization of conditional measurement-induced operations. We have identified a strategy, based on the ID device, able to minimize the effects of the noise due to the vacuum injection into the amplifier. A different filtering procedure, based on the OF device, has been deeply studied: it turned out that when a small portion of the state is analyzed through the OF, the visibility of the overall state, relative to a dichotomic measurement, is affected in a different way depending on the polarization basis in which the small portion has been measured. This tecnique is then not suitable to obtain an higher fidelity in the macro-states discrimination. Finally, we addressed a pre-selection scheme for the realization of a Bell's inequality test which do not suffer the same detection loopholes of the one based on post-selection strategies [VST$^+$10a]. The proposed method, based on the measurement of the reflected part of the wave-function in two different bases, does not allow to violate a Bell's inequality, since it induces the collapse of the correlations present in the macro-states in only a single polarization basis. These manipulation protocols exploited the use of a polarization preserving ultrafast optical shutter experimentally realized in our laboratories [SVG$^+$08].
Finally we have studied the application of multiphoton states to different quantum information protocols. We have demonstrated that the output field of an high gain optical parametric amplifier working in a collinear regime shows the sub-Rayleigh oscillation feature typical of a two-photon NOON states. The obtained fringe patterns suffer from a lower visibility respect to a pure NOON state, but the generated field results to be intense and the high flux regime can be adopted to perform high efficiency quantum lithography protocols [SVD$^+$08]. The analysis about the sub-Rayleigh behavior of multiphoton states has then be generalized by addressing the case of amplification of two-photon NOON states, obtaining an enhancement of the signal respect to the spontaneous emission case. Finally we showed theoretically that the collinear amplifier cannot be successfully used for amplifying N-photon states with N$>$2 due to the intrinsic $\frac{\lambda}{4}$ oscillation pattern of the crystal. To overcome this limitation, we propose to adopt a scheme for the amplification of a generic state based on a non-collinear QIOPA and we show that the state obtained by the amplification process preserves the $\frac{\lambda}{N}$ feature and exhibits a high resilience to losses [GCD$^+$08, VSSD09]. The resilience to losses of macro states has then be exploited in

order to obtain an enhancement in a minimally invasive metrology scenario [VST$^+$10b]. By performing the amplification process on the microscopic probe after the interaction with the sample, we have beaten the losses detrimental effect on the phase measurement which affects the single photon state after its interaction with the sample, and thus we have improved the achievable sensitivity in interferometrical experiments. In this case the enhancement in the sensitivity is not a scaling factor, as for the case of NOON-like oscillation pattern of the optical parametric amplifier, but consists in a constant factor which depends on the gain of the amplifier and on the losses condition in the investigated system.

At last the resilience to decoherence of the quantum state obtained by the amplification of an entangled couple is exploited to study the non-resonant interaction between the multiphoton state and a BEC shaped as a Bragg mirror. We have theorethically found that the entangled nature of the microscopic-macroscopic QIOPA system would imply the coherent displacement of the M-BEC system, depending on the polarization state of the injected single photon qubit. This system would represent a further example of macroscopic quantum state, fitting in the analysis of the transition from quantum to classical world performed in the present reasearch work [DSVC10].

In conclusion the multiphoton states of light, experimentally generated in our laboratories, have been considered as a paradigmatic example for the investigation of the quantum to classical transition, i.e. from the microscopic to the macroscopic world. Their generation and manipulation has been investigated in relation with the possibility of measuring the quantum properties in icreasing size quantum systems. The main obstacle in such an experimental demonstration turns out to be the inefficiency of performed measurement, which in presence of losses are unavoidable.At last the resilience to decoherence and to losses of multiphoton states has been exploited in different quantum information protocols: from quantum metrology to light atoms interface experiments.

Abbreviations

BEC Bose Einstein Condensate
BBO Beta-Barium-Bhorate Crystal
BS Beam Splitter
DFG Difference Frequancy generation
HWP Half waveplate
ID Intensity detection
M-BEC Mirror BEC
NL Non linear
NOON states of the form: $\frac{1}{\sqrt{2}}(|N\rangle|0\rangle + |0\rangle|N\rangle)$
OF Orthogonality Filter
OPA Optical Parametric Amplifier
PBS Polarizing Beam Splitter
POVM Positive-Operator-Valued Measure
QI Quantum Information
QIOPA Quantum Injected Optical Parametric Amplifier
QO Quantum Optics
QWP Quarter waveplate
SFG Sum Frequency generation
SHG Second Harmonic generation
SPDC Spontaneus Parametric Down Conversion

Publications

1. F. Sciarrino, C. Vitelli, F. De Martini, R. T. Glasser, H. Cable, and J. P. Dowling, *Experimental sub-Rayleigh resolution by an unseeded high-gain optical parametric amplifier for quantum lithography*, *Phys. Rev. A* **77**, 012324 (2008).

2. F. De Martini, F. Sciarrino, and C. Vitelli, *Entanglement Test on a Microscopic-Macroscopic System*, *Phys. Rev. Lett.* **100**, 253601 (2008).

3. R. T. Glasser, H. Cable, J. P. Dowling, F. De Martini, F. Sciarrino, and C. Vitelli, *Entanglement-seeded dual optical parametric amplification: application to quantum imaging and metrology*, *Phys. Rev. A* **78**, 012339 (2008).

4. N. Spagnolo, C. Vitelli, S. Giacomini, F. Sciarrino, and F. De Martini, *Polarization preserving ultra fast optical shutter for quantum information processing*, *Opt. Express* **16**, 17609 (2008).

5. C. Vitelli, N. Spagnolo, F. Sciarrino, and F. De Martini, *Amplification of polarization NOON states*, *JOSA B* **26**, 892 (2009).

6. N. Spagnolo, C. Vitelli, T. De Angelis, F. Sciarrino, and F. De Martini, *Wigner-function theory and decoherence of the quantum-injected optical parametric amplifier*, *Phys. Rev. A* **80**, 032318 (2009).

7. F. De Martini, F. Sciarrino, C. Vitelli, and F. S. Cataliotti, *Coherent Scattering of a Multiphoton Quantum Superposition by a Mirror BEC*, *Phys. Rev. Lett.* **104**, 050403 (2010).

8. C. Vitelli, N. Spagnolo, L. Toffoli, F. Sciarrino, and F. De Martini, *Quantum-to-classical transition via fuzzy measurements on high-gain spontaneous parametric down-conversion*, *Phys. Rev. A* **81**, 032313 (2010).

9. C. Vitelli, N. Spagnolo, L. Toffoli, F. Sciarrino, and F. De Martini, *Enhanced Resolution of Lossy Interferometry by Coherent Amplification of Single Photons*, *Phys. Rev. Lett.* **105**, 113602 (2010).

10. N. Spagnolo, C. Vitelli, F. Sciarrino, and F. De Martini, *Entanglement criteria for microscopic-macroscopic systems*, *Phys. Rev. A* **85**,052101 (2010).

11. C. Vitelli, N. Spagnolo, F. Sciarrino, and F. De Martini, *Measurement-induced quantum operations on multiphoton states* , *Phys. Rev. A* **82**, 062319 (2010).

Bibliography

[ACB+07] G. S. Agarwal, K. W. Chan, R. W. Boyd, H. Cable, and J. P. Dowling. Quantum states of light produced by a high-gain optical parametric amplifier for use in quantum lithography. *J. Opt. Soc. Am. B*, 24:270, 2007.

[AEM+95] M.H. Anderson, J.R. Ensher, M.R. Matthews, C.E. Wieman, and E.A. Cornell. Observation of bose-einstein condensation in a dilute atomic vapor. *Science*, 269:198, 1995.

[AK03] Guillaume Adenier and Andrei Khrennikov. Testing the fair sampling assumption for epr-bell experiments with polarizer beamsplitters. *arXiv:quant-ph/0306045*, 2003.

[AL06] M. Artoni and G.C. La Rocca. Optically tunable photonic stop bands in homogeneous absorbing media. *Phys. Rev. Lett.*, 96:073905, 2006.

[AMv+96] M.R. Andrews, M.-O. Mewes, N.J. van Druten, D.S. Durfee, D.M. Kurn, and W. Ketterle. Direct, nondestructive observation of a bose condensate. *Science*, 273:84, 1996.

[ARC+06] M. F. Andersen, C. Ryu, Pierre Clad, Vasant Natarajan, A. Vaziri, K. Helmerson, and W. D. Phillips. Quantized rotation of atoms from photons with orbital angular momentum. *Phy. Rev. Lett.*, 97:170406, 2006.

[AS98] C. O. Alley and Y. H. Shih. New type of einstein-podolsky-rosen-bohm experiment using pairs of light quanta produced by optical parametric down conversion. *Phys. Rev. Lett.*, 61:2921, 1998.

[BB06] A. I. Bishop and P. F. Barker. Subnanosecond pockels cell switching using avalanche transistors. *Rev. Sci. Instrum.*, 77:044701, 2006.

[BBB+08] J. D. Bancal, C. Branciard, Nicolas Brunner, Nicolas Gisin, Sandu Popescu, and Christoph Simon. Testing a bell inequality in multipair scenarios. *Phys. Rev. A*, 78:062110, 2008.

[BCC+04] R. Bonifacio, F.S. Cataliotti, M. M. Cola, L. Fallani, C. Fort, N. Piovella, and M. Inguscio. Decoherence effects in superradiant light scattering from a moving bose-einstein condensate. *J. Mod. Opt.*, 51:785, 2004.

[BcvH96] V. Bužek and M. Hillery. Quantum copying: Beyond the no-cloning theorem. *Phys. Rev. A*, 54(3):1844–1852, Sep 1996.

[Bel64] John Bell. On the einstein-podolski-rosen paradox. *Physics*, 1:195, 1964.

[BKA+00] A. N. Boto, P. Kok, D. S. Abrams, S. L. Braunstein, C. P. Williams, and J. P. Dowling. Quantum interferometric optical lithography: exploting entanglement to beat the diffraction limit. *Phys. Rev. Lett.*, 85:2733, 2000.

[Bos24] S.N. Bose. *Z. Phys.*, 26:178, 1924.

[Boy] R. W. Boyd. *Nonlinear Optics*. Elsevier.

[CDP+06] Marco Caminati, Francesco De Martini, Riccardo Perris, Fabio Sciarrino, and Veronica Secondi. Entanglement, epr correlations, and mesoscopic quantum superposition by the high-gain quantum injected parametric amplification. *Phys. Rev. A*, 73:032312, 2006.

[CdRF+05] C. W. Chou, H. de Riedmatten, D. Felinto, S. V. Polyakov, S. J. van Enk, and H. J. Kimble. Measurement-induced entanglement for excitation stored in remote atomic ensembles. *Nature*, 438:828, 2005.

[CHRB] Fabio Costa, Nicholas Harrigan, Terry Rudolph, and Caslav Brukner. Entanglement detection with bounded reference frames. *arXiv.org:0902.0935v1*.

[CHSH69] J. F. Clauser, M. A. Horne, A. Shimony, and R. A. Holt. Proposed experiment to test local hidden-variable theories. *Phys. Rev. Lett.*, 23:880, 1969.

[CLM+05] Gretchen K. Campbell, Aaron E. Leanhardt, Jongchul Mun, Micah Boyd, Erik W. Streed, Wolfgang Ketterle, and David E. Pritchard. Photon recoil momentum in dispersive media. *Phys. Rev. Lett.*, 94:94, 2005.

[CPHZ02] Z.-B. Chen, J.-W. Pan, G. Hou, and Y.-D. Zhang. Maximal violation of bell's inequalities for continuous variable systems. *Phys. Rev. Lett.*, 88:040406, 2002.

[CYZ+06] Y. A. Chen, T. Yang, A. N. Zhang, Z. Zhao, A. Cabello, and J. W. Pan. Experimental violation of bell's inequality beyond tsirelson's bound. *Phys. Rev. Lett.*, 95:020403, 2006.

[Dal99] F. Dalfovo. *Rev. Mod. Phys.*, 71:463, 1999.

[DBSS02] Francesco De Martini, Vladimir Buzek, Fabio Sciarrino, and Carlo Sias. Experimental realization of the quantum universal not gate. *Nature*, 419:815, 2002.

[DCS01] M. D'Angelo, M. V. Chekhova, and Y. Shih. Two-photon diffraction and quantum lithography. *Phys. Rev. Lett.*, 87:013602, 2001.

[DDDS+09a] R. Demkowicz-Dobrzanski, U. Dorner, B.J. Smith, J.S. Lundeen, W. Wasilewski, K. Banaszek, and I.A. Walmsley. Quantum phase estimation with lossy interferometers. *Phys. Rev. A*, 80:013825, 2009.

[DDDS+09b] U. Dorner, R. Demkowicz-Dobrzanski, B. J. Smith, J. S. Lundeen, W. Wasilewski, K. Banaszek, and I. A. Walmsley. Optimal quantum phase estimation. *Phys. Rev. Lett.*, 102:040403, 2009.

[De 98a] Francesco De Martini. Amplification of quantum entanglement. *Phys. Rev. Lett.*, 81:2842, 1998.

[De 98b] Francesco De Martini. Quantum superposition of parametrically amplified multiphoton pure states. *Phys. Lett. A*, 250:15, 1998.

[DHW+99] L. Deng, E. W. Hagley, J. Wen, M. Trippenbach, Y. Band, P. S. Julienne, J. E. Simsarian, K. Helmerson, S. L. Rolston, and W. D. Phillips. Four-wave mixing with matter waves. *Nature*, 398:218–220, 1999.

[dLC+06] H. de Riedmatten, J. Laurat, C. W. Chou, E. W. Schomburg, D. Felinto, and H. J. Kimble. Direct measurement of decoherence for entanglement between a photon and stored atomic excitation. *Phys. Rev. Lett.*, 97:113603, 2006.

[DMA+95] K.B. Davis, M.O. Mewes, M.R. Andrews, N.J. van Druten, D.S. Durfee, D.M. Kurn, and W. Ketterle. Bose einstein condensatio in gas of sodium atoms. *Phys. Rev. Lett.*, 75:3969, 1995.

[DNSD07] Tiziano De Angelis, Eleonora Nagali, Fabio Sciarrino, and Francesco De Martini. Experimental test of the no-signaling theorem. *Phys. Rev. Lett.*, 99:193601, 2007.

[Dow08] J. P. Dowling. Quantum optical metrology - the lowdown on high-noon states. *Contemp. Phys.*, 49:125, 2008.

[DS05] Francesco De Martini and Fabio Sciarrino. Non-linear parametric processes in quantum information. *Progr. Quantum Electron.*, 29:165, 2005.

[DSB+06] L. De Sarlo, R. Saers, S. Bartalini, F. S. Cataliotti, L. Fallani, C. Fort, I. Herrera, and M. Inguscio. From superradiant rayleigh scattering to bragg scattering. *Phys. Rev. Lett.*, 97:113603, 2006.

[DSS09a] Francesco De Martini, Fabio Sciarrino, and Nicolò Spagnolo. Anomalous lack of decoherence of the macroscopic quantum superpositions based on phase-covariant quantum cloning. *Phys. Rev. Lett.*, 103:100501, 2009.

[DSS09b] Francesco De Martini, Fabio Sciarrino, and Nicolò Spagnolo. Decoherence, environment-induced superselection, and classicality of a macroscopic quantum superposition generated by quantum cloning. *Phys. Rev. A*, 79:052305, 2009.

[DSV08] Francesco De Martini, Fabio Sciarrino, and Chiara Vitelli. Entanglement test on a microscopic-macroscopic system. *Phys. Rev. Lett.*, 100:253601, 2008.

[DSVC10] Francesco De Martini, Fabio Sciarrino, Chiara Vitelli, and Francesco Saverio Cataliotti. Coherent scattering of a multiphoton quantum superposition by a mirror bec. *Phys. Rev. Lett.*, 104:050403, 2010.

[Dur04] Gabriel A. Durkin. Light and spin entanglement. *Phd Thesis, Corpus Christi College, University of Oxford*, 2004.

[EGB+03] Manfred Eibl, Sascha Gaertner, Mohamed Bourennane, Christian Kurtsiefer, Marek Zukowski, and Harald Weinfurter. Experimental observation of four-photon entanglement from parametric down-conversion. *Phys. Rev. Lett.*, 90:200403, 2003.

[EHKB05] H. S. Eisenberg, J. F. Hodelin, G. Khoury, and D. Bouwmeester. Multiphoton path entanglement by nonlocal bunching. *Phys. Rev. Lett.*, 94:090502, 2005.

[Ein24] A. Einstein. *Sitzber. Kgl. Preuss. Akad. Wiss.*, 261, 1924.

[EKD+04] H. S. Eisenberg, G. H. Khoury, G. A. Durkin, Christoph Simon, and D. Bouwmeester. Quantum entanglement of a large number of photons. *Phys. Rev. Lett.*, 93:193901, 2004.

[EPR35] A. Einstein, B. Podolski, and N. Rosen. Can quantum-mechanical description of physical reality be considered complete? *Phys. Rev.*, 47:777, 1935.

[FBB+10] Franck Ferreyrol, Marco Barbieri, Rémi Blandino, Simon Fossier, Rosa Tualle-Brouri, and Philippe Grangier. Implementation of a nondeterministic optical noiseless amplifier. *Phys. Rev. Lett.*, 104:123603, 2010.

[Fen02] Mang Feng. Quantum computing in cavity qed with cold trapped ions by bichromatic radiation. *Phys. Rev. A*, 65(6):064301, May 2002.

[Fey82] R.P. Feynman. *Int. J. Theor. Phys.*, 21:467, 1982.

[Fiu01] J. Fiurasek. Conditional generation of sub-poissonian light from two-mode squeezed vacuum via balanced homodyne detection on idler mode. *Phys. Rev. A*, 64:053817, 2001.

[Fiu09] J. Fiurasek. Engineering quantum operations on traveling light beams by multiple photon addition and subtraction. *Phys. Rev. A*, 80:053822, 2009.

[FMA05] Radim Filip, Petr Marek, and Ulrik Lund Andersen. Measurement-induced continuous-variable quantum interactions. *Phys. Rev. A*, 71:042308, 2005.

[GAF+06] O. Glöckl, U. L. Andersen, R. Filip, W. P. Bowen, and G. Leuchs. Squeezed-state purification with linear optics and feedforward. *Phys. Rev. Lett.*, 97:053601, 2006.

[GCD+08] R. T. Glasser, H. Cable, J. P. Dowling, Francesco De Martini, Fabio Sciarrino, and Chiara Vitelli. Entanglement-seeded dual optical parametric amplification: application to quantum imaging and metrology. *Phys. Rev. A*, 78:012339, 2008.

[GLM04] V. Giovannetti, S. Lloyd, and L. Maccone. Quantum-enhanced measurements: Beating the standard quantum limit. *Science*, 306:1330, 2004.

[GLM06] Vittorio Giovannetti, Seth Lloyd, and Lorenzo Maccone. Quantum metrology. *Phys. Rev. Lett.*, 96:010401, 2006.

[GM97] N. Gisin and S. Massar. Optimal quantum cloning machines. *Phys. Rev. Lett.*, 79(11):2153–2156, Sep 1997.

[GSLD02] S. Giacomini, F. Sciarrino, E. Lombardi, and F. De Martini. Active teleportation of a quantum bit. *Phys. Rev. A*, 66:030302, 2002.

[Hel76] C. W. Helstrom. *Quantum Detection and Estimation Theory*. Academic Press, 1976.

[HKPS99] Lo Hoi-Kwong, Sandu Popescu, and Tim Spiller. *Introduction to Quantum Computation and Information.* World Scientific, 1999.

[HMD+06] J. Heersink, C. Marquardt, R. Dong, R. Filip, S. Lorenz, G. Leuchs, and U. L. Andersen. Distillation of squeezing from non-gaussian quantum states. *Phys. Rev. Lett.*, 96:253601, 2006.

[HMG+96] B. Huttner, A. Muller, J. D. Gautier, H. Zbinden, and N. Gisin. Unambiguous quantum measurement of nonorthogonal states. *Phys. Rev. A*, 54(5):3783–3789, Nov 1996.

[HWD08] S.D. Huver, C.F. Wildfeuer, and J.P. Dowling. Entangled fock states for robust quantum optical metrology, imaging, and sensing. *Phys. Rev. A*, 78:063828, 2008.

[ICSK+99] S. Inouye, A. P. Chikkatur, D. M. Stamper-Kurn, J. Stenger, D. E. Pritchard, and W. Ketterle. Superradiant rayleigh scattering from a bose-einstein condensate. *Science*, 285:571, 1999.

[IWS99] M. Inguscio, C. Wieman, and S. Stringari. *Bose-Einstein Condensation in Atomic Gases,*. IOS Press,Tokio, 1999.

[JG90] Juha Javanainen and Phillip L. Gould. Linear intensity dependence of a two-photon transition rate. *Phys. Rev. A*, 41:5088, 1990.

[JKP01] Brian Julsgaard, Alexander Kozhekin, and Eugene S. Polzik. Experimental long-lived entanglement of two macroscopic objects. *Nature*, 413:400, 2001.

[JPR09] Hyunseok Jeong, Mauro Paternostro, and Timothy C. Ralph. Failure of local realism revealed by extremely-coarse-grained measurements. *Phys. Rev. Lett.*, 102:060403, 2009.

[KB07] Johannes Kofler and Caslav Brukner. Classical world arising out of quantum physics under the restriction of coarse-grained measurements. *Phys. Rev. Lett.*, 99:180403, 2007.

[KB08] Johannes Kofler and Caslav Brukner. Conditions for quantum violation of macroscopic realism. *Phys. Rev. Lett.*, 101:090403, 2008.

[KBB09] J. Kofler, N. Buric, and C. Brukner. Macroscopic realism and spatiotemporal continuity. *arXiv.org:0906.4465*, 2009.

[KDDW+09] M. Kacprowicz, R. Demkowicz-Dobrzanski, W. Wasilewski, K. Banaszek, and I.A. Walmsley. Experimental quantum-enhanced estimation of a lossy phase shift. *arXiv:0906.3511*, 2009.

[KMW+95] Paul G. Kwiat, Klaus Mattle, Harald Weinfurter, Anton Zeilinger, Alexander V. Sergienko, and Yanhua Shih. New high-intensity source of polarization-entangled photon pairs. *Phys. Rev. Lett.*, 75:4337, 1995.

[KSSA98] T. E. Kiess, Y. H. Shih, A. V. Sergienko, and C. O. Alley. Einstein-podolsky-rosen-bohm experiment using pairs of light quanta produced by type-ii parametric down-conversion. *Phys. Rev. Lett.*, 71:3893, 1998.

[KTSC06] A. Kitagawa, M. Takeoka, M. Sasaki, and A. Chefles. Entanglement evaluation of non-gaussian states generated by photon subtraction from squeezed states. *Phys. Rev. A*, 73:042310, 2006.

[LBL+] J. A. Levenson, K. Bencheikh, D. J. Lovering, P. Vidakovic, and C. Simonneau.

[Leo93] Ulf Leonhardt. Quantum statistics of a lossless beam splitter: Su(2) symmetry in phase space. *Phys. Rev. A*, 48:3265, 1993.

[LHL+09] T.-W. Lee, S.D. Huver, H. Lee, L. Kaplan, S.B. McCracken, C. Min, D.B. Uskov, C.F. Wildfeuer, G. Veronis, and J.P. Dowling. Optimization of quantum interferometric metrological sensors in the presence of photon loss. *arXiv:0908.3008*, 2009.

[Lou00] Rodney Loudon. *The Quantum Theory of Light*. Oxford University Press, 2000.

[MCB+05] D. N. Matsukevich, T. Chanelire, M. Bhattacharya, S.-Y. Lan, S. D. Jenkins, T. A. B. Kennedy, and A. Kuzmich. Entanglement of a photon and a collective atomic excitation. *Phys. Rev. Lett.*, 95:040405, 2005.

[MD09] L. Maccone and G. De Cillis. Robust strategies for lossy quantum interferometry. *Phys. Rev. A*, 79:023812, 2009.

[MKTS+99] 1 Yoichi Suzuki Mikio Kozuma, Yoshio Torii, Toshiaki Sugiura, Takahiro Kuga, E. W. Hagley, and L. Deng. Phase-coherent amplification of matter waves. *Science*, 286:2309 – 2312, 1999.

[MLS04] M. W. Mitchell, J. S. Lundeen, and A. M. Steinberg. Super-resolving phase measurements with a multiphoton entangled state. *Nature*, 429:161, 2004.

[MMO+07] D. L. Moehring, P. Maunz, S. Olmschenk, K. C. Younge, D. N. Matsukevich, L.-M. Duan, and C. Monroe. Entanglement of single-atom quantum bits at a distance. *Nature*, 449:68–71, 2007.

[MO06] O. Morsch and M. Oberthaler. Dynamics of bose einstein condensates in optical lattices. *Rev. Mod. Phys.*, 78:179, 2006.

[MP95] S. Massar and S. Popescu. Optimal extraction of information from finite quantum ensembles. *Phys. Rev. Lett.*, 74(8):1259–1263, Feb 1995.

[MZM99] M. G. Moore, O. Zobay, and P. Meystre. Quantum optics of a bose-einstein condensate coupled to a quantized light field. *Phys. Rev. A*, 60:14911506, 1999.

[NBBA01] E. M. Nagasako, S. J. Bentley, R. W. Boyd, and G. S. Agarwal. Nonclassical two-photon interferometry and lithography with high-gain parametric amplifiers. *Phys. Rev. A*, 64:043802, 2001.

[NDSD07] Eleonora Nagali, Tiziano De Angelis, Fabio Sciarrino, and Francesco De Martini. Experimental realization of macroscopic coherence by phase-covariant cloning of a single photon. *Phys. Rev. A*, 76:042126, 2007.

[NOO+07] T. Nagata, R. Okamoto, J. L. O'Brien, K. Sasaki, and S. Takeuchi. Beating the standard quantum limit with four entangled photons. *Science*, 316:726, 2007.

[OFTBG09] Alexej Ourjoumtsev, Franck Ferreyrol, Rosa Tualle-Bruori, and Philippe Grangier. Preparation of non-local superpositions of quasi-classical light states. *Nature Physics*, 5:189, 2009.

[OJTBG07a] A. Ourjoumtsev, H. Jeong, R. Tualle-Brouri, and P. Grangier. Generation of optical 'schrödinger cats' from photon number states. *Nature*, 448:784, 2007.

[OJTBG07b] Alexej Ourjoumtsev, Hyunseok Jeong, Rosa Tualle-Bruori, and Philippe Grangier. Generation of optical "schrodinger cats" from photon number states. *Nature*, 448:784, 2007.

[OM88] Z. Y. Ou and L. Mandel. Violation of bell's inequality and classical probability in a two-photon correlation experiment. *Phys. Rev. Lett.*, 61:50, 1988.

[OPW+03] J. L. O'Brien, G. J. Pryde, A. G. White, T. C. Ralph, and D. Branning. Demonstration of an all-optical quantum controlled-not gate. *Nature*, 426:264–267, 2003.

[Par09] Matteo G. A. Paris. Quantum estimation for quantum technology. *Int. J. Quant. Inf.*, 7:125, 2009.

[PDS+06] S. Portolan, O. Di Stefano, S. Savasta, F. Rossi, and R. Girlanda. Decoherence-free emergence of macroscopic local realism for entangled photons in a cavity. *Phys. Rev. A*, 73(020201(R)):020101, 2006.

[Per95] A. Peres. *Quantum Theory: Methods and Concepts*. Kluwer Academic Publishers, 1995.

[Per96] Asher Peres. Separability criterion for density matrices. *Phys. Rev. Lett.*, 77(8):1413, 1996.

[Pop95] Sandu Popescu. Bell's inequalities and density matrices: revealing "hidden" nonlocality. *Phys. Rev. Lett.*, 74:2619, 1995.

[PPS+01] P. Pedri, L. Pitaevskii, S. Stringari, C. Fort, S. Burger, F. S. Cataliotti, P. Maddaloni, F. Minardi, and M. Inguscio. Expansion of a coherent array of bose-einstein condensates. *Phys. Rev. Lett.*, 81:220401, 2001.

[PSS+03] D. Pelliccia, V. Schettini, F. Sciarrino, C. Sias, and F. De Martini . Contextual realization of the universal quantum cloning machine and of the universal-not gate by quantum-injected optical parametric amplification. *Phys. Rev. A*, 68:042306, 2003.

[PST98] Jan Perina Jr., Bahaa E. A. Saleh, and Malvin C. Teic. Multiphoton absorption cross section and virtual-state spectroscopy for the entangled n-photon state. *Phys. Rev. A*, 57:3972, 1998.

[PWT+07] Robert Prevedel, Philip Walther, Felix Tiefenbacher, Pascal Bhi, Rainer Kaltenbaek, Thomas Jennewein, and Anton Zeilinger. High–speed linear optics quantum computing using active feed-forward. *Nature*, 455:65, 2007.

[Red] *Incompleteness, Nonlocality, and Realism*.

[RK07] Mark A. Rubin and Sumanth Kaushik. Loss-induced limits to phase measurement precision with maximally entangled states. *Phys. Rev. A*, 75:053805, 2007.

[RMD02] M. D. Reid, W. J. Munro, and Francesco De Martini. Violation of multiparticle bell inequalities for low- and high-flux parametric amplification using both vacuum and entangled input states. *Phys. Rev. A*, 66:033801, 2002.

[Sak94] J.J. Sakuray. *Modern Quantum Mechanics*. Addison-Wasleyr, 1994.

[SB03] Christoph Simon and Dik Bouwmeester. Theory of an entanglement laser. *Phys. Rev. Lett.*, 91:053601, 2003.

[SBB+09] Pavel Sekatski, Nicolas Brunner, Cyril Branciard, Nicolas Gisin, and Christoph SImon. Towards quantum experiments with human eyes as detectors based on cloning via stimulated emission. *Phys. Rev. Lett.*, 103:113601, 2009.

[SC07] Anil Shaji and Carlton M. Caves. Qubit metrology and decoherence. *Phys. Rev. A*, 76:032111, 2007.

[SSP+10] P. Sekatski, B. Sanguinetti, E. Pomarico, N. Gisin, and C. Simon. Cloning entangled qubits to scales one can see. *arXiv:1005.5083*, 2010.

[SVD+08] Fabio Sciarrino, Chiara Vitelli, Francesco De Martini, R. T. Glasser, H. Cable, and J. P. Dowling. Experimental sub-rayleigh resolution by an unseeded high-gain optical parametric amplifier for quantum lithography. *Phys. Rev. A*, 77:012324, 2008.

[SVD+09] Nicolò Spagnolo, Chiara Vitelli, Tiziano De Angelis, Fabio Sciarrino, and Francesco De Martini. Wigner-function theory and decoherence of the quantum-injected optical parametric amplifier. *Phys. Rev. A*, 80:032318, 2009.

[SVG+08] Nicolò Spagnolo, Chiara Vitelli, Sandro Giacomini, Fabio Sciarrino, and Francesco De Martini. Polarization preserving ultra fast optical shutter for quantum information processing. *Opt. Express*, 16:17609, 2008.

[TR04] S. Thanvanthri and M. H. Rubin. Ghost interference with an optical parametric amplifier. *Phys. Rev. A*, 70:063811, 2004.

[UMW+10] Mario A. Usuga, Christian R. Mueller, Christoffer Wittmann, Petr Marek, Radim Filip, Christoph Marquardt, Gerd Leuchs, and Ulrik L. Andersen. Noise-powered probabilistic concentration of phase information. *arXiv:1005.3706*, 2010.

[VPMM08] Giuseppe Vallone, Enrico Pomarico, Francesco De Martini, and Paolo Mataloni. Active one-way quantum computation with two-photon four-qubit cluster states. *Phys. Rev. Lett.*, 100:160502, 2008.

[VSSD09] Chiara Vitelli, Nicol Spagnolo, Fabio Sciarrino, and Francesco De Martini. Amplification of polarization noon states. *JOSA B*, 26:892, 2009.

[VST+10a] C. Vitelli, N. Spagnolo, L. Toffoli, F. Sciarrino, and F. De Martini. Quantum-to-classical transition via fuzzy measurements on high-gain spontaneous parametric down-conversion. *Phys. Rev. A*, 81:032313, 2010.

[VST+10b] Chiara Vitelli, Nicolò Spagnolo, Lorenzo Toffoli, Fabio Sciarrino, and Francesco De Martini. Enhanced resolution of lossy interferometry by coherent amplification of single photons. *Phys. Rev. Lett.*, 105(11):113602, 2010.

[WARZ05] Philip Walther, Markus Aspelmeyer, Kevin J. Resch, and Anton Zeilinger. Experimental violation of a cluster state bell inequality. *Phys. Rev. Lett.*, 95:020403, 2005.

[WM94] D.F. Walls and G.J. Milburn. *Quantum Optics*. Springer, 1994.

[WPA+04] P. Walther, J. W. Pan, M. Aspelmeyer, R. Ursin, S. Gasparoni, and A. Zeilinger. De broglie wavelength of a non-local four-photon state. *Nature*, 429:158, 2004.

[WSK+08] Witlef Wieczorek, Christian Schmid, Nikolai Kiesel, Reinhold Pohlner, Otfried Ghne, and Harald Weinfurter. Experimental observation of an entire family of four-photon entangled states. *Phys. Rev. Lett.*, 101:010503, 2008.

[WZ82] W. K. Wootters and W. H. Zurek. A single quantum cannot be cloned. *Nature*, 299:802, 1982.

[WZ01] Harald Weinfurter and Marek Zukowski. Four-photon entanglement from down-conversion. *Phys. Rev. A*, 64:010102(R), 2001.

[XRL+10] G. Y. Xiang, T. C. Ralph, A. P. Lund, N. Walk, and G. J. Pryde. Heralded noiseless linear amplification and distillation of entanglement. *Nature Photonics*, 4:316, 2010.

[ZFB10] A. Zavatta, J. Fiurasek, and M. Bellini. A high-fidelity noiseless amplifier for quantum light states. *arXiv:1004.3399*, 2010.

[Zur03] W. H. Zurek. Decoherence, einselection, and the quantum origins of the classical. *Rev. Mod. Phys.*, 75:715, 2003.

Experimental sub-Rayleigh resolution by an unseeded high-gain optical parametric amplifier for quantum lithography

Fabio Sciarrino,[1,2] Chiara Vitelli,[1] Francesco De Martini,[1] Ryan Glasser,[3] Hugo Cable,[3] and Jonathan P. Dowling[3]
[1]*Dipartimento di Fisica, Universitá di Roma "La Sapienza" and Consorzio Nazionale Interuniversitario per le Scienze Fisiche della Materia, Roma 00185, Italy*
[2]*Centro di Studi e Ricerche Enrico Fermi, Via Panisperna 89/A, Compendio del Viminale, Roma 00184, Italy*
[3]*Hearne Institute for Theoretical Physics, Louisiana State University, Baton Rouge, Louisiana 70803, USA*
(Received 18 July 2007; published 22 January 2008)

Quantum lithography proposes to adopt entangled quantum states in order to increase resolution in interferometry. In the present paper we experimentally demonstrate that the output of a high-gain optical parametric amplifier can be intense yet exhibits quantum features, namely, sub-Rayleigh fringes, as proposed by [Agarwal *et al.*, Phys. Rev. Lett. **86**, 1389 (2001)]. We investigate multiphoton states generated by a high-gain optical parametric amplifier operating with a quantum vacuum input for gain values up to 2.5. The visibility has then been increased by means of three-photon absorption. The present paper opens interesting perspectives for the implementation of such an advanced interferometrical setup.

DOI: 10.1103/PhysRevA.77.012324 PACS number(s): 03.67.Hk, 42.65.Lm

I. INTRODUCTION

Since the early days of quantum electronics, nonlinear optics has played a basic role both for its relevance as a fundamental chapter of modern science and for its technological applications [1]. Nonlinear parametric processes, due to the peculiar correlation properties of the generated photons, have been adopted to investigate the quantum properties of electromagnetic fields. In the last few years it has been proposed to exploit entangled quantum states in order to increase the resolution in quantum interferometry, specifically, for quantum lithography [2] and to achieve Heisenberg limited resolution [3]. In such framework, particular attention has been devoted to the generation of NOON states, path-entangled states of the form $\frac{1}{\sqrt{2}}(|N\rangle_{k1}|0\rangle_{k2}+|0\rangle_{k1}|N\rangle_{k2})$, of fundamental relevance since a single-photon phase shift φ induces a relative shift between the two components equal to $N\varphi$. This feature can be exploited to enhance phase resolution in interferometric measurements, leading to a sub-Rayleigh resolution scaling as $\frac{\lambda}{(2N)}$; λ being the wavelength of the field [4]. The generation of photonic NOON states has been the subject of intense theoretical research [5], but up to now the actual experimental implementation has been limited to *a posteriori* generation of two-, three-, and four-photons states [6–8] and to the conditional generation of a NOON state with $N=2$ [9]. The weak value of the generated number of photons strongly limits the potential applications to quantum lithography and quantum metrology. As an alternative approach to emulate the quantum resolution, it has been proposed to adopt classical, coherent light [10], effectively exploiting the nonlinearity of the absorbing material. The experimental results have been recently reported: Yablonovitch *et al.* proposed to use an interference technique with multiple-frequency beams achieving an experimental visibility of 3% [11] while Boyd *et al.* achieved a twofold enhancement of the resolution over the standard Rayleigh limit adopting a UV lithographic material excited by multiphoton absorption [12].

Recently it has been proposed to exploit a high-gain optical parametric amplifier acting on the vacuum field to generate fields with a high number of photons still exhibiting sub-Rayleigh periods: Fig. 1(a) [13]. The quantum lithography architecture involves the generation of correlated beams over the modes k_1 and k_2, the mixing over a beam splitter (BS), the phase shifting of one mode and then the recombination of the two modes over a second BS. Finally the output state is detected via a two-photon absorption over the outgoing modes. In the typical low-gain regime the quantum state $2^{-1/2}(|2\rangle_{k1}|0\rangle_{k2}-|0\rangle_{k1}|2\rangle_{k2})$ is generated by spontaneous parametric down conversion (SPDC) and a Hong-Ou-Mandel interferometer adopting a post-selection technique [6]. In Refs. [13–15] it has recently been theoretically shown that, for any gain of the parametric amplifier, the two-photon excitation rate presents a fringe pattern of the form $1+\cos 2\varphi$ which never falls below a visibility of 20%. Such an approach could lead to high resolution with a high number of photons overcoming the difficulty connected with the adoption of the NOON state with a low number of photons. At variance with the scheme based on classical radiation, the one here exploits quantum features of the OPA field.

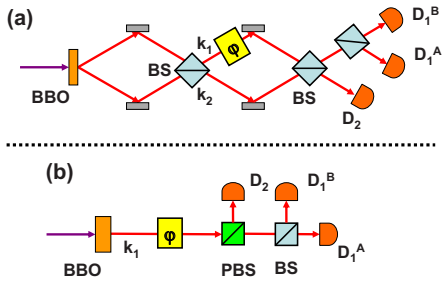

FIG. 1. (Color online) (a) Experimental scheme for quantum lithography based on spontaneous parametric down conversion. The two-photon absorption is simulated through a two-photon coincidence detection. (b) Configuration based on polarization entangled beams.

Entanglement Test on a Microscopic-Macroscopic System

Francesco De Martini,[1,2] Fabio Sciarrino,[3,1] and Chiara Vitelli[1]
[1]*Dipartimento di Fisica dell'Universitá "La Sapienza" and Consorzio Nazionale Interuniversitario per le Scienze Fisiche della Materia, Roma, 00185 Italy*
[2]*Accademia Nazionale dei Lincei, via della Lungara 10, I-00165 Roma, Italy*
[3]*Centro di Studi e Ricerche "Enrico Fermi", Via Panisperna 89/A,Compendio del Viminale, Roma 00184, Italy*
(Received 6 March 2008; published 26 June 2008)

A macrostate consisting of $\mathbf{N} \approx 3.5 \times 10^4$ photons in a quantum superposition and entangled with a far apart single-photon state (microstate) is generated. Precisely, an entangled photon pair is created by a nonlinear optical process; then one photon of the pair is injected into an optical parametric amplifier operating for any input polarization state, i.e., into a phase-covariant cloning machine. Such transformation establishes a connection between the single photon and the multiparticle fields. We then demonstrate the nonseparability of the bipartite system by adopting a local filtering technique within a positive operator valued measurement.

DOI: 10.1103/PhysRevLett.100.253601 PACS numbers: 42.50.Xa, 03.65.Ta, 03.67.Bg, 42.65.Lm

In recent years two fundamental aspects of quantum mechanics have attracted a great deal of interest: namely, the investigation of the irreducible nonlocal properties of nature implied by quantum entanglement and the physical realization of the "Schrödinger cat" [1,2]. The last concept, by applying the nonlocality property to a combination of a microscopic and macroscopic systems, enlightens the concept of the quantum state, the dynamics of large systems and ventures into a most intriguing philosophical problem, i.e., the emergence of quantum mechanics in real life. In recent years quantum entanglement has been demonstrated within a two photon system [3], within a single photon and atomic ensemble [4,5] and within atomic ensembles [6–8]. While, according to the 1935 proposal, the nonlocal correlations were conceived to connect the dynamics of two "microscopic" objects, i.e., two spins within the well-known EPR-Bohm scheme [3], in the present work the entanglement is established between a microscopic and a "macroscopic", i.e., multiparticle quantum object, via cloning amplification: Fig. 1. The amplification is achieved by adopting a high-gain nonlinear (NL) parametric amplifier acting on a single-photon input carrier of quantum information, i.e., a qubit state: $|\phi\rangle$. This process, referred to as "quantum-injected optical parametric amplification" (QI-OPA) [9,10] turned out to be particularly fruitful in the recent past to gain insight into several little explored albeit fundamental, modern aspects of quantum information, as *optimal* quantum cloning machines [9,11,12], *optimal* quantum U-NOT gate [13], quantum no-signaling [14]. Here, by exploiting the amplification process, we convert by a unitary transformation a single-photon qubit into a single macroqubit involving a large number of photons, typically 5×10^4. At variance with the previous works [14,15], here we demonstrate for the first time the entanglement between the microscopic qubit and the macroscopic one obtained by the amplification process. This result is achieved performing a local dichotomic measurement on the multiphoton field. Let us venture in a more detailed account of our endeavor.

An entangled pair of photons in the singlet state $|\Psi^-\rangle_{A,B} = 2^{-(1/2)}(|H\rangle_A|V\rangle_B - |V\rangle_A|H\rangle_B)$ was produced through a spontaneous parametric down-conversion (SPDC) by the NL crystal 1 (C1) pumped by a pulsed UV pump beam: Fig. 2. There $|H\rangle$ and $|V\rangle$ stands, respectively, for a single photon with horizontal and vertical polarization while the labels A, B refer to particles associated, respectively, with the spatial modes $\mathbf{k}_A$ and $\mathbf{k}_B$. Precisely, A, B represent the two spacelike separated Hilbert spaces coupled by the entanglement. The photon belonging to $\mathbf{k}_B$, together with a strong ultraviolet (UV) pump laser beam, was fed into an optical parametric amplifier consisting of a NL crystal 2 (C2) pumped by the beam $\mathbf{k}'_P$. The crystal 2, cut for collinear operation, emitted over the two modes of linear polarization, respectively, horizontal and vertical associated with $\mathbf{k}_B$. The interaction Hamiltonian of the parametric amplification $\hat{H} = i\chi\hbar\hat{a}_H^\dagger\hat{a}_V^\dagger + \text{H.c.}$ acts on the single spatial mode $\mathbf{k}_B$ where $\hat{a}_\pi^\dagger$ is the one photon creation operator associated with the polarization $\vec{\pi}$. The main feature of this Hamiltonian is its property of "phase-covariance" for "equatorial" qubits $|\phi\rangle$, i.e., representing equatorial states of polarization, $\vec{\pi} = 2^{-1/2}(\vec{\pi}_H + e^{i\phi}\vec{\pi}_V)$, $\vec{\pi}_{\phi\perp} = \vec{\pi}_\phi^\perp$, in a Poincaré sphere representation having $\vec{\pi}_H$ and $\vec{\pi}_V$ as the opposite "poles" [15]. The equatorial qubits are expressed in terms of a

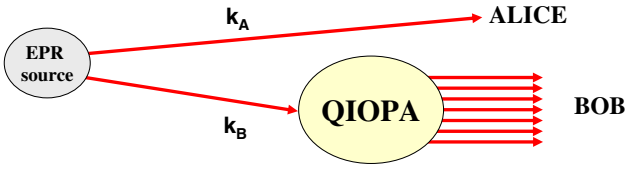

FIG. 1 (color online). Schematic diagram showing the single-photon quantum-injected optical parametric amplification.

Polarization preserving ultra fast optical shutter for quantum information processing

Nicoló Spagnolo[1], Chiara Vitelli[1], Sandro Giacomini[1], Fabio Sciarrino[2,1], and Francesco De Martini[1,3]

[1]*Dipartimento di Fisica dell'Universitá "La Sapienza" and Consorzio Nazionale Interuniversitario per le Scienze Fisiche della Materia, Roma 00185, Italy*
[2]*Centro di Studi e Ricerche "Enrico Fermi", Via Panisperna 89/A,Compendio del Viminale, Roma 00184, Italy*
[3] *Accademia Nazionale dei Lincei, via della Lungara 10, I-00165 Roma, Italy*
fabio.sciarrino@uniroma1.it

Abstract: We present the realization of a ultra fast shutter for optical fields, which allows to preserve a generic polarization state, based on a self-stabilized interferometer. It exhibits high (or low) transmittivity when turned on (or inactive), while the fidelity of the polarization state is high. The shutter is realized through two beam displacing prisms and a longitudinal Pockels cell. This can represent a useful tool for controlling light-atom interfaces in quantum information processing.

OCIS codes: (270.5585) Quantum Optics - Quantum information and processing

References and links

1. N. Gisin, G. Ribordy, W. Tittel, and H. Zbinden, "Quantum Cryptography," Rev. Mod. Phys. **74**, 145 (2002).
2. E. Knill, R. Laflamme, and G. Milburn, "A scheme for efficient quantum computation with linear optics," Nature (London) **409**, 46 (2001).
3. R. Raussendorf and H. J. Briegel, "A One-Way Quantum Computer," Phys. Rev. Lett. **86**, 5188 (2001).
4. S. Giacomini, F. Sciarrino, E. Lombardi, and F. De Martini, "Active teleportation of a quantum bit," Phys. Rev. A **66**, 030302(R) (2002).
5. R. Ursin,R. Ursin, T. Jennewein, M. Aspelmeyer, R. Kaltenbaek, M. Lindenthal, P. Walther, and A. Zeilinger, "Quantum teleportation across the Danube," Nature (London) **430**, 849 (2004).
6. T.B. Pittman, B.C. Jacobs, and J.D. Franson, "Demonstration of feed-forward control for linear optics quantum computation," Phys. Rev. A **66**, 052305 (2002).
7. R. Prevedel, P. Walther, F. Tiefenbacher, P. Bohl, R. Kaltenbaek, T. Jennewein, and A. Zeilinger "High-speed linear optics quantum computing using active feed-forward," Nature (London) **445**, 65 (2007).
8. P. Böhi, R. Prevedel, T. Jennewein, A. Stefanov, F. Tiefenbacher, and A. Zeilinger, "Implementation and characterization of active feed- forward for deterministic linear optics quantum computing," Appl. Phys. B **89**, 499-505 (2007).
9. G. Vallone, E. Pomarico, F. De Martini, and P. Mataloni,"Active one-way quantum computation with 2-photon 4-qubit cluster states," Phys. Rev. Lett. **100**, 160502 (2008).
10. K. Hammerer, A.S. Sorensen, and E.S. Polzik, "Quantum interface between light and atomic ensembles,"' quant-ph/0807.3358v1.
11. F. Cataliotti and F. De Martini, "Macroscopic Quantum Superposition and Entanglement in light reflection from Bose-Einstein Condensates," ArXiv: quant-ph/0804.1453v1.
12. C. Wittmann, D. Elser, U. L. Andersen, R. Filip, P. Marek, and G. Leuchs , "Experimental Noiseless Filtering of Continuous-Variable Quantum Information," ArXiv: quant-ph/0704.1918.
13. F. Sciarrino, E. Nagali, F. De Martini, M. Gavenda, and R. Filip, "Experimental entanglement restoration on entanglement-breaking channels," ArXiv: quant-ph/0804.3542

Entanglement-seeded, dual, optical parametric amplification: Applications to quantum imaging and metrology

Ryan T. Glasser,* Hugo Cable,† and Jonathan P. Dowling
Horace C. Hearne, Jr. Institute for Theoretical Physics, Department of Physics and Astronomy, Louisiana State University, Baton Rouge, Louisiana 70803, USA

Francesco De Martini, Fabio Sciarrino, and Chiara Vitelli
University of Rome "La Sapienza," Piazzale Aldo Moro, 2 00185 Roma, Italy
(Received 12 April 2008; revised manuscript received 18 June 2008; published 21 July 2008)

The study of optical parametric amplifiers (OPAs) has been successful in describing and creating nonclassical light for use in fields such as quantum metrology and quantum lithography [Agarwal *et al.*, J. Opt. Soc. Am. B **24**, 2 (2007)]. In this paper we present the theory of an OPA scheme utilizing an entangled state input. The scheme involves two identical OPAs seeded with the maximally path-entangled $|N00N\rangle$ state $(|2,0\rangle + |0,2\rangle)/\sqrt{2}$. The stimulated amplification results in output state probability amplitudes that have a dependence on the number of photons in each mode, which differs greatly from two-mode squeezed vacuum. A large family of entangled output states are found. Specific output states allow for the heralded creation of $N=4$ $N00N$ states, which may be used for quantum lithography, to write sub-Rayleigh fringe patterns, and for quantum interferometry, to achieve Heisenberg-limited phase measurement sensitivity.

DOI: 10.1103/PhysRevA.78.012339 PACS number(s): 03.67.Bg, 42.65.Yj, 03.67.Ac, 03.65.Ud

I. INTRODUCTION

Nonclassical states of light have been studied in depth both experimentally and theoretically since the emergence of quantum electronics. Squeezed light, in particular, has been applied to a variety of systems, including interferometry and lithography which show improvement beyond limitations imposed by classical optics [1–4]. One such device that creates a type of squeezed light is an optical parametric amplifier (OPA). OPAs are typically noncentrosymmetric crystals that exhibit a nonzero $\chi^{(2)}$ optical nonlinearity [5]. Pump, signal, and idler modes propagate through the crystal, and photons from the pump beam are down converted into lower energy photons in the signal and idler modes. Previous work focused on the case that the signal and idler modes couple to the vacuum at the input. This produces the two-mode squeezed vacuum state, which exhibits highly nonclassical behavior [2,3,6]. In the present paper we analyze a scheme in which two identical OPAs are seeded by entangled photon pairs. The scheme produces a heralded source for a large family of entangled states, of interest for applications in quantum metrology and imaging. These states are generated by conditioning the output on photodetection on two of the four total output modes.

A particularly useful heralded state that our scheme generates is the so-called "$N00N$" state with $N=4$. A $N00N$ state is a maximally path entangled state such that, in a Fock-state basis, $|N00N\rangle \propto |N\rangle_A|0\rangle_B + e^{iN\varphi}|0\rangle_A|N\rangle_B$, where φ is the relative phase difference between the two spatial modes A and B [4]. These states allow for superresolution by producing lithographic features with a minimum size of $\lambda/(2N)$, when incident on an N-photon absorbing substrate, thus allowing an N-fold enhancement over standard lithographic methods [1,4,7]. $N00N$ states have also been shown to exhibit supersensitivity in interferometric applications, thus reaching the Heisenberg limit of $\Delta\phi = 1/N$ [1,8–10]. Classically, in an interferometer using coherent light, precision in phase-uncertainty measurement is limited by the shot-noise limit of $\Delta\phi = 1/\sqrt{\bar{n}}$, where $\bar{n}$ is the average photon number. Experimentally, up to $N=4$ $N00N$ states have been reported and shown to exhibit both supersensitivity and superresolution [11,12]. However, implementing $N00N$-state generators that produce states of photon number greater than two, which simultaneously achieve high fidelities and high flux, is very challenging experimentally. Recently two of us proposed a scheme that scales well with N and works for an input of any superposition of $|N,N\rangle$ photons coupled with feedforward [13]. Our scheme, presented here, produces heralded $N=4$ $N00N$ states with relatively high probability, and is experimentally accessible.

In Sec. II we will review the process of optical parametric amplification and squeezing. In Sec. III we describe the entanglement-seeded, dual, optical parametric amplification scheme. Finally, in Sec. IV we analyze the properties of the output state, including probabilities and applications.

II. OPTICAL PARAMETRIC AMPLIFICATION

To obtain the input state for our scheme, some squeezing formalism will be reviewed. We will work in the Heisenberg picture and use a Fock (number) -state basis throughout the paper. Modes are represented with capital letters, such as mode A, mode B, and so on. The creation and annihilation operators for the respective modes are $\hat{a}^\dagger$, $\hat{a}$, $\hat{b}^\dagger$, and $\hat{b}$. The mode labels are dropped from the kets, but proceed in alphabetical order such that $|N\rangle_A|M\rangle_B \equiv |N,M\rangle$.

The unitary operator describing the action of an OPA is the two-mode squeezing operator [14],

*rglass1@lsu.edu
†hcable@phys.lsu.edu

Amplification of polarization NOON states

Chiara Vitelli,[1] Nicolò Spagnolo,[1] Fabio Sciarrino,[1,*] and Francesco De Martini[1,2]

[1]*Dipartimento di Fisica dell'Universitá "La Sapienza" and Consorzio Nazionale Interuniversitario per le Scienze Fisiche della Materia, Roma 00185, Italy*

[2]*Accademia Nazionale dei Lincei, Palazzo Corsini,Via della Lungara, 10, Roma 00165, Italy*

[*]*Corresponding author: fabio.sciarrino@uniroma.it*

Received October 3, 2008; revised January 23, 2009; accepted February 20, 2009; posted February 24, 2009 (Doc. ID 102302); published April 3, 2009

We analyze the quantum states obtained by optical parametric amplification of polarization NOON states. First we study, theoretically and experimentally, the amplification of a two-photon state by a collinear quantum injected optical parametric amplifier (QIOPA). We compare the stimulated emission regime with the spontaneous one, studied by Sciarrino *et al.* [Phys. Rev. A **77**, 012324 (2008)]. As a second step, we show that the collinear amplifier cannot be successfully used for amplifying N-photon states with $N>2$, and we propose to adopt a different scheme, based on a noncollinear QIOPA. We show that the state obtained by the latter amplification process preserves the λ/N feature and exhibits a high resilience to losses. Furthermore, measurement of part of the output state can be adopted to increase the pattern visibility. © 2009 Optical Society of America

OCIS codes: 270.4180, 190.4410, 120.3940.

1. INTRODUCTION

In the past few years it has been proposed to exploit quantum effects to provide resolution enhancement in imaging procedures. Among the numerous problems that are currently studied under the general name of "quantum imaging," investigations concerning the quantum limits of optical resolution have a special importance, as they may lead to new concepts in microscopy and optical data storage. Such so-called superresolution techniques, studied for a long time at the classical level with a view to beating the Rayleigh limit of resolution, were recently revisited at the quantum level [1,2]. It was shown that it is possible to improve the performance of superresolution techniques by use of nonclassical light [3,4]. This approach, named "quantum lithography," may lead in the future to innovative microscopy techniques, to recording image features that are much smaller than the wavelength of the light, or to improving optical storage capacity beyond the wavelength limit. In such a framework, path entangled NOON states $|\psi^N\rangle_{AB}=(1/\sqrt{2})(|N\rangle_A|0\rangle_B+|0\rangle_A|N\rangle_B)$ have been adopted to increase the resolution in quantum interferometry. Indeed, in such states a single-mode phase shift ϕ induces a relative shift between the two components equal to $N\phi$ [5]. This feature leads to sub-Rayleigh resolution scaling as $\lambda/2N$, where λ is the wavelength of the field [6] [Fig. 1(a)]. Analogously, multiphoton polarization entangled states can be exploited to carry out quantum lithography by adopting the scheme reported in Fig. 1(b), which converts polarization-entanglement into path-entanglement. The theoretical and experimental study of photonic NOON states [7–9] has led to the experimental generation of two-, three-, and four-photon states by post-selection [10–13] and to the conditional generation of a state with $N=2$ [14]. Very recently schemes for the generation of path entangled NOON states with high value of fidelity and arbitrary N have been proposed [8,15,16]. However, until now, the low number of photons generated has strongly limited the potential applications to quantum lithography and quantum metrology. Moreover a NOON state, like any superposition of macroscopic states, is supersensitive to losses: for a N-photon state a fractional loss $1/N$ would destroy the quantum effect responsible for the phase resolution improvement [17].

A natural approach to increase the number of photons and to minimize the effect of losses is to exploit a high optical parametric process. Recently the output radiation of an unseeded optical parametric amplifier (OPA) was exploited to demonstrate the typical $\lambda/4$ feature with a large number of photons [18] [Fig. 2(a)]. Even if the achieved visibility is equal to 20%, this value is sufficient for applications in lithography and imaging [16]. In such a framework it has been proposed to exploit stimulated parametric processes to improve the visibility and obtain higher signal values [19]. This process, also known as quantum injected optical parametric amplification, has found some important applications in the context of quantum information [20,21]. Let us stress that high resolution and intense light fields can also be obtained in a classical framework [22,23]. In that case the improved resolution relies on the nonlinear response of the recording medium rather than on the quantum features of the adopted light field.

In the present paper we investigate the task of the amplification of photonic NOON states by two different devices, both based on a quantum injected optical parametric amplifier (QIOPA). First, in Section 2, we review how a sub-Rayleigh $\lambda/2N$ resolution can be obtained by an interferometric device acting on a NOON state. Then, in Section 3 we study both theoretically and experimentally the amplification of a two-photon state by a collinear

Wigner-function theory and decoherence of the quantum-injected optical parametric amplifier

Nicolò Spagnolo,[1,2] Chiara Vitelli,[1,2] Tiziano De Angelis,[1] Fabio Sciarrino,[1,2] and Francesco De Martini[1,3]
[1]*Dipartimento di Fisica, "Sapienza" Università di Roma, Piazzale Aldo Moro 5, I-00185 Roma, Italy*
[2]*Consorzio Nazionale Interuniversitario per le Scienze Fisiche della Materia, Piazzale Aldo Moro 5, I-00185 Roma, Italy*
[3]*Accademia Nazionale dei Lincei, via della Lungara 10, I-00165 Roma, Italy*
(Received 12 May 2009; published 17 September 2009)

Recent experimental results demonstrated the generation of a macroscopic quantum superposition (MQS), involving a number of photons in excess of 5×10^4, which showed a high resilience to losses. In order to perform a complete analysis on the effects of decoherence on these multiphoton fields, obtained through the quantum injected optical parametric amplifier, we investigate theoretically the evolution of the Wigner functions associated to these states in lossy conditions. Recognizing the presence of negative regions in the W representation as an evidence of nonclassicality, we focus our analysis on this feature. A close comparison with the MQS based on coherent $|\alpha\rangle$ states allows us to identify differences and analogies.

DOI: 10.1103/PhysRevA.80.032318 PACS number(s): 03.67.−a, 03.65.Yz, 42.50.Ex, 03.65.Wj

I. INTRODUCTION

In the last decades the physical implementation of macroscopic quantum superpositions (MQSs) involving a large number of particles has attracted a great deal of attention. Indeed it was generally understood that the experimental realization of a MQS is very difficult and in several instances practically impossible owing to the extremely short persistence of quantum coherence, i.e., of the extremely rapid decoherence due to the entanglement established between the macroscopic system and the environment [1–4]. Formally, the irreversible decay toward a probabilistic classical mixture is implied theoretically by the tracing operation of the overall MQS state over the environmental variables [5,6]. In the framework of quantum information different schemes based on optical systems have been undertaken to generate and to detect the MQS condition. A cavity-QED scheme based on the interaction between Rydberg atoms and a high-Q cavity has lead to the indirect observation of macroscopic quantum superposition (Schrödinger cat) states and of their temporal evolutions. In this case the microwave MQS field stored in the cavity can be addressed indirectly by injecting in the cavity, in a controlled way, resonant or nonresonant atoms as *ad hoc* "measurement mouses" [7,8]. A different approach able to generate freely propagating beams adopts photon-subtracted squeezed states; experimental implementations of quantum states with an average number of photons of around four have been reported both in the pulsed and continuous wave regimes [9–12]. These states exhibit non-Gaussian characteristics and open new perspectives for quantum computing based on continuous-variable systems, entanglement distillation protocols [13,14], and loophole free tests of Bell's inequality.

In the last few years a novel "quantum injected" optical parametric amplification (QI-OPA) process has been realized in order to establish the entanglement between a single-photon and a multiphoton state given by an average of many thousands of photons, a Schrödinger cat involving a "macroscopic field." Precisely, in a high-gain QI-OPA "phase-covariant" cloning machine the multiphoton fields were generated by an optical amplifier system bearing a high nonlinear (NL) gain g and seeded by a single photon belonging to an Einstein-Podolski-Rosen (EPR) entangled pair [15–19].

While a first theoretical insight on the dynamical features of the QI-OPA macrostates and a thorough experimental characterization of the quantum correlations were recently reported [20,21], a complete quantum phase-space analysis able to recognize the persistence of the QI-OPA properties in a decohering environment is still lacking [22,23]. Among the different representations of quantum states in the continuous-variable space [24], the Wigner quasiprobability representation has been widely exploited as an evidence of nonclassical properties, such as squeezing [25] and EPR nonlocality [26]. In particular, the presence of negative quasiprobability regions has been considered as a consequence of the quantum superposition of distinct physical states [27].

In the present paper we investigate the Wigner functions associated to multiphoton states generated by optical parametric amplification of microscopic single-photon states. We focus our interest on the effects of decoherence on the macrostates and on the emergence of the "classical" regime in the amplification of initially pure quantum states. The Wigner functions of these QI-OPA generated states in presence of losses are analyzed in comparison with the paradigmatic example of the superposition of coherent, Glauber's states, $|\alpha\rangle$.

The paper is structured as follows. In Sec. II, we introduce the conceptual scheme and describe the evolution of the system both in the Heisenberg and Schrödinger pictures. Section III is devoted to the calculation of the Wigner function of the QI-OPA amplified field. We first consider a single-mode amplifier, which is analogous to the case of photon-subtracted squeezed vacuum. Then we derive a compact expression of the Wigner function in the case of a two-mode amplifier in the "collinear" case, i.e., for common k vectors of the amplified output fields. In Sec. IV, we introduce, for the collinear case, a decoherence model apt to simulate the decohering losses affecting the evolution of the macrostate density matrix. This evolution is then compared to the case of the coherent $|\alpha\rangle$ MQS. Section V is devoted to a brief review of the features of coherent state superpositions (CSSs). Hence in Sec. VI we derive an explicit analytic ex-

Coherent Scattering of a Multiphoton Quantum Superposition by a Mirror BEC

Francesco De Martini,[1,2] Fabio Sciarrino,[2] Chiara Vitelli,[1] and Francesco S. Cataliotti[3]

[1]*Dipartimento di Fisica, Università di Roma "La Sapienza," Piazzale Aldo Moro 2, I-00185 Roma, Italy*
[2]*Accademia Nazionale dei Lincei, Via della Lungara 10, I-00165 Roma, Italy*
[3]*Dipartimento di Energetica and LENS, Università di Firenze, via N. Carrara 1, I-50019 Sesto F.no (FI), Italy*

(Received 28 February 2009; published 3 February 2010)

We present the proposition of an experiment in which the multiphoton quantum superposition consisting of $\mathcal{N} \approx 10^5$ particles generated by a quantum-injected optical parametric amplifier, seeded by a single-photon belonging to an Einstein-Podolsky-Rosen entangled pair, is made to interact with a mirror-Bose-Einstein condensate (BEC) shaped as a Bragg interference structure. The overall process will realize a macroscopic quantum superposition involving a microscopic single-photon state of polarization entangled with the coherent macroscopic transfer of momentum to the BEC structure, acting in spacelike separated distant places.

DOI: 10.1103/PhysRevLett.104.050403 PACS numbers: 03.65.Ud, 03.67.−a, 03.75.Gg

In recent years, a great deal of interest has been focused on the ambitious problem of creating a macroscopic quantum superposition (MQS) of a massive object by an entangled optomechanical interaction of a tiny mirror with a single photon within a Michelson interferometer [1–5], then realizing a well-known 1935 argument by Erwin Schrödinger [6]. The present work is aimed at a similar scope but is not concerned with interferometers nor with solid mirrors. It rather exploits the process of nonresonant scattering by a properly shaped Bose-Einstein condensate (BEC) [7] of an externally generated multiparticle quantum photon state, a "macrostate" $|\Phi\rangle$, in order to create a joint atom-photon macrostate entangled by momentum conservation. Light scattering from BEC structures has been used so far to enhance their nonlinear macroscopic properties in superradiance experiments [8] to show the possibility of matter-wave amplification [9] and nonlinear wave mixing [10]. In the present work, we intend to discuss the linear *coherent scattering*, i.e., the *reflection* by a multilayered BEC of a large assembly of nearly monochromatic photons generated by a high-gain "quantum-injected" optical parametric amplifier (QI-OPA) in a Einstein-Podolsky-Rosen (EPR) configuration [11,12]. Very recently, it was demonstrated experimentally that the optical macrostate $|\Phi\rangle$ generated by the QI-OPA can indeed be entangled with, i.e., nonseparable from, a far apart single-photon state belonging to the injected EPR pair [13], thus resulting highly resilient to the decoherence due to losses [14]. By the present work, this condition will be extended to the mechanical motion of an atomic assembly by making the photonic macrostate $|\Phi\rangle$ to exchange linear momentum with a high reflectivity BEC optical mirror, here referred to as a "mirror BEC" (mBEC). This can be a novel and viable alternative to the realization of an entangled MQS of a massive object.

The layout of the experiment, Fig. 1, shows an EPR optical parametric amplifier, provided by Crystal 1, of a polarization entangled (π-entangled) pair of photons launched towards two distant measurement stations, here referred to as *Alice* (A) and *Bob* (B) [13,15]. One of the EPR photons emitted towards the Bob's site is injected into the QI-OPA which generates a corresponding macrostate $|\Phi\rangle$. The device operates in the collinear regime and amplifies with a large "gain" any injected single photon in a quantum superposition, i.e., a *qubit* $|\varphi\rangle_{k1}$, into a large number of photons, $\mathcal{N} \approx 10^5$, associated with a corresponding macroqubit $|\Phi^{\varphi}\rangle_{k1}$. These macrostates then drive the mechanical motion of the mBEC. Since these states are found to be entangled with the far apart single-photon emitted over the mode $\mathbf{k}_2$ and detected by Alice, the same entanglement property is then transferred to the position macrostate of the optically driven mBEC [Fig. 1(b)]. The optical part of the apparatus is the working QI-OPA device recently reported by [13,15] to which the reader is referred.

Micro-macro entangled light.—As shown in Fig. 1, the main uv beam is split in two beams and excites two nonlinear (NL) crystals cut for type II phase-matching. Crystal 1 is the spontaneous parametric down-conversion source of entangled photon couples of wavelength (wl) $\lambda' = 2\lambda'_P$, emitted over the modes $\mathbf{k}_i$ $(i = 1', 2)$ in the entangled *singlet* state $|\Psi^-\rangle_{k1',k2} = 2^{-1/2}(|H\rangle_{k1'}|V\rangle_{k2} - |V\rangle_{k1'}|H\rangle_{k2})$, where $H(V)$ labels the single-photon state horizontally (vertically) polarized. The photon associated with the mode $\mathbf{k}_2$ (the *trigger* mode) is coupled to a single mode (SM) fiber and filtered by a set of π-analyzing optical devices, namely, a Babinet compensator (B), a $\lambda'/2 + \lambda'/4$ wave plate set, a polarizing beam splitter (PBS), and an interference filter (IF) with a transmission linewidth $\Delta\lambda'$. At last, the *trigger* photon excites, at the Alice's site, the single-photon detector D_2^A delivering the *trigger* signal adopted to establish the overall quantum correlations. By a dichroic mirror (DM), the single photon created over the mode $\mathbf{k}'_1$ is made to merge into the mode $\mathbf{k}_1$ together with the uv beam associated with mode $\mathbf{k}'_P$ and then injected into the NL Crystal 2 where it stimulates the emission of many photon pairs over the two polarization

PHYSICAL REVIEW A **81**, 032123 (2010)

Quantum-to-classical transition via fuzzy measurements on high-gain spontaneous parametric down-conversion

Chiara Vitelli,[1,2] Nicolò Spagnolo,[1,2] Lorenzo Toffoli,[1] Fabio Sciarrino,[1,3] and Francesco De Martini[1,4]
[1]*Dipartimento di Fisica, "Sapienza" Università di Roma, Piazzale Aldo Moro 5, I-00185 Roma, Italy*
[2]*Consorzio Nazionale Interuniversitario per le Scienze Fisiche della Materia, Piazzale Aldo Moro 5, I-00185 Roma, Italy*
[3]*Istituto Nazionale di Ottica Applicata, Largo Fermi 6, I-50125 Firenze, Italy*
[4]*Accademia Nazionale dei Lincei, via della Lungara 10, I-00165 Roma, Italy*
(Received 20 January 2010; published 29 March 2010)

We consider the high-gain spontaneous parametric down-conversion in a noncollinear geometry as a paradigmatic scenario to investigate the quantum-to-classical transition by increasing the pump power, that is, the average number of generated photons. The possibility of observing quantum correlations in such a macroscopic quantum system through dichotomic measurement will be analyzed by addressing two different measurement schemes, based on different dichotomization processes. More specifically, we will investigate the persistence of nonlocality in an increasing size $\frac{n}{2}$-spin singlet state by studying the change in the correlations form as n increases, both in the ideal case and in presence of losses. We observe a fast decrease in the amount of Bell's inequality violation for increasing system size. This theoretical analysis is supported by the experimental observation of macro-macro correlations with an average number of photons of about 10^3. Our results shed light on the practical extreme difficulty of observing nonlocality by performing such a dichotomic fuzzy measurement.

DOI: 10.1103/PhysRevA.81.032123 PACS number(s): 03.65.Ta, 03.67.−a, 42.50.Xa

I. INTRODUCTION

For a long time the investigation of entanglement and nonlocality has been limited to quantum systems of small size [1]. Theoretical and experimental works on Bell's inequalities have been devoted to the study of single-particle states, in which dichotomic measurements have been performed [2]. Nonlocality tests have been achieved with single-photon states, produced by parametric down conversion, by detecting polarization correlations [3–5]. More recently, the violation of Bell's inequality has been shown with a larger number of photons: on Greenberger-Horne-Zeilinger (GHZ) [6] and cluster states [7] up to four photons.

On the other hand, the possibility of observing quantum phenomena at a macroscopic level seems to be in conflict with the classical description of our everyday world knowledge. The main problem for such observation arises from the experimental difficulty of sufficiently isolating a quantum system from its environment, that is, from the decoherence process [8]. An alterative approach to explain the quantum-to-classical transition, conceptually different from the decoherence program, has been given, very recently, by Kofler and Brukner, along the idea earlier discussed by Bell, Peres [9], and others. These authors have given a description of the emergence of macroscopic realism and classical physics in systems of increasing size *within quantum theory* [10]. They focused on the limits of the quantum effects observability in macroscopic objects, showing that, for large systems, macrorealism arises under coarse-grained measurements. More specifically, they demonstrated that, while the evolution of a large spin cannot be described classically when sharp measurements are performed, a fuzzy measurement on a large-spin system would induce the emergence of the Newtonian time evolution from a full quantum description of the spin state. However, some counterexamples to such a modelization have been found later by the same authors: some nonclassical Hamiltonians violate macrorealism despite coarse-grained measurements [11]. One example is given by the time-dependent Schrödinger catlike superposition, which can violate macrorealism by adopting a suitable "which emisphere" measurement. Therefore the measurement problem seems to be a key ingredient in the attempt to understand the limits of the quantum behavior of physical systems and the quantum-to-classical transition question. As a further step, Kofler, Buric, and Brukner also demonstrated [12] that macrorealism does not imply a continuous spatiotemporal evolution. Indeed, they showed that the same Schrödinger catlike nonclassical Hamiltonian, in contact with a dephasing environment, no longer violates a Leggett-Garg inequality, while it still presents a nonclassical time evolution. In a recent paper Jeong *et al.* [13] contributed to the investigation about the possibility of observing the quantum features of a system when fuzzy measurement are performed on it, finding that extremely coarse-grained measurements can still be useful to reveal the quantum world where local realism fails.

In this context, the possibility of obtaining macroscopic quantum systems in the laboratory has raised the problem of investigating entanglement and nonlocality in systems in which single particles cannot be addressed singularly. As shown in Ref. [14], the demonstration of nonlocality in a multiphoton state produced by a nondegenerate optical parametric amplifier would require the experimental application of parity operators. On the other hand, the estimation of a coarse-grained quantity, through collective measurements as the ones proposed in Ref. [15], would miss the underlying quantum structure of the generated state, introducing elements of local realism even in the presence of strong entanglement and in the absence of decoherence. The theoretical investigation on a multiphoton system, obtained via parametric down-conversion, has been also carried out by Reid *et al.* [16]. They analyzed the possibility of obtaining the violation of Bell's inequality by performing dichotomic measurement on the multiparticle quantum state. More specifically, in analogy with the spin

Enhanced Resolution of Lossy Interferometry by Coherent Amplification of Single Photons

Chiara Vitelli,[1,2] Nicolò Spagnolo,[1,2] Lorenzo Toffoli,[1] Fabio Sciarrino,[1,3,*] and Francesco De Martini[1,4]

[1]*Dipartimento di Fisica, Sapienza Università di Roma, piazzale Aldo Moro 5, I-00185 Roma, Italy*

[2]*Consorzio Nazionale Interuniversitario per le Scienze Fisiche della Materia, piazzale Aldo Moro 5, I-00185 Roma, Italy*

[3]*Istituto Nazionale di Ottica, largo Fermi 6, I-50125 Firenze, Italy*

[4]*Accademia Nazionale dei Lincei, via della Lungara 10, I-00165 Roma, Italy*

(Received 16 April 2010; revised manuscript received 14 July 2010; published 8 September 2010)

In the quantum sensing context most of the efforts to design novel quantum techniques of sensing have been constrained to idealized, noise-free scenarios, in which effects of environmental disturbances could be neglected. In this work, we propose to exploit optical parametric amplification to boost interferometry sensitivity in the presence of losses in a minimally invasive scenario. By performing the amplification process on the microscopic probe after the interaction with the sample, we can beat the losses' detrimental effect on the phase measurement which affects the single-photon state after its interaction with the sample, and thus improve the achievable sensitivity.

DOI: 10.1103/PhysRevLett.105.113602 PACS numbers: 42.50.Ex, 42.50.Dv, 42.50.St

The aim of quantum sensing is to develop methods to extract the maximum amount of information from a system with a minimal disturbance on it. Indeed, the possibility of performing precision measurements by adopting quantum resources can increase the achievable precision going beyond the semiclassical regime of operation [1–3]. In the case of interferometry, this can be achieved by the use of the so-called N00N states, which are quantum mechanical superpositions of just two terms, corresponding to all the available photons N placed in either the signal arm or the reference arm. The use of N00N states can enhance the precision in phase estimation to $1/N$, thus improving the scaling of the achievable precision with respect to the employed resources [4,5]. This approach can have wide applications for minimally invasive sensing methods in order to extract the maximum amount of information from a system with minimal disturbance. The experimental realization of protocols involving N00N states containing up to 4 photons have been realized in the past few years [6–10]. Other approaches [11,12] have focused on exploiting coherent and squeezed light to generated fields which approximate the features of N00N states. Nevertheless, these quantum states turn out to be extremely fragile under losses and decoherence [13], unavoidable in experimental implementations. A sample, whose phase shift is to be measured, may at the same time introduce high attenuation. Since quantum-enhanced modes of operations exploit fragile quantum mechanical features, the impact of environmental effects can be much more deleterious than in semiclassical schemes, destroying completely quantum benefits [14,15]. This scenario puts the beating of realistic, noisy environments as the main challenge in developing quantum sensing. Very recently, the theoretical and experimental investigations of quantum states of light resilient to losses have attracted much attention, leading to the best possible precision in optical two-mode interferometry, even in the presence of experimental imperfections [16–21].

In this work, we adopt a hybrid approach based on a high gain optical parametric amplifier operating for any polarization state in order to transfer quantum properties of different microscopic quantum states in the macroscopic regime [22,23]. By performing the amplification process of the microscopic probe after the interaction with the sample, we can beat the losses' detrimental effect on the phase measurement which affects the single-photon state after the sample. Our approach may be adopted in a minimally invasive scenario where a fragile sample, such as biological or artifacts systems, requires as few photons as possible impinging on it in order to prevent damages. The action of the amplifier, i.e., the process of optimal phase covariant quantum cloning, is to broadcast the phase information codified in a single photon into a large number of particles. Such multiphoton states have been shown to exhibit a high resilience to losses [24–26] and can be manipulated by exploiting a detection scheme which combines features of discrete and continuous variables. The effect of losses on the macroscopic field consists in the reduction of the detected signal and not in the complete cancellation of the phase information as would happen in the single-photon probe case, thus improving the achievable sensitivity. This improvement does not consist in a scaling factor but turns out to be a constant factor in the sensitivity depending on the optical amplifier gain. Hence, the sensitivity still scales as $\sqrt{N}$, where N is the number of photons impinging on the sample, but the effect of the amplification process is to reduce the detrimental effect of losses by a factor proportional to the number of generated photons.

Let us review the adoption of single photons in order to evaluate the unknown phase φ, Fig. 1(a). The phase φ introduced in the path k_2 is probed by sending to the sample N input photons, each one in the state

